
Doctoral Dissertations

Student Theses and Dissertations

Spring 2016

Composite confinement systems for RC column repair and construction under seismic loads: Concept, characterization and performance

Mostafa Fakharifar

Follow this and additional works at: https://scholarsmine.mst.edu/doctoral_dissertations



Part of the [Civil Engineering Commons](#)

Department: Civil, Architectural and Environmental Engineering

Recommended Citation

Fakharifar, Mostafa, "Composite confinement systems for RC column repair and construction under seismic loads: Concept, characterization and performance" (2016). *Doctoral Dissertations*. 2647.
https://scholarsmine.mst.edu/doctoral_dissertations/2647

This thesis is brought to you by Scholars' Mine, a service of the Missouri S&T Library and Learning Resources. This work is protected by U. S. Copyright Law. Unauthorized use including reproduction for redistribution requires the permission of the copyright holder. For more information, please contact scholarsmine@mst.edu.

COMPOSITE CONFINEMENT SYSTEMS FOR RC COLUMN REPAIR AND
CONSTRUCTION UNDER SEISMIC LOADS: CONCEPT, CHARACTERIZATION
AND PERFORMANCE

by

MOSTAFA FAKHARIFAR

A DISSERTATION

Presented to the Faculty of the Graduate School of the
MISSOURI UNIVERSITY OF SCIENCE AND TECHNOLOGY

In Partial Fulfillment of the Requirements for the Degree

DOCTOR OF PHILOSOPHY IN CIVIL ENGINEERING

2016

Approved by
Genda Chen, Advisor
Roger A. LaBoube
Mohamed A. ElGawady
Lesley H. Sneed
K. Chandrashekhara

© 2016

Mostafa Fakharifar

All Rights Reserved

PUBLICATION DISSERTATION OPTION

This dissertation has been prepared in the style such that the second section is composed of publications and submissions for publications in professional peer-reviewed journals. The corresponding journal specifications were used to format each of the papers presented in this dissertation.

Paper I entitled “Hybrid Jacketing for Rapid Repair of Seismically Damaged Reinforced Concrete Column”, presented from page 33 to 58 in this dissertation, has been published in Transportation Research Board (TRB): *Journal of the Transportation Research Board*, 2015, No. 2522, pages 70-78. DOI:10.3141/2522-07.

Paper II entitled “Rapid Repair of Earthquake Damaged RC Columns with Prestressed Steel Jackets”, presented from page 59 to 98 in this dissertation, has been accepted for publication in *Journal of Bridge Engineering* published by the American Society of Civil Engineers (ASCE), DOI: 10.1061/(ASCE)BE.1943-5592.0000840.

Paper III entitled “Seismic Performance of Post-Mainshock FRP/Steel Repaired RC Bridge Columns Subjected to Aftershocks”, presented from page 99 to 147 in this dissertation, has been published in *Composites: Part B Journal* (Elsevier Publishing) 2015, Volume 72, pages 183-198.

Paper IV present the manuscript entitled “Compressive Behavior of FRP-Confined Concrete-Filled PVC Tubular Columns”, presented from page 148 to 201 in this dissertation, which would be submitted to *Composites: Part B Journal* (Elsevier Publishing).

Paper V present the manuscript entitled “Concrete Filled FRP-PVC Tubular Columns for Ductile and Durable Bridge Behavior under Earthquake Loads”, presented from page 202 to 228 in this dissertation, which has been submitted to Transportation Research Board: *Journal of the Transportation Research Board*.

ABSTRACT

This study aims at developing, characterizing and validating an integrated composite confinement system of conventional jackets for: (1) repair and retrofit of existing bridge columns; and (2) construction of new bridge columns, subjected to earthquake excitations.

A new composite steel confinement jacket was proposed by combining a thin steel sheet and prestressing strands as a hybrid jacket, incorporating active and passive confining pressure on damaged RC columns. Both experimental and analytical studies were conducted to understand the performance and effectiveness of the proposed repair method. The experimental study involved two ½-scale lap-spliced deficient RC bridge columns originally tested to failure under reversed cyclic loading. The proposed jacket was designed and implemented to repair the damaged columns to achieve the required performance level after repair intervention for service and ultimate limit states. Experimental results indicated that both repaired columns exceeded the strength and ductility of their as-built columns. The stiffness of the second column designed for ultimate limit state was completely restored. Analytical studies and collapse analyses on the seismic performance of post-mainshock repaired bridges subjected to mainshock-aftershock sequences demonstrated the efficacy of the proposed technique under severe mainshock-severe aftershock attacks.

Another new composite confinement system of a fiber reinforced polymer (FRP) sheet wrapped around a polyvinyl chloride (PVC) tube with energy dissipation medium in between was developed for new bridge columns construction. This composite system is essentially a FRP-confined concrete-filled PVC tube, featuring exceptional durability properties of PVC materials in addition to high strength of the FRP fabrics. Experimental tests under uniaxial compression and flexural loading were undertaken to establish the representative stress-strain behavior of confined concrete filled PVC tubes (CCFPT). Experimental studies clearly demonstrated that the CCFPT system outperforms conventional FRP jacket. The intermediate energy dissipation medium is critical to make the post-peak behavior more ductile. Analytical studies were conducted and equations were derived for the prediction of the ultimate strength and strain of a CCFPT system.

ACKNOWLEDGMENTS

My most sincere gratitude and appreciation go to my advisor Professor Genda Chen for his tremendous help throughout my Ph.D. studies. His kind help, especially during the period of my back injury would never be forgotten. It has been a great honor and immense pleasure for me to have been worked with him. I do feel that I have been extremely fortunate to have Dr. Chen as a teacher and supervisor during my Ph.D. studies.

I would also like to thank all my committee members, Drs. Roger A. LaBoube, Mohamed ElGawady, Lesley H. Sneed, and K. Chandrashekhara for their valuable comments and guidance. I received great help from all of my committee members. Special thanks are extended to Dr. ElGawady on his technical comments during the repair method developed as part of this study. I would also like to thank Dr. Sneed for offering valuable comments on the numerical study, and Dr. Chandrashekhara for the new insight he gave me on finite element analysis. The pleasant experience of having my first course at Missouri S&T with Prof. LaBoube would never be forgotten as his class prepared me well toward my Ph.D. studies.

I sincerely appreciate the assistance of many staff in the Structures High Bay Lab at Missouri S&T, including Delbert Hampton, Jason Cox, John Bullock, Gary Abbott, Michael Lusher, Brian Swift and Scott Parker. I also owe thanks to Zachary T. Woolsey, Tim O'Connor, Kristian Krc and Alex Cain for their help throughout column specimen tests. I would like to thank my Persian friends in Rolla, MO for their friendship, and support during my Ph.D. years at Missouri S&T. Special thanks to my friend and my brother Amirhossein Rafati for his positive helpful character.

I am deeply indebted to my parents, my brother and my sister for their endless love. This work is dedicated to my mother for all her pure, unconditional love, prayers and emotional support.

Finally, my very special thanks go to my lovely wife, that we married couple of months prior to the completion of this dissertation. Her continuous love, beautiful smile, and encouragement are highly appreciated and will stay forever in my heart.

TABLE OF CONTENTS

	Page
PUBLICATION DISSERTATION OPTION	iii
ABSTRACT.....	iv
ACKNOWLEDGMENTS	v
TABLE OF CONTENTS.....	vi
LIST OF ILLUSTRATIONS.....	xi
LIST OF TABLES	xiv
SECTION	
1. INTRODUCTION	1
1.1. BACKGROUND	1
1.2. COMPOSITE STEEL CONFINEMENT FOR REPAIR/RETROFIT OF EXISTING CONSTRUCTION	3
1.2.1. Background on Earthquake Damage and Rehabilitation Through Confinement	3
1.2.2. Steel Jacketing for RC Column Confinement.....	5
1.2.3. RC Jackets for RC Column Confinement.....	6
1.2.4. FRP Jackets for RC Column Confinement.....	8
1.2.5. Prestressing Bars/Stands/FRP Belts for RC Column Confinement.....	18
1.2.6. Shape memory alloy (SMA) for RC Column Confinement	24
1.3.COMPOSITE FRP/PVC CONFINEMENT FOR NEW CONSTRUCTION..	25
1.3.1. FRP-Confined Concrete Filled PVC Tube System.....	26
1.4. RESEARCH OBJECTIVES AND SCOPE OF WORK.....	29
1.5. DISSERTATION OUTLINE.....	31
PAPER	
I. HYBRID JACKETING FOR RAPID REPAIR OF SEISMICALLY DAMAGED REINFORCED CONCRETE COLUMNS.....	33
ABSTRACT.....	33
INTRODUCTION	34
EXISTING SEIMSIC REPAIR/RETROFIT TECHNIQUES.....	34
EXPERIMENTAL PROGRAM	36

Original Column Design	36
Original Column Test to Failure	36
Repair Design of the Damaged Column	37
Materials	37
Repair Procedure.....	37
Repair Design and Performance Objectives	38
Instrumentation and Test to Failure of the Repaired Column.....	41
RESULTS AND DISCUSSION	42
Repair Efficiency	43
Strength Index (STRI)	43
Stiffness Index (STFI)	43
Ductility Index (DI)	44
Failure Mode	45
CONCLUSIONS.....	46
ACKNOWLEDGMENTS	47
REFERENCES	47
List of Tables	49
List of Figures	49
II. RAPID REPAIR OF EARTHQUAKE DAMAGED RC COLUMNS WITH PRESTRESSED STEEL JACKETS.....	59
Abstract	59
Introduction.....	60
Objectives and Research Significance	63
Experimental Program	64
As-built Column Specimens	65
Rapid Repair of the Damaged Columns with the Proposed PSJ.....	66
Materials	66
Design and Performance Objectives.....	67
Method and Procedure	68
Test Setup and Instrumentation.....	70
Test Results and Discussion.....	71

Behavior of As-built Columns	71
Hysteresis Behavior and Physical Observations of Repaired Columns.....	72
Performance Evaluation of the Proposed PSJ.....	74
Experimental Verification of Repair Mechanism in the PSJ.....	75
Comparative Cost Analysis.....	76
Conclusions.....	77
Acknowledgments.....	79
References.....	79
III. SEISMIC PERFORMANCE OF POST-MAINSHOCK FRP/STEEL REPAIRED RC BRIDGE COLUMNS SUBJECTED TO AFTERSHOCKS	99
ABSTRACT.....	99
1. Introduction.....	100
2. Post-earthquake resilience of mainshock-damaged bridges subjected to aftershocks.....	101
3. Repair of mainshock-damaged bridge piers	103
3.1. Hybrid repair jacket.....	103
3.2. Repair techniques	103
3.3. Repair performance objectives.....	104
4. Nonlinear finite element modeling of a prototype highway bridge.....	106
4.1. Constitutive laws of materials and column fiber modeling	108
4.2. Model validation with experimental results.....	109
5. Nonlinear static analysis	111
5.1. Column with minor damage.....	112
5.2. Column with moderate damage	112
5.3. Column with severe damage.....	113
5.3.1. Confining pressure variation on the column with severe damage ...	113
6. Incremental dynamic analysis.....	114
6.1. Damage/limit state	115
6.2. Mainshock-aftershock seismic ground motion records.....	116
6.3. IDA analysis results and discussion.....	117
7. Conclusions.....	121

Acknowledgments.....	123
References.....	123
IV. COMPRESSIVE BEHAVIOR OF FRP-CONFINED CONCRETE FILLED PVC TUBULAR COLUMNS	148
ABSTRACT.....	148
1. Introduction.....	149
2. Experimental program	152
2.1. Details of cylinder specimens	152
2.2. Material properties	154
2.2.1. Concrete	154
2.2.2. FRP.....	155
2.2.3. PVC.....	155
2.3. Instrumentation and testing procedure.....	156
3. Test results	157
3.1. Failure modes	157
3.2. Stress-strain behavior and ultimate condition.....	158
4. Analysis of test results	160
4.1. Stress-strain behavior	160
4.2. Influence of confinement pressure and detail	163
4.3. Influence of confinement type	165
5. Applicability of existing stress-strain models for CCFPT behavior prediction.	167
6. Conclusions.....	169
Acknowledgments.....	170
References.....	170
V. CONCRETE FILLED FRP-PVC TUBULAR COLUMNS FOR DUCTILE AND DURABLE BRIDGE BEHAVIOR UNDER EARTHQUAKE LOADS	202
ABSTRACT.....	202
INTRODUCTION	203
EXPERIMENTAL PROGRAM	205
Axial and Flexural Test Specimens.....	205
Material Properties	206
Concrete	206

FRP.....	207
PVC.....	207
Instrumentation and Testing Procedure	208
Stub Specimens Under Compression.....	208
Beam Specimens Under Transverse Bending.....	209
RESULTS AND DISCUSSION	210
Stub Specimens Failure Modes.....	210
Stub Specimens Stress-Strain Relationship	211
Comparison of Stress-Strain Behavior.....	211
Flexural Specimens Failure Modes.....	213
Flexural Specimens Load-Displacement Relationship	214
CONCLUSIONS.....	216
ACKNOWLEDGEMENTS.....	217
REFERENCES	217
List of Tables	218
List of Figures	218
SECTION	
2. SUMMARY, CONCLUSIONS AND RECOMMENDATIONS.....	229
2.1. SUMMARY OF RESEARCH WORK.....	229
2.2. CONCLUSIONS.....	233
2.2.1. Composite Steel Confinement for Repair/Retrofit	233
2.2.2. Composite FRP/PVC Confinement for New Construction	236
2.3. RECOMMENDATIONS	237
REFERENCES	238
VITA.....	248

LIST OF ILLUSTRATIONS

Figure	Page
PAPER I	
1 Comparison of existing retrofit/repair methods.....	51
2 Geometry and reinforcement details of the original column.....	52
3 Original column damage state	53
4 Repair procedure with the hybrid confining jacket.....	54
5 Hybrid jacket details	55
6 Column test setup and instrumentation.....	56
7 Cyclic and idealized force-displacement relationship of original and repaired column specimens.....	57
8 Concrete cracks associated with stress transfer through dowel bars at the column-foting connection	58
PAPER II	
1 Shear crack arrest mechanism and bridge pier collapse	88
2 Dimensions and reinforcement details of as-built RC columns.....	89
3 Damaged columns after removal of loose concrete.....	90
4 Final design of the PSJ.....	91
5 Repair method and procedure of Column 1	92
6 Test preparation	93
7 Location of strain gages on the jacket and reinforcement	94
8 Hysteresis loops	95
9 Failure modes.....	96
10 Envelope of actual and idealized load-displacement relationships of studied columns	97
11 Average strain-drift ratio relationships of repaired Columns 1 and 2	98
PAPER III	
1 (a) A scenario mainshock-aftershock acceleration time history; and (b) Arias intensity for mainshock only and for mainshock-aftershock sequence	132
2 Typical details of the bridge under investigation.....	133
3 Details of the hybrid repair jacket.....	134

4	(a) Stress states in the repair jacket along the shear crack due to hybrid jacket and prestressing strands only; (b) widening of the shear crack during aftershock on unrepaired columns	135
5	Schematic of various repair techniques	136
6	Various states of a five-span continuous bridge model	137
7	Constitutive models	138
8	Idealized column models	139
9	Hysteresis loops comparison and validation of numerical RC column models with lumped and distributed plasticity	140
10	Displacement time history comparison and shake table validation of the full-scale RC bridge with lumped and distributed plasticity models [63]	141
11	Pushover response curves of Bent 4 of the bridge under investigation with original and unrepaired columns as well as the repaired columns	142
12	Response spectra of far-fault (ensemble 1) unscaled ground motions and their corresponding target spectrum at various hazard levels	143
13	Response spectra of near-fault (ensemble 2) unscaled ground motions and their corresponding target spectrum at various hazard levels	144
14	Maximum drift versus spectral acceleration IDA curves under severe MS-severe AS far-fault motions (ensemble 1)	145
15	Maximum drift versus spectral acceleration IDA curves under severe MS-severe AS near-fault motions (ensemble 2)	146
16	Mean structural collapse capacity	147
PAPER IV		
1	Preparation of cylinder specimens	187
2	Details of cylinder specimens	188
3	Experimental stress-strain curves	189
4	PVC dogbone test specimen prior to and after tensile test	190
5	Hollow PVC tube deformation modes	191
6	Uniaxial compression test	192
7	Typical failure of cylinders under axial compression	193
8	Axial stress-strain behavior of cylinders	194
9	Influence of confinement pressure on stress-strain behavior of test specimens	196
10	Influence of confinement detail on stress-strain behavior	197

11	Comparison of representative axial stress-strain behavior of CFPT, FW, and CCFPT specimens.....	198
12	Influence of confinement type	199
13	Performance of various confinement models in predicting strength enhancement ratio (f'_{cc}/f'_{co}).....	200
14	Performance of various confinement models in predicting strain enhancement ratio ($\epsilon_{cu}/\epsilon_{co}$).....	201
PAPER V		
1	Details of studied specimens.....	222
2	Measured mechanical properties of PVC pipes.	223
3	Test setup.	224
4	Typical failure modes of stub columns.....	225
5	Axial stress-strain curves of stub specimens	226
6	Core concrete conditions of CFPT and CCFPT beam specimens after test	227
7	Load-deflection curves of flexural beams.....	228

LIST OF TABLES

Table	Page
PAPER I	
1 Idealized And Measured Responses Of Original And Repaired Column Specimens	50
PAPER II	
1 Parameters in Idealized Capacity Curves of As-built and Repaired Columns	85
2 Performance Measures of As-built and Repaired Columns.....	86
3 Comparative Cost Analysis of Three Repair Methods	87
PAPER IV	
1 Test matrix of cylinder specimens	178
2 Fresh and hardened concrete properties.....	179
3 Material properties of FRP sheets.....	180
4 Tensile properties of PVC dogbone specimens under tension	181
5 Measured properties of PVC tubes under axial compression	182
6 Test results of cylinder specimens	183
7 Average recorded strain reduction factor, k_e , for FW and CCFPT specimens	184
8 Models used to predict strength and strain enhancement ratios of confined specimens	185
9 Average relative error (%) of strength and strain enhancement ratio predictions.....	186
PAPER V	
1 Summary Of Stub Column Specimens Test Results	220
2 Summary Of Flexural Beam Specimens Test Results	221

1. INTRODUCTION

1.1. BACKGROUND

Recent earthquakes have demonstrated the seismic vulnerability and inadequacy of non-code conforming structures, in which the seismic codes of practice were not available or less stringent during the design and construction. In particular, the poor performance of substandard existing lifeline structures, such as reinforced concrete (RC) bridges that were constructed prior to the early 1970's has been observed during the past earthquakes. Prior to that, the seismic actions were not considered in design, or little attention was given to the dynamic inertia forces associated with earthquake excitations. This matter resulted in substandard construction where sparsely spaced transverse reinforcement was provided in RC columns, where significant plastification and nonlinearity, also known as plastic hinges, were anticipated to form. Moreover, longitudinal reinforcements were lap-spliced at column-footing interface due to ease of construction with short lap splice length. Bridges built prior to 1971 are seismically deficient due to: 1) lack of confinement due to sparsely spaced transverse reinforcement; and 2) short lap splices at the potential plastic hinge location [1]. Recent codes of practice have been updated to consider the seismic action effects on structures [2, 3]. Needless to mention, demolition and rebuilding all of the previously built, substandard construction is an arduous, costly action, in which due to time and budget constraints may not be a viable option. Therefore, extensive studies on seismic rehabilitation and retrofitting of existing bridges, to improve their strength, stiffness and ductility (deformability) were undertaken by different researchers (e.g., [2, 4-10] amongst many other). The bridge retrofitting program is a broad term that includes providing restrainers between expansion joints, increasing seat widths at the joints and jacketing the columns for improved seismic performance [2, 3].

Harsh environmental conditions necessitated a strong demand for more resilient, more durable and stronger structural members that are cost-effective with sound structural performance. Past studies have demonstrated the enhanced structural performance of concrete filled tube (CFT) systems, incorporating steel or fiber reinforced

polymer (FRP) confining tubes, as an improved form of gravitational and lateral load resisting system for tall buildings and bridge columns or pile-footings [11-22]. Concrete filled steel tube (CFST) and concrete filled FRP tube (CFFT) column systems are the two most common types of CFT system that have been investigated at both member and system level under static and simulated seismic loading conditions [11, 12, 14-21, 23-28]. The CFT system demonstrates remarkable properties in terms of enhanced structural performance (i.e., strength, stiffness, ductility and hysteretic capacity) and project economy and/or constructability [29]. In CFT system, confining tube serves both as a shoring system and permanent formwork, providing substantial continuous confining pressure to the encased concrete infill [11, 12, 14, 16]. Different studies demonstrated improved performance of hybrid tubular column members by incorporating steel and FRP tubes, referred to as hybrid double-skin tubular columns or beams, with remarkable hysteresis capacity against seismic excitations [30-33]. Durability of reinforced concrete (RC) structures and steel-concrete composite structures under severe environmental conditions (e.g. marine environments) has always been a major concern [34, 35]. It is estimated only in the U.S. over \$1 billion is spent annually for repair and replacement of waterfront piling systems [36]. This high cost has spurred great interest in alternative composite column and pile materials such as FRPs, recycled plastics, and hybrid materials. Consequently, FRP materials were considered as an attractive alternative for structures in marine and other harsh environments [37]. Considering the corrosion of steel tubes [28, 36], durability and potential bond issues in addition to the brittle failure of FRP materials (specifically in seismically active regions) [16, 38-40], polyvinyl chloride (PVC) tubes have also been used as an alternative to introduce the PVC confined tubular column system for bridge columns construction.

The research program presented in this study is focused on development, characterization and validation of integrated composite confinement system of conventional jackets for: (1) repair and retrofit of existing bridge columns; and (2) construction of new bridge columns. Composite confinement systems were developed by incorporating conventional confining jackets into one system to introduce more efficient and durable systems. The first part of this study focuses on a new composite steel confinement jacket for rehabilitation of existing bridge columns. The second part of this

study includes a new composite FRP/PVC concrete filled tubular column system for new bridge columns construction.

The following section first introduces the general background on damage due to earthquake excitations, followed by the related literature review in the areas of: (1) repair and retrofit of existing bridge columns using conventional confinement jackets; and (2) concrete filled tubular column systems for new bridge columns construction. At the end of this chapter, research objectives and scope of work are described and outlined in detail.

1.2. COMPOSITE STEEL CONFINEMENT FOR REPIAR/RETRPFIT OF EXISTING CONSTRUCTION

1.2.1. Background on Earthquake Damage and Rehabilitation Through Confinement. Past earthquakes have demonstrated catastrophic structural failure of earthquake-damaged structures subjected to cascading events, defined as events likely to be triggered by the main earthquake, such as aftershocks, explosions and tsunamis [41, 42]. Functionality of bridges in the post-earthquake event is vital to facilitate access for post-earthquake aftermath [43]. Bridges in seismically active areas are vulnerable to the risk of multiple mainshock-aftershock ground motions in quick succession. The March, 2011 Tohoku, Japan earthquake was succeeded by hundreds of aftershocks including at least thirty aftershocks greater than moment magnitude (M_w) of 6 [41]. Usually due to close occurrence of the mainshock-aftershock there would not be sufficient time for extensive time-taking bridge repair work. Mainshock-damaged structures are vulnerable to aftershocks even when only minor damage is present from the mainshock [41, 44, 45]. The May 12, 2008 Wenchuan earthquake with a M_w of 7.9 was followed by numerous aftershocks, where the August 5, 2008 aftershock (M_w larger than 6) [44] contributed to collapse of many of the structures sustaining damage from the mainshock event, and causing more loss of life (about 90,000 dead or missing) [44].

It has been well established that both the mechanical (strength, stiffness and ductility) and long term performance of concrete structures - normal strength [8, 21, 23, 26, 27, 37, 38, 46-50], high/ ultra-high strength [15-20, 28], self-consolidating/compacting [24, 51] and more recently recycled aggregate concrete [13, 25]- can be enhanced through the lateral confinement by a confining jacket (i.e., active or

passive confinement). Extensive studies on various forms of confining jackets from different materials (e.g., steel stirrups, steel spirals, hollow tubes/ prisms, prestressing strands; fiber reinforced polymer (FRP) composite stirrups, FRP tubes, FRP rings, pre/post-tensioned FRP shells, composite ropes; shape memory alloy (SMA) wraps; and hybrid confining jackets) have been implemented for strengthening and/or rehabilitation of existing structures; as well as for new construction [6, 7, 11, 52-62].

Advantageous use of external confinement at the potential plastic hinge regions has been extensively investigated for bridge and building columns [2, 53, 63]. Extensive studies have investigated the efficacy of different types of repair jackets with active or passive confining pressure [2]. For instance, study by He et al. [64] demonstrated advantages associated with fiber reinforced polymer (FRP) jackets for repair of damaged RC columns with or without fractured longitudinal reinforcement. Conventional thick steel and reinforced concrete jackets were the first and most widely utilized repair jackets. However, these jackets require labor intensive work and introduce additional seismic mass to the existing structure. Increasing the area of the original cross section would increase the stiffness and reduce the natural vibration period of the jacketed structure. Increased cross section increases the absorbed seismic action leading to higher shear demand on the rehabilitated column and higher moment demand on the foundation or the adjacent member [65]. Besides, under equal plastic rotation, the thin jacket is advantageous to create a more distributed plastic hinge length compared to a thick jacket; therefore the chance of reinforcement bar fracture would be less than a retrofitted column with a thicker jacket [66]. The negligible added weight from the FRP wrapping compared to the conventional steel and RC jacketing techniques is a promising feature. On the other side, FRP materials require application of adhesive epoxy, adequate impregnation of fibers prior to installation and curing time for the saturated fibers. Prestressing strands providing active confining pressure are another form of confinement for retrofit of existing RC columns. However, further tests proved that retrofitted columns with strands under cyclic loading experienced strength deterioration due to the high losses of the prestressing force of the confining strands. Spalling of cover concrete and penetration of the prestressed strands into the concrete caused the loss of confining pressure and the columns experienced strength decay [66].

Unlike extensive studies on the seismic retrofit of bridge columns, limited studies were implemented on rapid seismic repair of severely damaged bridge columns [8]. In this study, the term “retrofit” refers to upgrading of undamaged existing column, while “repair” refers to rehabilitation of a damaged column. According to the 2009 American Society of Civil Engineers Report Card for America’s Infrastructure, more than 26% of the nation’s bridges are either structurally deficient or functionally obsolete, and a \$17 billion annual investment is needed to substantially improve the current bridge conditions [67]. While the number of civil infrastructure systems increases worldwide rapidly, the number of deteriorated bridges, buildings and other structures also increase. Complete replacement of structure is likely to be an increasing financial burden, if rehabilitation and strengthening is a viable alternative [68]. Moreover, following an earthquake important structures are required to be rapidly strengthened for dispatching first aid to the earthquake struck region. Therefore, rapid repair of RC bridge columns is not only important for post-earthquake stability of the bridge, but also a matter of public safety to transport the emergency crew to the earthquake impacted area.

1.2.2. Steel Jacketing for RC Column Confinement. Rehabilitation of RC columns with steel jackets usually involves installation of steel halves around the column followed by field seam-welding of parts along the length of the jacket. Then the gap between the jacket and column is usually filled with cement based non-shrink grout [64, 69-71].

Chai et al. [5] studied the seismic retrofit of six RC columns with 610-mm in diameter, using steel jackets with on—site welds in the plastic hinge region. The test matrix included different longitudinal reinforcement configurations (i.e., lap-spliced or continuous longitudinal reinforcement). The tested columns were tested under constant axial load (1780 kN) and incrementally increasing reversed lateral cyclic loading until failure. Results from this study indicated that the lap-spliced columns are likely to fail due premature lap-splice failure (i.e., bond failure of lapped bars) of column’s longitudinal reinforcement, which result in rapid strength degradation of the tested columns at relatively low drift angles. Columns with continuous longitudinal reinforcement experienced less rapid strength deterioration, and the degradation was primarily due to lack of confinement in the plastic hinge region. Test results on the

retrofitted columns indicated the satisfactory performance of the rehabilitated columns in terms of strength, stiffness and hysteretic energy. Tests indicated that high tensile stresses were developed on the steel jacket, in addition to high vertical stresses due to local bending. Tests indicated a relative slip between the jacket and the grout infill along the jacket length. Moreover, an increased stiffness of the steel jacketed column by 10~15% was obtained. Columns with continuous longitudinal reinforcement experienced an improvement in displacement ductility of 3.5% to 6%. Such level of displacement ductility is a satisfactory level of performance by most recent seismic codes of practice (e.g. Caltrans [72]). Comprehensive analytical studies on seismic characteristics of steel-jacketed circular bridge columns by Chai [73] on the steel confinement effect on ultimate compressive strain of concrete and inhibition of concrete spalling, indicated significant improvement in concrete ultimate strain (4~9 times) the spalling strain of concrete. The confining steel also increases the curvature ductility and tensile strain in the extreme reinforcement fiber.

Study by Mitchell et al. [74] described the damages on bridges during the 1994 Northridge earthquake. Most of design deficiencies of the pre-1970 bridge construction included: sparsely spaced transverse reinforcement, inadequate reinforcement, lack of longitudinal restrainers across expansion joints, splice of longitudinal reinforcement at column-footing interface, and insufficient seat widths at joints and supports. The first step in retrofitting bridges included providing adequate restraints at expansion joints, followed by jacketing the bridge columns with confining jackets, mostly with steel jackets.

Aboutaha et al. [75] conducted an experimental study on eleven rectangular RC column with inadequate splices of different column widths and concrete confinement, under cyclic lateral loads without any axial load. The experimental test results indicated the efficacy of the retrofitting with rectangular steel jackets attaining stable hysteresis behavior beyond 4% drift ratio. Moreover, it was observed that for columns with larger diameter the adhesive anchor bolts are required to effectively maintain the integrity and continuity between the rectangular steel jacket and RC column.

1.2.3. RC Jackets for RC Column Confinement. RC jackets involve constructing a new RC jacket around the existing RC column, in which it usually involves enlarging the original column cross-section. Hence, that increases the seismic

inertia forces accordingly. In some cases, the reinforcement of the jacket is connected to the encased existing column through dowel anchor bars [66].

Bett et al. [76] conducted repair and retrofit of three 2/3-scale square RC columns with RC jackets. The three column specimens were constructed to 2/3-scale, using identical geometry and reinforcement. The test specimens had a 305-mm square cross section reinforced with eight 19-mm longitudinal bars, with 6-mm ties spaced at 200 mm, and a 25-mm cover. Spacing of the transverse reinforcement was intended to represent typical practice of column design in seismic regions of United States in the 1950s and early 1960s. One of the column specimens was tested and sustained severe damage. Then the column was repaired with RC jacket and re-tested under the same loading protocol. The remaining two column specimens were retrofitted by jacketing prior to testing. Columns were tested under a constant axial load and a single lateral displacement history up to failure. Test results indicated that the repaired column and the two retrofitted columns outperformed the original column. It was also observed that the repaired column with jacketing was much stiffer and stronger than the original column and performed almost as well as the retrofitted columns (i.e., RC jacket applied on intact, undamaged column prior to testing).

Rodriguez and Park [77] studied the performance of four columns using RC jackets to evaluate the jacketing effect on strength, stiffness and ductility of retrofitted columns. The tests included both damaged and undamaged RC columns using a 100-mm thick RC jacket. The columns had a 350-mm square cross-section and a 3.3-m height, including a stub at mid-height representing column segments between mid-heights of successive stories of an RC frame. A constant axial load of 20% of column nominal axial capacity (product of the gross column cross sectional area and the specified concrete compressive strength) was applied with a lateral cyclic loading regimen consisting of 2 cycles at each displacement ductility level until failure. The studied columns were typical of pre-1970 construction practice exhibiting inadequate flexural strength and transverse reinforcement. Two of the columns were tested in the as-built condition demonstrating poor hysteresis performance, as expected. The two damaged columns, in addition to the other two undamaged column specimens were retrofitted with RC jackets. Testing of the retrofitted column specimens indicated the very satisfactory performance of the column

specimens in terms of strength and stiffness-up to three times that of the original columns. Enhanced behavior in terms of energy dissipation was also observed for the jacketed columns. Moreover, the exiting damage sustained by columns during the first test proved not to have a dramatic impact on the seismic performance of the repaired columns. Test results indicated the satisfactory performance of the jacketed columns with RC overlays. However, as noted by the authors, the technique was very labor intensive.

1.2.4. FRP Jackets for RC Column Confinement. In recent decades, fiber reinforced polymers (FRP) have received great attention in retrofitting and repairing of RC members. In FRP composites fibers are the load bearing component which are bound with the aid of an adhesive material such as epoxy. Considering the strengthening scheme, fibers could then be oriented accordingly in the desired direction. For RC column confinement fibers are usually oriented in the hoop direction (perpendicular to the column longitudinal axis), while longitudinal fibers would function similar to column longitudinal reinforcement, increasing the column flexural strength.

Priestley and Seible [78] utilized glass FRP (GFRP) and epoxy injection to repair a 2/5-scale substandard circular RC bridge column with continuous longitudinal reinforcement. The as-built column was first tested to failure under a constant axial load (18% of the column nominal axial capacity) and reversed cyclic loading. The repair procedure included removing the loose, damaged concrete and epoxy injecting the existing cracks, followed by a full height GFRP jacket application. Test results indicated that the initial stiffness of the repaired column was fully restored, and higher displacement ductility was attained than that of the as-built column.

Saadatmanesh et al. [79] studied the seismic performance of five RC column with pre-1970 construction practice using FRP wraps. The studied columns had a 305-mm diameter and heights of 1800 mm. Columns with continuous and lap-spliced longitudinal reinforcement were considered in this study. The two types of active and passive confining pressure were applied by using the FRP composite straps. With active confinement, the confining pressure is applied to concrete columns prior to the progression of concrete damage. With passive confinement, concrete is subjected to damage (lateral dilation) before confinement is in effect through the buildup of hoop stress. Pressurized grout infill was used to achieve a 758 kPa level of active confining

pressure. Column specimens were tested under constant axial load (17.7% of column nominal axial capacity) and incrementally increasing reversed cyclic loading until failure. Six layers of FRP straps were applied in the plastic hinge region of the retrofitted columns, up to 635 mm above the column-footing interface. The retrofitting technique proved that significant improvement in terms of strength and ductility were obtained, in which a displacement ductility of 6 was achieved. Columns with continuous longitudinal reinforcement demonstrated significant improvement in terms of drift capacity (3.7% increased up to 5.5%).

Seible et al. [80] developed and validated a new seismic retrofit system for RC columns. The FRP jacket consisted of continuous carbon FRP (CFRP) prepreg tows wound in an automated fashion onto existing circular or rectangular RC columns, with variable jacket thickness along the column height based on experimentally validated design models. The FRP jacket design was implemented considering flexural plastic hinge confinement, shear strengthening, and/or lap-splice clamping, if required. Five large scale RC bridge columns were tested. The first pair of rectangular columns was tested in double flexure, with a height of 2.4 m and a 610 mm by 406 mm cross section. The applied load consisted of a constant axial load of 507 kN (6% of column nominal axial capacity) and lateral loading of incrementally increasing reversed cyclic loading with 3 cycles at each displacement ductility. The as-built column and the retrofitted column in shear demonstrated a displacement ductility of 3 and 12, respectively. While the as-built column exhibited a brittle shear failure with rapid strength loss at its peak strength, shear failure was avoided in the retrofitted specimen and a satisfactory behavior was obtained. The second pair of columns were tested for flexural retrofitting, in which the rectangular columns had a height of 3.658 m and a cross section of 730 mm by 489 mm. A constant axial load of 1780 kN (14.5% column nominal axial capacity) and incrementally increasing reversed cyclic loading up to failure were applied to the as-built and retrofitted column. While a displacement ductility of 3 was obtained for the as-built column, the retrofitted column exhibited a displacement ductility of 7. Finally, the CFRP jacket was implemented for lap-splice confinement of flexural dominant RC columns. The specimen height was 3.658 m with an outside diameter of 610 mm. The axial load was 1780 kN and incrementally increasing reversed cyclic loading up to failure was

applied. The retrofitted column was tested and bond failure of the lap-spliced reinforcement at a displacement ductility of five was observed. Post-test inspection revealed that the retrofitting applied was 20% less than the required design thickness, which does not meet the design requirements for lap splice clamping. A second test was performed where the required CFRP thickness was applied. The newly retrofitted column could reach a displacement ductility of 8, prior to starter bar rupture.

Saadatmanesh et al. [81] studied retrofitting five rectangular RC bridge columns using FRP straps. The columns were retrofitted up to 635-mm above the footing in the potential plastic hinge region (assumed twice the effective depth of column cross section). The 1800 mm long columns had dimensions of 240×368 mm. The transverse reinforcement of the original columns consisted of 3.8-mm diameter steel wire with 89-mm spacing along the column's height. Columns with continuous and lap-spliced reinforcement were examined. In the test matrix two columns constitute lap-spliced reinforcement, while the other three had continuous reinforcement. The reference column with lapped reinforcement exhibited significant strength degradation upon reaching displacement ductility of 3, whereas the retrofitted column with rectangular jacket demonstrated satisfactory performance up to displacement ductility of six, with little strength degradation. For columns with continuous reinforcement, the reference column failed in shear at displacement ductility of three. However, the other two retrofitted columns with rectangular and oval shaped jackets proved to be adequate for the column to reach a displacement ductility of six with no deterioration. Both the rectangular and oval jackets proved to be effective and no significant difference was observed between the two configurations.

Xiao and Ma [82] studied application of prefabricated composite jackets to retrofit and repair RC columns with lap-splice deficiency. The test program consisted of three RC columns with a diameter of 610 mm and a height of 2440 mm (1:2 scale column models). The column reinforcement consisted of 6.4 mm diameter hoops at 127 mm intervals and twenty 19.1 mm diameter longitudinal rebars (correspond to 2% steel ratio of the gross area of column section) lap-spliced at column footing interface, with the lap-splice length of 381 mm (lap splice length of 20×bar diameter). The columns were tested under reversed cyclic loading up to failure. The axial load was kept constant (712 kN)

and the incrementally increasing lateral displacement was applied at the column tip. The as-built column exhibited a rapid post-peak degrading behavior due to bond-slip of lapped bars at the column base. The other two columns were retrofitted with 4-ply and 5-ply of FRP and could reach to a displacement ductility of six. Besides, the as-built column was also repaired with 4-ply of FRP wraps and re-tested under the same loading protocol. The repaired column specimen demonstrated significantly improved behavior compared to the as-built specimen. However, significant pinching in the hysteresis response of the repaired column was observed. Moreover, Xiao and Ma developed an analytical bond model to predict the lateral force-displacement behavior of lap-spliced columns with and without lateral confinement, which resulted in satisfactory predictions when compared with experimental test results.

Sheikh and Yau [83] studied the seismic behavior of RC columns confined with steel and fiber reinforced polymers. Twelve 356 mm diameter and 1473 mm long columns were tested under constant axial load and reserved cyclic loading. Three groups of specimens were tested. Group one consisted of four columns that were conventionally reinforced with longitudinal and spiral steel reinforcement. The second group consisted of six RC columns that were strengthened with carbon fiber reinforced polymer (CFRP) or glass fiber reinforced polymer (GFRP) wraps. The last group contained two columns with different damage levels. The damage extent present in the first damaged column was flexural cracks, cover concrete spalling, and longitudinal reinforcement yielding. The second damaged column was tested until yielding of both longitudinal and transverse reinforcement was observed. The first damaged column was repaired with CFRP, while the second column was repaired with GFRP wraps. For both damaged columns the loose cracked concrete was removed and was then patched prior to FRP wrapping. The two repaired columns were re-tested and the obtained results indicated that the performance of the repaired specimens were comparable to the undamaged specimens that were strengthened. Overall, it was concluded that the use of FRP for retrofit or repair significantly enhances strength, ductility and energy absorption capacity of columns.

Cheng et al. [84] developed a rapid repair method for damaged RC bridge piers in the aftermath of an earthquake. In this study four hollow bridge piers were tested under pseudo-static loading up to failure, including fractured longitudinal bars. Dog-bone

shaped reinforcement bars were used for repair of the damaged specimens to replace the damaged longitudinal rebars segments in the plastic hinge region, and then confined with externally bonded CFRP wraps to increase the repaired specimens' lateral displacement capacity. Repaired columns were re-tested under similar loading protocol to that of the original as-built columns. Test results indicated that the fractured longitudinal bars can be repaired and the columns' deformation capacities were improved through CFRP wraps. However, the repaired columns exhibited lesser strength than anticipated due to concrete deterioration and buckling of longitudinal reinforcement in the inner layer of the hollow sections.

Li and Sung [85] studied the seismic repair of a shear-failure damaged circular bridge column under constant axial load and cyclic loading. The as-built column was a 2/5-scale RC circular bridge column which was shear deficient, and failed due to shear failure during testing. The repair procedure consisted of using non-shrinkage mortar with high-pressure epoxy injection, followed by applying 3-ply of CFRP wraps to enhance the shear strength. The repaired column was re-tested and significant improvement in terms of strength and ductility were obtained. Contrary to the as-built column with shear failure, the failure mode for the repaired column was altered to a ductile flexural failure mode. An analytical study was also implemented to predict the lateral force-displacement relationship of the experimental test results, and reasonably accurate results were obtained.

Belarbi et al. [86] repaired a 1/2 scale circular RC bridge pier under constant axial load and combined loading condition. The original column was tested to severe damage state under flexure, shear and torsion. The physical condition of the damaged column included spalled cover concrete, crushed core concrete and buckled longitudinal reinforcement. The damaged column was rehabilitated using CFRP sheets with fibers both in longitudinal and transverse direction. The longitudinal layers were applied first to compensate for the reduction in flexural strength due to yielding of longitudinal reinforcement in the original column, followed by CFRP wraps in the transverse direction to provide the required confinement in the plastic hinge region of the damaged column. A mechanical anchorage system was used to anchor the longitudinal CFRP sheets to the footing. Repaired column was re-tested and it was concluded that the repair method could

restore and even enhance the flexural and torsional capacity. However, the longitudinal CFRP sheets pulled out from the footing base at low load levels, and it was concluded that the longitudinal CFRP sheets may not have been required in this repair procedure.

Vosooghi et al. [87] reported the seismic repair of a large-scale two-span bridge model, damaged to the highest repairable level including visible reinforcement bars, initial buckling in some longitudinal bars, and initial concrete core damage in the previous tests. The damaged bridge was repaired using unidirectional CFRP jacketing and retested to evaluate the repair performance. In this repair, the loose concrete was replaced by fast setting grout, and the existing cracks were epoxy injected. The columns were then wrapped with CFRP sheets and were cured only for 54 hours prior to testing. Test results of the repaired column indicated that the lateral load capacity and the ductility capacity of the bridge bent were fully restored and the lateral service stiffness was nearly restored to that of the undamaged bent stiffness (87% of the undamaged bent stiffness).

Vosooghi and Saiidi [88] reported the seismic repair of two high-shear standard RC bridge columns using unidirectional CFRP wraps. Both RC columns were 1/3-scale standard circular RC bridge columns with continuous longitudinal reinforcement and spiral transverse reinforcement tested to near failure on a shake table test. The damage state for the columns included cracked and spalled cover concrete, visible spirals and longitudinal bars, buckled longitudinal bars, and damaged core concrete. For the two columns the cracked/crushed concrete was replaced by a fast-set non-shrink mortar, and epoxy injection was used to seal the existing cracks. According the repair design performance objective, different number of CFRP layers were used to repair the damaged columns. Retesting of the repaired columns indicated the lateral load and drift capacity of the columns were fully restored to that of the undamaged specimens. However, the service stiffness was partially restored due to existing damage from the initial test. It was also concluded that yielded spirals still contribute to the shear capacity of the repaired columns.

Elsouri and Harajali [89] studied the repair of RC columns including lap-splices using internal steel ties and/or CFRP wraps for plastic hinge confinement. Three full-scale rectangular RC columns with different longitudinal reinforcement ratios were tested

in this study. The columns were tested under lateral cyclic loading without axial load. The as-built columns exhibited a lap-splice failure due to slip of lapped bars in the plastic hinge and extensive concrete damage in the splice region. The repaired columns using CFRP wraps over the lapped reinforcement region resulted in obtainment of considerably larger lateral loads and energy dissipation capacities than the as-built columns. Analytical study also confirmed the efficacy of the CFRP wrap since assuming perfect bond between lap-spliced bars led to similar predictions of the experimental results.

Sun et al. [90] conducted an experimental study on rapid repair of severely earthquake-damaged bridge piers with flexural-shear failure mode. Six circular pier specimens were first tested to severe damaged state, and were then repaired using early strength concrete with high-fluidity and CFRP wraps. Four days later the repaired columns were re-tested. The obtained results indicate that the repair procedure was highly effective and the failure mode of as-built specimens was altered to ductile flexural failure. It was also concluded that the design provisions for bridge columns retrofit (i.e., no existing damage) are applicable for seismic repair of damaged bridge columns if shear strength contribution of the spirals in the repaired piers is disregarded and 1.5 times more FRP sheets than the retrofit scenario are provided.

Vosooghi and Saiidi [10] conducted seismic repair of one low-shear and one high-shear substandard RC bridge columns using CFRP jackets. The 1/4-scale original columns had insufficient transverse reinforcement and lap-spliced reinforcement at the column-footing interface. The columns were tested under constant axial load on shake table excitation. The apparent damage of the low-shear key column included extensive concrete cracks and spalling. Damage to the high-shear column included minimal spalling and shear cracks. The low-shear column was repaired using two plies of CFRP within the plastic hinge region and no CFRP outside the plastic hinge region. The high-shear column was repaired by applying two plies of CFRP along the entire height of the column. The repaired columns were tested under the same loading protocol to the original columns. Results indicated satisfactory performance of the repair method, in which the strength and ductility capacity were fully restored or enhanced. However, the service stiffness was lower than that of the original columns.

He et al. [59] conducted a comprehensive study on rapid repair of five 1/2-scale square standard RC bridge columns with different damage states. The damaged columns were repaired using externally bonded CFRP laminates oriented in longitudinal and transverse directions according to repair design. The original columns were tested to failure under constant axial load and combined cyclic lateral and torsional loading conditions. The apparent damage of the columns included cover concrete cracking/spalling, core concrete crushing, and longitudinal reinforcement yielding, buckling and fracture of some of the bars. Damaged columns were repaired using CFRP sheets and an anchorage system for longitudinal CFRP fibers, were buckled or fractured longitudinal rebars were left untreated. Testing of the repaired columns, under the same loading protocol, revealed restoration of the lateral strength and ductility of the repaired columns. However, initial stiffness of the columns was not fully restored to that of the original columns, due to accumulated damage from the first tests.

While different studies implemented anchorage system for FRP fabrics at column-footing interface, Rutledge et al. [91] investigated the seismic repair of two severely damaged RC columns containing buckled longitudinal bars by plastic hinge relocation. The two circular scaled RC columns were tested under constant axial load and a specific load history corresponding to that of two specific earthquakes applied as displacement to the top of the columns in static fashion. To repair the first column longitudinal CFRP anchors were used circumscribed by CFRP wraps in the hoop direction to confine the old plastic hinge. Additionally, CFRP wraps in the hoop direction were also provided over the expected new plastic hinge region to obtain higher curvature at the new plastic hinge location. Testing of the first repaired column under the same loading protocol indicated an increase in lateral strength capacity compared to that of the original column. However, due to additional confinement provided over the expected plastic hinge region, the plastic hinge did not form in the desired location. The second column was repaired similar to column one, except that no CFRP wraps were applied for confinement over the expected new plastic hinge region. Testing of the second repaired column indicated the satisfactory performance of the repair method in restoring and even increasing the strength with respect to the original column. The new plastic hinge was successfully relocated above the CFRP confined region, and the initial stiffness of the column was restored.

Yang et al. [92] reported an experimental study on the seismic repair of two ½-scale prototype bridge columns repaired using two types of mechanical couplers and CFRP jackets. This study was a new method on implementing two different types of mechanical couplers (“sleeve with lock shear bolt” and “swaged sleeve” couplers) in the plastic hinge region of repaired columns. Two ½-scale oval-shaped RC bridge columns with interlocking spirals had been tested to failure as part of another study under constant axial loading and reversed cyclic lateral loading resulting in combined flexure, shear, and torsion. The apparent damage to the columns included concrete crushing, yielding, buckling and fracture of longitudinal reinforcement, and yielding of transverse reinforcement in the plastic hinge region. Concrete cracking and spalling outside the plastic hinge region was also observed after the initial test of as-built columns. The repair procedure involved: (1) shoring the column; (2) demolishing and removing the concrete and spirals inside the plastic hinge; (3) severing and removing the damaged longitudinal bars; (4) straightening the column; (5) splicing new longitudinal bar segments to the existing bars with mechanical couplers; (6) casting new concrete; (7) preparing the concrete surface for CFRP wrap; and (8) installing the externally bonded CFRP wrap. The repair scheme for both columns were similar that involved removal of the longitudinal reinforcement bar segments within the plastic hinge and replacement with new bar segments of the same size spliced to existing longitudinal bars with mechanical couplers. For repair in order to remove and replace the longitudinal bars, the interlocking spirals were removed within the plastic hinge region. In order to compensate for the removed transverse interlocking spirals, CFRP wraps were used in the plastic hinge and non-plastic hinge regions of the repaired columns. For the first column, sleeve with lock shear bolt couplers were used to splice the new longitudinal reinforcement segments to the existing reinforcement. While for the second column the swaged sleeve couplers were used. Testing of repaired columns indicated that the repair method was successful in restoring the lateral and torsional strength to both columns. The lateral and torsional deformation capacity was restored to one column, while the other was not quantified due to early termination of testing. Test results also indicate that the lateral strength and deformation capacities of the columns could be restored with use of bar couplers in the plastic hinge region. However, the repair method resulted in reduced lateral and torsional

stiffness for the repaired columns. Moreover, repaired columns exhibited smaller energy dissipation per cycle as well as cumulative energy dissipation compared to the corresponding original columns.

Most recently, Yang et al. [93] conducted an experimental study on emergency repair of an RC bridge column with fractured bars using externally bonded prefabricated thin CFRP laminates and CFRP strips. The experimental study included a ½-scale RC bridge column specimen tested to failure under constant axial load and cyclic lateral loading. The original column had an oval-shaped cross section of 610 mm × 915 mm and an effective height of 3.35 m measured from the top of the footing to the centerline of applied load. The original column had a longitudinal and transverse reinforcement ratio of 2.13% and 1.32%, respectively. The apparent damage included buckled and fractured longitudinal bars. The repair procedure included repair of the column in the plastic hinge region and the footing. In summary, the repair technique involved the following steps: (1) cutting a 100 mm wide and 300 mm deep trench around the base of the column in the footing; (2) removing loose concrete from the column; (3) placing formwork and then a high-fluidity grout to restore the column cross section; (4) installing CFRP strips on the column surface; (5) wrapping a 1.2 m × 18.3 m epoxy-coated prefabricated laminate around the column to create a 7-ply jacket; (6) lowering the jacket into the trench until it touched the base of the trench; (7) filling the trench with an epoxy aggregate; (8) injecting a low-viscosity resin between the jacket and the column; and (9) installing CFRP fabric on the footing surface. The CFRP embedment length was designed as 305 mm. Since several reinforcing bars in the footing needed to be cut to facilitate the embedment of the CFRP strips and jacket, CFRP fabric was externally bonded to the top surface of footing to compensate for the loss of strength. 10 layers of 305 mm wide CFRP straps were designed on four sides of the column. Then, the repaired column was subjected to the same constant axial loading and cyclic lateral loading protocol (resulting in combined flexure, shear, and torsional moment loading) as applied to the original column. The obtained results indicate that the repair method was successful in restoring the lateral strength and deformation capacity of the repaired column.

1.2.5. Prestressing Bars/Strands/FRP Belts for RC Column Confinement. The superiority of active confinement over passive confinement, especially for lap-spliced RC columns, encouraged application of active confining pressure to retrofit and/or repair RC columns. Different studies implemented prestressed steel bars, steel cables, and steel strands to apply the active confining pressure in RC columns. On the other hand, some research studies aimed at applying the active confining pressure through FRP belts or FRP straps.

Coffman et al. [94] developed a simple, yet effective method to apply the confining pressure to retrofit lap-spliced RC columns using semicircular threaded reinforcing bars tightened by threaded swage couplers. Test program consisted of four lap-spliced RC columns (one reference column and three retrofitted columns). The studied specimens were intended to model the arrangement of bridge columns constructed in the 1950 to mid-1970 era. The columns were tested under constant axial load and incrementally increasing lateral cyclic loading condition. The reference un-retrofitted column failed due to slip between starter and column bars. The three retrofitted columns were rehabilitated only over the length of the column where the longitudinal bars were spliced with the dowel bars. The retrofit hoops used were grade 60 reinforcing steel formed into semicircular segments that were connected by swaged opposing threaded couplings. By tightening the stud connecting the hoop halves with a wrench, pre-stress was introduced into the hoops. The level of prestress in the hoops was approximately 350 MPa. Testing of actively confined retrofitted columns indicated that integrity of the column could be maintained and larger number of cycles could be sustained prior to lap failure. Then, this method was proposed to retrofit RC columns (excluding shear deficient columns) subjected to medium intensity shaking and long duration (correspond to large number of cycles).

Lin et al. [95] successfully implemented active confinement by prestressing 15 mm steel strands. However, further tests proved that the retrofitted columns under cyclic loading experienced strength deterioration due to the high losses of the prestressing force of the confining strands. Spalling of cover concrete and penetration of the prestressed strands into the concrete caused the loss of confining pressure and the columns experienced strength decay [66].

Flexural retrofitting of two RC circular columns using active confinement provided by prestressed wire wrap onto the column in the potential plastic hinge region was investigated at the University of California in May 1990 [96]. The two columns were wrapped with prestressing wires of 4.9 mm diameter at spacing of 30 mm and 6.6 mm, or corresponding to lateral confining pressure of 2.43 MPa and 11.2 MPa, respectively. The wires were stressed to 1207 MPa (corresponding to 70% of ultimate tensile strength capacity of wires). Testing of retrofitted columns indicated the excellent response with stable hysteresis loops of the retrofitted column reaching to drift angles of 4~5%. The columns failed due to low cycle fatigue of longitudinal reinforcement similar to failures of steel jacketed circular columns.

Researchers at University of Ottawa [3, 7, 97-100] performed extensive experimental studies on seismic rehabilitation of shear and lap-splice deficient columns by applying active confining pressure. Large number of RC columns with square and circular cross section including shear and lap-spliced deficiency were retrofitted and/or repaired using external prestressed strands and were tested under constant axial load and reserved cyclic loading. This technique involves external prestressing of concrete columns using prestressing strands, or high-strength steel straps. Saatcioglu and Yalcin [7, 97] investigated the prestressing strand technique on seven RC columns, of which five had circular cross section (610 mm diameter) and two had square cross section (550 × 550 mm). The columns had reinforcement detailing typical of pre-1970 RC bridge columns, including twelve No. 25 (25.4 mm diameter) longitudinal bars uniformly spaced, and No. 10 (9.5 mm diameter) hoops at 300 mm spacing, with the first hoop reinforcement placed at 75 mm above the base. All the columns were tested under reserved cyclic loading up to failure. For circular columns, first column was the non-retrofitted reference specimen. The second column was retrofitted using steel straps, and the remaining three specimens were retrofitted using 7-wire prestressing strands. The prestressing strands used were size 9 of grade 1860 MPa. Dywidag twisted ring anchors were used to join the ends of individual hoops. Different spacing and initial prestress levels were used as test parameters. Configuration 1 involved strands at 300 mm prestressed up to 25% of tensile capacity of strands. Configuration 2 included wires at 150 mm spacing prestressed with 25% of tensile capacity of strands, where configuration

3 included wires at 150 mm spacing with prestressed with 5% of tensile capacity of strands. Test results from non-retrofitted column resulted in a brittle shear failure as expected. The retrofitted column with the high strength steel straps could withstand up to 2% drift capacity only, and at 3% drift some of the straps ruptured and column failure shortly after that observed, hence the repair scheme was disregarded. All retrofitted columns with prestressed strands indicated improvement compared to the reference specimen. However, retrofitted column with configuration 2 resulted in the best performance, since the external confinement provided corresponded to the largest confinement pressure compared to the other two retrofit configurations. The studied method proved to be an effective retrofit intervention and a very economical retrofit solution. Square columns were retrofitted using the same technique. However, disk raisers were placed between strands and column sides to raise the prestress wire at three locations on every face, so as to improve the confinement effect provided by strands on prismatic cross sections. Obtained results from square columns accord to circular columns were non-retrofitted column demonstrated a brittle failure, while retrofitted column with strands placed at 150 mm spacing with an initial prestress of 25% of tensile capacity of strands demonstrated improved hysteresis behavior up to 5% drift ratio.

In summary, results from large number of tests [3, 7, 97-100] clearly indicated the superior performance of columns retrofitted with prestressed cables with active confining pressure (approximately 0.36 MPa) versus specimens retrofitted with identical cable arrangement with no prestressing confining pressure (approximately 0.06 MPa), creating essentially a “snug-tight” situation. However, test results indicated columns strength decay due to cover concrete spalling, penetration of the prestressing strands into the column, loss of confining prestress, and buckling of longitudinal reinforcement between wires spacing. Experimental tests by Beausejour [98] investigated the seismic retrofit of lap spliced columns with external prestressing using seven wire strands. Experimental tests revealed that retrofitted (i.e. undamaged) circular columns with lap spliced reinforcement ($20d_b$, where d_b : reinforcement bar diameter) experienced vertical cracks over the lap splice region due to significant elongation demand on the column longitudinal reinforcement.

Tests indicated despite the active confining pressure in the plastic hinge region, vertical cracks extended further up to the column and strands penetrated into cover concrete causing bond strength deterioration between lapped bars.

Miyagi et al. [101] developed an emergency repair method to rehabilitate shear-deficient rectangular RC columns using high-strength prestressed steel bars along with L-shaped corner blocks. The corner blocks were essentially used at four sides of the prism to anchor the steel bars at edges. Prior to installing the prestressed steel bars, four steel plates were affixed on each side of the column specimen, and then the steel bars were placed around the specimen. Four 250×250 mm square concrete prisms with a height of 500 mm under axial load and lateral cyclic loading were investigated in this study. The longitudinal and transverse reinforcement ratios for the specimens were 1.36% and 0.08%, respectively. To investigate the importance of active confinement through prestressing bars (5.4 mm diameter), three of the specimens were repaired with prestressed bars (reportedly prestressed to 490 MPa), while the last specimen was repaired with no prestressing present in the bars (essentially a snug-tight condition for the high-strength bars). In order to verify the effectiveness of the repair method at different damage levels, three damage levels were considered in the cyclic loading regimen. The three damage levels were classified according to the maximum crack widths observed after the cyclic testing, namely, level 1 corresponded to crack width not greater than 5 mm, level 2 corresponded to crack width between 5 to 10 mm, and damage level 3 corresponded to crack width greater than 10 mm. The first three as-built column specimens were tested to damage levels of 1, 2, and 3, respectively, while the last specimen was tested to damage level of 1 under constant axial load and reserved cyclic loading. Then, the first three damaged specimens were repaired using the high-strength prestressed steel bars. The last specimen was repaired using the high-strength bars with no prestressing pressure present in them. The obtained results indicated the efficacy of the proposed emergency repair method utilizing high-strength prestressed steel bars to restore the lateral capacity and axial capacity of damaged columns immediately after earthquake. It was also observed that prestressing force as an outstanding characteristic of this technique is an advantageous feature that incorporates the additional active confinement as well as passive confinement and shear strengthening. The proposed

method also proved to be a very quick and viable option with dry construction (i.e., no epoxy or adhesive requirement unlike FRP jackets) that required no heavy equipment.

Nesheli and Meguro [102] developed a retrofit method using external pressing with fibrous composite belts. In this study five shear-deficient square columns in the as-built condition and rehabilitated condition were tested under constant axial load and incrementally increasing lateral displacement excursions. The square columns were 250 mm and height of 625 mm, with a shear span to depth ratio of 2.5. The columns were reinforced with twelve No. 12 longitudinal reinforcement bars distributed evenly around the perimeter of the square cross section. Transverse reinforcement consisted of 4 mm steel hoops spaced at 100 mm. The first as-built column was tested as the bench mark and as expected demonstrated brittle shear failure. The remaining four specimens were retrofitted using FRP belts. The four specimens were divided into two groups were for group 1 carbon FRP was used, wherein for group 2 aramid FRP was used. Each group consisted of two retrofitted columns, one with non-prestressed belts and another with prestressed belts (active confinement). The prestressing level for CFRP belts was about 1/6 of the tensile strength of CFRP, while the AFRP belts were prestressed about 1/3 of the tensile strength of AFRP fibers. Prestressing was applied manually using a wrench. The FRP fibers were used with epoxy adhesives. The FRP belts were 30 mm wide, spaced every 75 mm in the 375 mm bottom region (potential plastic hinge zone) of the RC columns. Obtained results from retrofitted columns with non-prestressed and prestressed FRP belts demonstrated the high efficacy of the proposed system in altering the brittle shear failure to a ductile flexural failure. It was observed that despite the different initial confining pressures, yet the same lateral stiffness of the confining device, the deformation ductility of all retrofitted columns was similar. However, external prestressing proved effective in avoiding widening of the cracks, which would limit the level of concrete damage at large drift angles. Therefore, it was concluded that external prestressing is a beneficial technique compared to non-prestressed wraps for repair of earthquake damaged RC columns, where the cracks are already present.

Nesheli and Meguro [103] used a similar technique for rapid repair of earthquake-damaged RC column using lateral pre-tensioning (i.e., prestressing) of FRP belts on prismatic RC cross sections. In this study, similar to their previous study [102],

prestressed CFRP and AFRP belts were utilized to repair shear-failure damaged RC columns under pseudo static loading regimen. Repair process was straight forward and neither the damaged concrete was replaced by new concrete nor any repair intervention such as epoxy injection to cracks were undertaken. The obtained results proved the efficacy of the pre-tensioned FRP belts in restoring the lateral load capacity of damaged RC columns.

Kyoda et al. [104] developed an emergency repair method similar to Miyagi et al. [101] for prismatic damaged RC columns using fiber belts prestressing and plywoods. This study used a lashing belt device to apply the active confining pressure. The lashing belt was a combination of commercially available ratchet buckle and polypropylene fiber belt. In this study 250×250 mm shear-deficient prismatic RC columns were first damaged under pseudo static testing and were then repaired using lashing belts spaced at an interval of 65 mm through corner angles. Plywood or steel plates were attached first on the surfaces of the column and then the lashing prestressing belts were applied. Lightweight angles were placed at four corners between the column and lashing belt to prevent rubbing of belts at the corner zones. Then, repaired columns were re-tested and the proposed method proved to be an effective and rapid method for emergency repair of RC columns.

Most recently, Zhou et al. [105] conducted a comprehensive study on 25 circular RC columns rehabilitated with prestressed FRP strips. In this study carbon FRP and the newly introduced basalt FRP (BFRP) were used as prestressed external transverse reinforcement. RC columns with different damage levels were also investigated in this study, and were then repaired with prestressed FRP strips. The obtained test results of repaired RC columns under slow cyclic loading demonstrated the efficacy of prestressed FRP strips with active confining pressure. It was also concluded that as the damage extent present in columns prior to repair procedure increases, the efficacy of prestressed FRP strips is reduced. Moreover, test results indicated that surface grinding and epoxy bonding on the column surface results in the most appropriate strengthening response when prestressed FRP strips are used. BFRP strips, with considerably lower elastic modulus compared to CFRP strips proved to be ineffective and fractured easily.

Despite extensive research on the suitability of applying active confining pressure through FRP belts/strips to provide the required level of confinement, field application of prestressed FRP wraps resulted in unsatisfactory results. This is due to the natural tendency of composite materials to creep under sustained loading which can lead to rupture of the FRP wrap [66]. In the 1990s, California Department of Transportation (Caltrans) implemented composite overwraps to selected highway bridge support columns for seismic strengthening. The overwraps had epoxy-impregnated fiberglass (E-glass) tows in the circumferential direction and widely spaced Kevlar and glass tows in the vertical direction. The prestressed overwraps of each of two columns near Los Angeles ruptured almost 3 years after installation and 8~12 months after the January 1994 Northridge earthquake. Premature rupture of FRP wraps due to creep rupture caused failure of the wraps [106].

1.2.6. Shape Memory Alloy (SMA) for RC Columns Confinement. Shin and Andrawes [107, 108] investigated application of shape memory alloy (SMA) wraps in the plastic hinge region of RC columns to retrofit and/or repair columns using active confining pressure provided by thermally triggered recovery stress of pre-strained SMA spirals. The experimental study involved retrofitting four 1/3-scale RC columns retrofitted with SMA spirals and GFRP wraps under quasi-static lateral cyclic loading condition. Seismic repair of two damaged RC columns using SMA spirals were also investigated. The scaled RC columns were 254 mm in diameter with an effective height of 1270 mm. The columns were subjected to an axial load of 116 kN, corresponding to 5% of the column's gross section times compressive strength. Each column was reinforced with eight No. 4 (12.7 mm diameter) longitudinal reinforcement bars (2% volumetric ratio) and No. 2 hoops spaced every 102 mm to avoid shear failure. Three configurations were used to retrofit the columns. The first column served as the reference un-retrofitted specimen. The second specimen was retrofitted with GFRP wraps (10 layers GFRP in the plastic hinge). The third specimen was retrofitted using SMA spirals only (SMA spiral with 10 mm pitch in the plastic hinge). The fourth retrofitted specimen was confined by combining GFRP wraps and SMA spirals (hybrid jacket using 5 layers GFRP + SMA spiral with 20 mm pitch in the plastic hinge). All the retrofitted columns were also wrapped outside the plastic hinge region with 5 layers of GFRP from 508 mm

to 1016 mm above the footing, while the top remainder of the retrofitted columns was wrapped with 2 layers of GFRP. The SMA spirals were made of 2438 mm-long segments of 2 mm-diameter NiTiNb wires. To form a complete spiral around the column, the wires were spliced using U-clamps, which was tested and found to be capable of sustaining the ultimate strength of the wires. The pre-strained spirals were wrapped around the column with the desired pitch. While all the three retrofitted columns resulted in improvement and stable hysteresis loops compared to the as-built specimen, however, the obtained results from retrofitted columns using SMA and SMA+GFRP wraps indicated the superior performance of actively confined columns using SMA spirals. The GFRP retrofitted column dissipated 25% more hysteresis energy compared to the as-built column. The SMA and the SMA/GFRP columns were superior, since they dissipated 371% and 285% more hysteretic energy, respectively compared to the as-built column. Additionally, two 1/3-scale specimens were repaired using SMA spirals. The apparent damage from original tests included crushed concrete, fractured longitudinal bars, and excessive opening of transverse reinforcement. The repair method involved replacing the damaged concrete with quick-setting mortar, injecting epoxy into cracks, connecting the fractured longitudinal bars using rebar couplers, and wrapping the SMA spirals at the repaired region. Test results from repaired columns indicated that the lateral strength was fully restored, and the stiffness of the repaired column was also higher. However, a lower displacement capacity was obtained compared to the as-built columns. Overall, the obtained results indicated that actively confined RC columns using SMA spirals could effectively confine RC columns and could be used for retrofit and repair of RC bridge columns.

1.3. COMPOSITE FRP/PVC CONFINEMENT FOR NEW CONSTRUCTION

A significant demand exists for stronger and more durable structural members for applications in harsh environments like marine piles and highway columns. In such media, aggressive chemicals quickly deteriorate traditional RC and steel members. Concrete filled fiber reinforced polymer (FRP) tubes are a promising technology for such applications. FRP materials exhibit excellent strength-to-weight ratio, which are becoming increasingly attractive for structural repair and retrofit projects, as well as new

construction. Polyvinyl chloride (PVC) materials, exhibiting remarkable mechanical properties compared to other general purpose olefin plastics, demonstrate impressive ratio of cost to performance, specifically remarkable durability [109-111]. Investigation of soil buried PVC pipes dug up after 60 years of active use, indicated no deterioration and likely to have a further life expectancy of 50 years! [112]. PVC is one of the most important commercial plastics owing to its wide applications, low cost and its excellent properties, such as: (1) high electrical insulation; (2) high resistance for abrasion; (3) low diffusion for humidity; (4) remarkable resistance to water, bases, acids, alcohols, oils; (5) large elongation at break (i.e., ductile); (6) low creep deformation; (7) workability including (e.g. machining, cutting, welding/gluing for fabrication versatility); (8) consistency; and (9) excellent corrosion resistant, durability and mechanical stability (little change in mechanical strength and molecular structure) [113-115].

1.3.1. FRP-Confined Concrete Filled PVC Tube System. Past studies have demonstrated the enhanced structural performance of concrete filled tube (CFT) systems, using steel or FRP tubes [11-22]. Enhanced hysteresis behavior and improved fire resistance of concrete filled steel tubes (CFST) has been addressed in many studies [11, 12, 14, 16]. The main advantage of the CFST system is the full section confinement provided by the steel tube, where in return the concrete core prevents or delays buckling of the steel tube. This composite action results in enhanced stiffness, strength, ductility and overall stability of the CFST system. However, due to high modulus of elasticity of steel, large portion of the axial load is sustained by steel tube, which may cause premature buckling of the confining tube. Moreover, since the Poisson's ratio of steel relative to concrete is higher, the initial separation of steel tube and core concrete may delay engagement of the confinement mechanism. On the contrary, the modulus of elasticity for PVC tube is significantly smaller compared to steel (approximately 1/50 of steel modulus), that signifies substantially lesser axial load sustained by the PVC tube, thus eliminating the premature buckling of the PVC tube. Few research studies investigated other types of confining tubes, such as commercially available thermoplastic pipes, like high-density polyethylene (HDPE) and polyvinyl chloride (PVC) pipes [35, 109-111, 116-118] for improved durability of RC structures.

Study by Kurt [109] was the first attempt on implementing commercially available rigid plastic (acrylonitrile butadiene styrene (ABS) and PVC) pipe filled with concrete as a new composite column system, for structural applications.

Toutanji and Saafi [110, 116] then introduced a new hybrid column system for new construction consisting of concrete filled PVC tubes reinforced with external discrete FRP hoops at different spacings. In such hybrid system, PVC serves as the cast-in-place formwork, while the FRP-PVC tube provides additional confinement to the core concrete. Moreover, a few research studies on concrete filled PVC tubes were undertaken [35, 111, 118-120], however, experimental studies on CFT column system consisting of PVC tubes is very limited and confined to uniaxial compression tests [118].

Study by Gupta and Verma [119] on reinforced concrete filled PVC tubes subjected to harsh environmental condition indicated that “no degradation in the strength and ductility of reinforced concrete-filled poly-vinyl chloride tubular specimens was observed after submergence in sea water”. Test results on reinforced concrete filled PVC tubes submerged in saturated sea water (concentration 20 times higher than natural sea water) for 6 months revealed that the microstructure and chemical composition of the PVC jacket remained nearly identical after exposure to sea water (i.e., chemical action of sodium chloride and magnesium sulfate) [119]. It was then concluded that PVC tubes provide a safety jacket to encased concrete core that results in improved strength and ductility.

Most recently, Jian et al. [121] studied the performance of slender concrete-filled CFRP-PVC tubular (CFCT) columns of various slenderness ratios under uniaxial compression. However, only four CFCT specimens with discrete CFRP strips were tested. Moreover, there is a wealth of contradictory published data describing PVC, “a kind of elastic material” [121] or a ductile plastic material [35, 111, 118]. For instance, in studies by Refs [35, 111, 118, 119] ductile failure of PVC tube was observed up to complete collapse of the plastic tube. On the other hand, study by Ref [120] on concrete filled PVC tubes, demonstrated bursting (fracture) of the plastic tube toward the end the loading process.

The improved durability of PVC material allows potential applications of this system for wide variety of structural systems exposed to harsh environmental conditions

(marine and saline environments). Highway overhead sign structures, poles, and bridges are required to maintain their integrity in freezing weather conditions, where salt is frequently used for de-icing the roads. Similarly, marine piles and offshore platform structures are alternately submerged and exposed in harsh environment [122]. The exceptionally enhanced property of PVC materials in terms of durability and resiliency under harsh environmental conditions makes the PVC material as a promising and economically viable option for civil engineering applications.

Aging of the polymer, could affect the behavior of the FRP pipes/tubes and PVC pipes differently [35, 111]. Study by Li et al. [123] indicated that environmental conditioning - in a tank with boiled water and UV light for seven days only – resulted in 57-76% loss of strengthening efficacy, and 43-48% stiffness degradation of FRP after conditioning. On the contrary, study by Jakubowicz et al. [124] on accelerated and natural aging of PVC materials, indicated that aging in air at 80°C and 90°C for up to eight weeks caused no significant changes in mechanical properties and elongation at fracture of PVC material. Moreover, results of an ongoing research study [125] on long term (10-year results) performance of PVC demonstrated that all material properties except for thickness satisfy both the material specification at the time of installation, as well as with the current PVC specification [35, 125]. In summary, the harsh environment in northern Minnesota appeared to have had negligible effect on the engineering properties measured [125].

Offering exceptional durable long term properties over FRP materials against temperature cycle, wetting-drying cycle and UV light exposure, Wang and Yang [35] proposed the thermoplastic pipe confined concrete, using PVC pipes, as an appropriate system for new-built bridge piers.

PVC has outstanding anti-corrosion characteristics, and PVC coatings have been used as protective layer for on-shore and off-shore pipelines [126]. FRP jackets could be applied as an additional confining layer to the perimeter of PVC tubes, to compensate for the relatively weak confining properties of PVC pipes, introducing the composite confined concrete filled PVC tube (CCFPT) system, with exceptional durability and mechanical strength.

There are only two studies on confined concrete filled PVC tubes (CCFPT) conducted by Toutanji and Saafi [110, 116] and Jian et al. [121]. In both studies discrete FRP strips (i.e., partial wrapping) were utilized outside the PVC tube to provide additional confinement. Past studies (e.g. [127]) have demonstrated that in partial FRP wrapping where part of the concrete is unconfined, low ultimate confining pressure is present, which results in low strength enhancement. Moreover, the interaction and relation between FRP wrap, PVC tube and concrete core have not been systematically evaluated for this composite construction system [121]. An extensive review of the literature has revealed that the present study is the first to investigate the PVC tubes application through a carefully planned experimental program, which consists of companion concrete filled PVC tube (CFPT), confined concrete filled PVC tube (CCFPT), and FRP-wrapped (FW) specimens with identical geometrical and material properties. Past studies have indicated that FRP-wrapped specimens perform similar to CFPT (i.e., FRP tube-encased) specimens (e.g. [28, 128]). This new composite member owns both enhanced strength capacity of FRP materials, in addition to the superior corrosion resistance of PVC, which allows a feasible proposal for the application of this composite system in pile foundation and special environment (acid-based and sea water) [121]. Such new composite FRP-concrete-PVC column consists of an exterior FRP-PVC shell and a core concrete, which is lightweight, cost-effective, and environmentally resistant (superior corrosion resistance).

1.4. RESEARCH OBJECTIVES AND SCOPE OF WORK

The objective of this study is to develop, characterize, and validate an integrated composite confinement system of conventional jackets: (1) for repair and retrofit of existing bridge columns; and (2) construction of new bridge columns, subjected to earthquake excitations. Composite confinement systems were investigated to further improve the efficacy and durability of conventional confinement jackets.

Composite steel confinement system for repair and/or retrofit of existing bridge columns consists of a lightweight, hybrid prestressed jacket including thin sheet metal jacket circumscribed by discrete prestressed strands. The proposed composite confinement system introduces the enhanced properties of active confinement, in addition

to the higher energy dissipation capacity of the steel material into one confinement jacket. In order to characterize and evaluate the performance of the proposed confinement jacket under seismic loads, both experimental and analytical studies have been conducted in this research. The experimental study included two ½-scale RC column specimens with lap-spliced reinforcement at column-footing interface subjected to simulated earthquake loads tested to failure. To achieve the first objective of this study, the scope of the work included the following key steps: (1) evaluate the damage conditions of columns before repair; (2) propose design methodology for seismic repair of the damaged columns according to the required performance level/acceptance criteria to achieve after repair intervention; (3) implement the proposed composite steel jacket on damaged columns along with the instrumentation, and re-test the repaired columns under identical loading protocol applied to the original columns; (4) evaluate the repair intervention performance by comparing the obtained data from repaired columns against the response of the original columns; (5) develop nonlinear fiber element models of original and repaired columns and calibrate against experimental test results at member and system level; (6) conduct seismic assessment of post-repair response of two RC bridges repaired with hybrid jacket subjected to earthquake excitations of different intensities; (7) compare the post-repair seismic performance of the hybrid jacketed RC bridges with more conventional repair interventions, namely conventional thick steel and FRP jackets, subjected to aftershock attacks; and (8) conduct seismic collapse analysis on different repair interventions applied on earthquake damaged structures under aftershock attacks.

Composite FRP/PVC confinement system for new construction of bridge columns consists of a new hybrid concrete filled tubular column system. The composite FRP-concrete-PVC column consists of an exterior FRP-PVC shell and a core concrete, which is lightweight, cost-effective, and environmentally resistant (superior corrosion resistance). This composite system is essentially a FRP-confined concrete-filled PVC tube which consists of a FRP sheet wrapped around a PVC pipe with presence or absence of an energy dissipation medium in between. The following scope of work was implemented in an effort to attain this objective: (1) extensive review of applicable literature on existing concrete filled tube systems; (2) develop a research plan; (3) design, construct, and test stub column specimens, including concrete filled PVC tube (CFPT),

confined concrete filled PVC tube (CCFPT) and FRP-wrapped (FW) specimens, under monotonic axial compression; (4) design, construct, and test flexural beam specimens, including CFPT, CCFPT and FW specimens, under transverse four point load configuration; (5) compare the axial compressive behavior of CFPT (i.e., PVC confined) and CCFPT (i.e., FRP +PVC confined) specimens against companion FW (i.e., FRP confined) specimens; (6) compare the transverse flexural behavior of CFPT and CCFPT specimens against companion FW specimens; (7) investigate the interaction between FRP wrap, PVC tube, and encased concrete by introducing cushioning foam layer (energy dissipating medium) between FRP wrap and PVC tube; (8) conduct model performance assessment for FW and CCFPT specimens using seven of the most accurate existing stress-strain models; (9) derive closed-form relations for the ultimate stress and strain conditions for the proposed CCFPT system.

1.5. DISSERTATION OUTLINE

This thesis includes three sections. Section 1 gives an introduction to the subject area. The first section also explains the objective and scope of the work in this study, as well as a detailed literature review on different existing repair and retrofit methods for RC columns, and existing concrete filled tube systems, to establish the state-of-the-art on the proposed composite confinement systems.

Section 2 presents three published/accepted journal papers and two journal papers under review or in process. The first paper presents the composite steel jacket (also referred to as hybrid jacket or prestressed steel jacket) concept and experimental study on rapid repair of a severely damaged RC column subjected to simulated seismic loads using the proposed jacket. The second paper develops the design methodology for the composite steel jacket for different performance limit states, and the experimental results of repaired RC columns using the proposed jacket are presented. Moreover, comparative cost analysis of composite steel jacket versus conventional thick steel and FRP jackets are presented. The third paper presents the seismic assessment of post-mainshock FRP/steel repaired RC bridges subjected to aftershocks of multiple intensities, including near-fault and far-field earthquakes, utilizing calibrated fiber finite element models. The fourth paper focuses on experimental test results from axial compression of composite

FRP/PVC concrete filled tube system, and model performance assessment using existing stress-strain models are presented, and relations to establish the ultimate stress and strain condition of the proposed composite system are proposed. The fifth paper presents the experimental test results from uniaxial compression and flexural tests on composite FRP/PVC tubes and the effects of the inclusion of the energy dissipating foam layer between FRP wrap and PVC tube are investigated.

Section 3 summarizes the findings and conclusions of this study and proposes future research.

PAPER

I. HYBRID JACKETING FOR RAPID REPAIR OF SEISMICALLY DAMAGED REINFORCED CONCRETE COLUMNS

ABSTRACT

In this study, hybrid jacketing is proposed for rapid repair of seismically damaged concrete columns for bridge safety. The hybrid jacketing for a reinforced concrete (RC) column is composed of a thin cold-formed steel sheet wrapped around the column and its outside prestressing strands. While the prestressing strands can prevent buckling of the confining steel sheet, the steel sheet can in turn prevent the prestressing strands from cutting into concrete. The hybrid jacketing concept was validated with testing of a large-scale RC column with lap splice deficiency typical of pre-1970 bridge constructions in the Central U.S. Results from the original and repaired columns were compared in terms of hysteresis loops, strength, stiffness, ductility and energy dissipation. The hybrid jacketing proved to be effective in restoring structural behavior of the damaged column to prevent bridge collapse. Such a cost-effective solution can be implemented at bridge sites in hours. Design equations to establish the lateral force-displacement relationship of the tested column to design the hybrid jacket are derived in detail.

Keywords: Bridge, RC Column, Rapid Repair, Hybrid Confinement, Experimental Study

INTRODUCTION

Bridges are critical links in a surface transportation network. During an earthquake event, they are required to withstand strong ground motions so that emergency personnel and vehicles can be dispatched into the struck area for post-earthquake evacuation and response. Lessons learned from the past earthquakes testified the importance of bridge safety in the overall resilience of the highway transportation network. For example, the 1994 Northridge Earthquake caused the collapse of seven highway bridges in Los Angeles, California, and severely damaged many other bridges, resulting in significant disruption on the regional highway transportation network (1).

Bridges in seismically active areas are vulnerable to a series of mainshock-aftershock ground motions. The 2011 Tohoku Earthquake with a moment magnitude (M_w) of 9 was succeeded by hundreds of aftershocks including at least thirty aftershocks greater than M_w 6 (2). Due to the frequent occurrence of aftershocks, damaged bridges must be repaired in a short time with innovative techniques.

A large number of 12,000 bridges in the inventory of the State of California were constructed prior to the 1971 San Fernando Earthquake with common seismic deficiencies such as insufficient transverse reinforcement and lap splice reinforcement at column bases (3). To improve their safety, RC bridge columns have been retrofitted with various jacketing techniques/materials (4-11). However, very few studies addressed the rapid repair of severely damaged RC columns (12-14). The past studies for column retrofitting and repair have demonstrated the inadequacy of columns with a lap splice length of $20d_b$ (d_b is the reinforcement diameter) and the advantages of external jacketing to prevent potential lap splice failures (4, 10).

EXISTING SEISMIC RETROFIT/REPAIR TECHNIQUES

RC columns can be confined both *actively* and *passively*. With active confinement, the confining pressure is applied to concrete columns prior to the progression of concrete damage (3, 4, 10). With passive confinement, concrete is subjected to damage (lateral dilation) before confinement is in effect through the buildup of hoop stress (4). Figure 1(a) and 1(b) illustrate the schematics of cross sections of

passively and actively confined RC columns, respectively. In general, active confinement can improve the strength and ductility of concrete more significantly than passive confinement (4, 5). In particular, active confinement is preferred for inadequate lap spliced columns since concrete dilation is not required to activate the jacketing pressure, as concrete lateral dilation lead to bond deterioration between lapped bars (10). Priestley et al. (4) presented different seismic rehabilitation techniques of RC bridge columns using steel, concrete, fiber reinforced polymer (FRP) and prestressing strands. Different jackets based on the confining pressure provided are categorized and presented in Figure 1(c). Past studies proved the efficacy of different confining repair jackets (4-14). However, in addition to the high material cost and concerns about the long-term performance (prone to moisture), FRP materials were shown to suddenly rupture due to their linear elastic properties (4, 12). While thick steel jackets were available and economical with ductile behavior, material handling and high field installation costs were their major drawbacks (3, 4). Lin et al. (5) successfully implemented a seismic retrofitting system with active confinement using prestressing strands. However, tests indicated that the columns retrofitted with prestressing strands experience strength deterioration under cyclic loading due to high losses of the prestressing force in confining strands. The concrete cover spall during cyclic reversals and the penetration of prestressed strands into the concrete caused the loss of confining force.

The above-mentioned studies were focused on conventional thick steel or thin composite jacketing for the seismic retrofitting and repair of RC columns. This study aimed at developing a novel, hybrid passive-active jacketing technology with an inside lightweight steel sheet and outside prestressing strands to incorporate the active confining pressure along with the economical, ductile steel jacket, without requiring heavy equipment for field applications. The hybrid jacket requires no epoxy curing time, less expensive than FRP wraps and significantly lighter than conventional steel or concrete jackets with less labor intensive installations. The rapid repair technique is validated by designing and fabricating a large-scale RC bridge column, testing the column with substantial damage, repairing it with the proposed hybrid jacketing, and comparing the performances of the original and repaired columns. The hybrid jacket incorporates the additional advantages of both active and passive confinement into one repair jacket.

EXPERIMENTAL PROGRAM

Original Column Design

One 1/2-scale circular RC column was constructed and tested to failure in the Highway Structures Laboratory at Missouri S&T. The column represents typical pre-1970s bridge piers with column longitudinal reinforcement lap spliced at column-footing joints. The lap splice length was equal to $20d_b$ or 20 in. (508 mm) for No. 8 deformed rebar. As shown in Figure 2, the total height of the column was 167 in. (4242 mm) with an effective height of 132 in. (3353 mm) measured from the top of the footing to the centerline of the applied force. The column of 24 in. (610 mm) in diameter was reinforced with twelve No. 8 ($d_b=25$ mm) deformed bars with a longitudinal reinforcement ratio of 2.08%, and transversely confined with No. 4 ($d_b=12$ mm) spiral deformed bars at 4 in. (102 mm) spacing with a transverse reinforcement ratio of 0.9%. The measured yield strength of the longitudinal and transverse reinforcement bars was 60.6 ksi (418 MPa) and 78.5 ksi (541 MPa), respectively. The concrete compressive strength was 6,340 psi (44 MPa).

Original Column Test to Failure

The original column was tested to failure under an incrementally increasing lateral cyclic load while subjected to a constant axial load of approximately 133 kips (592 kN). The applied axial load simulated the imposed superstructure load and corresponded to approximately 7% of the nominal axial capacity. Three symmetric cycles were applied at each loading stage. Load-displacement hysteresis loops showed significant stiffness degradation and strength loss (75% of peak strength) at the completion of testing. As illustrated in Figure 3, the column failed due to lap splice reinforcement slippage. The damaged state of the column would be classified as extensive or DS-5 for imminent failure-visible reinforcement bars and compressive failure of the concrete core edge (13-14).

Repair Design of the Damaged Column

The repair materials and method were selected to meet the rapid repair requirement. To this end, repair grout, thin sheet metal, and prestressing strands were the only constituent components needed in the developed rapid repair technique.

Materials

A shrinkage-compensating fast setting repair grout, with one-day strength of 4,500 psi (31 MPa) was used to replace the degraded concrete from the damaged column. The average compressive strength of the repair grout at the test date of the repaired column was determined to be 4,560 psi (32 MPa). The hybrid jacketing was comprised of thin cold-formed sheet metal (passive confinement) enclosed by prestressing strands (active confinement). The steel jacketing had the yield strength of 98.5 ksi (680 MPa), tensile strength of 112 ksi (771 MPa) and elastic modulus of 30,050 ksi (207 GPa). According to the repair design, the sheet metal was 48 in. (1,220 mm) wide and 0.05 in. (1.27 mm) thick. The nominal ½ in. (12 mm) diameter, seven-wire strands had the ultimate tensile strength and modulus of elasticity of 281 ksi (1,937 MPa) and 29,100 ksi (200 GPa), respectively.

Repair Procedure

The damaged column was repaired in its bottom 48 in. (1,220 mm) with the proposed hybrid jacketing. To prevent premature compression damage in the jacketing, a 1 in. (25 mm) gap was left between the steel jacketing and the footing. The entire repair process was completed in four steps as illustrated in Figure 4:

1. Removing the cracked degraded concrete,
2. Placing repair grout to restore the column's original cross section,
3. Wrapping and welding the sheet metal around the column, and
4. Placing and prestressing strands around the steel jacket.

Several special considerations were taken into account in the proposed repair technique. First, existing cracks on the damaged column were not filled by epoxy injection to simulate an emergency repair scenario. Second, while the steel jacket could be directly wrapped on the damaged column and filled with the repair grout, the cross-section of the original column was restored prior to wrapping of the sheet metal with the

intent of studying the applicability of this method for bridge retrofit. Third, no surface preparation (such as primer to fill the voids) and adhesive materials (such as epoxy resin to bond the thin sheet metal onto the column) were needed; the proposed method thus requires no curing. Fourth, the force in prestressing strands would remove any gap between the sheet metal and the column. Fifth and lastly, the proposed repair scheme is similar to FRP jacketing without alteration of the original cross section (no increase in deadweight). Repair grout was allowed to cure for 12 hours, and then the lightweight sheet metal and prestressing strands were applied on the damaged column within four hours.

For real applications of the hybrid jacket on RC bridge columns, considering the long term performance, corrosion resistance and aesthetic requirements of the rehabilitated column, a protective layer should be provided to thin steel sheet. For corrosion protection, anti-corrosive paintings/coatings could be applied. For aesthetic requirements, a minimum of 1-inch concrete cover (preferably of high-performance concrete) applied either by shotcreting or by casing concrete over the jacket could be implemented.

Repair Design and Performance Objectives

The column repair was aimed at restoring shear strength and displacement ductility to prevent a lap splice failure of the repaired column. The height of plastic hinge to be repaired, L_{pz} , was calculated according to California Department of Transportation (Caltrans) Seismic Provisions (15). That is,

$$L_{pz} = \frac{3}{8} AR \times D \geq 1.5D \quad (1)$$

where AR = column aspect ratio, and

D = column diameter.

The shear strength of the column was based on those of individual components and checked against the factored shear (13). That is,

$$\frac{V^o}{\phi} < V_c + V_s + V_j \quad (2)$$

where V^o = base shear,

$\phi = 0.85$, and

V_c , V_s and V_j = shear resisted by concrete, existing transverse reinforcement, and jacket, respectively.

Since the existing steel hoop reinforcement in the plastic hinge region yielded during the original column test and no epoxy injection was applied to repair the concrete cracks, the existing transverse reinforcement and concrete contribution to the shear strength were neglected. The enhanced shear strength due to axial load was also neglected considering the effect of vertical ground motion during an earthquake event (16). The hybrid jacketing has two shear resisting components (4) for the repaired column: thin sheet metal and prestressing strands. The passive stress contribution of strands was considered in the calculation of shear capacity V_j .

$$V_j = V_{sj} + V_{sp} \quad (3)$$

$$V_{sj} = 0.5\pi t_j f_{yj} D \cot \theta \quad (4)$$

$$V_{sp} = 0.5\pi A_{ps} f_{ps} D s^{-1} \cot \theta \quad (5)$$

where V_{sj} and V_{sp} = shear enhancement from thin sheet metal and prestressing strands, respectively, and

θ = angle of the critical inclined shear-flexure crack to the column axis.

The required confining stress (f_l) to prevent the lap-splice failure (4) can then be determined by:

$$f_l = \frac{A_b f_s}{\mu p l_s} \quad (6-a)$$

$$p = \frac{\pi D'}{2n} + 2(d_b + c) \leq 2\sqrt{2}(d_b + c) \quad (6-b)$$

where A_b = cross sectional area of nonprestressed reinforcement bar,

f_s = 1.7 times reinforcement yield stress (= $1.7f_y$),

μ = coefficient of friction (assumed as 1.4),

l_s = lap splice length,

p = crack surface perimeter,

n = number of longitudinal lapped bars,

d_b = reinforcement bar diameter,

D' = core diameter (outside to outside dimension of the circular transverse

reinforcement), and

c = concrete cover thickness.

The maximum transverse strain for the lap splice confinement was limited to 0.001 to prevent splice failure, which is provided by the hybrid jacketing only. The contribution of yielded spirals in repaired columns is negligible (13, 14). For the tested column, the required confining pressure would be $f_l = 511$ psi (3.52 MPa).

The hybrid jacketing was designed to provide sufficient flexural confinement on the damaged column so that the target displacement ductility of 5.0 can be met after repair. The design parameters of the sheet metal (t_j = jacket thickness and f_{yj} = jacket yield strength) and prestressing strands (f_{ps} = level of prestressing stress, s = strand spacing, and A_{ps} = cross sectional area of prestressing strands) were then determined accordingly. In this study, the unified energy balanced approach by Mander et al. (17) for confined concrete was adopted to calculate the ultimate achievable strains in the confining jacket. The confined concrete ultimate compressive strains for the sheet metal and the prestressing strands (4) can be determined by:

$$\varepsilon_{cu_sj} = 0.004 + \frac{5.6 t f_{yj} \varepsilon_{sm}}{D f'_{cc}} \quad (7-a)$$

$$\varepsilon_{cu_sp} = 0.004 + \frac{\rho_s f_{pu} \varepsilon_{su}}{f'_{cc}} \quad (7-b)$$

where ε_{cu_sj} and ε_{cu_sp} = ultimate confined concrete strain due to sheet metal and prestressing strands, respectively,

t = steel jacket thickness,

f_{yj} = steel jacket yield strength,

ε_{sm} = strain at peak stress of confining reinforcement,

D = column diameter,

f'_{cc} = confined concrete compressive strength,

ρ_s = effective volumetric ratio of confining prestressing strands = $4A_{ps}/(D \times s)$,

f_{pu} = ultimate stress level of prestressing strands,

ε_{su} = fracture strain of prestressing strands,

A_{ps} = cross sectional area of the prestressing strands, and

s = spacing between the prestressing strands.

For the sheet metal and prestressing strands, the effect of lateral confining stress (f_l) on the confined concrete compressive strength (f'_{cc}) can be evaluated by:

$$f'_{cc} = f'_c \left[-1.254 + 2.254 \sqrt{1 + \frac{7.94 f_l}{f'_c} - \frac{2f_l}{f'_c}} \right] \quad (8-a)$$

$$f'_{cc} = f'_c \left[-1.254 + 2.254 \sqrt{1 + \frac{15.88 A_{ps} f_{pu}}{s D f'_c} - \frac{4 A_{ps} f_{pu}}{s D f'_c}} \right] \quad (8-b)$$

where f'_c = specified compressive strength of concrete,

$f_l = (2 \times t \times f_s) / D$, and

f_s = circumferential induced stress in the sheet metal.

Considering the repair performance objectives, shear design, lap-splice design, and flexural design with required displacement ductility, the final design of the repaired column is presented in Figure 5. The repair design includes a 0.05 in. (1.27 mm) thick, 48 in. (1,220 mm) wide sheet metal and 10 prestressing strands in the plastic hinge region. Specifically, 6 strands at 4 in. (102 mm) spacing were applied over the lap splice region and the remaining 4 strands at 6 in. (152 mm) outside the spliced end. Each strand was prestressed up to 14 kips (62 kN) and anchored with a twisted ring anchor from Dywidag-Systems International.

Instrumentation and Test to Failure of the Repaired Column

Linear variable differential transformers (LVDTs) and string potentiometers were used to measure displacement profile, average rotation, and curvature of the column specimen. In addition, the repaired column was instrumented with a total of 110 strain gages attached on the hybrid jacket (72 strain gages) and the inside reinforcement (38 strain gages) as illustrated in Figure 6. Six prestressing strands (No. 1-4, 6, and 8 from the footing) were instrumented with four transverse strain gages per strand at quarter points. The sheet metal was also instrumented with four transverse strain gages and four longitudinal strain gauges at quarter points at each of six levels as detailed in Figure 6.

Strain gages on the inside reinforcement prior to repair were attached on dowel bars, longitudinal and transverse reinforcement bars.

The original and repaired column test setup as shown in Figure 6 was identical. A constant axial load of 133 kips (592 kN) was applied with seven prestressing steel strands through a PVC pipe at the column center. The strands were fixed at the bottom of the footing and at the top of the column loading stub. The axial load was applied using a hydraulic jack and was held constant throughout the test. Each column specimen was laterally loaded through two actuators in incrementally increasing displacement control with three symmetric cycles at each level. The shear force and bending moment of the column when the actuators pushed the column away (south direction) was defined positive.

RESULTS AND DISCUSSION

The load-drift hysteresis loops and the load-displacement envelopes of the two column specimens are compared in Figure 7(a) and Figure 7(b), respectively. It can be observed from Figure 7(a) that the original as-built column specimen exhibited unstable hysteresis loops with rapid strength deterioration and pinched behavior due to slippage of the lapped bars at column base. Although it reached the nominal flexural strength of cross section, the original column specimen exhibited rapidly degrading post-elastic behavior at large drifts, which is inadequate in seismically active regions.

In comparison with the original column, the repaired column resulted in 15% increase in lateral strength capacity with stable hysteresis behavior. Figure 7(a) indicated that the “in-cycle strength degradation” of the original column was enhanced to a “cyclic strength degradation response” of the repaired column. The in-cycle strength degradation can lead to structural collapse under dynamic loading. The repaired column experienced flexural cracks at the column-footing interface at approximately 1.5% lateral drift with the column confinement provided in the plastic hinge. At the same time, the stress in the column was effectively transferred into footing without lap splice failure, resulting in surface cracks on the footing cover concrete at the location of dowel bars. The lap-spliced reinforcement reached yielding, as verified by the strain measurements. Further loading enlarged the flexural cracks at the column-footing interface and, under cyclic effect,

initiated severe cracking and pinching of the repair grout between the lapped bars. Eventually, crushing of the repaired grout was the governing failure causing the pullout between the dowel and longitudinal bars with no further yielding of the reinforcement.

The sheet metal effectively confined the cover concrete of the repaired column and prevented the concrete cover spalling. It also prevented strand penetration into the cover concrete at large drift angles. Hoop strain measurements indicated that the prestressing strands effectively maintained the confining pressure throughout the column test even though the cover concrete severely cracked.

Repair Efficiency

Strength, stiffness and ductility capacity were used to assess the structural behavior of the original and repaired column specimens. They were evaluated based on idealized elasto-perfectly-plastic load-displacement envelopes as displayed in Figure 7(b) (12-14). For the original column, the measured load-displacement envelope was idealized by setting the initial slope to pass through the first longitudinal reinforcement yielding and altering the post-elastic region so that areas under the measured and idealized envelopes were equal. For the repaired column, the initial elastic portion of the idealized envelope was acquired by connecting the origin of the measured envelope to a point at which the applied load is equal to one-half of the maximum measured load. The yield level was determined by equating the areas underneath the measured and idealized capacity curves. The three non-dimensional response indices for strength, stiffness and ductility are defined as follows.

Strength Index (STRI)

The strength index is defined as the ratio between the lateral strength of the repaired column (V_r) and that of the original column (V_o):

$$\text{STRI} = V_r / V_o \quad (9)$$

Stiffness Index (STFI)

The stiffness index is defined as the ratio between the service stiffness of the repaired column (K_r) and that of the original column (K_o):

$$\text{STFI} = K_r / K_o \quad (10)$$

Ductility Index (DI)

The ductility index is defined as the ratio between the ductility capacity of the repaired column (D_r^*) and that of the original column (D_o):

$$DI = D_r^* / D_o \quad (11)$$

$$D_r^* = D_r \times (K_o / K_r) = D_r / STFI \quad (12)$$

The ductility capacity is defined as the ratio of the ultimate displacement capacity to effective yield displacement, which can be obtained from the idealized curve (D_r and D_o). The ultimate displacement capacity was defined as the displacement corresponding to 80% of the maximum lateral measured strength. To account for the different initial stiffness of the original and repaired columns, the repaired column ductility (D_r^*) was modified as shown in Equation 12.

The three response indices for the tested columns are presented in Table 1. It can be seen from Table 1 that the improved seismic behavior of the repaired column over the original column is significant in terms of enhanced strength and ductility. Specifically, the strength of the repaired column is 115% of that of the original column; the ductility of the repaired column is 168% of that of the original column. These results demonstrate the efficacy of the proposed repair method as required in modern seismic codes. However, service stiffness of the repaired column is 83% of that of the original column mainly due to degraded material properties from the original test. In order to simulate an emergency post-earthquake repair, epoxy injection of cracks in the damaged column was not implemented, thus the repaired column stiffness was not completely restored compared to the original column.

Based on Caltrans Seismic Provisions (SDC 3.1.4.1) (15) a minimum displacement ductility capacity of 3 is required for RC columns. The repaired column could reach a displacement ductility capacity of 4.2 versus 2.5 of the original column (Ductility index= 168%). The repair jacket could also restore and even improve the strength of the repaired column versus the original column, satisfying the Caltrans Seismic Design Criteria (15). The initial stiffness of the repaired column was 83% of the original column, which is in the acceptable range (20% of the original column) for rapidly repaired RC bridge piers (12-14).

In order to compare the hybrid jacket with columns rehabilitated only with active prestressing strands, a retrofitted column from the Beausejour study (10) was selected. The selected column had comparable flexural strength capacity compared to the tested column in this study with similar lap splice length ($20d_b$). The retrofitted column with prestressing strands exhibited a maximum strength of 47 kips compared to 44 kips of the reference (unretrofitted) column (6.8% strength enhancement). The retrofitted column exhibited rapid strength decay due to loss of confining pressure in strands upon penetration of strands into cracked cover concrete. The drift capacity of the retrofitted column was 3% compared to 2% of the reference column (10). Therefore, the prestressing confinement alone was less efficient than the proposed hybrid jacket. It should also be noted that the Beausejour study (10) applied prestressing strands into the retrofitting of an existing column (i.e. undamaged/intact column specimen), while this study applied the hybrid jacket on a severely damaged column specimen.

Failure Mode

In terms of crack formation, propagation, and distribution in the plastic hinge region, the original and the repaired columns were quite dissimilar. For the original column, the flexural and vertical splitting cracks with limited plastic hinge progression over the height almost equal to the column diameter were the primary observed damage. The cracks mainly resulted from the bond failure of dowel bars at column-footing connection. No sign of stress transfer from the dowel bars to the footing was observed.

For the repaired column, after the hybrid jacket was removed at the completion of test, the vertical splitting cracks were found to be limited to the bottom gap. This indicated that the hybrid confinement was significant that the vertical splitting cracks did not extend further up to the column. Cracks initiating from the location of dowel bars were observed on the footing surface as illustrated in Figure 8. This is mainly because the hybrid confinement enabled the stress transfer through the dowel bars at the column-footing interface. Although extensive damage through cyclic tests was accumulated at the 1-inch gap between the top of the footing and bottom of the jacket, the hybrid jacket could effectively prevent splice failure. The most prominent structural feature of the proposed hybrid jacket over other jackets is to resist the shear crack opening both in

vertical and horizontal directions (i.e. enhanced aggregate interlock and higher shear strength), while the prestressing strands (similarly any unidirectional jacket such as FRP wraps) can resist the shear crack opening in the transverse direction only.

CONCLUSIONS

In this study, a new hybrid jacketing technology was developed to rapidly and effectively repair earthquake damaged bridge columns. Experimental tests on RC column specimens validated the effectiveness of the proposed repair technique. The tested columns were large scale, allowing an investigation of applicability, constructability, and efficacy of the proposed repair method in field conditions. The hybrid jacket requires no heavy installation equipment, no curing time of adhesive material, and thus a viable option for post-earthquake emergency repair. Based on the test results, the following conclusions can be drawn:

- The hybrid confinement is effective in preventing lap splice failure and improving the flexural strength and ductility.
- The proposed hybrid jacketing is lightweight and proves to be applicable as an emergency repair technique for bridge piers.
- The initial stiffness is partially restored due to existing damage in concrete and reinforcement.
- The confining pressure exerted by prestressing strands is adequate for shear transfer between the steel jacketing and column; no adhesive epoxy or dowel reinforcement is required.
- Sheet metal provides the required bearing strength and prevented cover concrete spalling and penetration of the prestressing cables.
- Prestressing cables could sustain the active confining pressure up to 6% lateral drift with no significant prestressing force loss.
- The proposed repair method is straightforward and the repair design equations can be readily used in practical applications.

ACKNOWLEDGMENTS

Financial support for this study was provided by the Department of Civil, Architectural, and Environmental Engineering at Missouri University of Science and Technology, and by the U.S. National Science Foundation under Award No. CMMI-1030399. The conclusions and opinions expressed in this paper are those of the authors only. The authors also appreciate the constructive comments made by five anonymous reviewers.

REFERENCES

1. DeBlasio, A. J., Zamora, A., Mottley, F., Brodesky, R., Zirker, M. E., and Crowder, M. *Effects of Catastrophic Events on Transportation System Management and Operations, Northridge Earthquake—January 17, 1994*. US Department of Transportation, Washington, D.C., 2002.
2. *United States Geological Survey*. USGS, 2012. <http://www.usgs.gov>. Accessed May, 2014.
3. *Seismic Retrofitting Manual for Highway Structures: Part 1, Bridges*. FHWA-HRT-06-032. FHWA, U.S. Department of Transportation, 2006.
4. Priestley, M. J. N., F. Seible, and G. M. Calvi. *Seismic Design and Retrofit of Bridges*. John Wiley & Sons, Inc., New York, 1996.
5. Lin, Y., Gamble, W.L. and Hawkins, N.M. *Testing of Bridge Piers, Poplar Street Bridge Approaches, East St. Louis, IL*. Department of Civil Engineering, University of Illinois at Urbana-Champaign, 1994.
6. Saiidi, M. S., and Mangoba, N. Seismic Retrofit of Flared Reinforced Concrete Columns in Multispan Viaduct: From Research to Field Implementation. In *Transportation Research Record: Journal of the Transportation Research Board, No. 1892*, Transportation Research Board of the National Academics, Washington, D.C., 2004, pp. 189-196.
7. Walkenhauer, B. J., McLean, D. I., Boone, C., and Lamont, M. Seismic Retrofitting of Cruciform-Shaped Columns by Jacketing with Fiber-Reinforced Polymer. In *Transportation Research Record: Journal of the Transportation Research Board, No. 2251*, Transportation Research Board of the National Academics, Washington, D.C., 2011, pp. 135-143.
8. Fakharifar, M., Sharbatdar, M. K., Lin, Z., Dalvand, A., Sivandi-Pour, A., and Chen, G. Seismic Performance and Global Ductility of RC Frames Rehabilitated with Retrofitted Joints by CFRP Laminates. *Earthquake Engineering and Engineering Vibration*, Vol. 13, No. 1, 2014, pp. 59-73.

9. Fakharifar, M., Chen, G., Lin, Z., & Woolsey, Z. Behavior and Strength of Passively Confined Concrete Filled Tubes. *In the 10th U.S. National Conference on Earthquake Engineering*, Anchorage, Alaska, July 21-25, 2014.
10. Beausejour, P. *Seismic Retrofit of Concrete Columns with Splice Deficiencies by External Prestressing*. Master thesis. University of Ottawa, ON, Canada, 2000.
11. Fakharifar, M., Dalvand, A., Arezoumandi, M., Sharbatdar, M. K., Chen, G., and Kheyroddin, A. Mechanical properties of high performance fiber reinforced cementitious composites. *Construction and Building Materials*, Vol. 71, 2014, pp. 510-520.
12. Fakharifar, M., Chen, G., Sneed, L., and Dalvand, A. Seismic performance of post-mainshock FRP/steel repaired RC bridge columns subjected to aftershocks. *Composites Part B: Engineering*, Vol. 72, 2015, pp. 183-198.
13. Vosooghi, A., and Saiidi, M. S. Design guidelines for rapid repair of earthquake-damaged circular RC bridge columns using CFRP. *Journal of Bridge Engineering*, Vol. 18, No. 9, 2012, pp. 827-836.
14. Vosooghi A, and Saiidi M. *Post-earthquake evaluation and emergency repair of damaged RC bridge columns using CFRP materials*. Center for Civil Engineering Earthquake Research, Department of Civil and Environmental Engineering, University of Nevada, Reno, Nevada, Report No. CCEER-10-05, 2010, p. 636.
15. *Seismic design criteria (SDC), version 1.4*. California Department of Transportation, Sacramento, CA, 2006.
16. Higazy, E. M. M., Elnashai, A. S., and Agbabian, M. S. Behavior of beam-column connections under axial column tension. *Journal of Structural Engineering*, Vol. 122, No. 5, 1996, pp. 501-511.
17. Mander J.B., Priestley M.J.N., and Park R. Theoretical stress-strain model for confined concrete. *Journal of Structural Engineering*, Vol. 114, No. 8, 1988, pp. 1804-1826.

List of tables:

TABLE 1 Idealized and measured responses of original and repaired column specimens

List of figures:

FIGURE 1 Comparison of existing retrofit/repair methods

FIGURE 2 Geometry and reinforcement details of the original column

FIGURE 3 Original column damage state

FIGURE 4 Repair procedure with the hybrid confining jacket

FIGURE 5 Hybrid jacket details

FIGURE 6 Column test setup and instrumentation

FIGURE 7 Cyclic and idealized force-displacement relationship of original and repaired column specimens

FIGURE 8 Concrete cracks associated with stress transfer through dowel bars at the column-footing connection

TABLE 1 Idealized And Measured Responses Of Original And Repaired Column Specimens

		Original	Repaired
Idealized response values	Inelastic base shear, kips (kN)	42.1 (187.2)	52.4 (233)
	Effective yield displacement, inches (mm)	1.1 (27.9)	1.63 (41.4)
	Ultimate displacement, inches (mm)	2.8 (71.12)	5.65 (143.5)
Measured results	Lateral strength, kips (kN)	48.91 (217.6)	56.16 (249.8)
	Initial service stiffness, kips/inch (kN/mm)	38.27 (6.7)	31.75 (5.63)
	Ductility, inch/inch (mm/mm)	2.5 (2.5)	4.2 (4.2)
Structural response indices	STRI (%)	115	
	STFI (%)	83	
	DI (%)	168	

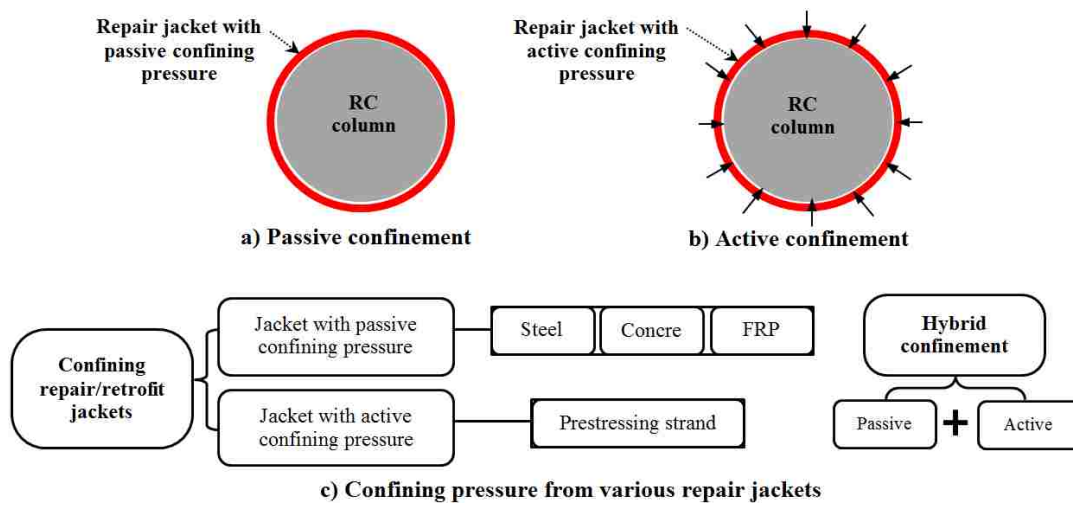


FIGURE 1 Comparison of existing retrofit/repair methods

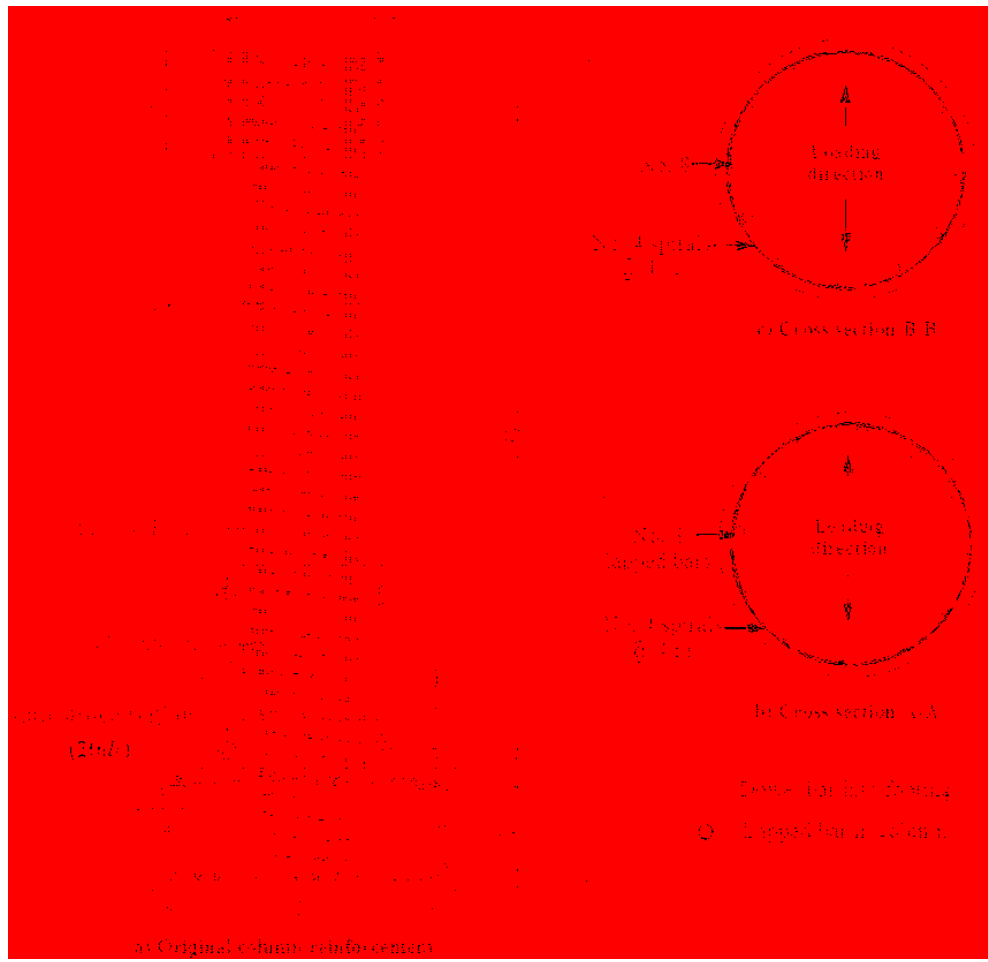


FIGURE 2 Geometry and reinforcement details of the original column

Conversion: No. 4(U.S.): No. 13(SI); No. 8(U.S.): No. 25(SI); 1 in. = 25.4 mm

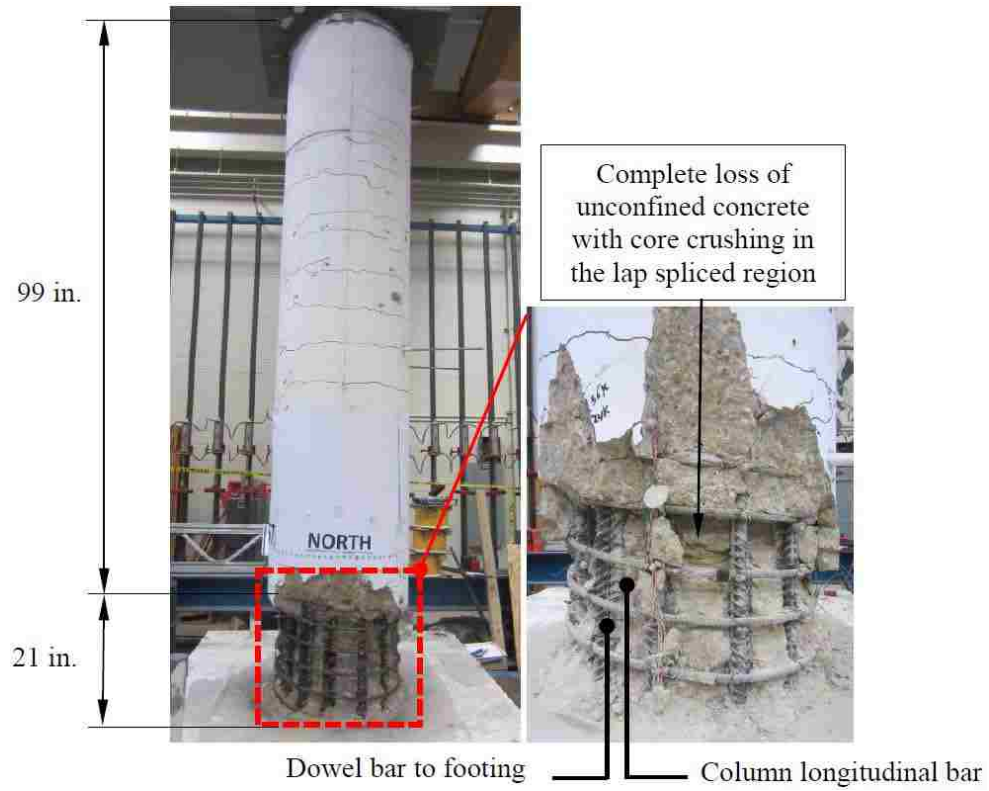


FIGURE 3 Original column damage state

Conversion: 1 in. = 25.4 mm

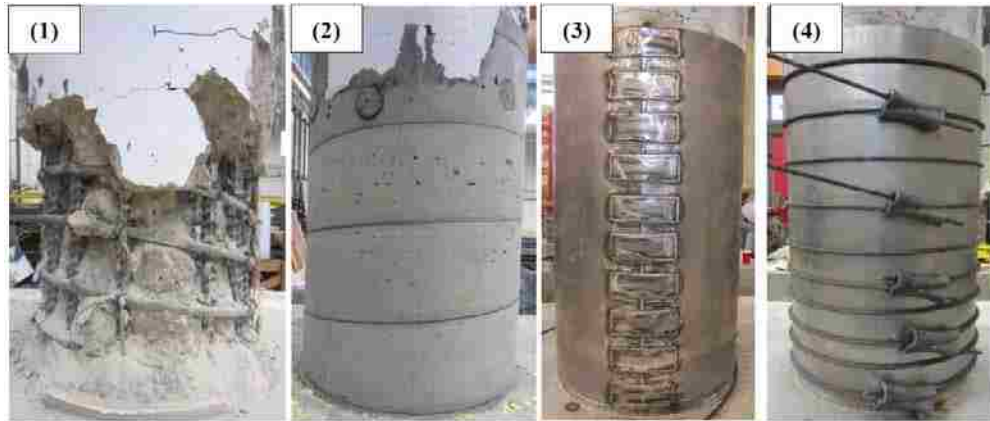


FIGURE 4 Repair procedure with the hybrid confining jacket

- (1) damaged column; (2) patched column with repair grout;
(3) sheet metal wrapping; (4) prestressing strands application

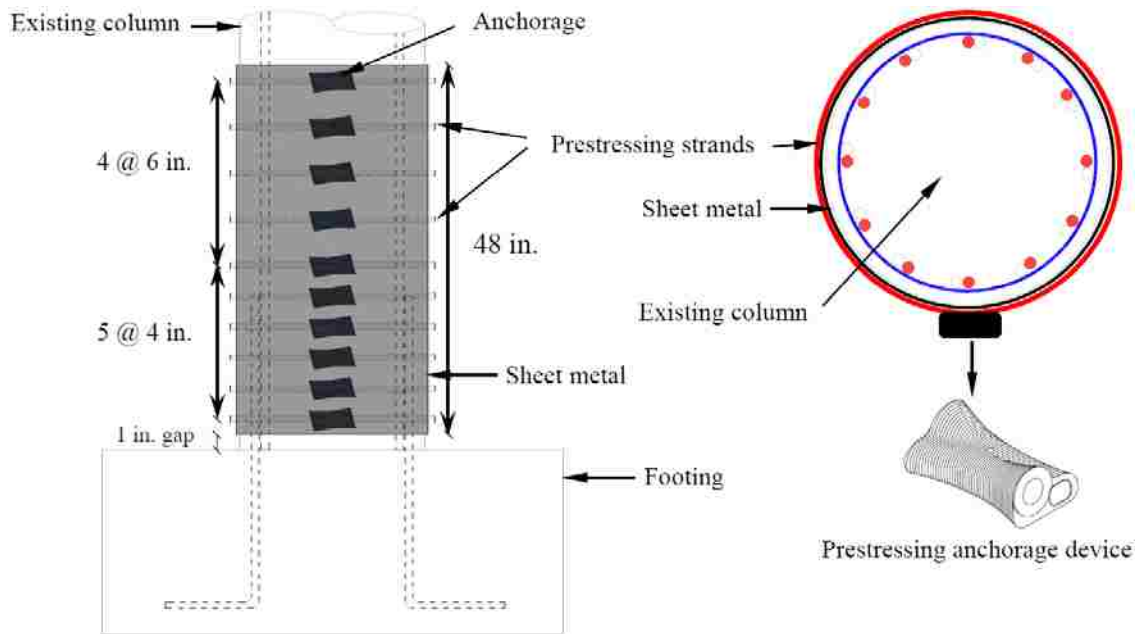


FIGURE 5 Hybrid jacket details

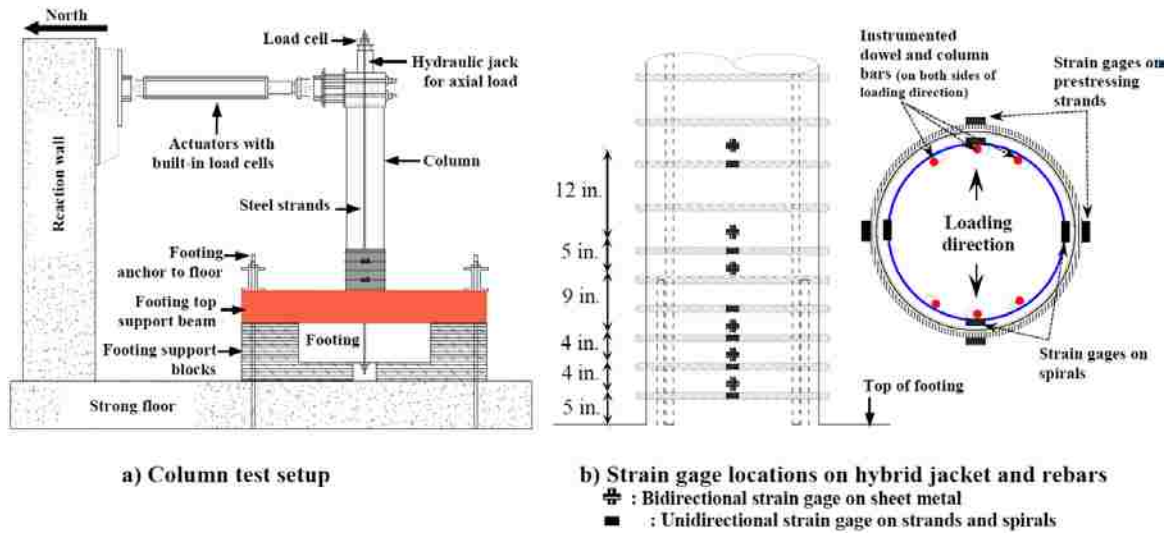


FIGURE 6 Column test setup and instrumentation

Conversion: 1 in. = 25.4 mm

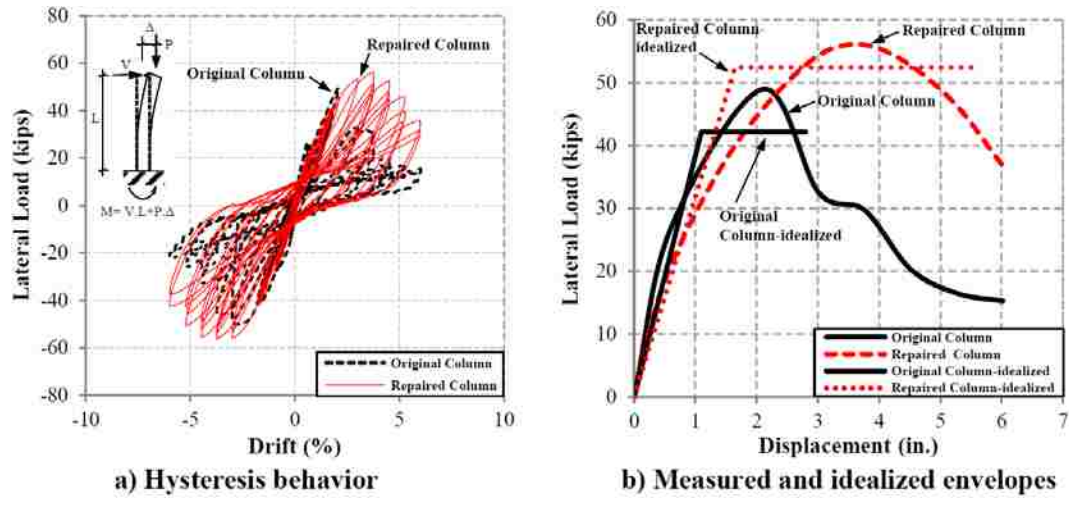


FIGURE 7 Cyclic and idealized force-displacement relationship of original and repaired column specimens

Conversion: 1 kips = 4.45 kN; 1 in. = 25.4 mm



FIGURE 8 Concrete cracks associated with stress transfer through dowel bars at the column-footing connection

* footing cracks marked with red dashed lines

II. RAPID REPAIR OF EARTHQUAKE DAMAGED RC COLUMNS WITH PRESTRESSED STEEL JACKETS

Abstract

In this study, a lightweight prestressed steel jacket (PSJ) is proposed and developed for rapid and cost-effective repair of a severely-damaged circular reinforced concrete column. PSJ is composed of several prestressed strands and a thin steel sheet restrained by them, which can be manually wrapped around and jointed to form a jacket on the column as part of a 12 h repair job by 2 workers. The prestressed strands restrain the thin sheet from buckling while the steel sheet in turn prevents the strands from cutting into cracked concrete and thus preserves the prestressing forces. The PSJ was validated with cyclic (reversed) testing of two large-scale columns with lap splice deficiency under incrementally increased displacements every three cycles. The ultimate strength and displacement ductility of the damaged column were respectively restored to 115% and 140% of those of the as-built column. The initial stiffness of the damaged column, however, was only restored to 84% of that of the as-built column since the PSJ was designed to restore the strength and ductility only. By connecting the damaged column to its footing through anchored dowel bars, the level of restoration in ultimate strength, initial stiffness, and displacement ductility were all increased by at least 20%.

Keywords: RC column repair; Seismic design; Prestressed jacket; Earthquake.

Introduction

Recent earthquakes have demonstrated catastrophic failures of buildings and bridges under a single mainshock or a series of mainshock-triggered events, such as aftershocks, explosions, and tsunamis. The March 11, 2011 Tohoku, Japan earthquake (moment magnitude M_w 9.0) was succeeded in one month by at least five aftershocks stronger than M_w 6.5 (USGS 2012). When a major earthquake occurs, the chance that aftershocks cause damage can be significant (Di Sarno 2013). For example, the M_w 6.3 February 22, 2011 Christchurch earthquake following the M_w 7.1 Canterbury earthquake on September 4, 2010, caused significant damage to the Christchurch building. The August 5, 2008 aftershock ($M_w > 6$) (USGS 2012), following the M_w 7.9 Wenchuan earthquake on May 12, 2008, contributed to the collapse of many structures that sustained damage from the mainshock (Yang 2009). Due to frequent occurrences of mainshock and aftershocks, damaged bridges along an emergency route must be rapidly repaired between multiple strong events to ensure safety of the bridges and enhance the resiliency of transportation network for post-earthquake response and recovery.

Bridges built prior to 1971 are seismically deficient due to: 1) lack of confinement associated with sparsely spaced transverse reinforcement in columns; and 2) short lap splices at potential plastic hinge locations (Laplace et al. 2005). Deficient columns can be retrofitted with passive and active external confinement in the plastic hinge regions (Caltrans 1996, Priestley et al. 1996, Buckle et al. 2006, Ying et al. 2006, Yarandi and Saatcioglu 2008, ElGawady et al. 2009, Andrawes et al. 2010, Fakharifar et al. 2014a, 2014b). Passive confinement can be provided by steel, reinforced concrete (RC), and fiber reinforced polymer (FRP) jackets (Chai et al. 1991, Priestley and Seible 1995, Silva et al. 2007). The level of passive confinement is completely determined by the dilation of column. Active confinement can be provided by prestressed strands and shape memory alloy (SMA) spirals (Saatcioglu and Yalcin 2003, Yarandi and Saatcioglu 2008, Andrawes et al. 2010), which can be changed by the initial pressure induced by mechanically prestressing and thermally induced stressing, respectively. Here, the term “retrofit” refers to upgrading of an undamaged existing column in contrast with the term “repair” for rehabilitation of a damaged column.

Conventional thick steel and RC jackets were among the first and most widely applied retrofit techniques for RC columns (Priestley et al. 1996). They are labor intensive and time consuming, and often require heavy lifting equipment during on-site installation. Increasing cross sectional area of the columns would increase both mass and stiffness of the existing columns, resulting in reduced vibration period of the jacketed structure. It often attracts more seismic demands (shear and moment) to the retrofitted columns and their connected members (Chai et al. 1991). Under the same plastic rotation in a retrofitted column, the thinner the jacket, the longer the plastic hinge length and the less likely rebar would fracture (Caltrans 1996, Buckle et al. 2006).

In comparison with the thick steel and RC jackets, FRP wrapping is attractive for its lightweight. However, it provided the retrofitted columns with lower stiffness and less energy dissipation, particularly when the transverse reinforcement of the columns decreased (Haroun and Elsanadedy 2005, Youm et al. 2006, Silva et al. 2007). Furthermore, it must be applied with adhesive epoxy, adequately impregnated, and sufficiently cured, which could be a time consuming process. To take advantage of ductile steel and lightweight FRP materials, thin steel sheet was used to retrofit a deficient RC column by Ying et al. (2006). The thin sheet was manually and rapidly wrapped around the column without use of any adhesives and equipment. However, the thin sheet was difficult to weld and thus bolted to form a jacket on the column. It was further confined by two halves of steel rings welded together to increase the shear capacity of the column in the plastic hinge region. Due to direct contact of hard surfaces among concrete, steel sheet, and steel ring, their system performance is less satisfactory than expected.

Prestressed strands were first introduced by Lin et al. (1994) to confine RC columns. Under cyclic loading, however, the retrofitted columns experienced strength degradation due to significant loss of the prestressing forces. The prestressing loss was associated with spalling of cover concrete and penetration of the prestressed strands into the concrete (Hawkins et al. 1999). The prestressing effect on the seismic retrofit of shear and lap-splice deficient columns was verified by comparing two groups of tests with approximately 0.36 MPa and 0.06 MPa confining pressures, respectively (Yalcin 1997, Mes 1999, Beausejour 2000, Saatcioglu and Yalcin 2003, Yarandi 2007, Yarandi and

Saatcioglu 2008, Sabri 2013). In addition to the above mechanisms for prestressing loss and thus strength degradation, this series of tests indicated that the buckling of longitudinal reinforcement between the strands contributed a sudden reduction of the column strength. The circular columns with $20d_b$ lap-spliced reinforcement (d_b = rebar diameter) tested by Beausejour (2000) indicated that the retrofitted columns with prestressed strands experienced concrete splitting/longitudinal cracks associated with lap slipping. Despite prestressing confinement in the plastic hinge region, the longitudinal cracks extended above the region and the strands penetrated into concrete cover, leading to debonding between the lapped rebar.

In comparison with the mechanically prestressed strands, thermally prestressed SMA spirals are easier to install in application (Andrawes et al. 2010, Shin and Andrawes 2011a). The thermally triggered recovery stress of prestrained SMA spirals was applied to provide actively confined pressure on the column in the plastic hinge region. With the use of FRP wrapping on the column inside the SMA spirals, the potential loss of active confinement by SMA spirals becomes less likely. Nevertheless, when cured, the FRP wrap is brittle and may fracture as the active confinement increases. As a result, the strength of retrofitted columns with prestressed SMA spirals can still degrade at large drifts as observed during tests (Shin and Andrawes 2011a).

Unlike the seismic retrofit of bridge columns, the rapid seismic repair of damaged columns was limited to relatively few attempts with the applications of SMA spirals and FRP wraps. SMA wires of 2 mm (0.079 in.) in diameter were wrapped in approximately 20 mm (0.79 in.) spacing and thermally prestressed around two 254-mm-diameter (10-in-diameter) RC columns that experienced concrete spalling, rebar buckling and fracture due to lateral loads (Shin and Andrawes 2011b). Each column was repaired in less than 15 h and tested in 24 h. The stiffness, strength, and displacement ductility of the two repaired columns were successfully restored to their respective parameters prior to damage. However, the maximum drift ratio or deformability of the repaired columns was significantly reduced due to substantially stiffening effect. Vosooghi and Saiidi (2012) repaired two 407-mm-diameter (16-in-diameter) RC columns with a relatively long lap splice length ($36d_b$) after they had been tested to a damage state (DS) of minimal concrete spalling and possible shear cracks or DS-2 (Vosooghi and Saiidi 2010b). The effects of

spirals, concrete and carbon FRP jacket on the shear capacity of the damaged columns were characterized (Vosooghi and Saiidi 2012). He et al. (2013) further investigated the repair efficacy of carbon FRP wraps on severely damaged RC columns of 560 mm × 560 mm (22 in × 22 in) in square cross section. Under flexural and torsional loads, the stiffness, strength, and ductility of the repaired columns can sometimes be restored to those of their as-built columns.

Objectives and Research Significance

To meet the urgent need for rapid repair of earthquake-damaged bridge columns, repair techniques with the following features would be desirable: ductile material (e.g. steel and alloy), lightweight jacket (e.g. thin steel and FRP sheet), minimum curing of repair materials (e.g. steel and alloy), and sustained active confinement (e.g. prestressed strands and SMA spirals). Ductile materials often give a warning signal prior to the failure of a repair system, which is critical to save lives during strong aftershocks. Lightweight allows field installation in a short time without requiring heavy lifting equipment. Minimum material curing returns the damaged bridges to service immediately after the completion of repair work. Active confinement can help restore stiffness, strength, and ductility of the columns to be repaired. Referring to the existing retrofit/repair jackets summarized in the previous section, a combination of a thin cold-formed steel sheet and several prestressed strands wrapped outside the steel sheet is proposed and referred to as a prestressed steel jacket (PSJ).

The objectives of this study are to develop and validate the proposed PSJ for rapid repair (≤ 24 h) of severely damaged RC columns with spiral transverse reinforcement and short lap-splice length ($20d_b$), and investigate the mechanical mechanism of the PSJ for performance improvement of the repaired columns in terms of ultimate strength, initial stiffness, and displacement ductility. The proposed hybrid jacket combines the passive confinement by a thin cold-formed steel sheet directly wrapped around a damaged column with the active confinement by prestressed strands wrapped around the steel sheet.

The thin steel metal can prevent high performance prestressed strands from cutting into spalling or damaged concrete while the prestressed strands can restrain the

thin sheet from buckling. The constrained effect of the steel metal and strands expects to sustain their high performance over a large range of lateral drifts and makes the PSJ superior to most, if not all, repair techniques in terms of the stiffness, strength, and ductility of rapidly repaired columns. At the same time, the constrained jacket system is light and easy to install in field applications.

In addition to the constrained effect, the sheet metal can arrest the widening of a shear crack both horizontally and vertically as illustrated in Fig. 1(a) or both flexural and longitudinal splitting cracks in other cases. The bi-directional resistance to the crack opening mainly comes from the load bearing capability of steel in any direction (i.e., isotropic), in addition to the friction between the sheet metal and concrete under the prestressing force. As a result, the enhanced aggregate interlock along the shear or flexural crack surface can increase the concrete shear strength of damaged columns or the bond strength between lap-spliced bars when repaired by the PSJ. In contrast, any unidirectional jacket such as prestressed strands, SMA wires, and transverse FRP can only resist the shear or splitting crack opening horizontally, contributing less to the concrete shear strength and little to the flexural strength of the columns. This advantageous feature of the proposed PSJ is vital to the safety of earthquake damaged RC columns threatened by strong aftershocks since the lateral displacement of the repaired columns could increase and result into the collapse of the bridge due to continuous widening of existing shear cracks as illustrated in Fig. 1(b) or flexural cracks. The less widening of shear or flexural cracks are also translated into higher stiffness of the repaired columns.

SMA spirals can be used to replace prestressing strands in the proposed PSJ. However, the thermally prestressing process with SMA spirals may require longer time in installation due to high heat conductivity of the sheet metal. Although performed well during small-scale column tests, SMA spirals could be costly for full-size columns even if feasible in applications.

Experimental Program

Two 1/2-scale circular RC columns were first constructed and tested to failure under pseudo-static cyclic (reversed) loads (Chen et al. 2010), then repaired with the

proposed PSJ, and finally tested again under the same load protocol in Structural Engineering Research Laboratory (SERL) at Missouri University of Science and Technology. This process allows the simulation and testing of applicability, constructability, and performance of the proposed repair jacket following a major earthquake event. For convenience, the two as-built specimens are designated as Column 1 and Column 2. The damaged Column 1 was rapidly repaired in about 12 h to restore stiffness, strength, and ductility while the damaged Column 2 was repaired with the intent of increasing strength in 24 h. The two repaired specimens are designated as Column 1-R and Column 2-R, respectively.

As-built Column Specimens

The two column specimens represent typical circular bridge piers with dowel bars from their footing and discontinuous longitudinal reinforcement at the pier-footing joint, which are commonly encountered in the Eastern coast and Midwest of the U.S (Chen et al. 2010). They are identical with a lap splice length of $20d_b$. The main reinforcement in Column 1 was uncoated while the reinforcing bars in Column 2 were coated with enamel. The original study by Chen et al. (2010) was to investigate the effect of enamel coating on the cyclic behavior of columns.

Fig. 2 illustrates the dimensions and reinforcement details of each specimen, including a load stub, column, and footing. The overall height of the specimen was 4242 mm (167 in.) with an effective column height of 3353 mm (132 in.) measured from the top of the footing to the centerline of the load stub and a lap splice length of 508 mm (20 in.) from the top of the footing. The column was 610 mm (24 in.) in diameter and reinforced with 12 No. 25 (#8) deformed reinforcement bars. Its transverse reinforcement consisted of No. 13 (#4) spiral deformed bars spaced at 102 mm (4 in.). The reinforcing steel was in compliance with ASTM 615 (ASTM 2012a). The measured yield strengths of longitudinal and transverse reinforcement bars was 418 MPa (60.6 ksi) and 541 MPa (78.5 ksi), respectively. The concrete compressive strength was selected to be representative to the columns constructed prior to 1971, 34.5 MPa (5000 psi) (Laplace et al. 2001, Vosooghi and Saiidi 2013) with additional 10% accounting for strength increase over a period of approximately 45 years. The concrete compressive strength measured on

the date of test according to ASTM C39 (ASTM 2012b) was 44 MPa (6340 psi). Each column was post-tensioned to approximately 592 kN (133 kips) corresponding to 7% of the nominal axial capacity, which represents gravity load of the bridge superstructure. At the center of the load stub, the column was laterally subjected to an incrementally increasing cyclic (reversed) load. The test setup and load protocol are identical to those for repaired columns as discussed later. The two columns were tested to complete failure when the residual strength was reduced by 75% from the measured peak strength.

At the completion of tests, the lap-splice failure conditions of Column 1 and Column 2 are illustrated in Fig. 3. Complete bond loss between lapped bars, core concrete crushing and reinforcement buckling were observed. According to ATC-32 (Rojahn et al. 1997), and Vosooghi and Saiidi 2012 criteria, their conditions were classified as significant damage and extensive damage (DS-5: imminent failure-visible reinforcement bars and compressive failure of the concrete core edge, initiation of reinforcement buckling), respectively.

Rapid Repair of the Damaged Columns with the Proposed PSJ

Materials A shrinkage-compensated, cement-based, and fast setting repair grout with mineral aggregates was used to replace degraded concrete from the damaged columns. At the date of tests, the average grout compressive strength of three samples in accordance with ASTM C109 (ASTM 2011) was 31 MPa (4560 psi) and 40 MPa (5820 psi) for Column 1 and Column 2, respectively. The average compressive strength of the grout used for Column 2 jacketing was 32 MPa (4651 psi).

Tension tests on the sheet metal specimens were conducted according to the ASTM A370 (ASTM 2012c). The sheet metal had the following properties: 680 MPa (98.5 ksi) in yield strength, 771 MPa (112 ksi) in ultimate strength, and 207 GPa (30,050 ksi) in the Modulus of Elasticity. The nominal 12.7 mm (½ in.) diameter seven-wire strands had an ultimate tensile strength and modulus of elasticity of 1,937 MPa (281 ksi) and 200 GPa (29,100 ksi), respectively. The headed No. 13 (#4) bars for Column 2 repair had the measured yield strength and modulus of elasticity of 468 MPa (68 ksi) and 212 GPa (29,430 ksi), respectively. For improved anchorage, each anchored dowel bar included two end heads and one middle head as shown in Fig. 4(d).

Design and Performance Objectives The goal of column repairs was mainly to restore shear strength and displacement ductility to prevent premature lap splice failure of the repaired columns. The design parameters of the steel sheet (t_j = jacket thickness, f_{yj} = jacket yield strength, and E_j = jacket modulus) and prestressed strands (f_{ps} = level of prestressing, s = strand spacing, and A_{ps} = cross sectional area of prestressed strands) were then determined accordingly. For Column 2-R, a load transfer mechanism was designed from the column to its footing through headed dowel bars that were part of the expanded column section and anchored into the footing as shown in Figs. 4(c, d). The headed dowel bars were carefully designed and detailed to ensure that the transferred load can be resisted by the existing footing.

The height of a plastic hinge region to be repaired, L_{pz} , was calculated according to Caltrans (2006):

$$L_{pz} = \frac{3}{8} AR \times D \geq 1.5D \quad (1)$$

where AR = column aspect ratio, and D = column diameter. The shear strength of a repaired column was calculated and checked against the factored shear (Caltrans 2006). That is,

$$\frac{V^o}{\phi} < V_c + V_s + V_j \quad (2)$$

where V^o = base shear, $\phi = 0.85$, and V_c , V_s and V_j = shear resisted by concrete, existing transverse reinforcement, and jacket, respectively.

Since the existing spiral transverse reinforcement in the plastic hinge region yielded during the as-built column tests and no epoxy was injected into the concrete cracks, the existing transverse reinforcement and concrete contribution to the shear strength were neglected. The PSJ has two shear resisting components (Priestley et al. 1996) for the repaired columns: thin sheet metal (V_{sj}) and prestressed strands (V_{sp}).

$$V_j = V_{sj} + V_{sp} \quad (3)$$

$$V_{sj} = 0.5\pi t_j f_{yj} D \cot \theta \quad (4)$$

$$V_{sp} = 0.5\pi A_{ps} f_{ps} D s^{-1} \cot \theta \quad (5)$$

where θ = angle of the critical inclined shear-flexure crack to the column axis.

The required confining stress (f_l) to prevent the lap-splice failure (Priestley et al. 1996) can then be determined by:

$$f_l = \frac{A_b f_s}{\mu p l_s} \quad (6)$$

$$p = \frac{\pi D'}{2n} + 2(d_b + c) \leq 2\sqrt{2}(d_b + c) \quad (7)$$

where A_b = cross sectional area of nonprestressed longitudinal reinforcement bars, $f_s = 1.7f_y$ and f_y = yield strength of longitudinal reinforcement, μ = coefficient of friction (assumed as 1.4), l_s = lap splice length, p = crack surface perimeter, n = number of longitudinal lapped bars, d_b = reinforcement bar diameter, D' = concrete core diameter (outside to outside dimension of the spiral transverse reinforcement), and c = concrete cover thickness.

The PSJ was designed to ensure that the repaired column can reach a displacement ductility of 3.0 accounting for different initial stiffness of the as-built and repaired columns, according to Vosooghi and Saiidi 2012 and Caltrans 1996. In this study, the unified stress-strain model of Mander et al. (1988) was adopted.

The final design of the two repaired columns is summarized in Fig. 4. Both columns included a jacket of a 1.27 mm (0.05 in.) thick, 1,220 mm (48 in.) wide steel sheet and 10 prestressing strands in the plastic hinge region. Specifically, 6 strands at 102 mm (4 in.) spacing were applied over the lap splice region and the remaining 4 strands at 152 mm (6 in.) spacing outside the spliced region. The strands were prestressed up to 1,034 MPa (150 ksi), corresponding to a confinement stress of 3.3 MPa (0.48 ksi). However, the repaired sections of Columns 1 and 2 were 610 mm (24 in.) and 660 mm (26 in.), respectively. The increased diameter in the repaired Column 2 was to accommodate the addition and concrete cover of 10 headed anchor bars outside the original cross section.

Method and Procedure Both damaged columns were repaired in the bottom 1,220 mm (48 in.) with the proposed PSJ. To prevent premature compression damage, the jacket stops at 25 mm (1 in.) distance from its footing. Column 1 was repaired in three steps as illustrated in Fig. 5: 1) restoring the damaged column to its original cross section with repair grout; 2) wrapping a thin sheet metal around the restored column and welding

the two ends of the sheet when tightly pressed against the column with the aid of ratchet straps; and 3) wrapping and prestressing strands to complete the jacket. The prestressing equipment for strands is illustrated in Fig. 5(d).

Column 2 was repaired in five steps. Step 1 was to restore the damaged column to its original cross section as done for Column 1. Step 2 was to drill five holes with 25 mm (1 in.) in diameter into the footing by 250 mm (10 in.), which were evenly distributed on either side of the loading plane as shown in Fig. 4(c), remove concrete debris from the holes with compressed air, fill the holes with Epcon G5 high strength epoxy, and insert No. 13 (#4) headed bars into them as illustrated in Fig. 4(d). After the epoxy had been cured, Step 3 began and was to pour a 25-mm-thick (1-in-thick) grout jacket around the column and cover the headed dowel bars up to 1,245 mm (49 in.) from the top of footing. After grout curing, the repair process of the damaged Column 2 was completed by placing the thin steel and prestressed strands in Steps 4 and 5 in the same way as Steps 2 and 3 for Column 1.

Several considerations taken during the repair process are warranted of special attention. First, existing cracks on the damaged column were not filled with epoxy to simulate an emergency repair scenario. Second, the sheet metal was thin enough to be manually wrapped around the damaged column. Third, while the thin sheet could be directly wrapped around the damaged column and their gap filled with repair grout, the cross section of the as-built column was restored prior to wrapping of the steel sheet with the intent of testing the applicability of the PSJ for bridge retrofit as well. Fourth, no surface preparation or bonding adhesives were needed in between the steel sheet and the column; the proposed method thus requires no curing of the jacketing materials after the loose concrete has been replaced by repair grout. Fifth and last, similar to FRP jacketing, the lightweight steel sheet and prestressing strands were applied on the damaged column by a two member crew within 4 h after repair grout was applied and cured in 8 h to replace loose concrete (and cover the headed bars) of the damaged column. For Column 2 repair, drilling anchor holes into the footing and anchoring the headed bars with epoxy took additional 12 h.

When long-term performance and aesthetic requirement of the repaired columns are a concern in field applications, a protective or architectural layer can be added to the

proposed PSJ. For corrosion protection, anti-corrosive paintings/coatings could be applied on outside surface of the jacket. To meet aesthetic requirements, a minimum of 25-mm-thick (1-in-thick) concrete cover (preferably high-performance concrete) could be applied either by shotcreting or casting it over the jacket.

Test Setup and Instrumentation

The test setup of each column specimen is shown in Fig. 6(a). The column footing was fixed through a footing top rigid frame that was anchored into the strong floor. The column was post-tensioned along its centerline by a PVC-encased 7-wire steel strand that was anchored at the bottom of the footing and at the top of a hydraulic jack placed above the load stub. The hydraulic jack was placed to provide an axial load of approximately 592 kN (133 kips). The repaired column was laterally loaded by two actuators with a pseudo-static cyclic (reversed) force in displacement control with three symmetric cycles applied at each load increment (Chen et al. 2010). The shear force and bending moment of the column were defined positive when the actuators pushed the column away.

Each repaired column was instrumented with 76 strain gages attached on the jacket and 52 strain gages on the internal reinforcement. As shown in Fig. 7, the strain gages on the steel sheet were installed at various elevations both longitudinally and transversely and the strain gages on the prestressed strands transversely only. The strain gages on three dowel and reinforcing bars near the extreme concrete fibers of the column in the loading plane were placed at approximately 102 mm (4 in.), 305 mm (12 in.) and 457 mm (18 in.) above the footing. Four strain gages were also attached on each of the lowest four spirals at quarter points within and perpendicular to the loading plane. “Confinement” strain gages in the loading plane were installed to measure the dilation of concrete under compressive stresses, which were then used to compute the confining pressure. The “shear” strain gages perpendicular to the loading plane were used to measure the shear strains. The strain gages on the repair jacket were located at approximately the same elevation as those on the internal transverse reinforcement.

In addition, each of the headed anchor bars for Column 2-R was instrumented with three strain gages (Sg1-Sg3) as illustrated in Fig. 4(d). Ten linear variable differential transformers (LVDTs) and linear position transducers (LPTs) were mounted

at the base of each column as illustrated in Fig. 6(b) to measure the column rotation, caused by the separation of Column 1 from its footing or the anchorage slip in Column 2, and the steel sheet slip. Additional three pairs of LPTs were installed on a reference frame to measure the lateral displacement of the tested columns.

Test Results and Discussion

Behavior of As-built Columns

The behavior of the two as-built columns was detailed in Chen et al. (2010). For convenience, it is briefly summarized here. The as-built column specimens exhibited rapid strength deterioration associated with inadequately spliced bars. At 0.5% drift ratio, flexural cracks initiated at column bases. The columns experienced the peak lateral load at approximately 1% drift when the main reinforcement yielded as indicated by the strain gages attached on the lapped bars. At that loading level, longitudinal splitting cracks occurred over the spliced region and new flexural cracks appeared at higher elevation of the columns. As the test progressed, the flexural cracks were widened and coalesced with the splitting cracks, indicating bond deterioration between the spliced bars. At 3% drift, cover concrete spalling and core concrete crushing occurred and the lapped bars experienced significant slippage. As a result, both as-built columns exhibited a pinched hysteretic behavior typical of the lap-spliced columns. Throughout the test, Column 1 experienced no rebar buckling but Column 2 had two longitudinal rebar buckled at the column base as shown in Fig. 3(d). Correspondingly, Column 1 eventually failed at the end of dowel bars while Column 2 at the column-footing joint. These differences were attributed to the effect of enamel coating on lap-spliced bond.

The load-displacement curves of Column 1 and Column 2 were compared in Chen et al. (2010). Due to the effect of enamel coating, the hysteresis energy absorption of Column 2 was over 5% higher than those of Column 1. In two consecutive cycles at the same displacement, Columns 1 and 2 experienced a maximum drop of load capacity by 35.2% and 11.6%, respectively.

Hysteresis Behavior and Physical Observations of Repaired Columns

Fig. 8(a) compares the base shear-drift ratio hysteresis loops of repaired Column 1-R and as-built Column 1. Note that the applied load reported in Chen et al. (2010) was from one hydraulic actuator and corrected from two actuators in this paper. As shown in Fig. 8(a), the strength drop in two consecutive cycles at the same drift ratio corresponding to the maximum strength was significantly reduced from the as-built (35.2%) to the repaired column (11.1%). At the maximum strength, the strength envelope changed over a similar drift increment from dramatically-dropped in Column 1 (approximately 37.7%) to gradually-reduced in Column 1-R (approximately 9.5%). This analysis indicated that the unstable in-cycle strength deterioration of Column 1 was enhanced to the stable cyclic strength degradation of Column 1-R, preventing the potential collapse associated with in-cycle deterioration (ATC-62/FEMA P440A 2008). The area enclosed by the column hysteresis loops as shown in Fig. 8(a) or the hysteresis energy absorption increased from 135.4 kN.m (1198 kip.in) in Column 1 to 228.0 kN.m (2018 kip.in) in Column 1-R.

Column 1-R exhibited the first flexural crack at the column-footing joint (unjacketed portion) at 0.15% drift. The crack was rapidly widened till approximately 1.2% drift when the repair jacket effectively confined the lap-spliced column so that the confined dowel bars can transfer the strain from the column to its footing as indicated by the appearance of a few minor cracks on the footing at the location of main reinforcing bars as illustrated in Fig. 9(a). At that loading level, the internal lapped reinforcing bars yielded as indicated by the readings from attached strain gages. As the test progressed, longitudinal tensile splitting cracks were observed in theunjacketed gap. At 1.8% drift ratio, the main reinforcing bars were at the onset of strain hardening and the longitudinal strains of the sheet metal increased rapidly as indicated by the internal and surface strain gages, respectively. This important observation verified that, upon significant elongation of longitudinal bars, the steel sheet restrained the formation of flexural cracks over the lap-spliced region through friction between the metal and concrete. It signified the importance of sheet metal in transforming the unidirectional hoop stress state generated by conventional jackets or prestressed strands into a biaxial stress state by the proposed jacket. Further loading caused crushing of the repair grout between lap-spliced bars under

the confining pressure provided by the jacket, resulting in the pullout of reinforcing bars at the column-footing joint. Post-test inspections revealed that the longitudinal splitting cracks on the column were limited to the 25 mm (1 in.) unjacketed gap only; the prestressed jacket had confined the column so tightly that the damage in the gap area did not extend further up to the column.

Fig. 8(b) compares the base shear-drift ratio hysteresis loops of Column 2 and Column 2-R. Due to the difference between positive (push) and negative (pull) actuator displacement capacities, unsymmetric displacement cycles were applied beyond a drift ratio of 7.0% to ensure that the column was tested to failure. As shown in Fig. 8(b), the strength drops in two consecutive cycles at the same drift ratio corresponding to the maximum strength were approximately 11.6% and 14.2% for the as-built and repaired columns, respectively. The hysteresis energy absorption increased from 142.4 kN.m (1260 kip.in) in Column 2 to 850.7 kN.m (7529 kip.in) in Column 2-R.

At 2% drift, the steel sheet was observed to slide up for approximately 4.5 mm as illustrated in Fig. 9(b) and the headed dowel bars appeared to yield. Throughout the remaining tests, no further sliding was observed in the steel sheet due to its firm contact with the column (friction force) as a result of active pressure provided by the prestressed jacket. As shown in Fig. 8(b), the in-cycle strength reduction in the drift range of 2.0-4.5% was insignificant. At 6.8% drift, the repaired column exhibited a slightly hardening hysteretic behavior. After removal of the repair jacket at the end of tests, it can be observed from Fig. 9(c) that the repair grout overlay experienced distributed flexural cracks at the top and bottom portions of the 1220 mm (48 in.) repaired section. The prestressed jacket has effectively confined the lap-spliced joint and dowel connection from the column to its footing, thus requiring no adhesive to bind the jacket with the repair grout. No pullout of the headed dowel bars was observed throughout the test. However, at large drift angles, the headed dowel bars experienced buckling and finally low cycle fatigue fracture in the unjacketed gap at the column-footing joint. The plastic hinge was formed at the column-footing joint as expected.

In both columns, the steel sheet confined by prestressed strands inhibited the concrete spalling and prevented strands from penetrating into the concrete cover even at large drift angles. It also arrested the longitudinal splitting cracks in the lap-spliced

region. Strain measurements verified that the active confining pressure provided by prestressed strands remained effective throughout the tests. No plastic hinges were observed in the middle of columns. Although the existing cracks above the steel jacket were slightly widened under increasing loads, no additional cracks were generated.

Performance Evaluation of the Proposed PSJ

Performance of the repaired columns was evaluated in terms of the restoration or improvement of stiffness, strength, and ductility. Therefore, the envelope of load-displacement hysteresis loops similar to Fig. 8, referred to as the actual capacity curve as shown in Fig. 10, was determined and idealized into an elastic-plastic curve for each column. To do so, the ultimate displacement included in the capacity curve is defined as the displacement at which 20% strength reduction in three consecutive cycles has been reached (ATC-62/FEMA P440A 2008) to ensure that the columns or their supporting structures are stable. For as-built (original) columns, the actual capacity curve was idealized by setting the initial stiffness to pass through the first yield point of longitudinal reinforcement and adjusting the yield strength so that areas under the actual and idealized curves up to the ultimate displacement were equal. Due to the prior yielding, the first yield point of the reinforcement in the repaired columns when loaded was not associated with the initial stiffness of the repaired columns. Therefore, for the repaired columns, the initial stiffness of the idealized capacity curve was determined by the slope of a straight line from the origin to a point of the actual curve at which 50% of the maximum strength has been achieved. The idealized capacity curve of each column is compared in Fig. 10 with its corresponding actual capacity curve. Note that the idealized curve stops at the ultimate displacement.

The yield strength, effective yield displacement, and ultimate displacement of idealized capacity curves are summarized in Table 1 for the as-built and repaired columns. The initial stiffness can then be calculated by dividing the yield strength by the effective yield displacement. The displacement ductility is calculated by dividing the ultimate displacement by the effective yield displacement. The calculated initial stiffness, the calculated displacement ductility, and the ultimate strength directly obtained from the actual capacity curve are summarized in Table 2 as performance measures of the as-built

and repaired columns. Table 2 indicated an increase of displacement ductility from 2.5 in the as-built Column 1 to 3.5 in the repaired Column 1-R and from 2.8 in the as-built Column 2 to 6.7 in the repaired Column 2-R. Both repairs met the seismic design criteria requirement for minimum displacement ductility of 3 for ductile RC columns (Caltrans 2006). Therefore, the proposed rapid repair on Column 1 proved appropriate for the serviceability limit state while the repair on Column 2 was sufficient for the ultimate limit state or regarded as a permanent repair.

The level of restoration for a particular performance measure (i.e. ultimate strength, initial stiffness, or displacement ductility) is defined as a ratio of the measure between the as-built column and the repaired column. It can be calculated from Table 2 that the strength restorations are 115% and 156%, the stiffness restorations are 84% and 100%, and the ductility restorations are 140% and 239% for Columns 1 and 2, respectively. Therefore, both the ultimate strength and displacement ductility of the repaired column exceeded those of its as-built column. The initial stiffness of the repaired Column 1-R was less than that of the as-built Column 1 since the repair design was focused on the restoration of strength and ductility only. However, introducing headed dowel bars in Column 2-R successfully restored the initial stiffness of the as-built Column 2, which is promising to address a real challenge in repair of earthquake damaged columns (Vosooghi and Saiidi 2010a, 2010b, Vosooghi and Saiidi 2012, He et al. 2013).

Experimental Verification of Repair Mechanism in the PSJ

To further understand how the proposed PSJ performed during tests, the data sets recorded from the strain gages on Levels 1 and 2 as illustrated in Fig. 7 in the load plane of Column 1-R are averaged and presented in Figs. 11(a, c) for the longitudinal strain of sheet metal and the transverse strain of prestressed strands, respectively. The corresponding average strains are presented in Figs. 11(b, d) for Column 2-R. Fig. 11(e) compares the average strains on the spirals of as-built Column 1 and repaired Column 1-R while Fig. 11(f) is for the corresponding comparison of Column 2 and Column 2-R.

The nearly rectangular strain-drift hysteresis loops as shown in Figs. 11(a, b) strongly suggest a friction force transfer mechanism between the thin sheet metal and its

confined concrete, which was availed by prestressed strands. The height of the hysteresis loops appears constant at different drifts, which verified the effectiveness of “constant” prestressing mechanism throughout testing. The rotational angle of the hysteresis loops for Column 1-R is significantly smaller than that of Column 2-R likely due to the effect of headed dowel bars in Column 2-R. The average tensile and compressive longitudinal strains of Column 1-R was 672 and 958 $\mu\epsilon$, respectively. At large drifts, the sheet metal of Column 2-R was subjected to tensile and compressive longitudinal strains up to 2412 and 895 $\mu\epsilon$, respectively. The peak strains corresponded to the maximum applied base shear to the repaired column, both within the yield strain of sheet metal.

As shown in Figs. 11(c, d), the average transverse strains of prestressed strands steadily increased with the applied displacement. This result indicated a satisfactory performance of the thin sheet metal in preventing the potential loss of prestressing force (active confining pressure) of prestressed strands. The peak transverse strains of 1317 and 2482 $\mu\epsilon$ on the strands of Columns 1-R and 2-R, respectively, are comparable with the typical design strains of 1000-4000 $\mu\epsilon$ for lap splice slippage retrofitting. The level of the peak strains indicated that the strands were in elastic range. The presence of prestressing force by the strands reduced the transverse strain of spirals to within the yield strain of spiral reinforcement, as indicated in Figs. 11(e, f), which clearly indicated less concrete core dilation when repaired with prestressed strands.

Comparative Cost Analysis

The maintenance of buildings and bridges is subjected to tight budget constraints. Therefore, cost effectiveness of any retrofit/repair technique is a critical factor to determine whether the developed technique can be widely implemented in practice. This section provides a comparative cost analysis of the proposed PSJ and two commonly-used repair methods: conventional steel and FRP jackets.

To have a fair comparison basis, steel and FRP jackets were designed and detailed for the same criteria as used in the repair of two damaged columns with the PSJ (no anchored dowel bars) according to existing retrofitting guidelines (Prierstley et al. 1996, Buckle et al. 2006). The steel jacket uses a 10-mm (0.4 in.) thick steel shell with the minimum yield strength of 400 MPa (58 ksi) and the modulus of elasticity of 200 GPa

(29,000 ksi). The steel jacket is 50 mm (2 in.) larger in diameter than the existing column. The 25 mm gap between steel jacket and the column is filled with non-shrinkage repair grout. For installation, two identical steel plates are prepared and rolled into two halves of a cylindrical shell in factory. The two halves are transported to the project site, placed around the existing column, welded at seams, and filled with repair grout. The FRP jacket includes 12 plies of carbon FRP sheets that have a tensile strength of 3800 MPa (550 ksi), modulus of elasticity of 227 GPa (33,000 ksi), and a rupture strain of 1.67%. The FRP jacket includes carbon fibers as load bearing component and epoxy resins as fibers binder. It can be manually wrapped around a column with the wet-layup process.

The itemized costs of various retrofit/repair methods are calculated and compared in Table 3. The cost items include materials, shipping and handling, equipment rentals, and installation labors. The sample prices of various items are referred to Sarrazin (2004). They do not reflect the current prices and are subjected to changes depending on the location of projects. For site setup, clearing, and scaffolding during installation, hourly rates for skilled workers (i.e. welders) and general workers were assumed to be \$35 and \$25, respectively. For some items such as crane rental, the minimum (Min.) cost was also taken into account for small projects. It can be seen from Table 3 that the grand totals for the steel jacket, carbon FRP jacket, and the proposed PSJ are \$7,005, \$4,820, and \$1,684, respectively, making the PSJ a cost-effective solution.

Conclusions

The proposed PSJ repair technique with several prestressed strands restraining a thin steel sheet that is wrapped around a damaged RC column has been developed and demonstrated effective and cost competitive. Based on the experimental study on two 3.35-m-tall (132-in-tall) cantilevered columns with 610 mm (24 in) in diameter, the following conclusions can be drawn:

- The PSJ is a lightweight system of steel materials with no curing requirement. It can be manually installed by a two-member crew in 4 h after fast setting cementitious grout to replace loose concrete in the damaged column has been cured in 8 h. It is a cost-effective technique for post-earthquake emergency repair.

- When repaired with the PSJ, the ultimate strength and displacement ductility of the damaged column were respectively restored to 115% and 140% of those of Column 1 in as-built condition. The PSJ effectively prevented the premature lap-splice failure of the repaired Column 1-R. The initial stiffness of the damaged column, however, was only restored to 84% of that of the as-built column since the PSJ was designed to restore the ultimate strength and ductility only. The PSJ applied sufficient passive and active confining pressure on the column surface to prevent cover concrete from spalling. The 1.27-mm-thick (0.05-in-thick) steel sheet had the required shear strength to sustain the potential penetration of the 12.7-mm-diameter (0.5-in-diameter) seven-wire strands that were spaced 102 mm and 152 mm (4 in. and 6 in.) within and outside the spliced region, respectively. The strands in turn restrained the thin steel sheet from potential buckling.
- The prestressing forces in various strands or the active confinement applied on the repaired column suffered little or no loss up to 8% drift. Therefore, the friction force between the sheet metal and the column remained steady throughout the test and effectively restrained flexural cracks in the plastic hinge region from widening. No adhesive between the steel sheet and the column is required.
- Both the as-built and repaired columns with lap splice deficiency did not exhibit appreciable hardening behavior beyond the yield strength, irrespective of the level of confining pressure in the plastic hinge region.
- When repaired with the PSJ and anchored dowel bars, the ultimate strength, initial stiffness, and displacement ductility of the damaged column were restored to 156%, 100%, and 239% of those of Column 2 in as-built condition. Ten 12.5-mm-diameter (0.5-in-diameter) headed bars, which were anchored into the footing by 250 mm (10 in) deep and embedded in 25-mm-thick (1-in-thick) cementitious grout, added significant stiffness in the lap-spliced region of the column and thus provided an effective load transfer mechanism that can compensate for potential lap splice failures.

- In comparison with Column 1-R, the anchored dowel bars in Column 2-R increased the level of restoration in ultimate strength, initial stiffness, and displacement ductility by at least 20%. However, additional 12 h are required to drill holes in the column footing and install the headed bars with adhesives, amounting to a total of 24 h repair time for a two-member crew. As such, the PSJ with anchored dowel bars can be used for a permanent repair.

Acknowledgments

Financial support for this study was provided in part by the U.S. National Science Foundation under Award No. CMMI-1030399 and the Department of Civil, Architectural, and Environmental Engineering at Missouri University of Science and Technology. The views, opinions, findings, and conclusions reflected in this paper are those of the authors only and do not necessarily reflect the official views or policies of the sponsors. Special thanks are due to Mr. Christian Dahl from Headed Reinforcement Corp. for his donation of headed anchor bars. Thanks are also extended to Zachary T. Woolsey, Timothy O'Connor, John A. Cain, and John Bullock for their assistance throughout column repair and testing processes. The authors also appreciate the constructive comments made by three anonymous reviewers.

References:

Andrawes, B., Shin, M., and Wierschem, N. (2010). "Active confinement of reinforced concrete bridge columns using shape memory alloys." *Journal of Bridge Engineering*, 15(1), 81-89.

ASTM. (2011). "Standard test method for compressive strength of hydraulic cement mortars (Using 2in. or [50-mm] Cube Specimens)." ASTM C109–11/C109M-11, West Conshohocken, PA.

ASTM. (2012a). "Standard specification for deformed and plain carbon steel bars for concrete reinforcement." ASTM A 615/A 615-12, West Conshohocken, PA.

ASTM. (2012b). "Standard test method for compressive strength of cylindrical concrete specimens." ASTM C 39/C 39M-12, West Conshohocken, PA.

ASTM. (2012c). "Standard test methods and definitions for mechanical testing of steel products." ASTM A 370, West Conshohocken, PA.

ATC-62. (2008). "Effects of strength and stiffness degradation on seismic response". ATC-62/FEMA P440A, prepared by the Applied Technology Council for the Federal Emergency Management Agency, Applied Technology Council, Redwood City, California.

Beausejour, P., (2000). "Seismic Retrofit of Concrete Columns with Splice Deficiencies by External Prestressing". Master thesis. University of Ottawa, Ottawa, ON, Canada.

Buckle, I., Friedland, I., Mander, J., Martin, G., Nutt, R., and Power, M. (2006). "Seismic retrofitting manual for highway structures: Part 1—Bridges." FHWA-HRT-06-032, Federal Highway Administration, McLean, VA.

Calderone, A.J., Lehman, D.E.; Moehle, J.P. (2000). "Behavior of reinforced concrete bridge columns having varying aspect ratios and varying lengths of confinement," Pacific Earthquake Engineering Research Center, PEER 2000/08.

Caltrans, (1996). Earthquake Retrofit Guidelines for Bridges, Memo to Designers 20-4, California Department of Transportation, Sacramento, California.

Caltrans. (2006). Seismic design criteria (SDC), version 1.4, California DOT, Sacramento, CA.

Chai I, Y. H., Priestley, M. N., and Seible, F. (1991). "Seismic retrofit of circular bridge columns for enhanced flexural performance." ACI Structural Journal, 88(5).

Chen, G.D., Volz, J.S., Brow, R.K., Yan, D.M., Reis, S., Wu, C.W., Tang, F.J., Werner, C., and Tao, X. (2010). "Coated steel rebar for enhanced concrete-steel bond strength and corrosion resistance". Final Report Submitted to Missouri Department of Transportation, No. OR 11-004.

Coffman, H. L., Marsh, M. L., and Brown, C. B. (1993). "Seismic durability of retrofitted reinforced-concrete columns." Journal of Structural Engineering, 119(5), 1643-1661.

Di Sarno, L. (2013). "Effects of multiple earthquakes on inelastic structural response". Engineering Structures, 56, 673-681.

ElGawady, M., Endeshaw, M., McLean, D., and Sack, R. (2009). "Retrofitting of rectangular columns with deficient lap splices." *Journal of Composites for Construction*, 14(1), 22-35.

Elnabelsya , G. (2000). "Seismic retrofitting of concrete bridge columns with CFRP laminate". Master thesis. University of Ottawa, Ottawa, ON, Canada.

Elnabelsya, G., (2013). "Use of Carbon Fiber Reinforced Polymer Sheets as Transverse Reinforcement in Bridge Columns". PhD thesis. University of Ottawa, Ottawa, ON, Canada.

Fakharifar, M., Sharbatdar, M., Lin, Z., Dalvand, A., Sivandi-Pour, A., and Chen, G. (2014a). "Seismic performance and global ductility of RC frames rehabilitated with retrofitted joints by CFRP laminates." *Earthquake Engineering and Engineering Vibration*, 13(1), 59-73.

Fakharifar, M., Chen, G., Lin, Z., & Woolsey, Z. (2014b). Behavior and strength of passively confined concrete filled tubes. In the 10th U.S. National Conference on Earthquake Engineering: July 21-25, 2014, Anchorage, Alaska.

Haroun, M. A., and Elsanadedy, H. M. (2005). "Fiber-reinforced plastic jackets for ductility enhancement of reinforced concrete bridge columns with poor lap-splice detailing." *Journal of Bridge Engineering*, 10(6), 749-757.

Hawkins, N.M., Kaspar, I.I., and Karshenas, M., (1999), "Seismic Retrofit of Poplar Street Interchange in East St. Louis," *Structures Congress*, ASCE, April, 1999.

He, R., Grelle, S., Sneed, L. H., & Belarbi, A. (2013). "Rapid repair of a severely damaged RC column having fractured bars using externally bonded CFRP". *Composite Structures*, 101, 225-242.

Laplace, P., Sanders, D., Saiidi, M. & Douglas, B., (2001). "Experimental study and analysis of retrofitted flexure and shear dominated circular reinforced concrete bridge columns subjected to shake table excitation": Center for Earthquake Engineering Research, Department of Civil Engineering, University of Nevada, Reno.

Laplace, P. N., Sanders, D. H., Saiidi, M. S., Douglas, B. M., and El-Azazy, S. (2005). "Performance of concrete bridge columns under shake table excitation." *ACI structural journal*, 102(3).

Lin, Y., Gamble, W.L. and Hawkins, N.M., (1994). "Report to ILLDOT for Testing of Bridge Piers Poplar Street Bridge Approaches, East St. Louis, IL." Department of Civil Engineering, University of Illinois at Urbana-Champaign.

Mander, J. B., Priestley, M. J. N., and Park, R. (1988). "Theoretical stress-strain model for confined concrete." *J. Struct. Eng.*, 10.1061/(ASCE) 0733-9445(1988)114:8(1804), 1804–1826.

Mes, D. (1999). "Seismic retrofitting of concrete bridge columns by external prestressing". Master thesis. University of Ottawa, Ottawa, ON, Canada.

Priestley, M., and Seible, F. (1995). "Design of seismic retrofit measures for concrete and masonry structures." *Construction and Building Materials*, 9(6), 365-377.

Priestley, M. N., Seible, F., & Calvi, G. M. (1996). "Seismic design and retrofit of bridges". John Wiley & Sons, New York.

Rojahn, C., Mayes, R., Anderson, D., Clark, J., Hom, J., Nutt, R., and O'Rourke, M. J. (1997). "Seismic design criteria for bridges and other highway structures". New York, USA: John Wiley & Sons; p. 198.

Saatcioglu, M., & Yalcin, C. (2003). "External prestressing concrete columns for improved seismic shear resistance". *Journal of Structural Engineering*, 129(8), 1057-1070.

Sabri, A., (2013). "Seismic Retrofit of Concrete Columns by Transverse Prestressing". Master thesis. University of Ottawa, Ottawa, ON, Canada.

Sarrazin, J. (2004). "A comparative analysis of seismic retrofit techniques for reinforced concrete bridge columns". Master thesis. University of Ottawa, Ottawa, ON, Canada.

Shin, M., and Andrawes, B. (2011a). "Lateral cyclic behavior of reinforced concrete columns retrofitted with shape memory spirals and FRP wraps." *Journal of Structural Engineering*, 137(11), 1282-1290.

Shin, M., and Andrawes, B. (2011b). "Emergency repair of severely damaged reinforced concrete columns using active confinement with shape memory alloys." *Smart Materials and Structures*, 20(6), 065018.

Silva, P.F., Ereckson, N., & Chen, G.D. (2007). "Seismic Retrofit of Bridge Joints in Central U.S. with Carbon Fiber-Reinforced Polymer Composites." *ACI Struct. J.*, 104-S22, 207-217.

USGS. (2012). United States Geological Survey. <http://www.usgs.gov/> (visited on June 14, 2015).

Vosooghi A, Saiidi M. (2010a). "Post-earthquake evaluation and emergency repair of damaged RC bridge columns using CFRP materials". Center for Civil Engineering Earthquake Research, Department of Civil and Environmental Engineering, University of Nevada, Reno, Nevada, Report No. CCEER-10-05; 2010. p. 636.

Vosooghi, A., and Saiidi, M. (2010b). "Seismic Damage States and Response Parameters for Bridge Columns," *Structural concrete in performance-based seismic design of Bridges*, P. F. Silva and R. Valluvan, eds., American Concrete Institute, Farmington Hills, MI, SP-271-2, pp. 27-44.

Vosooghi, A., & Saiidi, M. S. (2012). "Design guidelines for rapid repair of earthquake-damaged circular RC bridge columns using CFRP". *Journal of Bridge Engineering*, 18(9), 827-836.

Vosooghi, A., and Saiidi, M. S. (2013). "Shake-table studies of repaired reinforced concrete bridge columns using carbon fiber-reinforced polymer fabrics." *ACI Structural Journal*, 110(1).

Yalcin, C., (1997). "Seismic Evaluation and Retrofit of Existing Reinforced Concrete Bridge Columns". PhD thesis. University of Ottawa, Ottawa, ON, Canada.

Yang, J., (2009). "Nonlinear Responses of High-Rise Buildings in Giant Subduction Earthquakes". PhD thesis. California Institute of Technology, CA, USA.

Yarandi, M. S., (2007). "Seismic Retrofit and Repair of Existing Reinforced Concrete Bridge Columns by Transverse Prestressing". PhD thesis. University of Ottawa, Ottawa, ON, Canada.

Yarandi, M., & Saatcioglu, M. (2008). Rapid seismic repair of shear damaged concrete bridge columns by transverse prestressing. In the 14th World Conference on Earthquake Engineering: October 12-17, Beijing, China.

Ying, X., Chen, G., Silva, P. F., LaBoube, R. A., & Yen, P. W. (2006). "Thin steel sheet wrapping on RC columns and steel plate strengthening on beam-column joints for seismic ductility and capacity improvements". In 100th Anniversary Earthquake Conference. Earthquake Engineering Research Institute.

Youm, K. S., Lee, H. E., & Choi, S. (2006). "Seismic performance of repaired RC columns". Magazine of Concrete Research, 58(5), 267-276.

Table 1. Parameters in Idealized Capacity Curves of As-built and Repaired Columns

Column	P_{cr} (kN)	P_{cr} (kN)	P_{cr} (kN)	P_{cr} (kN)	P_{cr} (kN)	P_{cr} (kN)
1	28,274.3	232,952.4	2,977.1	4,411.6	51,12.8	147,275
2	126,211.9	2,017,663	39,761.2	48,319	86,434	125,112.8

Table 2. Performance Measures of As-built and Repaired Columns

Column	As-Built	As-Built	As-Built	As-Built	As-Built	As-Built	As-Built
1	1176.139	2498.372	8738.23	5817.1	2.5	0.5	
2	1234.455	1456.789	2123.456	3210.987	1.2	0.7	

Table 3. Comparative Cost Analysis of Three Repair Methods

Item									
Materials									
Steel plate	12.6 kg	200kg	\$220						
Mounting plate	\$2,200/lot	0.35lot	\$770						
Carbon FRP sheet				\$2.0/m ²	90m ²	\$180			
Thin sheet metal							\$7.57/m ²	150m ²	\$1,135.5
Sealants							\$6.75/ea	10 pieces	\$67.5
Anchorage blocks							\$3.0/ea	10 pieces	\$30.0
Fabrication									
Two 100 es. 100 circular steel	\$300	3m	\$300						
Transportation									
Steel plate	\$200	Min	\$200						
Equipment material							\$200	Min	\$200
Rental									
Crane	\$40/h	22h	\$880						
Motor pump	\$300	1m	\$300						
Scaffolding	\$350	1m	\$350						
Personnel hiring							\$50/h	8h	\$400
Installation									
Skilled worker	\$35/h	22h	\$770				\$35/h	4h	\$140
Worker	\$25/h	87h	\$2,175				\$25/h	4h	\$100
Blasting gun/flow primer apparatus for 1" hole				\$350/m ²	3m ²	\$1,050			
Blasting gun/flow primer apparatus for 3/4" hole				\$80/m ²	33m ²	\$2,640			
Grand total			\$7,005			\$4,820			\$1,684

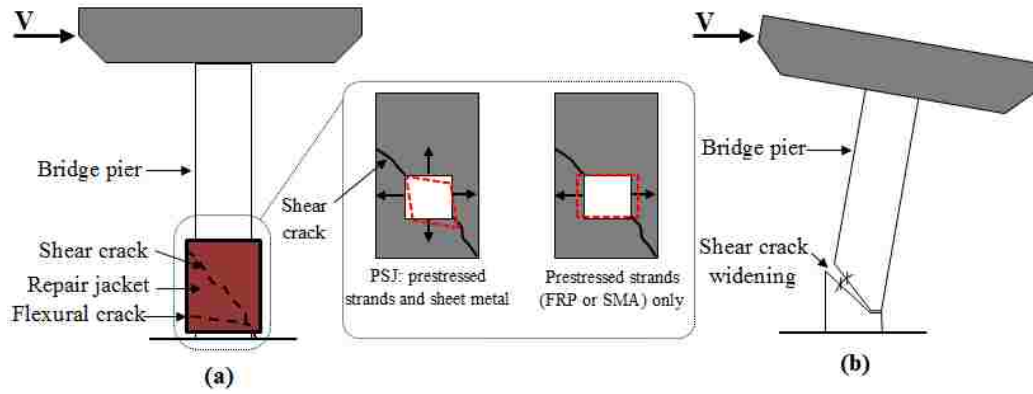


Figure 1. Shear crack arrest mechanism and bridge pier collapse: (a) bidirectional versus unidirectional restraints on crack opening, and (b) potential pier collapse due to continuous crack widening under aftershocks.

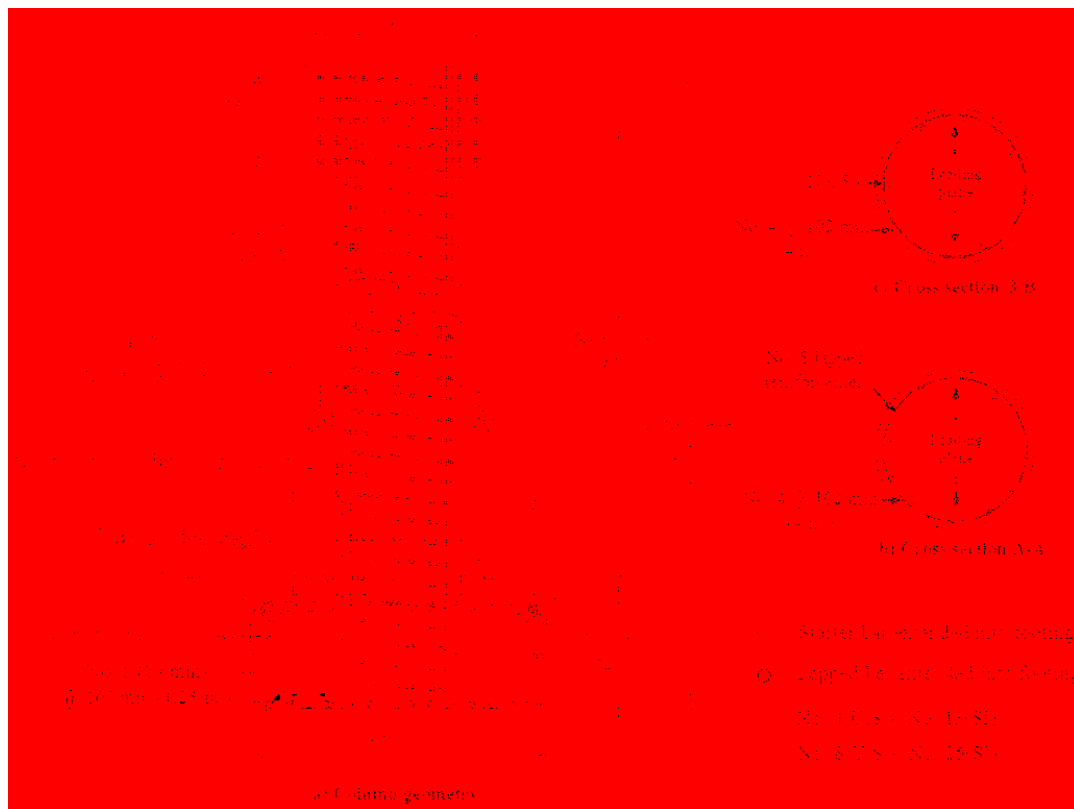


Figure 2. Dimensions and reinforcement details of as-built RC columns.

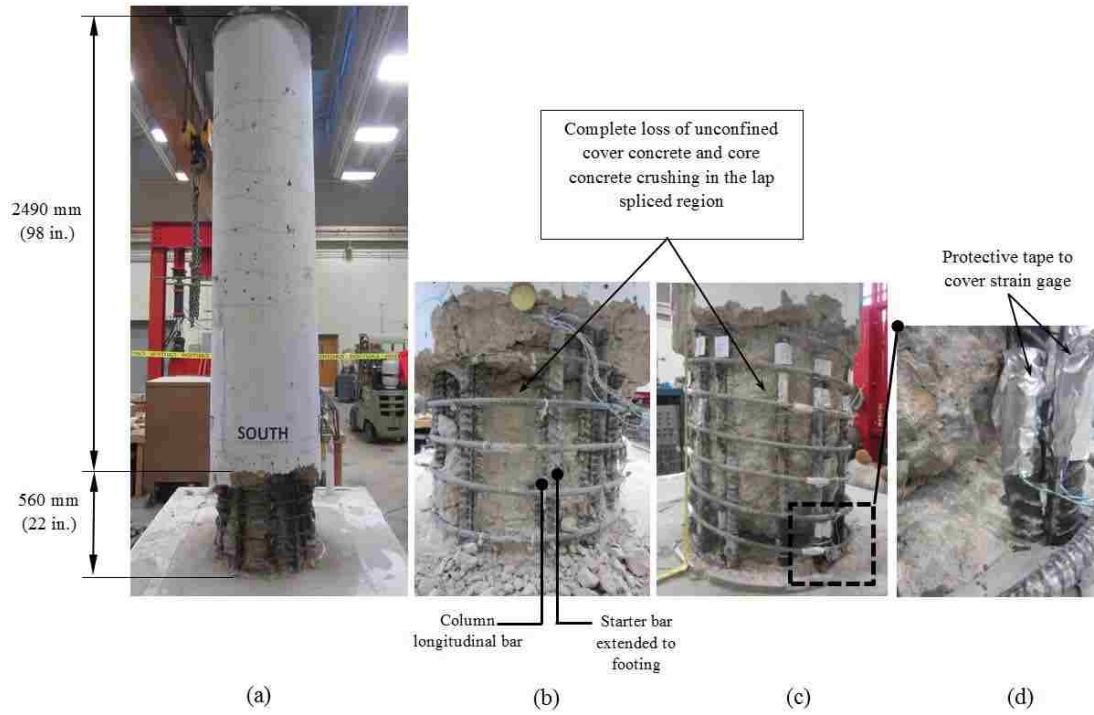


Figure 3. Damaged columns after removal of loose concrete: (a) plastic hinge region, (b) condition of Column 1, (c) condition of Column 2, (d) buckled longitudinal rebar.

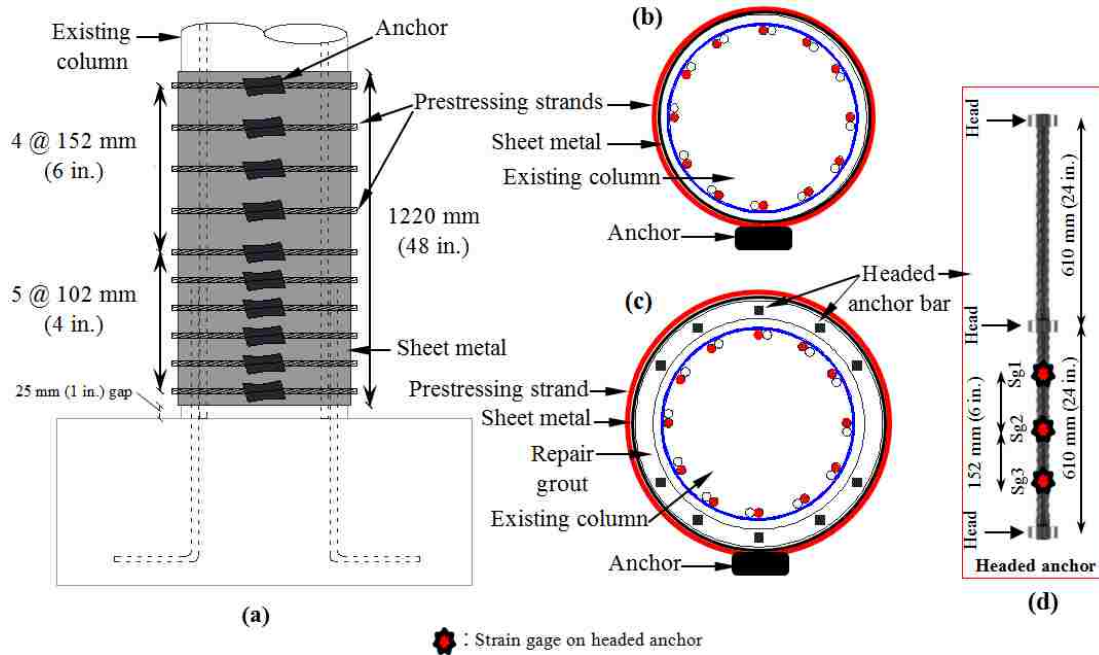


Figure 4. Final design of the PSJ: (a) plastic hinge repair for two damaged columns, (b) cross section of repaired Column 1, (c) cross section of repaired Column 2, and (d) No. 4 (12 mm) headed anchors.

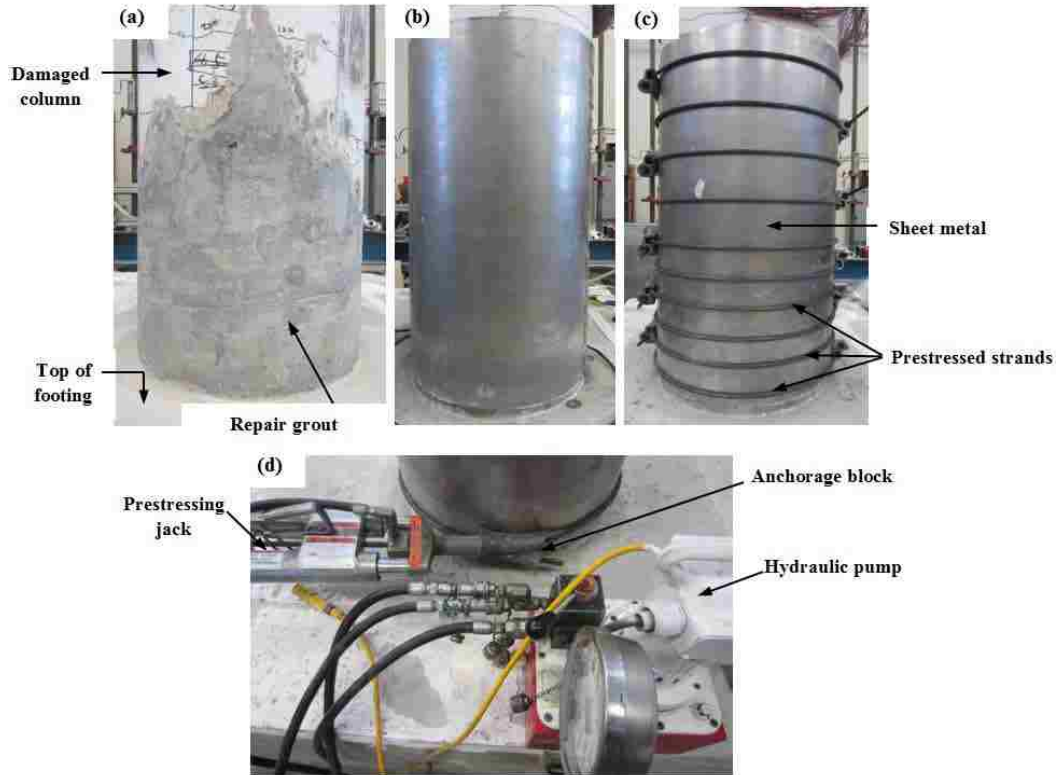
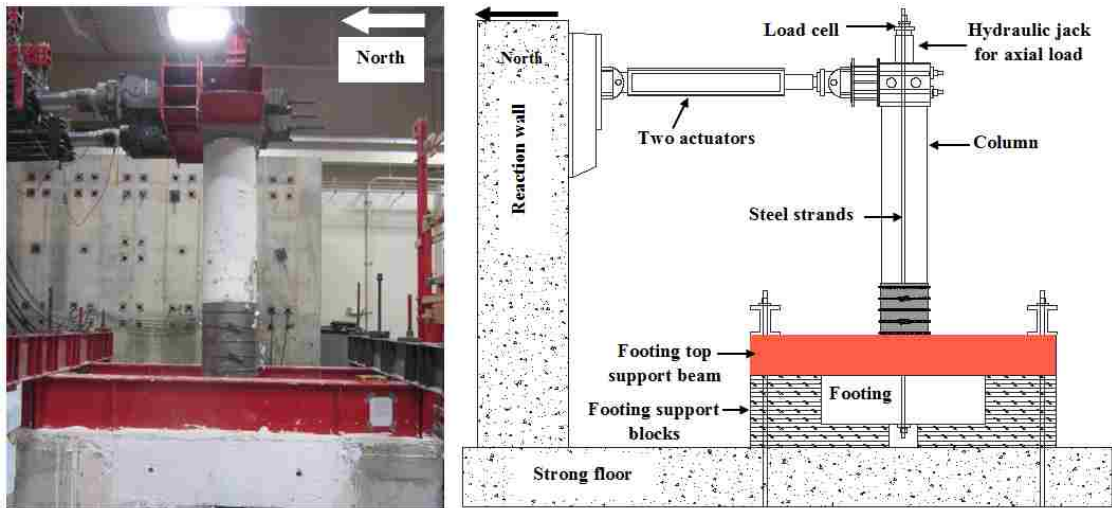


Figure 5. Repair method and procedure of Column 1: (a) restoration to the original column cross section, (b) thin sheet metal wrapping and joining, (c) strands wrapping and prestressing, (d) prestressing equipment.



(a)



(b)

Figure 6 Test preparation: (a) column setup, and (b) LVDTs and LPTs at the column-footing joint.

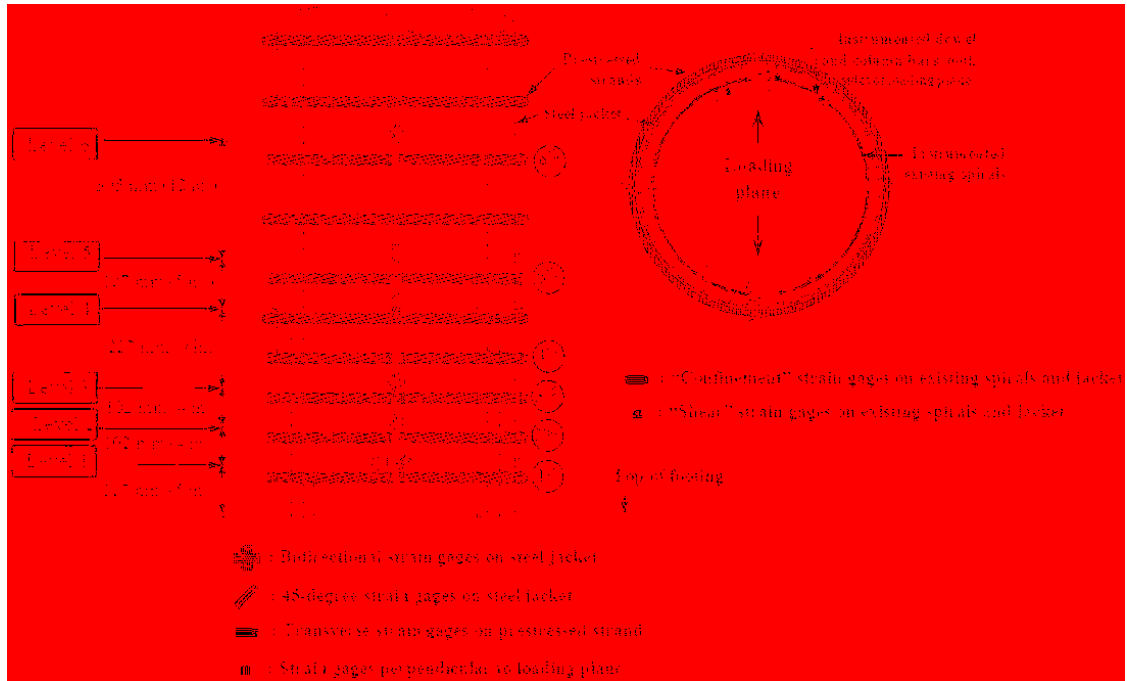


Figure 7. Location of strain gages on the jacket and reinforcement.

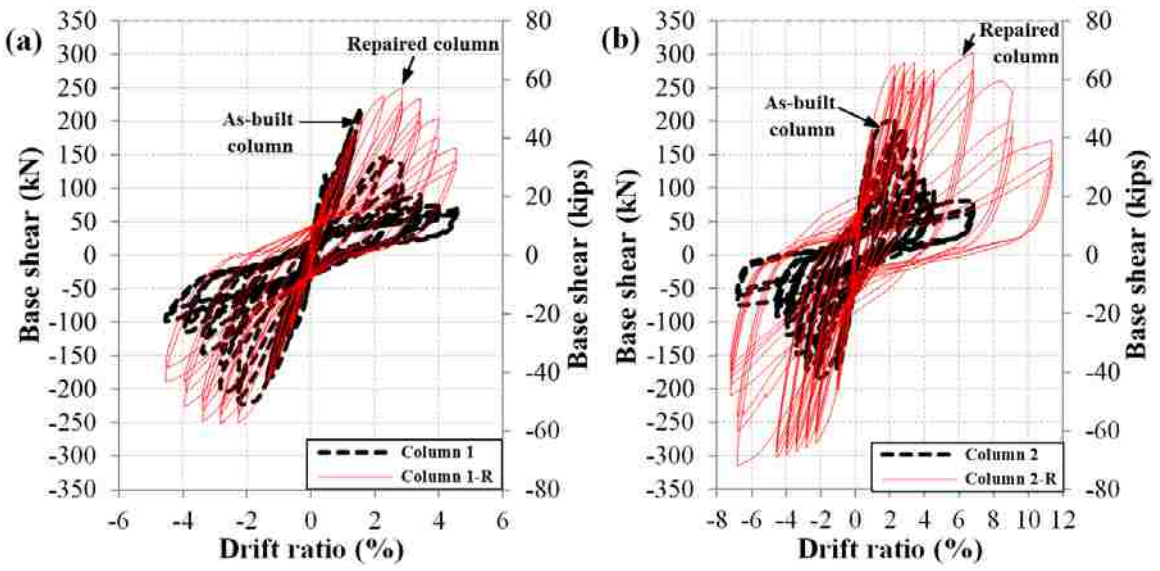


Figure 8. Hysteresis loops: (a) repaired Column 1-R compared to as-built Column 1, and (b) repaired Column 2-R* compared to as-built Column 2.

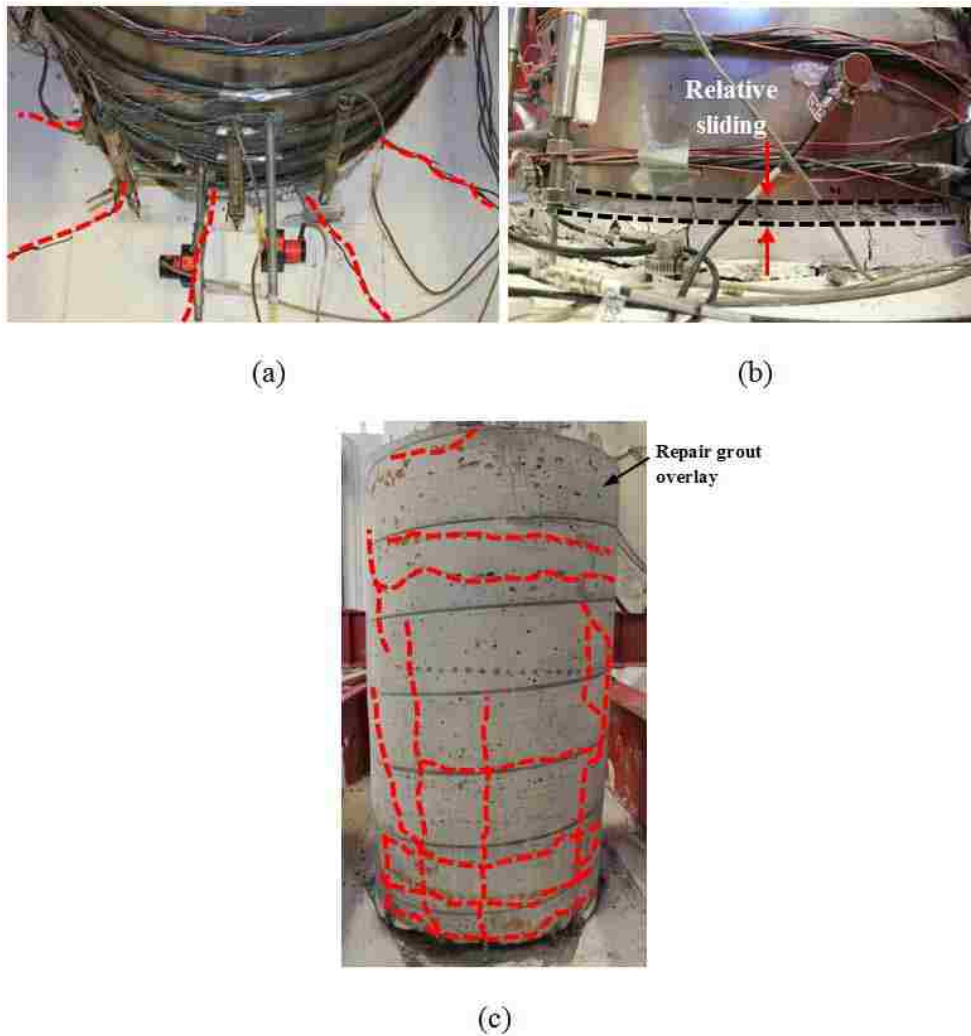


Figure 9. Failure modes: (a) concrete cracks on the top of footing associated with stress transfer through dowel bars in Column 1-R, (b) slip of steel jacket in Column 2-R, and (c) flexural cracks of repair grout overlay of Column 2-R after the jacket was removed at the completion of tests. Cracks are highlighted in dashed lines.

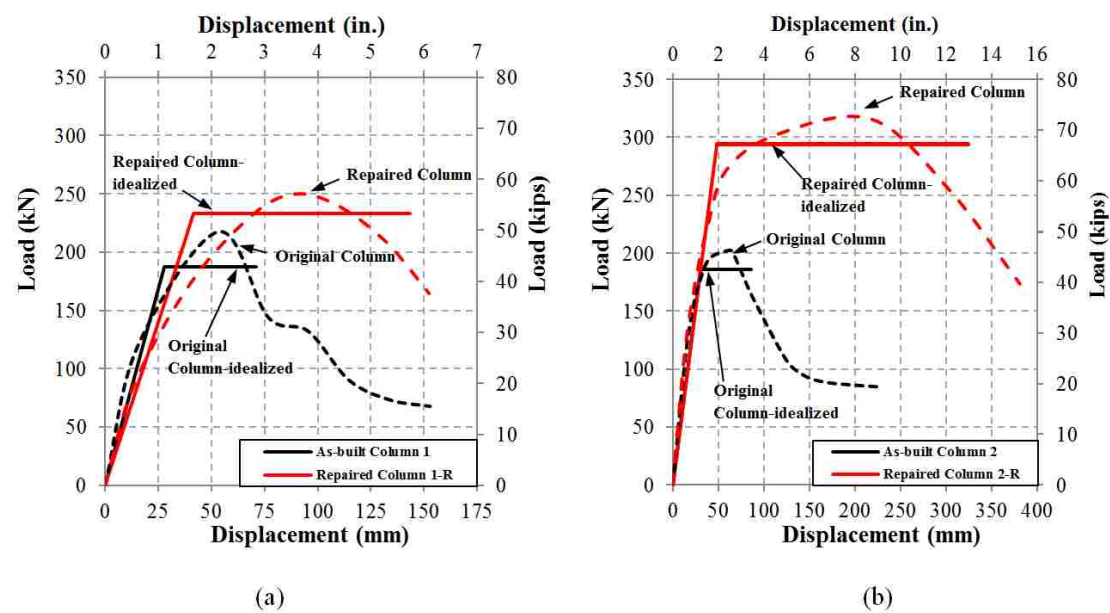


Figure 10. Envelope of actual and idealized load-displacement relationships of studied columns: (a) Column 1, and (b) Column 2.

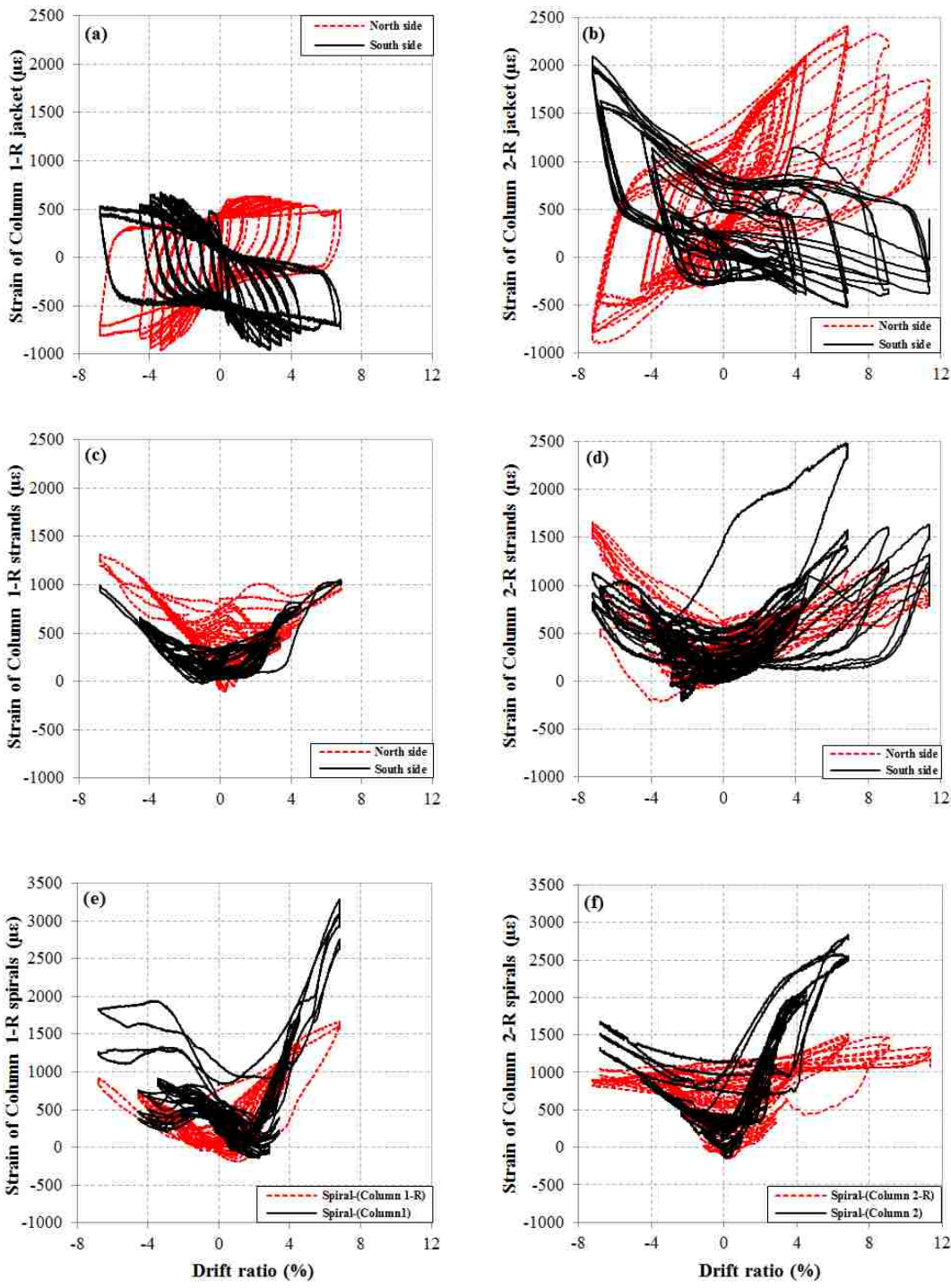


Figure 11. Average strain-drift ratio relationships of repaired Columns 1 and 2: (a, b) longitudinal strain on sheet metal, (c, d) transverse strain on prestressed strands, and (e, f) transverse strain on spirals.

III. SEISMIC PERFORMANCE OF POST-MAINSHOCK FRP/STEEL REPAIRED RC BRIDGE COLUMNS SUBJECTED TO AFTERSHOCKS

ABSTRACT

This study compares the performances of three types of repair jackets on mainshock (MS) earthquake-damaged RC bridge columns subjected to aftershock (AS) attacks. These repair jackets include fiber reinforced polymers (FRP), thick steel, and thin steel wrapped with prestressing strands. Results obtained from incremental dynamic time history analyses on refined numerical finite element bridge models were utilized to evaluate the efficacy of different repair jackets application on the post-MS collapse safety of RC bridges subjected to AS attacks of various intensities. Numerical results indicated that the three repair jackets can effectively improve the bridge collapse capacity by approximately 20% under severe MS-severe AS even though they cannot restore the initial stiffness of damaged columns. Repair jackets for the severe MS-damaged columns were ineffective under moderate AS events and thus not required. Steel repair jackets exhibited higher energy dissipation under MS-AS sequences than FRP jackets. In the case of FRP jackets, bidirectional fiber wraps are recommended for plastic hinge confinement of MS-damaged bridge columns subjected to aftershocks.

Keywords: *A. Carbon-carbon composites (CCCs); C. Finite element analysis (FEA); C. Numerical analysis; repair and retrofit.*

1. Introduction

Bridges are required to withstand a disastrous earthquake without collapses, and retain sufficient capacity along emergency routes prior to/during potential aftershocks in order to promptly dispatch emergency vehicles to the impacted area [1]. In seismically active areas, bridges are subjected to the combined effect of a mainshock (MS) and a series of aftershocks. For example, the March 2011 Tohoku, Japan, earthquake with a moment magnitude (M_w) of 9 was succeeded by hundreds of aftershocks with at least thirty of them greater than M_w 6 [2]. Compared to the MS, the aftershocks may have significant intensity with a longer effective duration, and different spectral shape, energy content and specific energy density [3]. Since the structural condition of damaged bridges immediately after the MS is often unknown due to strong motion variations and their propagation to structural behaviors [4], predicting the load-carrying capacity of repaired bridges during an aftershock (AS) becomes even more uncertain and challenging. While prediction of the post-earthquake load-carrying capacity of damaged structures is a challenging task [4] (still topic of extensive ongoing research!), it becomes even more onerous when the inelastic structural response under the aftershock (AS) event is considered [5].

Rapid repair of the damaged bridge columns after the MS event is essential for post-earthquake functionality and collapse prevention of the bridges under subsequent aftershocks. Usually due to close occurrences of MS and AS events, there is typically limited time for repair application. Different forms/types of fiber reinforced polymer (FRP) materials have been extensively studied for rehabilitation and new constructions in various structures [6, 7]. Retrofit and repair of reinforced concrete (RC) columns with FRP wraps, prestressed FRP belts, post-tensioned FRP shells, continuous composite fiber ropes, thick steel jackets, RC jackets, prestressing strands and shape memory alloy (SMA) wraps have also been investigated in extensive studies [8-31].

Bridge columns are one of the most vulnerable structural elements during seismic events [18-31]. The post-mainshock load carrying capacity of earthquake damaged bridges depends on the extent of damage present in RC columns [4, 18-21, 26]. While extensive studies have been conducted on the significance and efficacy of retrofit jackets

under MS events [18-31], this study is a preliminary attempt to investigate the efficacy of FRP repair jacket application on MS-damaged RC bridge piers subjected to AS attacks of various intensities, often termed as multiple earthquakes. Different studies have evaluated the MS-AS sequences on structures [1,3,5 amongst others], however, there is no comprehensive study on different repair jackets application on MS-damaged RC bridge structures subjected to AS attacks of various intensities. The only relevant work to this study is the work by Lee et al. [32] to evaluate the post-repair behavior of RC bridge columns under four sets of as-recorded ground motions, without taking into account the variation of AS attacks. Therefore, it is imperative to understand and quantify the significance and efficacy of different rapid repair techniques during uncertain AS events.

2. Post-earthquake resilience of mainshock-damaged bridges subjected to aftershocks

Bridges subjected to a seismic event may experience damage to different extents, depending on their strengths, dynamic characteristics and intensity of seismic event. Many studies have indicated the seismic vulnerability of MS-damaged bridge columns, if subjected to potential aftershocks, as substantial damage could accumulate during the MS event [18-26]. Therefore, the MS-damaged columns must be rapidly repaired prior to the occurrence of an AS event in practice. Then, the question that remains unanswered is how significant and effective various repair techniques are under AS attacks of various intensities. Fig. 1(a) illustrates a scenario MS-AS (or often termed foreshock-aftershock) acceleration time history with sufficient time between the MS and AS events to ensure that bridges cease to vibrate before the AS event occurs. The Arias intensity [33] of the MS only is compared in Fig. 1(b) with that of the MS-AS sequence. It can be seen from Fig. 1(b) that the energy for the MS-AS sequence accumulates over a longer time than that for the MS only, which could contribute to the so-called “long duration” effect on the behavior of damaged bridges.

The primary goal of this study is to evaluate the significance and effectiveness of transverse confinement provided on MS-damaged RC columns by three repair techniques for the increase of the structural collapse capacity of bridges subjected to AS events. These repair techniques include carbon FRP (i.e., CFRP jacket), conventional thick steel

jackets, and thin steel jackets wrapped with prestressing strands (i.e., hybrid jacket). Their effects on the post-repair behavior of bridges are compared under both near- and far-fault earthquakes and under different MS-AS sequences in terms of earthquake intensity. Recommendations on the fiber orientation of CFRP repair jackets for MS-damaged bridge columns are made. It should be emphasized that this manuscript is aimed at evaluating the efficacy of repair jackets on earthquake-damaged RC bridge columns. Interested reader for an in-depth review on the inelastic structural behavior of different systems under various intensities of MS-AS sequences, especially those exhibiting moderate to severe stiffness degradation, strength deterioration and pinching response, should refer to the relevant references in this area ([1,3,5], amongst many others).

To investigate the significance and efficacy of repair techniques for bridge columns, a prototype highway bridge was modeled and analyzed. Multi-span continuous concrete box-girder bridges have been increasingly constructed in the U.S. In particular, single-column bents were found to be most vulnerable to seismic excitations as observed during previous earthquake events [18-21, 23-28]. Therefore, a five-span box-girder bridge near Los Angeles, representative of a typical modern overpass [34] detailed and constructed according to the Caltrans Seismic Design Criteria [35], was selected as a prototype structure in this study. As shown in Fig. 2(a), the first and last spans were 36.5 m each and the three middle spans were 45.7 m each, making the overall bridge length 210.3 m. The box girder was supported on two abutments and four intermediate single-column bents. As indicated in Fig. 2(b), each column was 6.7 m tall and 1.2 m in diameter. It was reinforced with 28 No. 10 longitudinal deformed bars ($d_b=32.8$ mm, #10 in Customary Unit) and No. 4 spiral transverse deformed bars ($d_b=12$ mm, #4 in Customary Unit) at 89 mm spacing as illustrated in Fig. 2(b). The column aspect ratio is well above 2.5, indicating the dominant flexural behavior and a potential flexural failure due to formation of a plastic hinge. The foundation of each column consisted of 10 RC piles and a RC pile cap. The design yield strength of the reinforcing steel was 420 MPa. The design compressive strength of the concrete was 35 MPa.

3. Repair of mainshock-damaged bridge piers

3.1. Hybrid repair jacket

In this study, a new hybrid repair jacket recently proposed by the authors [36] will be compared with CFRP and conventional thick steel repair jackets. As shown in Fig. 3, the hybrid repair/retrofit jacket is comprised of a thin cold-formed steel sheet wrapped around a RC column and prestressing strands that are applied outside the steel sheet. The steel sheet and strands provide passive and active confinement on the repaired/retrofitted RC column, respectively. While the prestressing strands can prevent buckling of the confining steel sheet, the thin steel sheet can in turn prevent the prestressing strands from penetrating into cracked cover concrete and thus losing effective confinement. The thin cold-formed sheet metal is 1.27 mm thick and directly wrapped around the existing column after grout materials replacing the damaged concrete during the MS loading have been hardened as illustrated in Figs. 3(a, b). The repair is completed by placing and prestressing the strands and then welding the tightened sheet metal to form a cylinder around the damaged column. The hybrid jacket is flexible and easy to install for rapid application after a MS event with no heavy equipment requirement, so light that it adds no seismic inertial force, and requires no column surface preparation and adhesive material application. The most prominent structural feature of the hybrid jacket is that the thin steel sheet can resist shear crack opening both vertically and horizontally as illustrated in Fig. 4, while the prestressing strands (similar to any unidirectional jackets such as FRP, continuous composite ropes or SMA wires) can resist the shear crack opening in the transverse direction only. Thus, due to the enhanced aggregate interlock provided [37], concrete shear strength in the hybrid jacketed column is larger than that in columns with prestressing strands (FRP, composite ropes or SMA) only (detailed discussion in the results section 6.3.).

3.2. Repair techniques

Three repair techniques are considered in this study. In addition to the hybrid jacket as discussed in Section 3.1, a CFRP repair jacket and a conventional thick steel repair jacket are included in numerical analysis. The CFRP jacket was chosen as the first

repair technique due to its excellent strength-to-weight ratio, which becomes increasingly attractive for structural repair/retrofit projects [18, 19]. The disadvantage of the CFRP jacket is its requirement for surface preparation and adhesive application on a damaged RC column. The steel jacket was the first and the most widely used retrofit technique [18] due to its availability, price, and ductile behavior when compared with FRP materials with brittle failure. However, the steel jacket can not only involve intensive labor work in application but also increase the original cross section of the damaged column, thus changing the dynamic characteristics of a bridge and increasing the flexural strength of the column. As a result, a thick steel jacketed column would be subjected to an increased plastic shear demand and potentially trigger other failure modes in other capacity protected elements such as foundation [18, 19]. Therefore, active prestressing strands were considered as another repair technique. They can provide active confining pressure without increasing the cross section of the damaged column. However, potential penetration of the prestressed strands into the cracked cover concrete caused the loss of confining pressure in the active strands [18, 19]. To incorporate the low price of steel jackets into the benefit of active confining pressure, the hybrid confinement jacket was proposed and considered as the third seismic repair intervention [36].

3.3. Repair performance objectives

The bridge column repair design is aimed at restoring the shear strength and providing the required confining pressure in the plastic hinge. The repair jacket design procedure is briefly described here. The height of plastic hinge to be repaired, L_{pz} , was calculated according to the California Department of Transportation Seismic Provisions [35].

$$L_{pz} = \frac{3}{8} AR \times D \geq 1.5D \quad (1)$$

where AR = column aspect ratio, and D = column diameter.

The shear strength of a RC column was based on those of individual components and checked against the factored shear [20]. That is,

$$\frac{V^o}{\phi} < V_c + V_s + V_j \quad (2)$$

where V^o = base shear, $\phi = 0.85$, and V_c , V_s and V_j = shear resisted by concrete, existing transverse reinforcement, and repair jacket, respectively. Due to unknown extent of damage from a MS event, the shear resistance of the concrete and spirals were neglected, and the repair jacket was designed to resist the shear demand. The shear resistance for the different repair techniques was determined as follows [18-20]:

$$V_{cj} = 0.5\pi t_j f_{cj} D \cot \theta \quad (3)$$

$$V_{sj} = 0.5\pi t_j f_{yj} D \cot \theta \quad (4)$$

$$V_{sp} = 0.5\pi A_{ps} f_{ps} D s^{-1} \cot \theta \quad (5)$$

where V_{cj} , V_{sj} and V_{sp} = shear enhancement from CFRP jacket, steel jacket and prestressing strands, respectively; t_j = jacket thickness (CFRP or steel); D = column diameter; f_{cj} = hoop stress in the CFRP jacket; f_{yj} = steel jacket yield stress; A_{ps} = cross sectional area of prestressing strand; f_{ps} = level of prestressing stress in the strand; s = vertical spacing between prestressing strands; and θ = angle of the critical inclined shear-flexure crack to the column axis. For the hybrid repair jacket, the shear resistance was calculated as the contribution from both the steel jacket and the prestressing strands (i.e. $V_{sj} + V_{sp}$).

The required jacket thickness and spacing between prestressing strands to provide the adequate confining pressure in the plastic hinge region of damaged columns were calculated as follows [18, 19].

$$t_{cj} \geq \frac{215D}{E_{cj}} \quad (7)$$

$$t_{sj} \geq \frac{f_l D}{400} \quad (8)$$

$$s \leq \frac{A_{ps} (f_{ps} + 200)}{D} \quad (9)$$

where t_{cj} = CFRP jacket thickness; t_{sj} = steel jacket thickness; f_l = confining pressure in the plastic hinge region; E_{cj} is the CFRP modulus of elasticity; and the remaining parameters were defined previously. The maximum spacing between the prestressing strands should not exceed six times the diameter of the longitudinal reinforcing bar [19].

Fig. 5 schematically illustrates three types of repair jackets applied on the RC columns of the five-span bridge described in Section 3. The jacket height was determined to be $L_{pz} = 1,830$ mm. For all of the repair jackets, a 25-mm gap was considered between the bottom of the jacket and the adjacent member to avoid any undesirable force transfer to the adjacent member as specified in Fig. 5(a).

The CFRP jacket was assumed to have a tensile strength of 3800 MPa, modulus of elasticity of 227 GPa, and a rupture strain of 1.67%. The selected composite CFRP repair system consisted of unidirectional high strength carbon fabric with fibers perpendicular to the column longitudinal axis as indicated in Fig. 5(a). The required jacket thickness for the studied bridge columns was calculated as 2.98 mm (6 layers).

A 6.3-mm thick A36 steel with minimum yield strength of 400 MPa was required for the thick steel repair technique. Due to availability, a 10-mm thick steel jacket with yield strength of 400 MPa and modulus of elasticity of 200 GPa was considered as shown in Fig. 5(b). A 25 mm gap was left between the column and the jacket and later filled with repair grout.

For the hybrid jacket, the thin sheet metal used had yield strength of 680 MPa, tensile strength of 771 MPa, and elastic modulus of 207 GPa. Considering field application and formability of the sheet metal around an existing column without specialized equipment, a 1,830 mm wide sheet with a thickness of 1.27 mm was considered. The nominal 12 mm diameter seven-wire strands with the ultimate tensile strength of 1,937 MPa and modulus of elasticity of 200 GPa were considered for repair design. The spacing between strands and the required prestressing pressure in the strands were calculated as 728 MPa and 185 mm, respectively.

4. Nonlinear finite element modeling of a prototype highway bridge

The five-span bridge as shown in Fig. 2 was modeled with fiber based elements to explicitly simulate concrete and reinforcing steel fibers as illustrated in Fig. 6(a). On one hand, throughout this study, the bridge deck and box girder were observed to experience elastic deformation and thus can be equivalently modeled by elastic frame elements. On the other hand, the bridge columns experienced inelastic deformation to various degrees under MS excitations as shown in Fig. 6(a) or during AS events after different repair

strategies had been implemented as indicated in Fig. 6(b, c). As such, only the discretization of a representative column cross section into many fibers is detailed and presented in Fig. 6. The bridge model was subjected to uniform ground motions in transverse direction at all supports.

To illustrate the general capability of such a computational model under a scenario MS-AS event as shown in Fig. 1(a), Fig. 6 schematically presents the overall bridge behavior with different column repair strategies implemented. Specifically, Fig. 6(a) shows an incipient collapse state of the five-span bridge subjected to a high intensity MS event. Figs. 6(b, c) indicate the influence of existing damage from the MS event on the post-MS behavior of the bridge. Column failure as indicated in Fig. 6(b) could be avoided if repair jackets were installed prior to the AS attack as shown in Fig. 6(c). Note that the bridge deformation presented in Fig. 6 is amplified by 100 times for clarity.

The finite element models presented in Fig. 6 were developed and analyzed using SeismoStruct nonlinear analysis software [38]. The program is capable of predicting the large displacement behavior of space frame structures under static and dynamic loading with both geometric nonlinearity (P- Δ effect) and material inelasticity properly taken into account [39]. The fiber based modelling approach using the inelastic beam-column element discretized by uniaxial fiber elements was adopted to develop the numerical models. The calibrating parameters of nonlinear fiber discretized column elements were checked against two analytical column modeling strategies [40, 41]. Many studies [4, 20, 21, 39-44] have demonstrated the accuracy of adequately calibrated fiber elements in predicting the lateral force-displacement hysteresis relationship of different structural systems under static and dynamic loading conditions. The element cross sections were represented by assemblages of longitudinally oriented, unidirectional steel and concrete fibers as shown in Fig. 6. Each fiber was associated with a prescribed uniaxial stress-strain relationship that could be specified to represent the unconfined cover concrete, confined core concrete (i.e. steel confined or CFRP confined), or longitudinal reinforcement. The sectional stress-strain state of the inelastic column elements was then obtained through the integration of the nonlinear uniaxial stress-strain of individual fibers. Hilbert-Hughes-Taylor integration scheme [43] was utilized to acquire the global flexibility matrix of flexibility-based elements that take into account the potential strain

softening or localized deformations. The obtained forces and inelastic deformations were then distributed through fiber-based sections spread along the element length with each section represented by an integration point. The fiber discretized plane sections were assumed to remain plane throughout the analysis with strain compatibility between the longitudinal reinforcement and the surrounding concrete. Bond-slip deformations, shear deformations, P-delta effects, and strain rate effects on material properties were considered analytically.

4.1. Constitutive laws of materials and column fiber modeling

The Menegotto-Pinto [45] steel model with Filippou [46] hardening rules and Fragiadakis [47] additional memory rule for higher numerical instability/accuracy under transient seismic loading was used for the reinforcing steel material. To incorporate the accumulated damage in steel reinforcement, the steel properties were modified [20] to consider the Bauschinger effect [48], which resulted in lowering the reversed yield stress and the reversed stiffness. For concrete the nonlinear variable confinement model of Madas and Elnashai [49] with Martinez-Rueda [50] cyclic rules was used. The variable confinement algorithm enabled the explicit computation of the relation between the concrete lateral dilation and straining of the transverse reinforcement computed at every analysis step. For the FRP confined concrete, the Ferracuti and Savoia [51] model following the constitutive relationship and cyclic rules proposed by Mander et. al. [52] and Yankelevsky and Reinhardt [53] under compression and tension, respectively was utilized. This model implements the Spoelstra and Monti [54] model for the confining effect of FRP wrapping. The FRP material was considered as linear elastic material up to rupture with zero compressive strength.

The effect of lateral confining pressure on concrete model in compression is illustrated in Fig. 7(a). The typical stress-strain relationships for virgin and damaged steel reinforcement are presented in Fig. 7(b). In the case of retrofit, the jacket is applied on the intact column cross section with no damage. For a repair scenario, the repair jacket is implemented after a column has experienced some extent of damage. As shown in Fig. 7(b), due to existing damage, the initial stiffness and post-yield strain hardening of steel reinforcement are reduced [20, 21].

Fig. 8 details two idealized column fiber models. Each model includes an inelastic spring defined as “zero length link element” to represent bond-slip and shear deformation behaviors as typically included into a member pinching/degrading hysteresis response. The spring was constrained to the coincident column node with “Equal DOF”. Both lumped plasticity (inelastic plastic hinge element) and distributed plasticity (inelastic distributed element) frame elements were investigated in this study. The bond-slip spring [44] was modelled through a symmetric curve link element in tension and compression as the backbone envelope of a smooth hysteresis loop with deterioration behavior [55, 56]. The hysteresis loops were determined to conform to the appropriate hysteretic model [57] for inelastic time history analysis with strength/stiffness degradation.

The approximate shear deformation of link element was included by using the cracked cross section to calculate the elastic shear stiffness of a member [57]. In this way, shear stiffness degradation is proportionate to the member’s flexural stiffness. Note that fiber discretized sections with uniaxial constitutive laws were used in the finite element model and the fiber element is incapable of accurately aggregating shear deformations.

4.2. Model validations with experimental results

The authors have previously validated the analytical model of FRP jacketed concrete columns [58]. To further validate the computational model for the evaluation of bridge behavior under MS-AS sequences, several full-scale RC column/bridge test results under multiple series of ground motions were taken as discussed below.

An RC cantilever column [59] typical of modern bridge construction - like the one in Fig. 2 - was tested under constant axial load and unidirectional quasi-static incrementally increasing lateral displacement up to failure was selected [59]. Figs. 9(a) and 9(b) demonstrate the high accuracy of both lumped and distributed plasticity elements in predicting the hysteretic behavior of the experimental column specimen in terms of strength, stiffness and displacement capacity.

A full-scale RC bridge column subjected to a series of six incremental ground motions developed by PEER and NEES [60] as part of a blind prediction contest was selected. The input ground motions commenced with the low intensity excitations succeeded by high intensity motions to bring the bridge column to the incipient collapse

state. The numerical model was developed adopting the proposed recommendations by Bianchi et al. [61]. Figs. 9(c) and 9(d) demonstrate the capability of the numerical models in reproducing the dynamic hysteresis behavior of the studied bridge pier. The selected pier specimen exhibits a significantly high level of nonlinearity (both material inelasticity and geometric nonlinearity). The numerical models could successfully capture the seismic response of the pier specimen subjected to six seismic sequences of various intensities.

Another RC cantilever column (Column A10) tested under a constant axial load and a random cyclic displacement history was considered [62]. The applied displacement history simulated a sequence of five seismic events (minor, moderate, minor, major and severe earthquakes) to investigate the effects of load path and multiple earthquakes on the accumulated damage in RC columns. Figs. 9(e) and 9(f) indicate the reasonably accurate results obtained from the numerical simulations under numerous inelastic displacement excursions.

To further validate the proposed modeling procedures in simulating the response of bridges subjected to seismic sequences, a large-scale bridge specimen tested in a pseudo-dynamic manner was selected [63]. The bridge specimen was subjected to two successive input motions in shake table tests, including the design level earthquake and then the 1.2 times the design earthquake. The bridge deck was modelled using elastic frame elements [64]. Both distributed plasticity and lumped plasticity elements were adopted to model the bridge columns. For the lumped plasticity model, the plastic hinge length and the strain penetration depth were calculated according to Priestley et al. [57]. The middle-column displacement time histories predicted with the distributed and lumped plasticity models are compared with experimental results in Fig. 10. The results indicate the adequacy of both types of element formulations in predicting the displacement time history and the maximum displacement with reasonable accuracy.

In summary, the developed finite element models were shown to provide sufficient accuracy in terms of initial stiffness, yield strength, base shear capacity, loading and reloading path, and pinching effect. They were therefore adopted for performance-based evaluation of the five-span bridge in the current study.

5. Nonlinear static analysis

Nonlinear static analysis commonly referred to as static pushover analysis (SPA) was conducted for a single column bent of the bridge under investigation. The SPA was performed to assess the post-repair lateral load-carrying capacity of a damaged column. Different levels of damage resulted from minor, moderate and severe MS were approximated in the numerical column model using the approach as described below. Then, the repair was incorporated onto the damaged column and the SPA was utilized to determine the post-repair lateral load carrying capacity of the bridge column. It should be noted that this procedure was approximate for a preliminary evaluation of the CFRP jacket design before an extensive number of nonlinear dynamic time history analyses (NTHA) under MS-AS sequences are executed.

The extent of damage in bridge columns after a seismic event largely depends on the intensity, frequency content, and duration of ground motions [1, 5, 65-68]. Therefore, different damage levels from MS attacks of various intensities must be defined to properly reflect the effect of existing damage on the post-repair behavior of columns under AS attacks. In this study, three damage levels were considered, namely minor, moderate and severe. Subsequently, prior to SPA analysis, a total of 240 NTHA of the bridge bent using minor, moderate and severe magnitude earthquake records were undertaken. Such a process is also termed as cloud approach in the context of probabilistic seismic demand analysis [69]. Eighty ground acceleration time histories were considered at each magnitude level, 40 of which represented far-fault motions and 40 included near-fault characteristics. In other words, the bridge bent was analyzed under 80 minor, 80 moderate and 80 severe magnitude time histories, respectively. The selected ground motions are detailed in Section 6.2.

During the NTHA analyses, the state of stress and strain in the steel and concrete fibers at the selected integration points, the maximum drift demand, and the hysteretic behavior of the RC column were monitored against the damage limit states as described in Section 6.1 to evaluate the extent of damage/nonlinearity in the steel and concrete fibers. As expected, records from severe earthquakes caused the highest extent of material nonlinearity and minor earthquakes resulted in a least extent of damage.

Monitoring the stress-strain state of selected fibers allowed for an approximate incorporation of different damage states under MS attacks of various intensities. The reinforcing steel properties were reduced for damaged RC columns [20]. Based on the reduced material properties for steel and concrete and the relevant recommendations [20, 66-68], three numerical models of the column bent were developed incorporating three levels of damage: minor, moderate and major.

The lateral load carrying capacity of the bridge column (Bent 4) was established through the SPA. The damaged bridge column was analyzed in four cases with unrepaired, CFRP repaired, steel repaired and hybrid repaired jackets, respectively. For the repaired column, one repair jacket was considered prior to the SPA. Figs. 11(a-c) illustrate the capacity curves of the column with minor, moderate and severe damage, respectively. For the severely damaged column, the effect of confining pressure due to different number of CFRP layers is shown in Fig. 11(d). As a point of reference, the capacity curve for the original column with no prior damage is included in Fig. 11.

5.1. Column with minor damage

Fig. 11(a) illustrates the lateral load carrying capacity of the column with minor damage associated with a minor MS. It can be seen that the material degradation due to the minor earthquake was insignificant as the unrepaired column experienced only a 10.8% strength reduction compared to the original column with no damage. The ultimate displacement capacity of the damaged column is essentially equal to the original column. Each of the repair jackets was shown to be relatively ineffective on the strength and displacement capacity of the repaired column. However, the conventional thick steel jacket had the highest strength increase of the repair alternatives considered due to increased cross section.

5.2. Column with moderate damage

Fig. 11(b) illustrates the capacity curve of the column with moderate damage from a moderate MS. While the original column exhibits a hardening post-yield behavior, the unrepaired column demonstrated a plateaued response at nominal yield strength due to the damage from the MS. The initial elastic stiffness of the unrepaired column is

approximately 87.4% that of the original column due to reduced stiffness of steel reinforcement and cracked concrete. The peak lateral strength and drift capacity of the unrepaired bridge were reduced by 26.2% and 15.4%, respectively, compared to the original column. On the other hand, the CFRP, steel and hybrid repaired column exhibited a peak strength of 817 kN, 908 kN and 862 kN, respectively. These strengths respectively corresponded to 80.1%, 89.9% and 85.3% of the strength of the original column. The repair jackets cannot restore the peak strength of the original column. However, the repaired columns exhibited a hardening behavior with less than 20% strength reduction, which is acceptable in most seismic codes (e.g. Caltrans [35]). The initial elastic stiffness cannot be restored with repair jackets.

5.3. Column with severe damage

Fig. 11(c) shows the capacity curve of the column with severe damage. In comparison with Figs. 11(a, b), it can be seen from Fig. 11(c) that the increased damage from a high intensity MS dramatically decreased the seismic capacity of the unrepaired column. In this case, the effect of repair jackets becomes significant as the unrepaired column stiffness was reduced to 68.1% of the original column. The unrepaired column reached its peak strength at a relatively small drift level (around 2.41%). The peak strength and displacement capacity of the damaged column in the unrepaired condition was 73.1% and 46.0% of the original column, respectively. The repaired columns exhibited satisfactory performance since they prevented premature strength deterioration and the obtainment of considerable lateral drift. Even so, all the three repair jackets cannot restore the stiffness of the original column due to severe damage from the MS.

5.3.1. Confining pressure variation on the column with severe damage

In order to evaluate the adequacy of the CFRP jacket design to provide the required confining pressure in the plastic hinge region of the studied column in the severe damage state, different levels of confining pressure (i.e., different number of CFRP layers) were considered. As shown in Fig. 11(d), a confining pressure of 815 kPa, 2489 kPa, 4096 kPa and 8193 kPa (corresponding to 2, 6, 10 and 20 layers of CFRP, respectively) were considered in the plastic hinge region. It can be observed that the

repair design with 6 layers of CFRP seemed appropriate since additional CFRP layers contributed a marginal increase of the load carrying capacity of the column. On the other hand, insufficient confinement (2 layers of CFRP) resulted in significant degradation of post-peak behavior.

Overall, none of the repair jackets could restore the initial elastic stiffness of the repaired column to that of the original column. This observation is consistent with experimental studies [21, 23-25]. However, the confining pressure associated with repair jackets contributed significantly to the drift capacity of the repaired columns.

6. Incremental dynamic analysis

The SPA indicates that the load carrying capacity of a bridge subjected to an AS event is directly related to the level of damage that the bridge has experienced during the previous MS event. However, the SPA lacks a rigorous theoretical foundation since the nonlinear response of a bridge is assumed to be related to the response of an equivalent single-degree-of-freedom system [70]. The inherent inability of SPA to correctly determine the seismic demands, specifically for structures that deform far into their inelastic range of behavior (expected for structures subjected to MS-AS sequence) has been clearly documented in many studies [58, 70, 71].

Therefore, incremental dynamic analysis (IDA) [72] was incorporated to accurately evaluate the seismic demand and capacity of a repaired bridge under various sets of MS-AS sequences so that the bridge structural collapse capacity can be predicted satisfactorily [70, 71]. Each IDA requires a series of NTHA of the bridge structure under incrementally increasing ground excitations. The IDA analysis starts from a very low (non-negative) scaling factor multiplied by the intensity measure (IM) of each unscaled ground motion time history. The scaling factor for each run is incrementally increased until the structural median collapse is reached. Each data point on the IDA curve corresponds to a single NTHA for the structure subjected to one ground motion time history scaled to one intensity level. This procedure is repeated to obtain all the data points – from elastic to inelastic and finally to global dynamic instability - for the full range of IDA curves.

The use of peak ground acceleration (PGA) as an IM for structures with the dominant first mode of vibration may result in biased structural response predictions [72]. For structures with a moderate period of vibration, the maximum drift ratio as a damage measure (DM) changes little when subjected to a group of scaled and unscaled ground records so long as the 5% damped first mode spectral acceleration ($Sa(T_1,5\%)$) remains the same. Therefore, the $Sa(T_1,5\%)$ is adopted as the IM in this study as often recommended in the literature [72,73].

Engineering demand parameter (EDP) is the output of the IDA analysis that elicits the state of structural damage in terms of its response under different earthquake records. For brevity, the IDA results are presented only in terms of maximum drift ratio as the demand parameter.

6.1. Damage/limit state

The damage states considered include: minor, moderate, extensive and collapse and were correlated with the quantitative engineering demand parameters. The drift-based limit states developed by Dutta and Mander [74] were adopted to define the bridge columns drift limits. The drift limits considered for the bridge columns were 0.008, 0.01, 0.025, 0.05 and 0.075 for no damage, minor, moderate, extensive and collapse damage states, respectively. However, these constant drift limits better serve as a global (system) response quantity. For a more accurate evaluation, the strain limit states (local response quantity) [57] was incorporated as well. Using the moment curvature and pushover analysis the strain limits can be related to drift limit states. The maximum compressive strain in the confined core concrete and the maximum tensile strain in the longitudinal reinforcing steel were considered as the strain-based limit states [57].

In addition, the bar buckling and bar fracture damage states were calculated according to the equations developed by Berry and Eberhard [40]. The complete failure limit state of a column was defined as the lateral drift level beyond the peak strength when the column reaches zero strength; it can be calculated according to Mackie and Stojadinovic [75].

6.2. Mainshock-aftershock seismic ground motion records

The ground motions used in this study were selected from the Pacific Earthquake Engineering Research Center (PEER) Strong Motion Database [76], which was developed to provide several standardized sets of ground motions for the PEER's Transportation Research Program. The selected ground motions are neither site-specific nor structure specific (i.e., unbiased).

Two bins of earthquake records were considered to generate the MS-AS excitation sequences. Ensemble 1 constitutes far-fault records. Ensemble 2 constitutes near-fault records. The acceleration response spectra of the two ensembles of unscaled ground motions are presented in Figs. 12 and 13, respectively. Each ensemble constitutes records of large, moderate and minor magnitude.

Two seismic sequences from each ensemble of earthquake records were considered: (1) severe MS-moderate AS and (2) severe MS-severe AS, each resulting in 80 scenario MS-AS ground motions. For example, the severe MS-moderate AS sequence in ensemble 1 includes 40 far-fault records from earthquakes of large magnitude as shown in Fig. 12(a) and 40 far-fault records from earthquakes of moderate magnitude as shown in Fig. 12(b). Similarly, the severe MS-severe AS in ensemble 1 includes 40 far-fault records from earthquakes of large magnitude in Fig. 12(a) as MS events and the same 40 far-fault records as AS events. Similar procedure was used to generate the earthquake records in ensemble 2. No paired seismic sequence mixed from ensemble 1 and ensemble 2 was considered in this study (i.e., no near fault MS-far fault AS or opposite). Hence, a total of 160 paired accelerations (40 severe MS-moderate AS and 40 severe MS-severe AS from ensemble 1 and 2) were used in the following IDA. To ensure that the bridge ceases to vibrate at the end of the MS record, twenty seconds of zero acceleration was introduced between the MS and AS events as illustrated in Fig. 1(a).

For each intensity level, the selected ground motions were scaled to match the Los Angeles-California site (location of the studied bridge in California) response spectrum for three different hazard levels, namely 50% probability of exceedance in 50 years (minor earthquake), 10% probability of exceedance in 50 years (moderate earthquake), and 2% probability of exceedance in 50 years (severe earthquake) (Figs. 12, 13). The

target response spectra were utilized to scale the original records at each intensity level. The selected unscaled ground motions from the severe (Fig. 12(a)), moderate (Fig. 12(b)) and minor (Fig. 12(c)) intensity record sets from ensemble 1 were scaled considering the 2%, 10% and 50% in 50 years target response spectra, respectively, to calculate the scaled severe, moderate and minor magnitude records for ensemble 1. The same procedure was adopted to scale the original records from the ensemble 2 set of records. The characteristics of ensemble 1 and 2 record sets are detailed below.

Ensemble 1 (far-fault): for this set the large magnitude suite of records consists of 40 broad-band ground motions that their response spectra match the median and log standard deviations predicted for a large magnitude ($M_w=7$) strike-slip earthquake at a distance of 10 km. The moderate magnitude motions constitute 40 broad-band ground motions with their response spectra matching the median and log standard deviations predicted for a moderate magnitude ($M_w=6$) strike-slip earthquake at a distance of 25 km. The minor magnitude ground motions (for NTHA analyses) consist of 40 records obtained by scaling the large magnitude records [77]. The selected set of ground motions as the far fault records represent a very broad range of spectral amplitudes up to two orders of magnitude. These set of records cover a broad range of intensities at sites located near active crustal earthquake sources [76]. The acceleration response spectra of the ensemble 1 ground motions are presented in Figs. 12(a)-12(c), respectively.

Ensemble 2 (near-fault): For this set the large magnitude ground motions consists of 40 records containing strong velocity pulses of varying periods. The velocity pulses are typically observed in the near fault ruptures due to directivity effects. The minor (for NTHA analyses) and moderate magnitude ground motions consist of 40 records each obtained from scaling the large magnitude records [77]. The acceleration response spectra of the ensemble 2 ground motions are presented in Figs. 13(a)-13(c).

6.3. IDA analysis results and discussion

For brevity IDA results are presented in Figs. 14 and 15 only in terms of the spectral acceleration at the first mode period of vibration as an intensity measure and the maximum drift as an engineering demand parameter.

For each series of analyses, four cases were considered with bridge columns unrepaired (Fig. 14(a) and Fig. 15(a)), repaired with CFRP jacket (Fig. 14(b) and Fig. 15(b)), repaired with conventional steel jacket (Fig. 14(c) and Fig. 15(c)), and repaired with hybrid jacket (Fig. 14(d) and Fig. 15(d)). All columns of the studied bridge were repaired prior to the AS event. Each IDA curve corresponds to one MS-AS pair of ground motions. Due to space limitations, only the IDA curves for severe MS-severe AS ground motions are presented in Fig. 14 for far-fault records (ensemble 1) and Fig. 15 for near-fault records (ensemble 2). To evaluate the impact of damage from the MS-AS sequence compared to an MS event only, the median of the IDA results for the bridge subjected to severe MS only (i.e., no AS event) is superimposed on Figs. 14(a) and 15(a) accordingly (red dotted line). In the following discussion, the structural collapse capacity is defined as the maximum spectral acceleration that a bridge can withstand.

It can be seen from Figs. 14(a) and 15(a) that the occurrence of severe MS-severe AS events significantly reduced the mean structural collapse capacity of the unrepaired bridge from 3.15g to 1.23g (60.9% reduction) under far-fault motions and from 3.06g to 1.33g (56.5% reduction) under near-fault motions. Correspondingly, the maximum drift that the unrepaired bridge can sustain prior to collapse was reduced from 5.74% to 4.13% under far-fault motions and from 5.56% to 4.16% under near-fault motions. They correspond to 27.9% and 25.2% reduction in maximum attainable drift level prior to collapse, respectively. Based on the obtained mean collapse capacity and maximum drift, the bridge designed with modern seismic detailing can adequately sustain a severe MS event as expected. However, the existing damage from a severe MS event had significantly reduced the strength/deformation capacity of the unrepaired bridge for the subsequent severe AS event of the similar magnitude to the MS event. However, it should be noted that the severe MS-severe AS is an extreme scenario and the obtained collapse capacity is the lowest bound for the structural collapse capacity (i.e., AS event is often considered of smaller intensity compared to the MS event).

It can be observed from Figs. 14(b-d) that the mean structural collapse capacities for the CFRP, conventional steel, and hybrid repaired bridge columns under severe MS-severe AS sequences from far-fault records were respectively 1.47g, 1.52g and 1.51g, or 19.51%, 23.6% and 22.8% increase in comparison with the unrepaired bridge (1.23g).

Similarly, under near-fault records as shown in Figs. 15(b-d), the mean structural collapse capacities for the CFRP, conventional steel, and hybrid repaired bridge columns under severe MS-severe AS sequences were 1.53g, 1.59g and 1.56g, or 15.9%, 20.5% and 18.2% increase in comparison with the unrepaired bridge (1.33g). The abovementioned results for the severe MS-severe AS sequences are summarized in Figs. 16(a, b) for far-fault and near-fault motions, respectively. Once again, the three repair jackets can all increase the mean structural collapse capacity of the damaged bridge columns under severe AS by approximately 20%. By monitoring the stress-strain state of concrete and reinforcing steel fibers during extensive analyses, the primary damage/nonlinearity was in the form of steel yielding instead of confined concrete crushing. Hence, the additional confinement by jacketing proved to be effective, but to limited extent under severe AS events.

Figs. 16(c, d) present the summary of IDA results for severe MS-moderate AS sequences for far-fault and near-fault motions, respectively. In this case, the occurrence of a moderate AS event reduced the mean structural collapse capacity of the unrepaired bridge from 3.15g to 2.75g (12.7% reduction) under far-fault motions and from 3.06g to 2.84g (7.2% reduction) under near-fault motions. These reductions demonstrate a conservative, but reasonable approximation of the structural capacity reduction by SPA (26.2%). For the repaired bridge subjected to far-fault ground motions, the mean structural collapse capacities (2.78g, 2.75g and 2.85g) with CFRP, steel and hybrid repair jackets were close to the collapse capacity (2.75g) of the unrepaired bridge. Similarly, under near-fault ground motions, the mean structural collapse capacities (2.91g, 2.95g and 2.90g) with CFRP, steel, and hybrid repair jackets were also close to the collapse capacity (2.84g) of the unrepaired bridge.

The effect of earthquake types can also be evaluated from Figs. 16(a, b). For MS events only, the mean structural collapse capacity (3.06g) under near-fault motions is smaller than that (3.15g) under far-fault motions. This is expected due to the directivity and short pulse effects of near-fault records. However, for both severe MS-severe AS and severe MS-moderate AS sequences, the mean structural collapse capacity of the repaired bridges under near-fault motions was larger than that under far-fault motions. For instance, for the CFRP jacketed bridge under the severe MS-moderate AS sequence, the

collapse capacities were 2.78g and 2.91g for ensemble 1 (far-fault) and ensemble 2 (near-fault), respectively. Li et al. [3] reported the far-fault aftershocks resulted in smaller collapse capacity for steel frame buildings. This is mainly because the stiffness of the damaged columns, even repaired with confining repair jackets, is always lower than that of the original columns. The increased vibration period of the bridge due to the column damage is likely close to the pulse duration of near-fault motions, so as it could potentially lessen the effect of pulse type records on a damaged/softened bridge structure.

CFRP, steel and hybrid jackets can all increase the mean structural collapse capacity of the bridge subjected to severe MS-severe AS events. However, the mean collapse capacity for the CFRP jacketed columns was slightly smaller than that of both conventional and hybrid steel jackets. This is mainly because the isotropic steel jackets can resist stress in any direction as shown in Fig. 4(a), resulting in more significant energy dissipation and higher stiffness of the steel jacketed column than that of the CFRP jacketed column. This result is consistent with experimental results of an extensive series of tests on damaged RC columns repaired with steel or CFRP jackets [78]. While both jacketing materials improved the seismic behavior of the repaired columns, “the energy dissipation capacity and stiffness of the steel jacketed columns were consistently larger than that of the CFRP jacket repaired columns” [78]. Based on the comparable performance of conventional steel and hybrid jackets, fabrics with bidirectional fibers are recommended in the case of CFRP jacket for plastic hinge confinement of earthquake damaged RC columns. Bidirectional fibers could lessen the stiffness degradation of RC columns during an AS event as the longitudinal fibers can restrain the opening of flexural cracks as illustrated in Fig. 4(b). While shear deformation is somehow negligible during the first seismic event for a flexural dominant modern RC bridge column, it becomes non-negligible during the second severe seismic event for a column with yielded steel and cracked/crushed concrete.

Overall, the abovementioned results clearly indicate that the CFRP, steel and hybrid jackets are effective for severe MS-severe AS events but ineffective for severe MS-moderate AS events, irrespective of the fault type studied. However, if a bridge suffers minor damage during a moderate earthquake but is inspected and considered safe to remain open to traffic after the earthquake event, high-cycle traffic load fatigue may

cause failure of the damaged RC columns. In this case, the columns with minor damage are still required to be repaired. This is because the minor existing damage of RC columns such as concrete cracks and slightly yielded steel bars can potentially lead to the significantly reduced structural capacity during high-volume traffic fatigue loads. The capacity reduction could make the damaged bridge vulnerable to moderate aftershocks.

7. Conclusions

Results from a comprehensive study on the seismic collapse capacity of the mainshock-damaged highway RC bridge that is representative of modern bridge construction practices are presented in this manuscript. Calibrated analytical models of the bridge were subjected to numerous series of mainshock-aftershock sequences of various intensities. Three repair techniques (CFRP, conventional thick steel and hybrid jacket) were considered to be applied after the MS attack (i.e. prior to AS). The collapse capacity and drift capacity of CFRP jacketed bridge columns under severe MS-severe or moderate AS were quantified and compared with steel jacketed columns. Different repair jackets were compared to address the differences that may arise on the post-repair response of rehabilitated bridges subjected to potential aftershocks. Based on the obtained results, the following conclusions can be drawn:

1- The accumulated damage of bridges under multiple earthquakes is closely related to the intensity of seismic events. Although adequate for a single severe MS event, RC bridges designed with modern seismic codes can significantly degrade when subjected to severe MS-severe AS sequences. Confining repair jackets, including CFRP, can increase the post-repair collapse capacity of severely MS-damaged columns by approximately 20% under severe AS events.

2- Moderate AS events resulted in a slight decrease of the residual collapse capacity of the damaged bridge columns previously attacked by a severe MS. Therefore, confining repair jackets are insignificant and not required for severely damaged bridge columns under moderate AS events unless post-earthquake high-volume traffic induced fatigue loads are a concern.

3- The confining pressures provided by CFRP, steel and hybrid jackets are comparable in improving the post-repair collapse capacity of damaged columns subjected

to AS events. Repair interventions that provide only lateral confining pressure (including CFRP, steel and hybrid jackets) cannot restore the stiffness of the repaired column to that of the original column. In comparison with the CFRP jacket, both steel and hybrid jackets provide more energy dissipation and relatively higher stiffness of repaired columns (attracting larger ductility demand in turn). In the case of CFRP repair, bidirectional FRP jackets are recommended for severe MS-damaged columns subjected to severe AS.

4- For severe-MS damaged bridge columns subjected to severe AS, an appropriately designed (i.e., not exceeding the residual shear strength of the damaged column, the flexural capacity and the overturning capacity of the original footing due to increased force demands) force transfer system (such as FRP or double headed steel anchors) is recommended to improve the efficacy of repair intervention. Anchorage could compensate for the loss of reduced steel reinforcement properties and could restore and even improve the flexural capacity of the repaired column compared to that of the original column.

5- Compared to far-fault ground motions, near-fault ground motions resulted in smaller collapse capacity for the original bridge with no prior damage under severe MS events but larger capacity for the damaged bridge under severe MS-severe AS and severe MS-moderate AS sequences, irrespective of repair methods. This is due to the potential match of the lengthened vibration period of the damaged bridge with the pulse duration in near-fault motions.

Current study is limited only to one regular bridge configuration under two record sets. Future studies may be directed to consider other bridge configurations such as multiple-column bents and irregular column heights, shear/shear-flexure columns, and a mixed combination of records (i.e., far field mainshock-near fault aftershock and opposite) from different earthquake types (as-recorded crustal ground motions, subduction, inslab and interface record sets) for a comprehensive performance assessment of FRP/steel repaired columns under multiple earthquakes. The effect of soil-structure interaction with the inclusion of the pile-footing-pier failure on the significance and efficacy of repair jackets should be investigated.

Acknowledgments

Prof. R. Pinho and Dr. F. Bianchi's kind assistance by sharing some of the experimental data for model validations are highly appreciated. The first author would like to acknowledge Messrs. Zachary T. Woolsey and Timothy O'Connor during the experimental part of this study. Financial support for this study was provided by the Department of Civil, Architectural, and Environmental Engineering at Missouri University of Science and Technology, and by the U.S. National Science Foundation under Award No. CMMI-1030399. The conclusions and opinions expressed in this paper are those of the authors only and do not necessarily reflect the official views or policies of the sponsors.

References

- [1] Chang, L., Peng, F., Ouyang, Y., Elnashai, A. S., & Spencer Jr, B. F. (2012). Bridge seismic retrofit program planning to maximize postearthquake transportation network capacity. *Journal of Infrastructure Systems*, 18(2), 75-88. [http://dx.doi.org/10.1061/\(ASCE\)IS.1943-555X.0000082](http://dx.doi.org/10.1061/(ASCE)IS.1943-555X.0000082).
- [2] USGS, United States Geological Survey. <http://www.usgs.gov/> (2012).
- [3] Li, Y., Song, R., & Van De Lindt, J. W. (2014). Collapse Fragility of Steel Structures Subjected to Earthquake Mainshock-Aftershock Sequences. *Journal of Structural Engineering*. [http://dx.doi.org/10.1061/\(ASCE\)ST.1943-541X.0001019](http://dx.doi.org/10.1061/(ASCE)ST.1943-541X.0001019).
- [4] Terzic V, Stojadinovic B. Evaluation of Post-Earthquake Axial Load Capacity of Circular Bridge Columns. *ACI Structural Journal*. 2014;111(1-6).
- [5] Di Sarno, L. (2013). Effects of multiple earthquakes on inelastic structural response. *Engineering Structures* 2013; 56, 673-681. with discussion by J. Ruiz-Garcia and reply in *Engineering Structures* 2014; 58, 110-113.
- [6] Nardone, F., Di Ludovico, M., De Caso y Basalo, F. J., Prota, A., & Nanni, A. (2012). Tensile behavior of epoxy based FRP composites under extreme service conditions. *Composites Part B: Engineering*, 43(3), 1468-1474.

[7] Lin, Z., Fakhairfar, M., Wu, C., Chen, G., Bevans, W., Gunasekaran, A. V. K., & Sedighsarvestani, S. (2013). Design, Construction and Load Testing of the Pat Daly Road Bridge in Washington County, MO, with Internal Glass Fiber Reinforced Polymers Reinforcement (No. NUTC R275).

[8] Yan, Z., Pantelides, C. P., & Reaveley, L. D. (2007). Posttensioned FRP composite shells for concrete confinement. *Journal of Composites for Construction*, 11(1), 81-90. [http://dx.doi.org/10.1061/\(ASCE\)1090-0268\(2007\)11:1\(81\)](http://dx.doi.org/10.1061/(ASCE)1090-0268(2007)11:1(81)).

[9] Rousakis, T. C., & Tourtouras, I. S. (2014). RC columns of square section—Passive and active confinement with composite ropes. *Composites Part B: Engineering*, 58, 573-581.

[10] Rousakis, T. C., Kouravelou, K. B., & Karachalios, T. K. (2014). Effects of carbon nanotube enrichment of epoxy resins on hybrid FRP–FR confinement of concrete. *Composites Part B: Engineering*, 57, 210-218.

[11] Anggawidjaja, D., Ueda, T., Dai, J., & Nakai, H. (2006). Deformation capacity of RC piers wrapped by new fiber-reinforced polymer with large fracture strain. *Cement and Concrete Composites*, 28(10), 914-927.

[12] Choi, E., Kim, J. W., Rhee, I., & Kang, J. W. (2014). Behavior and modeling of confined concrete cylinders in axial compression using FRP rings. *Composites Part B: Engineering*, 58, 175-184.

[13] Garcia, R., Hajirasouliha, I., Guadagnini, M., Helal, Y., Jemaa, Y., Pilakoutas, K., ... & Saiidi, M. (2014). Full-scale shaking table tests on a substandard RC building repaired and strengthened with Post-Tensioned Metal Straps. *Journal of Earthquake Engineering*, 18(2), 187-213.

[14] Janke, L., Czaderski, C., Ruth, J., & Motavalli, M. (2009). Experiments on the residual load-bearing capacity of prestressed confined concrete columns. *Engineering Structures*, 31(10), 2247-2256.

[15] Fakharifar, M., Dalvand, A., Arezoumandi, M., Sharbatdar, M. K., Chen, G., & Kheyroddin, A. (2014). Mechanical properties of high performance fiber reinforced cementitious composites. *Construction and Building Materials*, 71, 510-520.

[16] Shimomura, T., & Phong, N. H. (2007, July). Structural performance of concrete members reinforced with continuous fiber rope. In FRPRCS-8 Conference University of Patras, Patras, Greece.

[17] Del Prete, I., Bilotta, A., & Nigro, E. (2015). Performances at high temperature of RC bridge decks strengthened with EBR-FRP. *Composites Part B: Engineering*, 68, 27-37.

[18] Priestley, M. N., Seible, F., & Calvi, G. M. (1996). *Seismic design and retrofit of bridges*. John Wiley & Sons, New York.

[19] Buckle, I., Friedland, I., Mander, J., Martin, G., Nutt, R., & Power, M. (2006). *Seismic retrofitting manual for highway structures: part 1-bridges* (No. FHWA-HRT-06-032).

[20] Vosooghi, A., & Saiidi, M. S. (2012). Design guidelines for rapid repair of earthquake-damaged circular RC bridge columns using CFRP. *Journal of Bridge Engineering*, 18(9), 827-836. [http://dx.doi.org/10.1061/\(ASCE\)BE.1943-5592.0000426](http://dx.doi.org/10.1061/(ASCE)BE.1943-5592.0000426).

[21] Vosooghi A, Saiidi M. Post-earthquake evaluation and emergency repair of damaged RC bridge columns using CFRP materials. Center for Civil Engineering Earthquake Research, Department of Civil and Environmental Engineering, University of Nevada, Reno, Nevada, Report No. CCEER-10-05; 2010. p. 636.

[22] Fakharifar, M., Chen, G., Lin, Z., & Woolsey, Z. (2014). Behavior and strength of passively confined concrete filled tubes. In the 10th U.S. National Conference on Earthquake Engineering: July 21-25, 2014, Anchorage, Alaska.

[23] Yang, Y., Sneed, L. H., Saiidi, M. S., & Belarbi, A. (2014). "Repair of Earthquake-Damaged Bridge Columns with Interlocking Spirals and Fractured Bars," Caltrans, Final Report CA 14-2179, Missouri University of Science and Technology, University of Nevada, and University of Houston, July 2014.

[24] He, R., Sneed, L. H., & Belarbi, A. (2014). Torsional Repair of Severely Damaged Column Using Carbon Fiber-Reinforced Polymer. *ACI Structural Journal*, 111(3), 706-715.

[25] He, R., Grelle, S., Sneed, L. H., & Belarbi, A. (2013). Rapid repair of a severely damaged RC column having fractured bars using externally bonded CFRP. *Composite Structures*, 101, 225-242.

[26] He, R., Sneed, L. H., & Belarbi, A. (2013). Rapid Repair of Severely Damaged RC Columns with Different Damage Conditions: An Experimental Study. *International Journal of Concrete Structures and Materials*, 7(1), 35-50.

[27] Saatcioglu, M., & Yalcin, C. (2003). External prestressing concrete columns for improved seismic shear resistance. *Journal of Structural Engineering*, 129(8), 1057-1070.

[28] ElGawady, M., Endeshaw, M., McLean, D., & Sack, R. (2009). Retrofitting of rectangular columns with deficient lap splices. *Journal of Composites for Construction*, 14(1), 22-35.

[29] Fakharifar, M., Lin, Z. B., Wu, C. L., Mahadik-Khanolkar, S., Leventis, N., & Chen, G. D. (2013). Microstructural characteristics of polyurea and polyurethanexerogels for concrete confinement with FRP system. *Advanced Materials Research*, 742, 237-242.

[30] Micelli, F., Angiuli, R., Corvaglia, P., & Aiello, M. A. (2014). Passive and SMA-activated confinement of circular masonry columns with basalt and glass fibers composites. *Composites Part B: Engineering*, 67, 348-362.

[31] Andrawes, B., Shin, M., & Wierschem, N. (2009). Active confinement of reinforced concrete bridge columns using shape memory alloys. *Journal of Bridge Engineering*, 15(1), 81-89. [http://dx.doi.org/10.1061/\(ASCE\)BE.1943-5592.0000038](http://dx.doi.org/10.1061/(ASCE)BE.1943-5592.0000038).

[32] Lee, D. H., Park, J., Lee, K., & Kim, B. H. (2011). Nonlinear seismic assessment for the post-repair response of RC bridge piers. *Composites Part B: Engineering*, 42(5), 1318-1329.

[33] Arias, A. (1970). "A Measure of Earthquake Intensity," R.J. Hansen, ed. *Seismic Design for Nuclear Power Plants*, MIT Press, Cambridge, Massachusetts, pp. 438-483.

[34] Ketchum, M., Chang, V., and Shantz, T. (2004). "Influence of design ground motion level on highway bridge costs." Rep. PEER 6D01, Pacific Earthquake Engineering Research Center, Univ. of California, Berkeley, CA.

[35] Caltrans. (1999). *Seismic Design Criteria*, 1.4, California DOT, Sacramento, CA.

[36] Fakharifar, M., Chen, G., Arezoumandi, & M., ElGawady, M. Hybrid jacketing for rapid repair of seismically damaged reinforced concrete columns. *Transportation Research Record: Journal of the Transportation Research Board.*, 2015, in press.

[37] Jirawattanasomkul, T., (2013). “Ultimate shear behavior and modeling of reinforced concrete members jacketed by fiber reinforced polymer and steel”. PhD thesis. Hokkaido University, Sapporo, Japan.

[38] Seismosoft. (2013). “SeismoStruct – A computer program for static and dynamic nonlinear analysis of framed structures”. <www.seismosoft.com>

[39] Ferracuti, B., Pinho, R., Savoia, M., & Francica, R. (2009). Verification of displacement-based adaptive pushover through multi-ground motion incremental dynamic analyses. *Engineering Structures*, 31(8), 1789-1799.

[40] Berry, M. P., & Eberhard, M. O. (2007). Performance modeling strategies for modern reinforced concrete bridge columns, PEER Report 2007/07, Pacific Engineering Research Center, University of California, Berkeley, California.

[41] Haselton, C.B., A.B. Liel, S. Taylor Lange, and G.G. Deierlein. (2008). Beam-Column Element Model Calibrated for Predicting Flexural Response Leading to Global Collapse of RC Frame Buildings, PEER Report 2007/03, Pacific Engineering Research Center, University of California, Berkeley, California.

[42] Billah, A. H. M., & Alam, M. S. (2014). Seismic performance evaluation of multi-column bridge bents retrofitted with different alternatives using incremental dynamic analysis. *Engineering Structures*, 62, 105-117.

[43] Scott, M. H., & Fenves, G. L. (2006). Plastic hinge integration methods for force-based beam–column elements. *Journal of Structural Engineering*, 132(2), 244-252.

[44] Zhao, J., & Sritharan, S. (2007). Modeling of Strain Penetration Effects in Fiber-Based Analysis of Reinforced Concrete Structures *Concrete Structures*. *ACI structural journal*, 104(2).

[45] Menegotto M., Pinto P.E. (1973). Method of analysis for cyclically loaded R.C. plane frames including changes in geometry and non-elastic behaviour of elements under combined normal force and bending. Symposium on the Resistance and Ultimate Deformability of Structures Acted on by Well Defined Repeated Loads, International Association for Bridge and Structural Engineering, Zurich, Switzerland, pp. 15-22.

[46] Filippou F.C., Popov E.P., Bertero V.V. (1983). Effects of bond deterioration on hysteretic behaviour of reinforced concrete joints. Report EERC 83-19, Earthquake Engineering Research Center, University of California, Berkeley.

[47] Fragiadakis M., Pinho R., Antoniou S. (2008) "Modelling inelastic buckling of reinforcing bars under earthquake loading," in Progress in Computational Dynamics and Earthquake Engineering, Eds. M. Papadrakakis, D.C. Charmpis, N.D. Lagaros and Y. Tsompanakis, A.A. Balkema Publishers – Taylor & Francis, The Netherlands.

[48] Kent, D. C., & Park, R. (1973). Cyclic load behaviour of reinforcing steel. *Strain*,9(3), 98-103.

[49] Madas P. and Elnashai A.S. (1992) "A new passive confinement model for transient analysis of reinforced concrete structures," *Earthquake Engineering and Structural Dynamics*, Vol. 21, pp. 409-431.

[50] Martinez-Rueda J.E., Elnashai A.S. (1997) "Confined concrete model under cyclic load," *Materials and Structures*, Vol. 30, No. 197, pp. 139-147.

[51] Ferracuti B., Savoia M. (2005) "Cyclic behaviour of FRP-wrapped columns under axial and flexural loadings," *Proceedings of the International Conference on Fracture*, Turin, Italy.

[52] Mander J.B., Priestley M.J.N., Park R. (1988) "Theoretical stress-strain model for confined concrete," *Journal of Structural Engineering*, Vol. 114, No. 8, pp. 1804-1826.

[53] Yankelevsky, D. Z., & Reinhardt, H. W. (1989). Uniaxial behavior of concrete in cyclic tension. *Journal of Structural Engineering*, 115(1), 166-182. [http://dx.doi.org/10.1061/\(ASCE\)0733-9445\(1989\)115:1\(166\)](http://dx.doi.org/10.1061/(ASCE)0733-9445(1989)115:1(166)).

[54] Spoelstra, M. R., & Monti, G. (1999). FRP-confined concrete model. *Journal of composites for construction*, 3(3), 143-150. [http://dx.doi.org/10.1061/\(ASCE\)1090-0268\(1999\)3:3\(143\)](http://dx.doi.org/10.1061/(ASCE)1090-0268(1999)3:3(143)).

[55] Sivaselvan, M. V., & Reinhorn, A. M. (1999). Hysteretic models for cyclic behavior of deteriorating inelastic structures. Report MCEER-99-0018, MCEER/SUNY/Buffalo. Nov. 5. 1999.

[56] Sivaselvan M., Reinhorn A.M. (2001) "Hysteretic models for deteriorating inelastic structures," *Journal of Engineering Mechanics*, ASCE, Vol. 126, No. 6, pp. 633-640, with discussion by Wang and Foliente and closure in Vol. 127, No. 11. [http://dx.doi.org/10.1061/\(ASCE\)0733-9399\(2000\)126:6\(633\)](http://dx.doi.org/10.1061/(ASCE)0733-9399(2000)126:6(633)).

[57] Priestley, M. J. N., Calvi, G. M., and Kowalsky, M. J. (2007). Displacement based seismic design of structures, Istituto Universitario di Studi Superiori Press, Pavia, Italy.

[58] Fakharifar M, Sharbatdar MK, Lin Z, Dalvand A, Sivandi-Pour A, Chen G. Seismic performance and global ductility of RC frames rehabilitated with retrofitted joints by CFRP laminates. *Earthq Eng Eng Vib* 2014;13(1):59–73.

[59] Calderone, A., Lehman, D. E., & Moehle, J. P. (2001). Behavior of reinforced concrete bridge columns having varying aspect ratios and varying lengths of confinement. Pacific Earthquake Engineering Research Center.

[60] PEER; (2010). http://nisee2.berkeley.edu/peer/prediction_contest/?page_id=25 [last access 07.24.14].

[61] Bianchi F., Sousa R., Pinho R. (2011) “Blind prediction of a full-scale RC bridge column tested under dynamic conditions”, Proceedings of the 3rd International Conference on Computational Methods in Structural Dynamics and Earthquake Engineering (COMPDYN 2011), Corfu, Greece, Paper no. 294.

[62] Kunnath, S. K., El-Bahy, A., Taylor, A. W., & Stone, W. C. (1997). Cumulative seismic damage of reinforced concrete bridge piers. In Technical Report NCEER (No. 97-0006). US National Center for Earthquake Engineering Research.

[63] Pinto, A.V., Verzeletti, G., Pegon, P., Magonette, G., Negro, P., and Guedes, J., 1996. Pseudo- Dynamic Testing of Large- Scale R/C Bridges, Report EUR 16378, Ispra (VA), Italy.

[64] Seismosoft (2013). SeismoStruct ver. 6.0 - Verification Report.

[65] Liel, A. B., Haselton, C. B., & Deierlein, G. G. (2010). Seismic collapse safety of reinforced concrete buildings. II: Comparative assessment of nonductile and ductile moment frames. *Journal of Structural Engineering*, 137(4), 492-502.

[66] Abdelnaby, A., Elnashai, A. (2014) "Performance of Degrading Reinforced Concrete Frame Systems under Tohoku and Christchurch Earthquake Sequences," *Journal of Earthquake Engineering*, Vol. 18(7) pp. 1009-1036 (DOI:10.1080/13632469.2014.923796).

[67] Luco N, Bazzurro P, Cornell CA. Dynamic versus static computation of the residual capacity of a mainshock-damaged building to withstand an aftershock. In: *Proceedings of the thirteenth world conference on earthquake engineering*, Paper No. 2405. 2004.

[68] Bazzurro, P., Cornell, C. A., Menun, C., & Motahari, M. Guidelines for seismic assessment of damaged buildings. In: *Proceedings of the thirteenth world conference on earthquake engineering*, Paper No. 1708. 2004.

[69] Mackie K, Wong J-M, Stojadinović B. Integrated probabilistic performance-based evaluation of benchmark reinforced concrete bridges. Technical Report 2007/09, University of California Berkeley, Pacific Earthquake Engineering Research Center, Berkeley, CA, 2008.

[70] Villaverde, R. (2007). Methods to assess the seismic collapse capacity of building structures: State of the art. *Journal of Structural Engineering*, 133(1), 57-66.

[71] Chopra, A.K., and Goel, R.K. (2002). "A modal pushover analysis procedure for estimating seismic demands for buildings". *Earthquake Engineering and Structural Dynamics*, 31(3): 561–582.

[72] Vamvatsikos, D., & Cornell, C. A. (2002). Incremental dynamic analysis. *Earthquake Engineering & Structural Dynamics*, 31(3), 491-514.

[73] Tehrani, P., & Mitchell, D. (2013). Seismic Risk Assessment of Four-Span Bridges in Montreal Designed Using the Canadian Bridge Design Code. *Journal of Bridge Engineering*. [http://dx.doi.org/10.1061/\(ASCE\)BE.1943-5592.0000499](http://dx.doi.org/10.1061/(ASCE)BE.1943-5592.0000499).

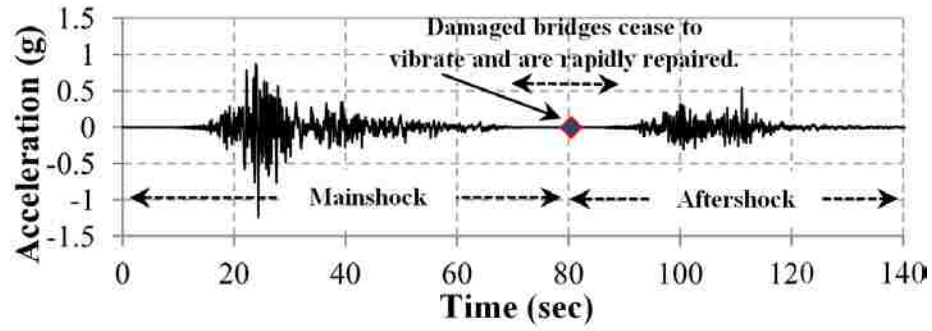
[74] Dutta, A., & Mander, J. B. (1998). Seismic fragility analysis of highway bridges. In *Proceedings of the INCEDE-MCEER Center-to-Center Project Workshop on Earthquake Engineering Frontiers in Transportation Systems* (pp. 22-23).

[75] Mackie, K. R., & Stojadinović, B. (2007). R-factor parameterized bridge damage fragility curves. *Journal of Bridge Engineering*, 12(4), 500-510. [http://dx.doi.org/10.1061/\(ASCE\)1084-0702\(2007\)12:4\(500\)](http://dx.doi.org/10.1061/(ASCE)1084-0702(2007)12:4(500)).

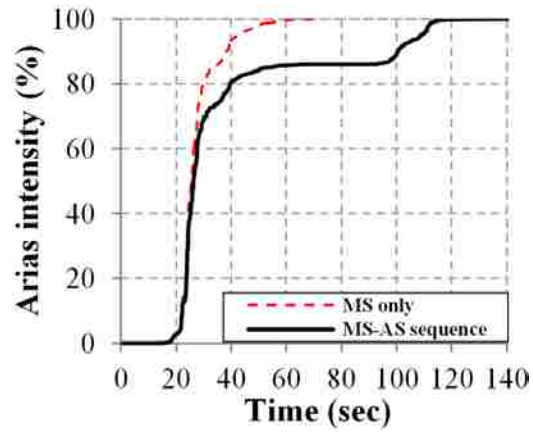
[76] Baker, J. W., T. Lin, S. K. Shahi, and N. Jayaram. (2011). *New Ground Motion Selection Procedures and Selection Motions for the PEER Transportation Research Program*. PEER Report 2011/03, Berkeley, CA: Pacific Earthquake Engineering Research Center.

[77] Bearman, C.F. (2012) *Post-earthquake assessment of reinforced concrete frames*, M.S. Thesis, Department of Civil and Environmental Engineering, University of Washington, Seattle, WA.

[78] Youm, K. S., Lee, H. E., & Choi, S. (2006). Seismic performance of repaired RC columns. *Magazine of Concrete Research*, 58(5), 267-276.



(a)



(b)

Fig. 1. (a) A scenario mainshock-aftershock acceleration time history; and (b) Arias intensity for mainshock only and for mainshock-aftershock sequence.

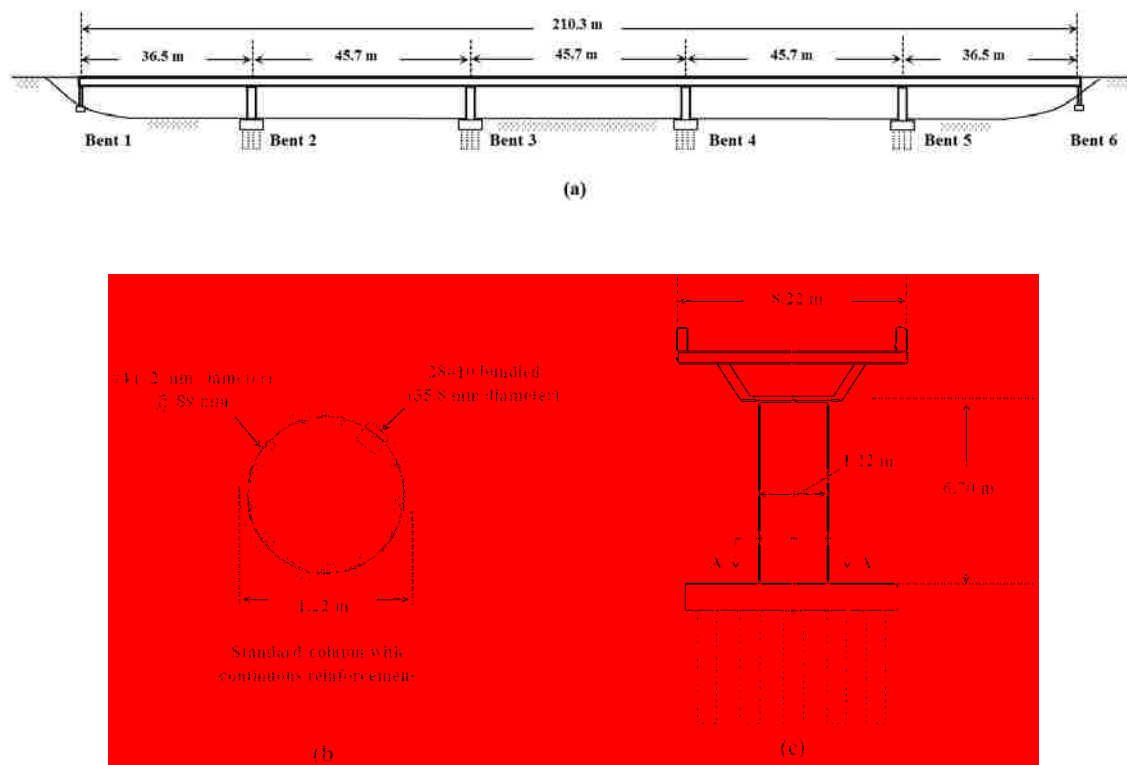


Fig. 2. Typical details of the bridge under investigation: (a) elevation; (b) cross section A-A of column; (c) cross section at columns (adopted from [34]).

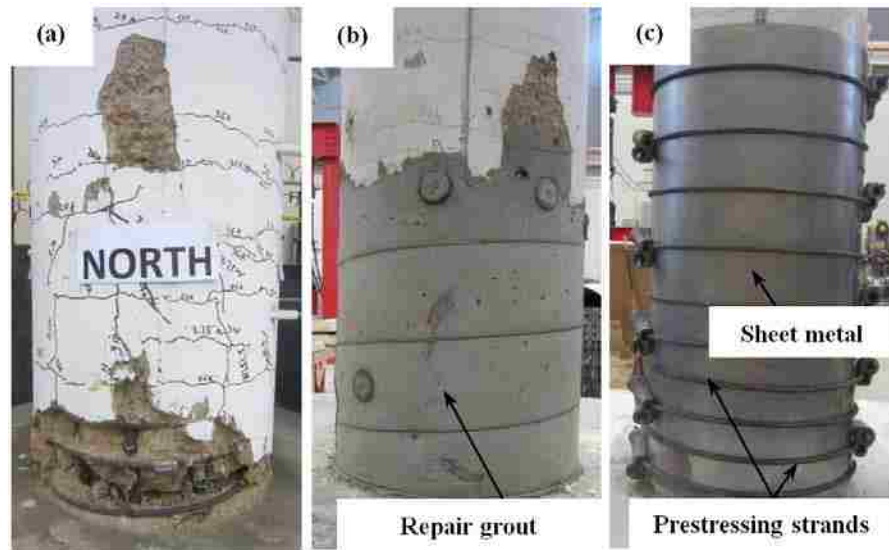


Fig. 3. Details of the hybrid repair jacket: (a) damaged column; (b) the damaged column restored to original cross section; (c) thin sheet metal wrapped around the column with prestressing strands.

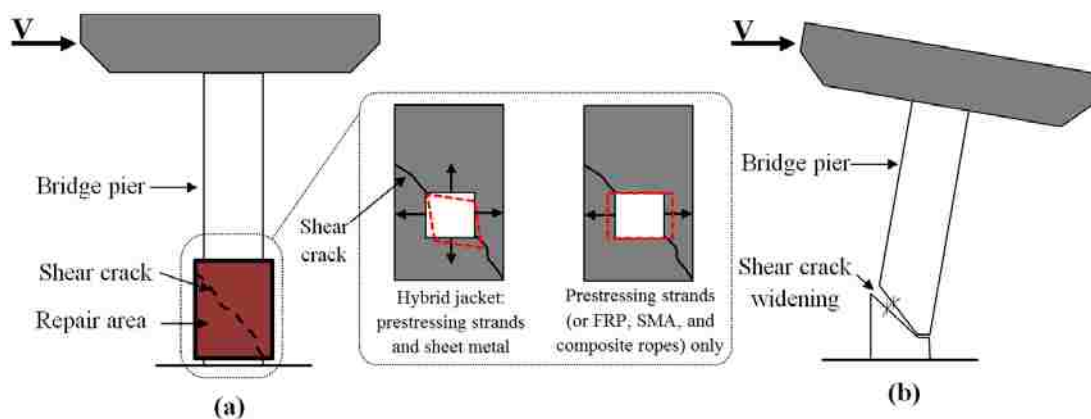


Fig. 4. (a) Stress states in the repair jacket along the shear crack due to hybrid jacket and prestressing strands only; (b) widening of the shear crack during aftershock on unrepaired columns.

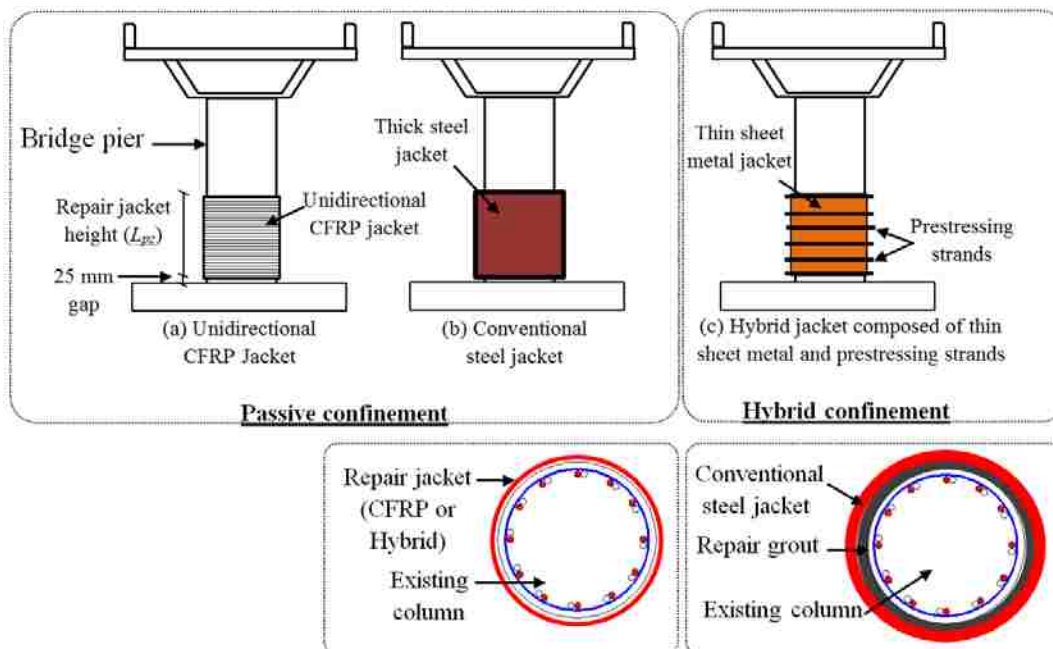


Fig. 5. Schematic of various repair techniques: (a) CFRP jacket; (b) conventional steel jacket; and (c) hybrid jacket.

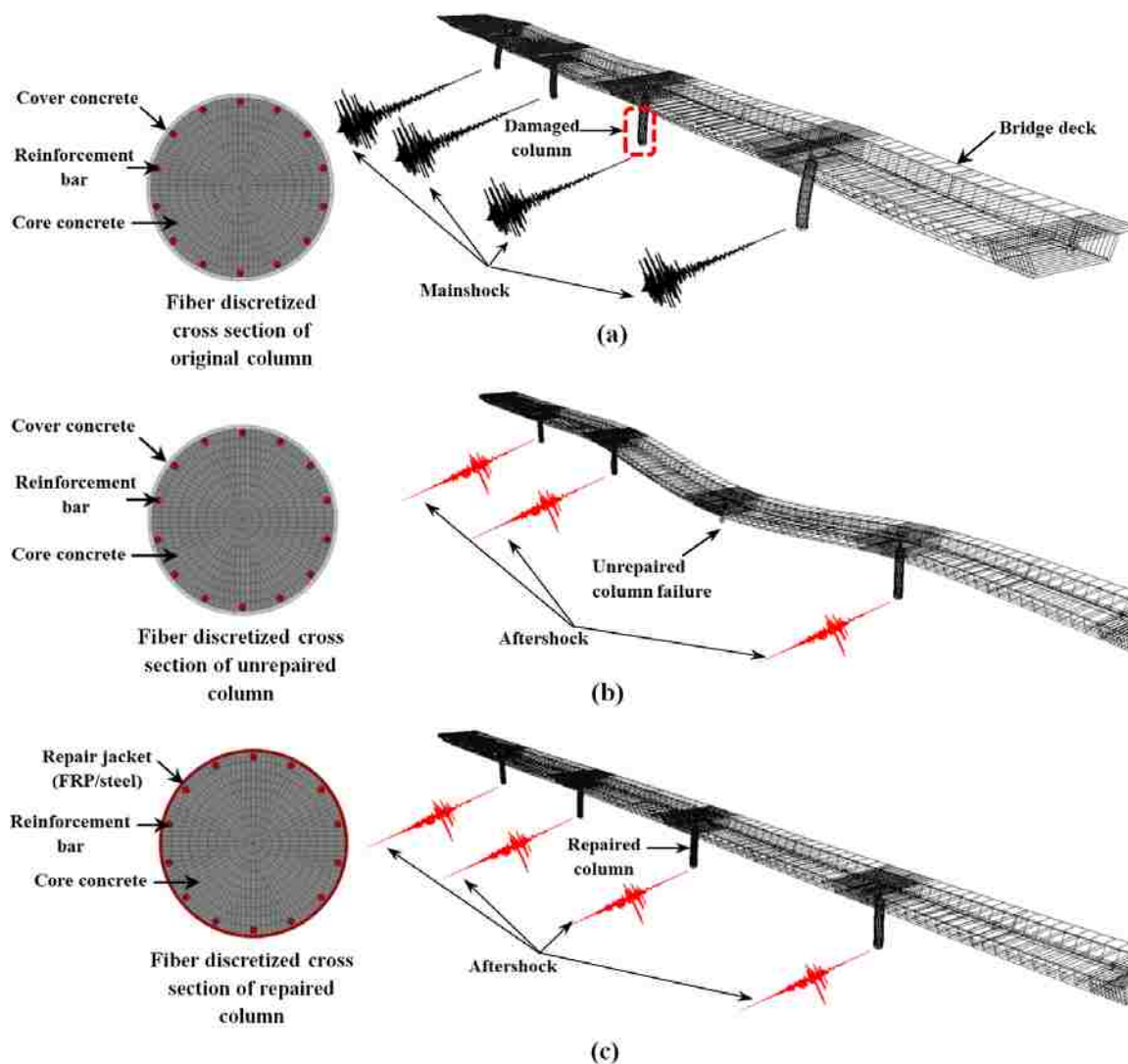


Fig. 6. Various states of a five-span continuous bridge model with: (a) the damaged RC column during mainshock; (b) the unrepaired RC column failure during aftershock, causing incipient collapse of the entire bridge; (c) the repaired RC column during aftershock.

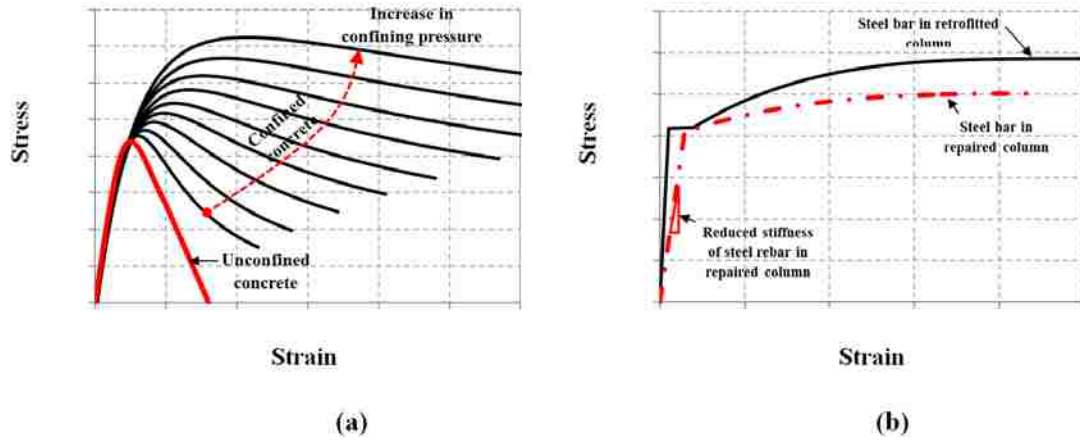


Fig. 7. Constitutive models for (a) unconfined and confined concrete; (b) steel reinforcement in retrofitted and repaired columns.

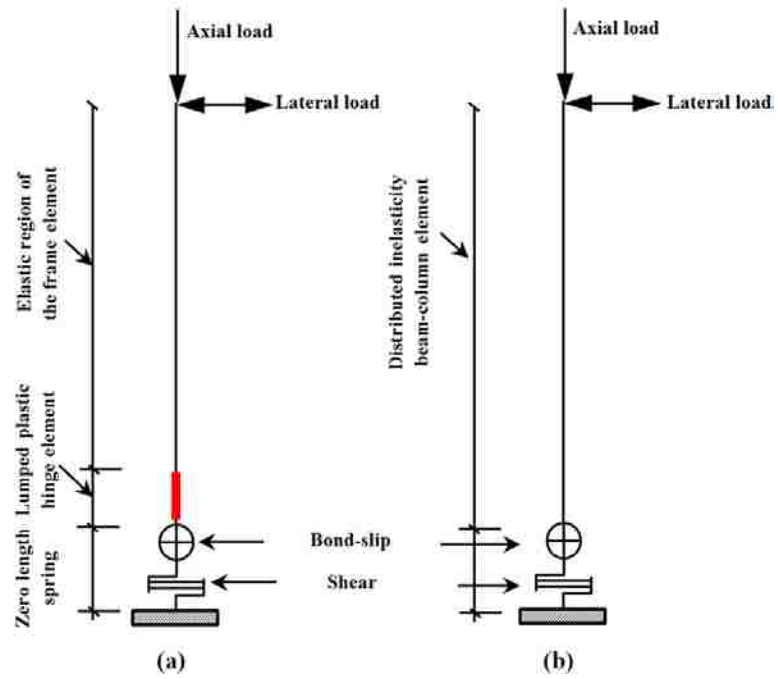


Fig. 8. Idealized column models with (a) lumped plastic hinge element; (b) distributed plasticity element.

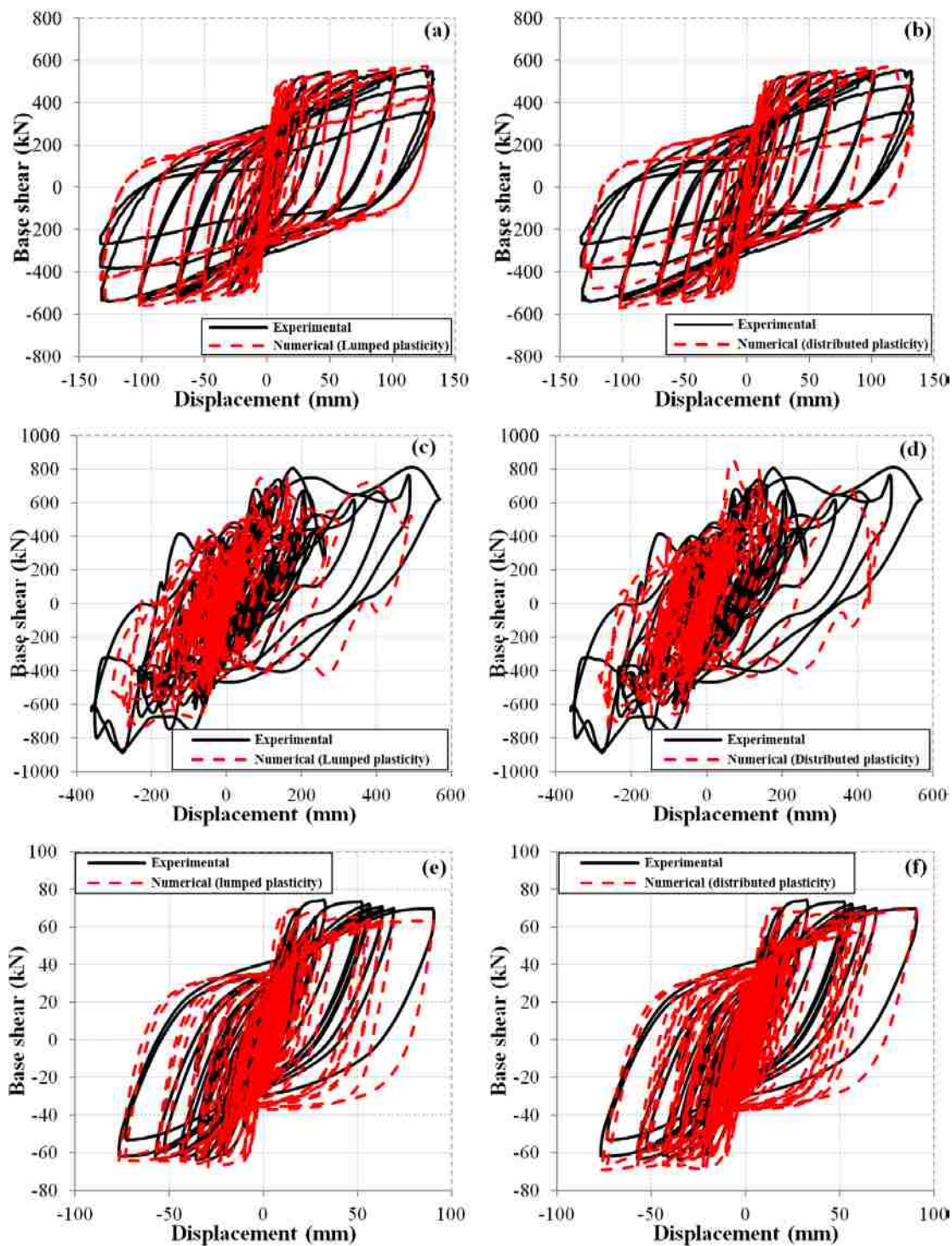


Fig. 9. Hysteresis loop comparison and validation of numerical RC column models with lumped and distributed plasticity: (a, b) under symmetric cyclic load reversals [59]; (c, d) under earthquake ground accelerations on shake table [60]; (e, f) under random cyclic displacement reversals [62].

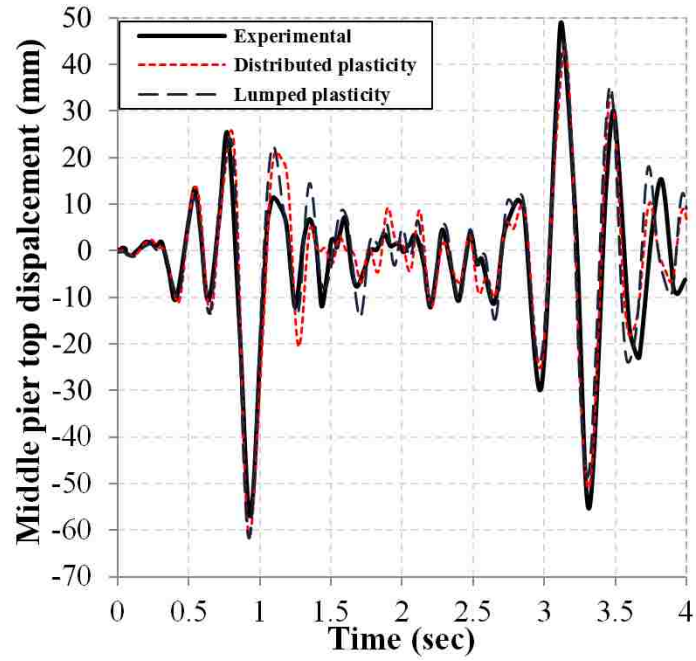


Fig. 10. Displacement time history comparison and shake table validation of the full-scale RC bridge with lumped and distributed plasticity models [63].

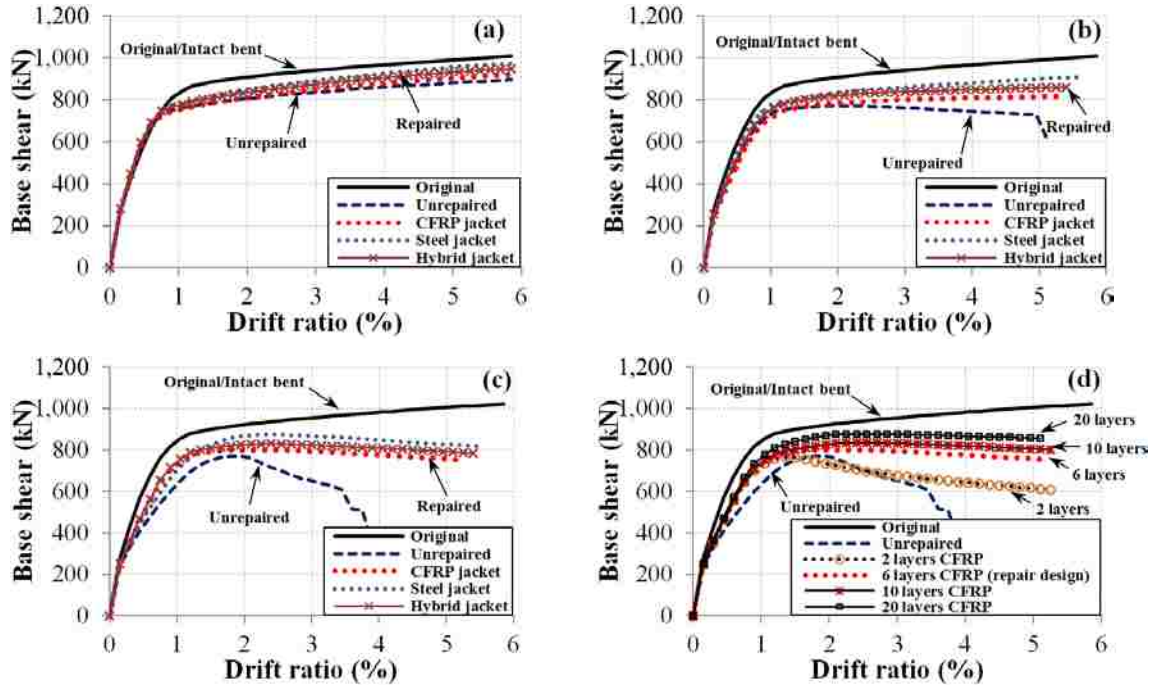


Fig. 11. Pushover response curves of Bent 4 of the bridge under investigation with original and unrepaired columns as well as the repaired columns with (a) CFRP, steel and hybrid jackets for minor damage; (b) CFRP, steel and hybrid jackets for moderate damage; (c) CFRP, steel and hybrid jackets for severe damage; (d) CFRP jacket with various numbers of layers for severe damage.

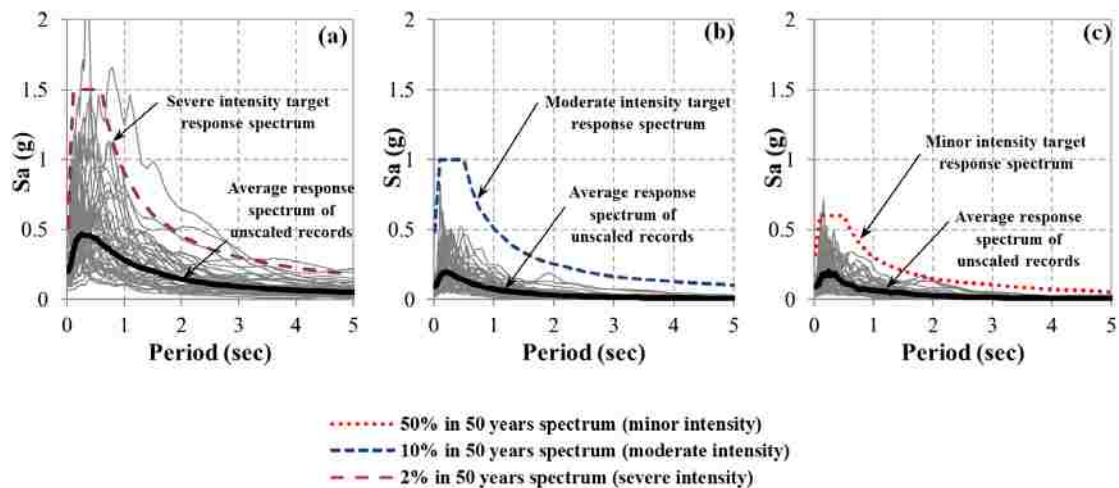


Fig. 12. Response spectra of far-fault (ensemble 1) unscaled ground motions and their corresponding target spectrum at various hazard levels: (a) severe; (b) moderate; (c) minor magnitudes.

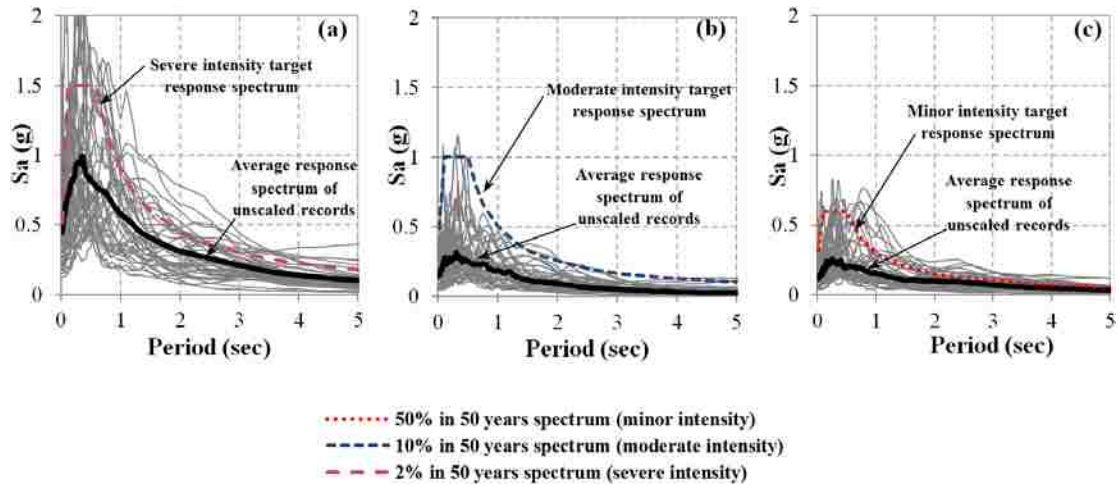


Fig. 13. Response spectra of near-fault (ensemble 2) unscaled ground motions and their corresponding target spectrum at various hazard levels: (a) severe; (b) moderate; (c) minor magnitudes.

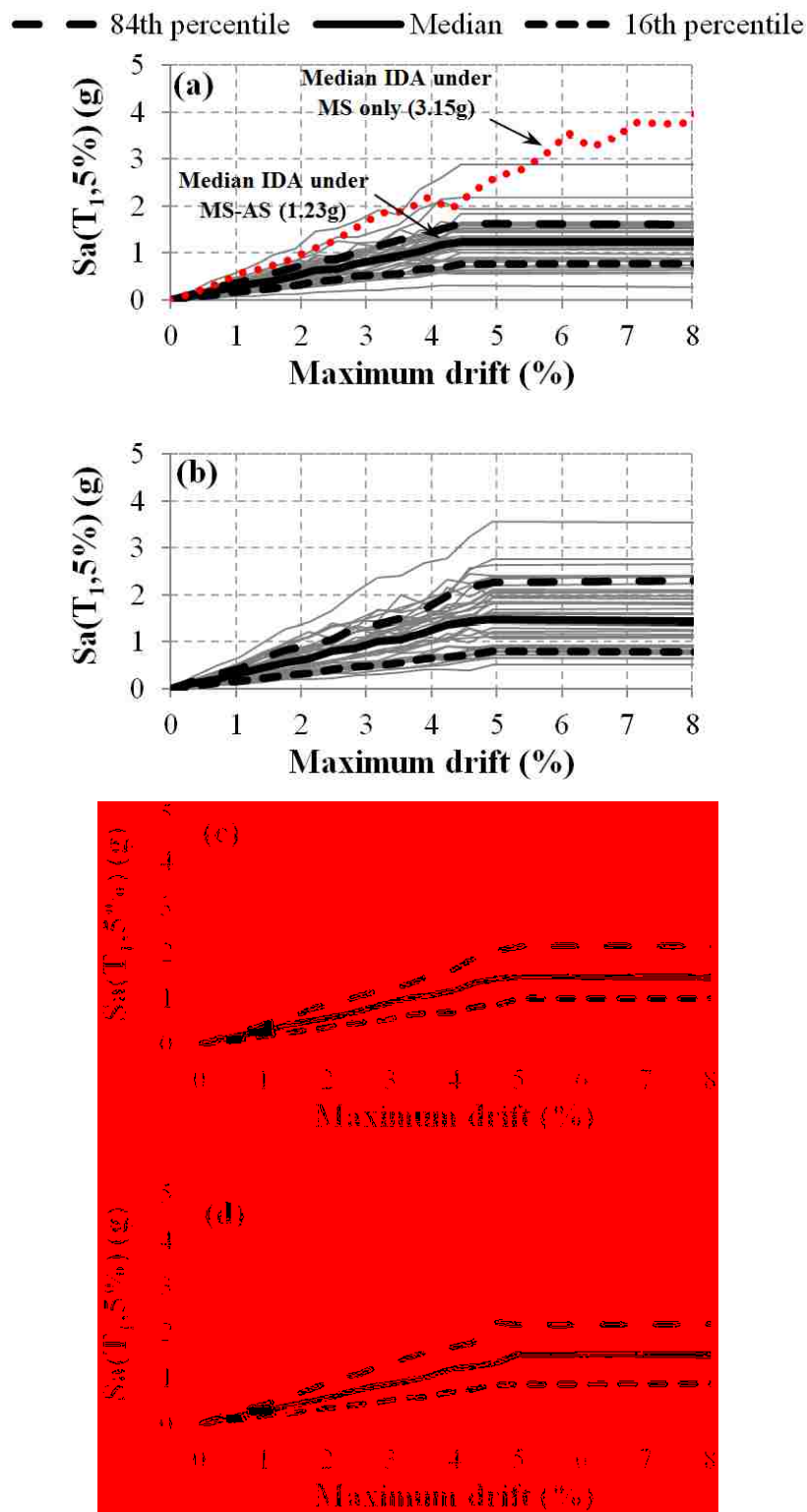


Fig. 14. Maximum drift versus spectral acceleration IDA curves under severe MS-severe AS far-fault motions (ensemble 1): (a) unrepaired; (b) CFRP jacket; (c) conventional steel jacket; (d) hybrid jacket.

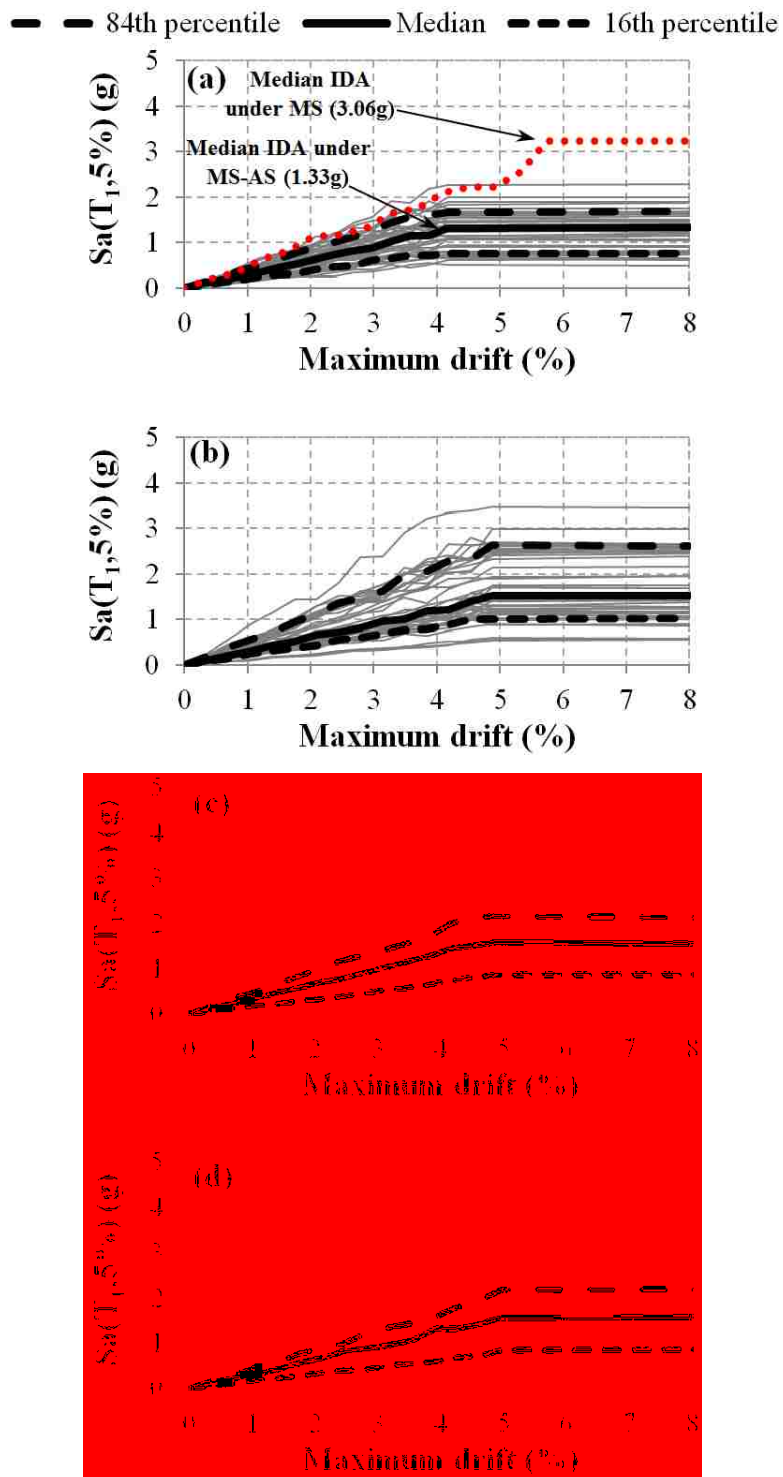


Fig. 15. Maximum drift versus spectral acceleration IDA curves under severe MS-severe AS near-fault motions (ensemble 2): (a) unrepaired; (b) CFRP jacket; (c) conventional steel jacket; (d) hybrid jacket.

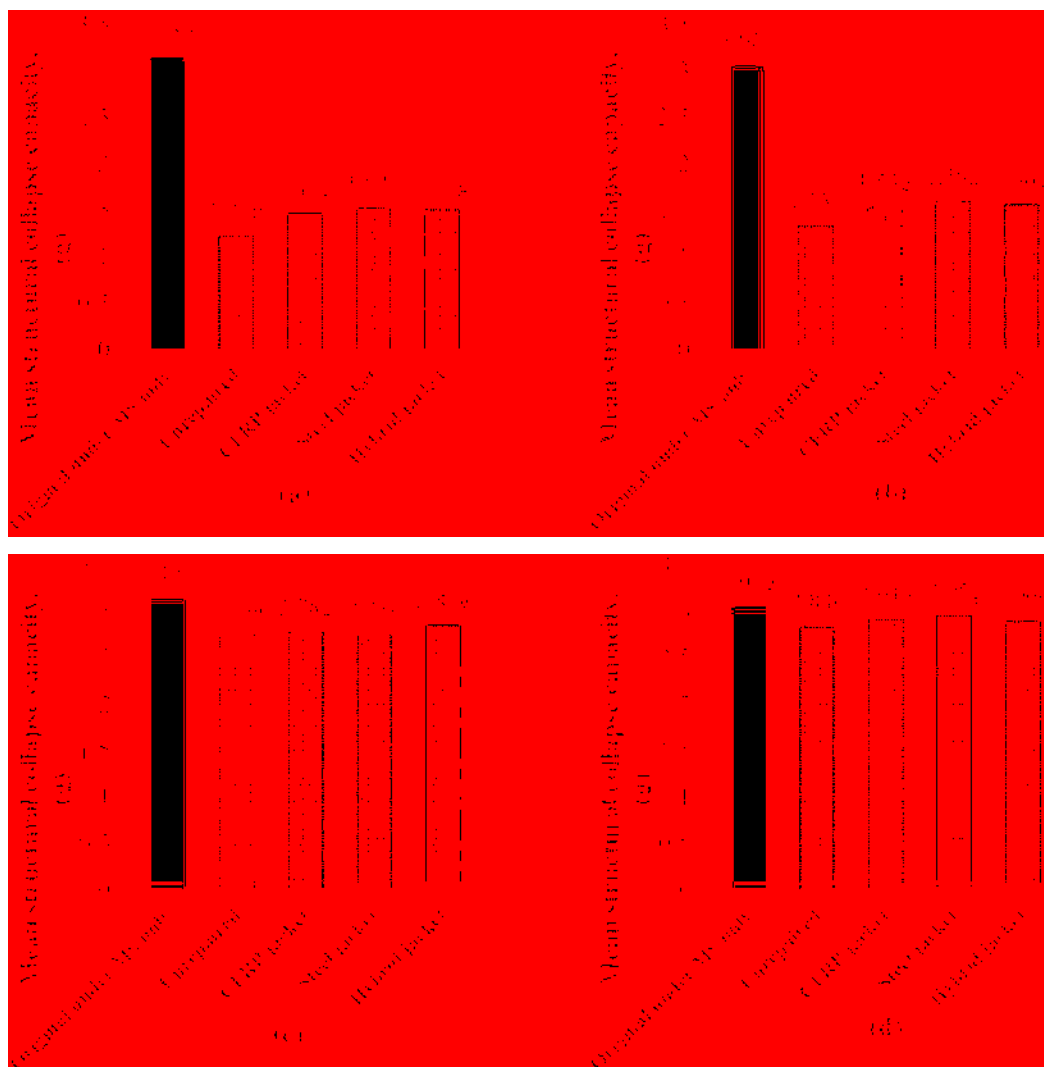


Fig. 16. Mean structural collapse capacity under (a) severe MS-severe AS far-fault motions (ensemble 1); (b) severe MS-severe AS near-fault motions (ensemble 2); (c) severe MS-moderate AS far-fault motions (ensemble 1); (d) severe MS-moderate AS near-fault motions (ensemble 2).

IV. COMPRESSIVE BEHAVIOR OF FRP-CONFINED CONCRETE-FILLED PVC TUBULAR COLUMNS

ABSTRACT

This paper presents a new composite confinement system of FRP wrap and PVC tube with and without an impact absorption medium (compressible foam) in between. The compressive behavior of the proposed FRP-confined concrete filled PVC tube (CCFPT) was investigated and compared with those of the concrete filled PVC tube (CFPT) and FRP-wrapped (FW) concrete cylinder. The effect of compressible foam on the post-peak strain behavior of the CCFPT specimen was explored. The applicability of seven existing FRP-confined stress-strain relationships to predict the strength and ductility enhancement of FW and CCFPT specimens was evaluated. A total of 14 FW, 5 CFPT, and 17 CCFPT specimens with 152 mm in diameter and 305 mm in height were tested under monotonically increasing axial loads in compression. The key parameters examined included the type and thickness of FRP wraps, the presence and thickness of compressible foam, and loading area. Test results indicated that, without compressible foam, the CCFPT cylinders resembled the FW cylinders in stress-strain relationships with brittle failures upon FRP rupture and immediately-followed PVC fracture due to sudden transfer in confining pressure. With compressible foam, the CCFPT cylinders can combine the strength of the FW cylinders and the ductility of the CFPT cylinders. This is because the soft PVC tube in CCFPT cylinders slightly contributes to axial strength and confining pressure of the concrete cylinders, copes with significant concrete dilation, and becomes extremely ductile after the impact energy generated at FRP rupture has been absorbed by the foam through impedance modulation. The stress-strain model by Lam and Teng can reasonably predict both the ultimate strength and the ultimate strain of CCFPT specimens by a relative error of 8.3% and 26.4%, respectively.

Keywords: *A. Carbon-carbon composites (CCCs); B. Strength; B. Plastic deformation; D. Mechanical testing; FRP-confined concrete-filled PVC tube.*

1. Introduction

It has been well established that both the mechanical (strength, stiffness and ductility) and long term performance of concrete structures (normal strength [1-12], high/ultra-high strength [13-19], self-consolidating/compacting [20, 21] and more recently recycled aggregate concrete [22, 23]) can be enhanced through the lateral confinement by a confining jacket (i.e., active or passive confinement). Various forms of confining jackets from different materials have been extensively studied for strengthening/rehabilitation of existing structures and for new constructions [24-37], including steel stirrups, steel spirals, hollow tubes/prisms, prestressing strands, fiber reinforced polymer (FRP) composite stirrups, FRP tubes, FRP rings, pre/post-tensioned FRP shells, composite ropes, shape memory alloy (SMA) wraps, and hybrid (active and passive) confining jackets.

Past studies have demonstrated the enhanced structural performance of concrete filled tube (CFT) systems with steel or FRP confinement as an improved form of gravitational and lateral load resisting system for tall buildings/bridge columns and pile-footings [10, 14-19, 22, 32, 38-40]. Concrete filled steel tube (CFST) and concrete filled FRP tube (CFFT) columns are the two most common types of CFT systems that have been investigated at both member and system levels under static and simulated seismic loading conditions (e.g. [3-5, 10, 13-19, 21, 23, 32, 38, 39]). The CFT systems demonstrated remarkable properties in terms of enhanced structural performance (i.e., strength, stiffness, ductility and hysteretic capacity) and project economy/constructability (e.g. reduced tube thickness due to the composite action between concrete and confining tube [41]). While a steel tube serves as shoring system/permanent formwork and provides substantial continuous confining pressure to the concrete infill [15, 32, 38, 39], the encased concrete can improve fire resistance of the steel tube. Other studies also demonstrated the improved performance of hybrid tubular columns by incorporating steel and FRP tubes, referred to as hybrid double-skin tubular columns or beams with remarkable hysteresis capacity against seismic excitations [42-45].

Durability of reinforced concrete (RC) structures and steel-concrete composite structures under severe environmental conditions (e.g. marine environments) has always

been a major concern [46, 47]. It was estimated that the U.S. alone annually spent over \$1 billion for repair and replacement of waterfront piling systems [48]. This high cost has spurred great interest in alternative composite column/pile materials such as FRPs, recycled plastics, and hybrid materials. Consequently, FRP materials were considered an attractive alternative for structures in marine and other harsh environments [6].

Considering the corrosion-induced durability of steel tubes [13, 48] and bond issues as well as the brittle failure of elastic FRP tubes, particularly in seismically active regions [2, 15, 49, 50], several studies have been conducted on commercially available thermoplastic pipes, such as high-density polyethylene (HDPE) and polyvinyl chloride (PVC) [47, 51-56] for the improved durability of RC structures. PVC materials, exhibiting remarkable mechanical properties compared to other general purpose olefin plastics, demonstrate impressive ratio of cost to performance, specifically durability [51, 52, 56]. PVC is a polymer-based material which is vastly utilized in the construction industry. Investigation on soil buried PVC pipes after 60 years of active use [57] indicated no deterioration and likely to have a further life expectancy of 50 years! PVC is one of the most important commercial plastics owing to its wide applications, low costs and excellent properties such as (1) high electrical insulation; (2) high resistance for abrasion; (3) low diffusion for humidity; (4) remarkable resistance to water, bases, acids, alcohols, oils; (5) large elongation at break (i.e., ductile); (6) low creep deformation; (7) workability including (e.g. machining, cutting, welding/gluing for fabrication versatility); (8) consistency; (9) excellent corrosion resistant, durability and mechanical stability (little change in mechanical strength and molecular structure); and (10) safety due to its fire retarding properties [58-60]. The thermal conductivity of PVC is only 0.45~0.6% of a steel tube, which provides a stable curing condition for the core concrete to achieve high performance and high durability [55, 56]. Kurt [51] made the first attempt in implementing commercially available rigid plastic (acrylonitrile butadiene styrene and PVC) pipes filled with concrete as a new composite column system for structural applications. Toutanji and Saafi [52, 53] then introduced a new hybrid column system for new construction consisting of concrete filled PVC tubes reinforced with external discrete FRP hoops at different spacings. In such a hybrid system, PVC serves as the cast-in-place formwork while the FRP-PVC tube provides additional confinement to the

core concrete. Moreover, a few research studies on concrete filled PVC tubes were undertaken [47, 55, 56, 61, 62]. However, experimental studies on CFT columns consisting of PVC tubes are limited to uniaxial compression tests [55]. The study by Gupta and Verma [61] on RC filled PVC tubes subjected to harsh environmental condition indicated that “no degradation in the strength and ductility of RC-filled poly-vinyl chloride tubular specimens was observed after submergence in sea water”. Test results on RC filled PVC tubes submerged in saturated sea water (concentration 20 times higher than natural sea water) for 6 months revealed that the microstructure and chemical composition of the PVC jacket remained nearly identical after exposure to sea water (i.e., chemical action of sodium chloride and magnesium sulfate) [61]. It was then concluded that PVC tubes provide a safety jacket to their encased concrete core with improved strength and ductility. Most recently, Jian et al. [63] studied the performance of slender concrete-filled carbon FRP-PVC tubular (CFCT) columns of various slenderness ratios under uniaxial compression. However, only four CFCT specimens with discrete carbon FRP strips were tested. Moreover, there is a wealth of contradictory published data on PVC, “a kind of elastic material” [63] or a ductile plastic material [47, 55, 56]. For instance, the ductile failure of a PVC tube was observed up to a complete collapse of the plastic tube [47, 55, 56, 61]. On the other hand, bursting (fracture) of the plastic tube toward the end the loading process was demonstrated with CFPT [62].

The main advantage of a CFST system is full concrete section confinement by the steel tube that is in turn constrained by the concrete and delayed from buckling. This composite action results in enhanced stiffness, strength, ductility and overall stability of the CFST system. However, due to high modulus of elasticity, the steel tube is subjected to a large portion of the axial load capacity and can still be buckled. On the contrary, the modulus of elasticity for PVC tubes is approximately 1/50 of that of steel. The axial load carried by the PVC tube is substantially less than that by a steel tube of same size, which makes the PVC tube experience no premature buckling.

Harries and Carey [64] were among the first researcher who investigated the effect of unbonded FRP wrap on the performance of FRP-confined concrete cylinders by introducing an approximately 0.08 mm thick plastic wrap used in kitchen between the FRP wrap and concrete cylinder. Their tests clearly indicated a reduction in the maximum

obtainable confined concrete strength due to the use of the plastic wrap. Later, Xiao et al. [32] further evaluated the application of foam between the FRP wrap and steel tube in confined concrete-filled steel tubes.

In this study, a new composite confinement system with a FRP wrap outside a PVC tube with an energy dissipation medium in between is investigated. The energy dissipation medium is a thin, compressible, rubber-based foam that is designed to (1) regulate the change in confinement provided by the FRP wrap so that significant axial deformation of the confined cylinder without strength enhancement can be achieved prior to FRP rupture, and (2) dissipate impact energy generated by the FRP rupture so that the PVC tube is not fractured under slowly increased confinement. The FRP-confined concrete filled PVC tubular (CCFPT) cylinder with an energy dissipation medium could be advantageous over others when the brittle failure of FRP materials is not desirable for RC structures in high seismicity regions. Therefore, the compressive behavior of CCFPT cylinders is characterized under monotonically increasing axial loads in compression and compared with those of the CFPT and FRP-wrapped (FW) specimens. The key parameters to be examined include the type and thickness of FRP wrap, the presence and thickness of compressible foam, and compressive loading area. To this endeavor, 17 CCFPT, 5 CFPT, and 14 FW cylinders with 152 mm in diameter and 305 mm in height were cast with normal strength concrete. The ultimate strength and strain as well as the stress-strain relationships are investigated and discussed. The potential of predicting the compressive behavior of CCFPT cylinders with seven existing stress-strain models developed for FRP-confined cylinders is assessed.

2. Experimental program

2.1. Details of cylinder specimens

All the CCFPT, CFPT, and FW specimens were fabricated, cured and tested in the Structural Engineering High-Bay Research Laboratory (SERL) at Missouri University of Science and Technology. The cast specimens and the quality control/quality assurance/reference cylinders according to ASTM C39-12 [65] and C496-11 [66] and flexural beam specimens according to ASTM C78-10 [67] were covered with wet burlap

and plastic wraps. For each CFPT specimen, a Grey Schedule 40 PVC pipe was cut to the required length (i.e., 305 mm) and then affixed at one end to a wood board as illustrated in Fig. 1(a), which functioned as a stay-in-place formwork during concrete casting. A FRP wrap was applied using a manual wet layup process, which required wrapping of an epoxy-resin impregnated fiber sheet around a PVC tube for each CCFPT specimen or around a precast concrete cylinder for each FW specimen. As illustrated in Fig. 1(b), the two ends of each specimen were then ground using a surface-grinding machine to remove irregularities, unevenness, and soft concrete and ensure that the specimen ends were orthogonal to its longitudinal axis. To avoid direct axial load transfer from loading platens, the FRP wrap was recessed by 5 mm at both ends of each CCFPT or FW specimen. The confinement materials for all specimens are summarized in Table 1.

The cylinder specimens under axial compressive loading were identified according to the confinement material (i.e., FRP, PVC, or FRP+PVC), where the FRP type, number of FRP layers, and PVC tube type are specified. Confinement tube is designated as either FW (i.e., FRP-wrapped confined), CFPT (i.e., concrete filled PVC tube), or CCFPT (i.e., confined concrete filled PVC tube). The symbols G, and C are used to represent the type of FRP-confinement, namely: carbon (C), or glass (G) preceded by the number of layers. For CFPT and CCFPT specimens the letter G was used in specimen designation to specify the PVC pipe schedule/color followed by a number that determines the PVC pipe schedule (ASTMD1785 [68] standard pressure rating). As stated earlier, the gray Schedule 40 PVC pipe was used for manufacturing all the CFPT, and CCFPT specimens in this study, hence the G40 designation was used accordingly. A final number was provided to identify between nominally identical specimens. Details on all the compressive specimens according to their type of confinement are presented later in Table 6. For example, a FRP-wrapped specimen confined with one layer of carbon FRP, which is the first in its group would be labelled as FW-1C#1. Similarly, a CFPT specimen encased by the gray Schedule 40 PVC tube, and is third in its group would be labelled as CFPT-G40#3. Lastly, a CCFPT specimen encased by the gray Schedule 40 PVC tube and one layer of carbon FRP, and is the first in its group would be labelled as CCFPT-G40-1C#1.

As stated earlier, two companion CFPT specimens with 12-mm gap at both ends (i.e., CFPT-G40-w gap#1 and 2) were tested (see Fig. 2(d)). This gap was provided at both ends of the specimen to avoid compressive axial load resisted by the PVC tube. These specimens were tested to compare the relative performance of the CFPT system when either the entire cross section (i.e., PVC tube and concrete infill) or the infill concrete only is loaded.

Moreover, four CCFPT specimens including a foam layer between the PVC tube and FRP wrap as shown in Fig. 2(e) were added into the test matrix, and designated as CCFPT-G40-1G-foam#1, 2, 3 and 4 specimens, respectively. Effect of the thickness of the foam layer on the axial stress-axial strain relationship of CCFPT specimens were studied by comparing the performance of two different thicknesses of the foam layer. For CCFPT-G40-1G#1 and 2 specimens, a 4.175-mm foam layer was utilized. For CCFPT-G40-1G#3 and 4 specimens, a 1-mm foam layer was affixed on the PVC tube prior to the FRP wrap application. All the four specimens were identical in terms to the encased concrete, PVC tube and FRP wrap properties, except the thickness of the foam layer varied.

2.2. Material properties

2.2.1. Concrete

A normal strength concrete mix with a target unconfined compressive strength (f'_{co}) of 50 MPa at 28 days was used in the fabrication of cylinder specimens. The concrete mix was delivered by a local ready-mix concrete supplier (Rolla, MO). It consisted of ASTM Type I Portland cement as binder, crushed limestone with a maximum nominal aggregate size of 25 mm from the Potosi quarry (Potosi, MO), and river sands (Jefferson City plant, MO). Quality control/quality assurance (QC/QA) companion cylinders (ASTM:C39 [65] and ASTM:C496 [66]) and beams (ASTM:C78 [67]) were also cast from the mix. Table 2 presents fresh and hardened concrete properties of the mix in the present study.

Plain concrete cylinders with 152 by 305 mm dimensions were tested at selected time intervals to determine the in-place unconfined concrete strength, f'_{co} . The average

compressive strength of axially loaded specimens throughout the period of testing was 49.5 MPa.

2.2.2. FRP

Table 3 compares the manufacturer-specified with measured properties of carbon and E-Glass fibers used in the preparation of cylinder specimens. The measured data was based on flat coupon tests (ASTMD3039 [69]). At least five tensile tests were conducted for each type of FRP fabrics. For each CCFPT or FW specimen, the PVC tube or concrete cylinder was first brushed with a thin layer of epoxy resin and then manually wrapped with an epoxy impregnated FRP sheet in the hoop direction. For CCFPT and FW specimens, the FRP sheet was overlapped with 152 mm and 144 mm, respectively, to prevent premature debonding failure.

2.2.3. PVC

Commercially available Grey schedule 40 PVC pipes (as per ASTM D1785 [68]) used for water supply with a nominal pressure of 1.24 MPa were used to prepare CFPT and CCFPT specimens. The selected PVC pipe as shown in Fig. 2 had grey color with an inside diameter (ID) of 152 mm and a minimum wall thickness of 7.11 mm. All the CFPT, CCFPT, and FW specimens had a concrete core of 152 mm in diameter and 305 mm in height as shown in Table 1. Details of the CFPT, CCFPT, and FW specimens are illustrated in Fig. 2.

Mechanical properties of the PVC pipes were obtained by testing a minimum of five tensile dogbone coupon specimens (as per ASTM D638 [70]) as reported in Table 4. Each tensile PVC coupon specimen was instrumented with two electrical strain gages in axial and transversal directions, and a clip-on extensometer to determine the modulus of elasticity and Poisson's ratio. Fig. 3(a) depicts the typical tensile stress-strain behavior of the PVC material. The PVC coupon specimens exhibited significantly ductile behavior reaching to an average fracture strain of 46% (i.e., 2~3 times that of mild structural steel). The typical failure of PVC pipe tensile coupon specimens is illustrated in Fig. 4, where significant plastic elongation is evident. As shown in Fig. 3(a), the tensile behavior of PVC materials under tension can be divided into four regions: 1) linear-elastic; 2) onset

of yielding and nonlinear up to the ultimate strength; 3) post-peak strain-softening; and 4) yielding plateau with 80% of the ultimate strength till fracture. PVC materials exhibited a substantially lower strength but higher ductility than FRP materials. The ductile behavior was observed from discoloration and white patches due to the flow of resin in Fig. 4 with stable post-peak residual strength up to a large fracture strain.

To evaluate the material property of PVC tubes used in CFPT and CCFPT specimens, two hollow PVC tube specimens were axially loaded in compression. They failed due to local elephant foot buckling and global buckling as illustrated in Fig. 5. The axial stress-strain relationships of the hollow PVC tubes under axial compression are illustrated in Fig. 3(c). The material properties of PVC tubes obtained from the axial compression tests are given in Table 5. By comparing Table 5 with Table 4, the measured mechanical properties (yield stress and ultimate strength) of PVC pipes under tension and compression differ by less than 1%.

2.3. Instrumentation and testing procedure

For each cylinder specimen, three vertical linear variable differential transformers (LVDTs) were evenly distributed around the cylinder perimeter to measure axial deformation between the top and bottom sections of the specimen, as illustrated in Fig. 6(b). In addition, three horizontal LVDTs located at the mid-height of the cylinder were evenly distributed around the specimen to measure the lateral dilation (i.e., radial expansion) of the specimen under axial compressive loading. Moreover, PVC tube or FRP sheet of the specimen was instrumented at mid-height with three unidirectional strain gages to measure axial strains to correct the LVDT measurements at the early stage of loading. This is because the LVDT measurements at the early stage are often inaccurate due to potential slack in the test setup [72]. The hoop strain of a PVC tube or FRP sheet was also measured with three evenly-distributed unidirectional strain gages at mid-height outside the overlap region. For FW and CCFPT specimens, one additional hoop strain gage was installed on the overlap region of the FRP wrap. This strain gage was used to measure the potential discrepancy of hoop strain in the overlap region of the FW and CCFPT specimens. The average of the three strain measurements outside the overlap region is reported as the hoop strain of the specimen.

Axial load was applied on the composite cross section of concrete and PVC tube in some CFPT cylinder specimens as shown in Fig. 2(d). In this case, the PVC tube is in a biaxial stress state with the direct axial stress and the hoop stress due to concrete dilation. For comparison, the PVC tube in other CFPT specimens was reset to leave a 12-mm gap at both ends, making the PVC tube subjected to the uniaxial hoop stress only as seen in Fig. 2(d).

After 28 days of curing, specimens were tested in displacement control at approximately 0.5 mm per minute on a 2670-kN capacity MTS testing machine in the Highbay Structures Laboratory. Prior to testing, both ends of the specimens were ground with a concrete end grinding machine to ensure a uniform distribution of the applied axial load. For each CFPT and CCFPT specimen, the load was applied to its entire cross section (i.e., PVC tube and concrete). A data acquisition system was utilized to record the load, displacement, and strain of specimens throughout each test. The unconfined concrete compressive strength (f'_{co}) was determined at the time of testing, and its corresponding axial strain (ε_{co}) was calculated according to Tasdemir et al. [71] as follows:

$$\varepsilon_{co} = (-0.067 f'_{co} + 29.9 f'_{co} + 1053) \times 10^{-6} \quad (1)$$

where f'_{co} is in MPa.

3. Test results

3.1. Failure modes

The test results of all specimens are summarized in Table 6. The typical failure modes observed during tests are illustrated in Fig. 7 for various types of confinement materials.

The FW specimens and the CCFPT specimens without a thin layer of foam exhibited a brittle rupture of FRP wraps either over the entire height, as shown in Figs. 7(a, b, g, and h), or around the mid-height, as shown in Figs. 7(c, d, i and j). The rupture of FRP wraps in the specimens immediately resulted in catastrophic failure of the core concrete due to loss of confinement. The CFPT specimens exhibited a very ductile behavior with gradual post-peak strength degradation and experienced no cracking or

PVC fracture as the core concrete continued to dilate and push the PVC wall outwards to bulge and deform significantly as shown in Fig. 7(e). Due to non-uniform dilation of the core concrete, the highly stressed region of the PVC tube showed discoloration or white patch due to the flow of resin, as shown in Fig 7(f). The core concrete was thoroughly crushed and somewhat pulverized and the PVC tube remained intact. The typical shear cone formation for the CFPT-G40-w gap#1 in Fig. 7(f) can be observed due to discoloration of the highly stressed region on the PVC tube. The FW and CCFPT specimens exhibited similar shear cone type failure to a less degree depending on the ultimate dilation of the confining jacket.

Further examination on the CCFPT specimens without a thin layer of foam indicated that the PVC tube immediately fractured upon FRP rupture due to sudden transfer of the confining pressure from the FRP sheet to the PVC tube, regardless of the type and number of FRP layers. The PVC tube was not able to absorb a large amount of surge energy released from the rupture of FRP sheet. Indeed, the rupture of CCFPT specimens was more explosive than that of FW specimen as a louder sound was heard during tests of the CCFPT specimens. As a result, the core concrete in the CCFPT specimens was damaged more severely than that of the FW specimens.

However, the CCFPT specimens with a thin layer of foam between the FRP sheet and PVC tube demonstrated a ductile behavior similar to their CFPT counterparts with no FRP wrap. In this case, the FRP rupture in each CCFPT specimen was gradual since the progressive fracture of fibers caused tearing and splintering of the FRP sheet along the specimen's height as shown in Figs. 7(k, l). The observed behavior was similar to the failure mode of confined concrete filled FRP tubes with inclined fibers reported by Vincent and Ozbakkaloglu [72]. Contrary to the local rupture of FRP wrap in the CCFPT with no foam, introduction of the foam in a CCFPT specimen resulted in a more-like distributed rupture of the FRP wrap. In this case, the PVC tube remained intact upon FRP rupture; no catastrophic failure occurred.

3.2. Stress-strain behavior and ultimate condition

The ultimate axial strength (f'_{cu}) recorded at the failure of a specimen and its corresponding axial strain (ϵ_{cu}) as well as the FRP hoop rupture strain ($\epsilon_{h,rupt}$) of each

confined specimen are reported in Table 6; the axial stress-strain relationships are presented in Fig. 8. The ultimate strength (f'_{cu}) and the peak stress (f'_{cc}) are presented in Table 6 according to the type of stress-strain relationships. For stress-strain relationship that consisted of a descending post-peak branch, the ultimate strength (f'_{cu}) was lower than the recorded peak stress (f'_{cc}); both the ultimate strength (f'_{cu}) and the peak stress (f'_{cc}) are reported. For stress-strain relationship with a monotonically increasing second branch, the ultimate strength (f'_{cu}) and peak stress (f'_{cc}) were equal; only f'_{cc} is reported in Table 6. To establish the axial stress-strain relationships of all CFPT and CCFPT specimens except CFPT-G40-w gap#1, 2, the applied load on the confined concrete for a given axial strain was determined by subtracting the axial load resisted by the PVC tube from the total load applied. The load acting on the PVC tube was determined based on the results of hollow PVC tube compression tests, assuming that the load-strain behavior of PVC tubes used in a CFPT or CCFPT specimen is equal to that of the corresponding hollow PVC tube.

The ultimate condition of FW and CCFPT specimens without any foam was quite clear due distinct rupture of the FRP wrap observed during testing. However, for CFPT specimens and the CCFPT specimens with a thin layer of foam (CCFPT-G40-1G-foam#1, 2, 3 and 4), no catastrophic failure was observed; tests were terminated after excessive compression (i.e. 7%). As shown in Table 6, the ultimate conditions (i.e., f'_{cu} , ϵ_{cu} and $\epsilon_{h,rupt}$) for these specimens corresponded to 20% drop below the recorded peak stress (i.e., threshold of $0.8 f'_{cc}$). This threshold has been widely adopted in similar studies (e.g., [72]); it was used herein for the sake of consistency since the method used in determining the ultimate condition may significantly influence the ultimate strain. With such a threshold, all CFPT specimens without gap have a relatively small strain enhancement ratio ($\epsilon_{cu}/\epsilon_{co}$) since they still demonstrate a stable load-carrying capacity upon 40% drop from the measured peak stress as shown in Fig. 8(e).

The ultimate hoop rupture strain ($\epsilon_{h,rupt}$) of each specimen obtained from the average of three lateral strain gages installed outside the overlapping FRP region is tabulated in Table 6. Past studies have indicated that the hoop rupture strains obtained from FRP-confined concrete specimens and double skin tubular columns are usually smaller than the ultimate tensile strain (ϵ_{fu}) of component fibers as advertised by

manufacturers [4, 5, 13, 73-77]. Different contributory causes for this phenomena have been cited in the literature, including: (1) cracking of the confined concrete results in non-uniform strain distribution and stress concentration on the FRP wrap, (2) curvature of the FRP reduces its strain capacity, (3) geometric imperfection of the column, (4) non-uniform bonding of the FRP to the column, (5) misalignment of fibers, and (6) geometric discontinuity within the FRP overlap [3, 5, 76]. This apparent in-situ FRP jacket inefficiency could result in low confining pressure. The strain reduction factor (k_ε) reported in Table 6 is calculated for FW and CCFPT specimens by:

$$k_\varepsilon = \frac{\varepsilon_{h,rupt}}{\varepsilon_{fu}} \quad (2)$$

Note that the strain reduction factor (k_ε) presented for the CCFPT specimen with a thin layer of foam (i.e., CCFPT-G40-1G-foam#1, 2, 3 and 4) in Table 6 is approximate only since there was no distinct hoop rupture of FRP definable in these specimens.

4. Analysis of test results

4.1. Stress-strain behavior

When concrete is confined by an enclosing material (e.g., FRP sheet or PVC tube) and subjected to monotonically increasing axial compression, passive confining pressure is developed in the jacket as the enclosed concrete tends to dilate laterally due to Poisson's effect, resulting in a multiaxial state of stress. The hoop stress in the confining jacket increases as the internal pressure develops between the jacket and the confined concrete. Hence, confinement action depends on two main factors: 1) radial stiffness of the confining jacket restraining the concrete from being dilated; and 2) lateral dilation of the concrete under axial compression. Depending on the type of confinement materials, distinct stress-strain relationships were obtained as shown in Fig. 8. Specifically, the axial behavior of confined specimens consists of three regions. In the first region, irrespective of the confinement type (PVC tube, FRP tube, or PVC+FRP tube), the behavior of the confined specimen is similar to that of unconfined plain concrete since the core concrete is not severely cracked to allow the required dilation and engage with the confining device. In the second region around the peak stress of corresponding unconfined

concrete, excessive cracking results in a state of unstable volumetric dilation of the confined concrete that is then restrained by the confining tube from further deformation and cracking. This region of the stress-strain relationship is characterized by a transitional curve in the vicinity of the unconfined concrete compressive strength. Eventually, a third region is defined when the confining device is fully engaged. Depending on the level of existing confinement pressure provided by PVC tube and/or FRP sheet, the tested specimens in this study exhibited either a descending or monotonically ascending stress-strain curve.

The CFPT specimens exhibited a post-peak strain-softening and ductile behavior without sudden strength loss as shown in Fig. 8(e). When adequately confined (i.e., 3 layers of FRP), the FW specimens and the CCFPT specimens with no foam exhibited a monotonically ascending strain-hardening response up to FRP's rupture as shown in Figs. 8(b, d, h and k). It can also be observed in Figs. 8(h, k) that some of the CCFPT specimens experienced a small drop in strength after the transition point between the initial ascending branch and the following branch. The gradual softening can be attributed to uneven micro-cracking of the encased concrete and local deformation of the PVC tube. However, when adequate confinement by FRP is provided (i.e., CCFPT-G40-3C#1, 2 and 3 and CCFPT-G40-3G#1, 2 and 3), the CCFPT specimens exhibited a monotonically ascending axial stress-strain response in the second branch. Therefore, the post-peak stress-strain relationship of the CCFPT specimens is influenced by stiffness of the confining jacket. A similar conclusion was drawn for FRP-confined columns (e.g., [5, 77]).

For lightly confined FW and CCFPT specimens (i.e., with 1-ply of FRP), the strength enhancement ratio (f'_{cc}/f'_{co}) and strain enhancement ratio ($\epsilon_{cu}/\epsilon_{co}$) were significantly smaller than those of their companion ones with adequate confinement (i.e., with 3-ply of FRP) as reported in Table 6.

The CFPT specimens with gaps at both ends (CFPT-G40-w gap#1 and 2) demonstrated a pre-peak behavior similar to their companion specimens with no gap. Around the peak stress, the unconfined concrete outside the PVC tube started to crush, resulting in rapid post-peak strength degradation on the axial stress-strain relationship as shown in Fig. 8(f). However, the PVC tube in this series of specimens still demonstrated

a very ductile behavior, similar to CFPT specimens with full height tube. The shear type failure and the direction of a shear crack associated with the discolored region on the PVC tube is highlighted in Fig. 7(f). The presence of the PVC tube, even when it partially confined the concrete core in the middle portion, allowed the obtainment of excessive axial strain.

The CCFPT specimens with a thin layer of foam exhibited a distinct axial stress-strain relationship due to the cushioning property or space provided by the foam layer between the PVC tube and FRP wrap. All the four specimens demonstrated consistent behavior up to the peak stress with a smooth, gradual post-peak strength reduction as marked in Fig. 8(j). The post-peak strength reduction was completely stable since the space occupied by and the flexibility of the foam regulated the confinement pressure, reducing or eliminating impact effect on the PVC tube and thus preventing the PVC tube from sudden fracture. The effect of the foam thickness becomes significant on the second region of the post-peak axial stress-strain relationship (i.e., plateaued region on the axial stress-strain relationship after the drop of post-peak strength). The thicker the foam in specimens (i.e., CCFPT-G40-1G-foam#1 and 2 versus CCFPT-G40-1G-foam#3 and 4), the larger the strength drop observed before the GFRP wrap starts to provide the confining pressure. The greater strength reduction for the specimens with thicker foam is due to the larger gap provided by the foam layer, allowing larger dilation of the core concrete before the FRP wrap becomes completely engaged. In other words, the FRP wrap becomes engaged at a larger level of axial strain and the FRP wrapped cylinder hence experienced a larger strength loss. Therefore, different ultimate axial strains can be obtained by changing the foam layer thicknesses. Moreover, presence of the foam layer delayed the onset of GFRP rupture as marked in Fig. 8(j), compared to the CCFPT specimens without foam. As a result, the specimens with foam are very ductile with gradual rupture of the GFRP.

In summary, a sudden rupture of the entire GFRP wrap in specimens without a foam layer resulted in immediate fracture of the PVC tube. However, the GFRP wrap in specimens without a foam layer exhibited a progressive rupture that did not lead to immediate fracture of the PVC tube due to the space or the impact absorption provided by the foam. In essence, the presence of the foam layer (i.e., CCFPT-G40-1G-foam#1, 2,

3 and 4) altered the failure mode of CCFPT specimens from brittle to ductile failure, as shown in Fig. 7(k, l).

4.2. Influence of confinement pressure and detail

As expected, increase in the number of FRP layers in the FW and CCFPT specimens led to an increase of ultimate conditions (i.e., f'_{cu} and ϵ_{cu}) as seen in Table 6, and improved the strength enhancement ratio (f'_{cu}/f'_c) and strain enhancement ratio ($\epsilon_{cu}/\epsilon_{co}$). Figs. 9(a, b) illustrate the influence of lateral confinement pressure (f_{lu}) provided by different number of FRP layers on the axial stress-strain relationships of the FW and CCFPT specimens, respectively. In preparation of the FW and CCFPT specimens, the number of FRP layers was determined to provide a comparable nominal confinement ratio (f_{lu}/f'_{co}) between the FW and CCFPT specimens so that a meaningful comparison can be made between the two types of specimens. The nominal confinement ratio (f_{lu}/f'_{co}) represents the lateral confinement pressure (f_{lu}) divided by the in-place unconfined concrete strength (f'_{co}). When a uniform confinement pressure is assumed around a circular cross section, it can be calculated by [5, 13, 72, 78]:

$$\frac{f_{lu}}{f'_{co}} = \frac{2t_f f_{fu}}{Df'_{co}} = \frac{2t_f E_f \epsilon_{fu}}{Df'_{co}} \quad (3)$$

where t_f = total nominal thickness; E_f = the modulus of elasticity; ϵ_{fu} = the ultimate tensile strain of fibers; and D = the diameter of confined concrete. However, as mentioned earlier and reported in Table 6, the FRP hoop rupture strain ($\epsilon_{h,rupt}$) is often lower than that of the ultimate tensile strain of fibers (ϵ_{fu}) obtained from flat coupon tests and/or reported by manufacturers. Therefore, a strain reduction factor, k_ϵ , was introduced; the actual confinement ratio ($f_{lu,a}/f'_{co}$) was calculated and presented in Table 6 by:

$$\frac{f_{lu,a}}{f'_{co}} = \frac{2t_f f_{fu} k_\epsilon}{Df'_{co}} = \frac{2t_f E_f (\epsilon_{fu} k_\epsilon)}{Df'_{co}} = \frac{2t_f E_f \epsilon_{h,rupt}}{Df'_{co}} \quad (4)$$

The nominal confinement ratio (f_{lu}/f'_{co})_{PVC} of a PVC tube can be calculated in a similar way:

$$\left(\frac{f_{lu}}{f'_{co}} \right)_{PVC} = \frac{2t_{PVC} f_{y,PVC}}{D_{int} f'_{co}} \quad (5)$$

where t_{PVC} = thickness; $f_{y,PVC}$ = yield strength; D_{int} = inside diameter of the PVC tube. For $f_{lu} = 3.8$ MPa, the nominal confining ratio of a Grey Schedule 40 PVC tube was determined to be approximately 0.08 as presented in Table 6. This level of confinement pressure is very small and approximately half of the confinement pressure provided by 1 ply of CFRP or GFRP.

Figs. 9(a, b) show the axial stress-strain relationships of FW and CCFPT specimens with various actual confinement ratios ($f_{lu,a}/f'_{co}$). The actual confinement ratios ($f_{lu,a}/f'_{co}$) with 1- and 3-ply of FRP are approximately equal to 0.12 and 0.37, respectively, regardless of the type of FRP (both CFRP and GFRP). Depending on the level of lateral confining pressure, either a descending or monotonically ascending first-post-peak behavior can be observed in Fig. 9. Although similar in shape of the axial stress-strain relationship, the ultimate conditions (i.e., f'_{cu} and ϵ_{cu}) were affected by the type of FRP particularly when the number of FRP plies increases as shown in Table 6. This is because the ultimate rupture strain of fibers (ϵ_{fu}) is strongly related with the attainable ultimate axial strain of the FW and CCFPT specimens as demonstrated for FRP-confined concrete [75, 79]. For example, the FW and CCFPT specimens with 3-ply of GFRP (FW-3G#2 in Fig. 9(a) and CCFPT-G40-3G#2 in Fig. 9(b)) experienced greater strength enhancement ratio (f'_{cc}/f'_{co}) and strain enhancement ratio ($\epsilon_{cu}/\epsilon_{co}$) than those specimens with 3-ply of CFRP (FW-3C#2 in Fig. 9(a) and CCFPT-G40-3C#2 in Fig. 9(b)). As presented in Table 6, the FW and CCFPT specimens with GFRP had a significant increase of strain capacity (ϵ_{cu}) and a moderate increase of peak stress (f'_{cc}) than those with CFRP. Although the CCFPT specimens with 3-ply of FRP as presented in Figs. 8(h, k) exhibited a slight strength loss right after the initial peak, the strength loss is temporary and the ultimate strength and strain were improved significantly in comparison with specimens with 1-ply of FRP as shown in Figs. 8(g, i).

Fig. 10(a) compares the axial stress-strain relationships of CFPT specimens without and with gap at both ends. The presence of gap does not affect the linear ascending region up to the peak stress but does change the post-peak response. While the CFPT-G40#1 specimen without gap shows continuous strength degradation due to gradual plastification of the PVC tube, the CFPT-G40-w gap#1 (with gap) demonstrates a rapid and unstable strength loss due to local crushing of the unconfined concrete in the

gap region. After significant crushing of the unconfined concrete in CFPT-G40-w gap#1 specimen (similar in CFPT-G40-w gap#2), the specimen recovered to undergo further axial deformation and the plastic plateau region, similar to CFPT-G40#1 specimen. Comparison of CFPT-G40#1 and CFPT-G40-w gap#1 specimens also allows a understanding of the axial load resisted by the PVC tube in CFPT specimens. While the entire composite cross section of CFPT-G40#1 specimen was axially loaded, only the core concrete of CFPT-G40-w gap#1 was loaded. However, the two specimens had an approximate peak stress of 50 MPa, which represents the in-place unconfined concrete strength (f'_{co}). Fig. 10(a) and the strength enhancement ratio (f'_{cc}/f'_{co}) reported in Table 6 for CFPT specimens (CFPT-G40#1, 2 and 3) and CFPT specimens with gap (CFPT-G40-w gap#1 and 2) clearly indicate that the axial load resisted by the PVC tube is negligible.

Fig. 10(b) compares the axial stress-strain relationships of CCFPT specimens with and without a foam layer between the PVC tube and the FRP wrap. The CCFPT specimens with a foam layer (CCFPT-G40-1G-foam#1 and 3) had more significant post-peak strength drop and ultimate strain (ϵ_{cu}) enhancement than those of CCFPT specimen without a foam layer (CCFPT-G40-1G#2). The foam layer reduced the strain demand on the GFRP wrap which resulted in slower development of confining pressure and thus higher ultimate axial strain. In addition to the improvement in mechanical property, the foam between the PVC tube and FRP wrap can also reduce the impact susceptibility of CCFPT columns under impact loading [80], which is beyond the scope of current study. The presence of foam indicates a reduction of strength enhancement ratio (f'_{cc}/f'_{co}) of CCFPT specimens. The effect of foam thickness can also be observed in Fig. 10(b). The increase in foam thickness (CCFPT-G40-1G-foam#1) results in a greater post-peak strength loss and larger ultimate axial strain.

4.3. Influence of confinement type

Fig. 11 compares the representative axial stress-strain relationships of specimens with various confinement details (i.e., PVC in CFPT, FRP+PVC in CCFPT, and FRP in FW). The CFPT specimen demonstrates a similar behavior to the unconfined concrete up to peak stress but is followed by a strength plateau region. In comparison with CFPT specimens, the adequately confined CCFPT specimens demonstrate a bilinear response

similar to its companion FW specimens. However, it can be seen from Fig. 11 and Table 6 that CCFPT specimens often developed higher ultimate axial stresses (f'_{cu}) and ultimate axial strains (ϵ_{cu}) than those of FW specimens with the same number of FRP layers. This is attributed to the additional confinement on the core concrete by the PVC tube. Although the PVC tube provided relatively low confinement, it provides a mechanism to uniformly distribute the stress induced by concrete dilation and thus reduces the stress concentration due to uneven concrete cracking on the FRP wrap. The rupture of the FRP wrap is thus governed by the overall dilation behavior of the PVC tube, which results in obtainment of larger hoop rupture strains (i.e., larger k_ϵ). A similar observation on the influence of the effect of stress concentration on FRP jacket has been previously reported in the literature (e.g., [81]). Table 6 indicates that the CCFPT specimens consistently exhibited larger strain reduction factors (k_ϵ) than the FW wrapped specimens. Hence, considerably higher strain enhancement ratios were observed for the CCFPT specimens.

The average hoop strain reduction factors (k_ϵ) and corresponding standard deviations (SD) from the FW specimens and CCFPT specimens without a foam layer are presented in Table 7 for each type of confinement material. As stated earlier, no distinct hoop rupture of FRP wraps was observed for these specimens. The obtained results indicate that the confinement type affects the mean k_ϵ with an average value of 0.744 and 0.839 for the FW and CCFPT specimens, respectively. The k_ϵ comparison indicates that the FRP wrap in the CCFPT composite system is more efficient than that in the FW specimen. Table 7 also indicates that, while the mean k_ϵ values for the CFRP ($k_\epsilon= 0.715$) and GFRP ($k_\epsilon= 0.781$) wrap in the FW specimens are close, those for the CFRP ($k_\epsilon= 0.785$) and GFRP ($k_\epsilon= 0.903$) in the CCFPT configuration are quite different.

Lim and Ozbakkaloglu [82] recently proposed a strain reduction factor (k_ϵ) equation for FRP-confined normal and high strength concrete [4, 82] as follows.

$$k_\epsilon = 0.9 - 2.3f'_{co} \times 10^{-3} - 0.75E_f \times 10^{-6} \quad (6)$$

where f'_{co} and E_f are in MPa. This expression is applicable for FRP-confined concrete with an unconfined concrete strength up to 120 MPa and a FRP's modulus of elasticity of $100,000 \text{ MPa} \leq E_f \leq 640,000 \text{ MPa}$ which is confined by any of CFRP, GFRP, AFRP, high-modulus CFRP (HM CFRP), and ultra-high-modulus CFRP (UHM CFRP). GFRP-confined specimens with E_f lower than 60,000 MPa or ϵ_f greater than 4.0%

were excluded in the development of Eq. (6) [82]. For the tested specimens in this study, the obtained strain reduction factors (k_ϵ) for the CFRP and GFRP from Eq. (6) would be 0.6 and 0.73, respectively, which are not so far away from the measured mean value (0.79) for all the tested specimens. Therefore, Eq. (6) may be applied to determine the k_ϵ , for the tested CCFPT specimens since the soft PVC tube in CCFPT specimens contributes little to the axial load capacity; their ultimate strength is mainly due to the confinement provided by the FRP wrap. Consequently, the CCFPT specimens failed similarly to the FW specimens.

Fig. 12 plots the strength enhancement ratio (f'_{cc}/f'_{co}) and strain enhancement ratio ($\epsilon_{cu}/\epsilon_{co}$) as a function of actual confinement ratio ($f_{lu,d}/f'_{co}$) for various confinement types. The obtained trend lines for strength and strain enhancement ratios for FW and CCFPT specimens indicate their similar behavior with a nearly identical trend line for strength enhancement ratio (Fig. 12(a)). However, the CCFPT specimens demonstrate greater improvement in strain enhancement ratio ($\epsilon_{cu}/\epsilon_{co}$) compared to companion FW specimens (Fig. 12(b)).

5. Applicability of existing stress-strain models for CCFPT behavior prediction

To appropriately design a CCFPT system, axial strength and strain enhancement ratios must be determined accurately. In this section, seven existing strength and strain models as presented in Table 8 are verified against the obtained experimental results from the FW and CCFPT specimens to understand their applicability for the proposed composite system. Six models [84-89] were chosen from over 80 models reviewed and reported by Ozbakkaloglu et al. [5]. The last model was selected from the most recent study by Ozbakkaloglu and Lim [4] in which a new design-oriented model was developed using 3042 test results from carefully chosen experimental tests through an extensive review of the literature. Since these models were developed to predict the ultimate conditions of FRP-confined concrete with a monotonically increasing axial stress-strain relationship (i.e., ascending behavior of second region), FW and CCFPT specimens that exhibited ascending post-peak behaviors were selected for this verification.

To measure the accuracy of various models, an average relative error (ARE) is defined as follows:

$$ARE = \frac{\sum_{i=1}^N \left| \frac{mod_i - exp_i}{exp_i} \right|}{N} \quad (7)$$

where mod_i represents the model prediction, exp_i denotes the experimental value, and N is the total number of datasets (tested specimens). The strength enhancement ratio (f'_{cc}/f'_{co}) and strain enhancement ratio ($\epsilon_{cu}/\epsilon_{co}$) were evaluated for FW specimens with adequate transverse confinement (i.e., 3 ply of FRP) and CCFPT specimens with no foam layer (CCFPT-G40-1G#1, 2, and 3).

The predicted strength and strain enhancement ratios ($(f'_{cc}/f'_{co})_{model}$ and $(\epsilon_{cu}/\epsilon_{co})_{model}$) are compared in Figs. 13 and 14 with the test results ($(f'_{cc}/f'_{co})_{experimental}$ and $(\epsilon_{cu}/\epsilon_{co})_{experimental}$). Table 9 presents the ARE of strength and strain enhancement ratio predictions for FW and CCFPT specimens. For strength enhancement ratio prediction, all the studied models perform reasonably well for FW and CCFPT specimens with an ARE less than 15%. The Wei and Wu [88] unified stress-strain model of FRP-confined concrete provided the most accurate strength prediction for both the FW and CCFPT test specimens. For strain enhancement ratio prediction, only Ozbakkoglu and Lim [4], Youssef et al. [89], and Lam and Teng [86] resulted in an ARE less than 15% for FW specimens. The model by Ozbakkoglu and Lim [4] is most accurate with an ARE of 6.97% for the FW specimens. The Shehata et al. [87] model is least accurate in strain enhancement ratio prediction for the FW specimens. The strain enhancement prediction accuracy for CCFPT specimens is overall less accurate than that for FW specimens. For example, Ozbakkoglu and Lim [4], Lam and Teng [86], and Youssef et al. [89] gave an ARE less than 30%. The Ozbakkoglu and Lim [4] model is the most accurate in strain enhancement prediction for the CCFPT specimens. This particular model was developed as a unified strain enhancement relation based on an extensive number of carefully chosen FRP-confined concrete tests, wherein the axial strain (ϵ_{cu}) is quantified as a non-linear function of the most affecting parameters on strain enhancement, namely, confinement jacket stiffness, hoop rupture strain ($\epsilon_{h,rupt}$), and unconfined concrete strength (f'_{co}). Other models such as Benzaid et al. [84] and Bisby et al. [85] introduced a linear

relationship between the strain enhancement and lateral confinement pressure, resulting in a relatively large deviation of model predictions compared to test results.

6. Conclusions

Based on visual observations, test results, and statistical analyses, the following conclusions can be drawn:

1- The PVC tube in a CFPT cylinder added little to axial load capacity due to its low modulus of elasticity. Even so, leaving a small PVC gap at two ends of the cylinder resulted in rapid post-peak strength degradation due to crushing of the unconfined concrete. The PVC tube also provided a relatively low confining pressure on the cylinder. But it can cope with significant concrete dilation and make the concrete cylinder ductile with a strain softening post-peak response. No fracture or crack was observed in PVC tubes tested.

2- By introducing additional confinement, the FRP wrap on a CCFPT cylinder can effectively delay outward local buckling of the confined PVC tube and restrain the lateral dilation of the encased concrete, thus increasing both strength and strain capacities of the cylinder.

3- The post-peak stress-strain behavior of a CCFPT cylinder proved to be significantly affected by the confining pressure from FRP wrap. When adequately confined by FRP, both carbon and glass FRP resulted in a monotonically increasing stress-strain behavior with an ascending second region. In comparison with carbon wraps, glass wrapping provided significantly greater strain enhancement for the CCFPT cylinder.

4- The CCFPT cylinder exhibited a brittle, explosive-type failure with a sudden loss of axial load capacity since FRP rupture suddenly transferred substantial confining pressure to the PVC tube that fractured instantaneously. By introducing an impact energy absorption medium of compressible foam between the FRP wrapping and the PVC tube, the confined CFPT demonstrated highly ductile behavior similar to the regular CFPT. However, the post-peak strength was reduced as the thickness of the foam increased.

5- The stress-strain curves of CCFPT specimens without compressible foam resembled those of FW specimens with slightly larger ultimate strength and significantly

larger ultimate strain. Therefore, the energy dissipation ability of the CCFPT specimens is significantly higher than that of the FW specimens.

6- The seven existing stress-strain models assessed can accurately predict the ultimate strength of axially-loaded CCFPT columns with an average relative error of less than 15%. The unified stress-strain model by Wei and Wu [88] provided the most accurate ultimate strength predictions for CCFPT and FW specimens. Unlike the ultimate strength, the ultimate strain was predicted with an average relative error of as high as 67%. The model by Ozbakkaloglu and Lim [4] gave the most accurate ultimate strain predictions for CCFPT and FW specimens with 26.3% and 6.97% error, respectively. Overall, the model by Lam and Teng [86] can reasonably predict both the ultimate strength and the ultimate strain of CCFPT specimens by 8.3% and 26.4%, respectively.

Additional tests are required to further understand the mechanical behavior and durability of FRP-PVC-concrete composite columns under axial loads. The types of FRP fabrics, the schedules of PVC pipes [68], and pipe diameters should be investigated accordingly.

Acknowledgments

Financial support for this study was provided in part by the U.S. National Science Foundation under Award No. CMMI-1030399 and the Department of Civil, Architectural, and Environmental Engineering at Missouri University of Science and Technology. The views, opinions, findings, and conclusions reflected in this paper are those of the authors only and do not necessarily reflect the official views or policies of the sponsors. Thanks are extended to Dr. Zhibin Lin, Zachary T. Woolsey, Timothy O'Connor, Amir Ghazanfari, and Hassan Golpour for their assistance in concrete casting.

References

- [1] Mander JB, Priestley MJ, Park R. Theoretical stress-strain model for confined concrete. *Journal of structural engineering*. 1988;114(8):1804-26.
- [2] Nanni A, Bradford NM. FRP jacketed concrete under uniaxial compression. *Construction and Building Materials*. 1995;9(2):115-24.

- [3] Teng J, Lam L. Behavior and modeling of fiber reinforced polymer-confined concrete. *Journal of Structural Engineering*. 2004;130(11):1713-23.
- [4] Ozbakkaloglu T, Lim JC. Axial compressive behavior of FRP-confined concrete: Experimental test database and a new design-oriented model. *Composites Part B: Engineering*. 2013;55:607-34.
- [5] Ozbakkaloglu T, Lim JC, Vincent T. FRP-confined concrete in circular sections: Review and assessment of stress–strain models. *Eng Struct*. 2013;49:1068-88.
- [6] Nanni A, Norris M, Bradford N. Lateral confinement of concrete using FRP reinforcement. *ACI Special Publication*. 1993;138.
- [7] Lopez A, Galati N, Alkhrdaji T, Nanni A. Strengthening of a reinforced concrete bridge with externally bonded steel reinforced polymer (SRP). *Composites Part B: Engineering*. 2007;38(4):429-36.
- [8] Teng J, Chen J, Smith ST, Lam L. Behaviour and strength of FRP-strengthened RC structures: a state-of-the-art review. *Proceedings of the ICE-Structures and Buildings*. 2003;156(1):51-62.
- [9] Fam AZ, Rizkalla SH. Confinement model for axially loaded concrete confined by circular fiber-reinforced polymer tubes. *ACI Structural Journal*. 2001;98(4).
- [10] Zaghi AE, Saiidi MS, Mirmiran A. Shake table response and analysis of a concrete-filled FRP tube bridge column. *Composite Structures*. 2012;94(5):1564-74.
- [11] Vosooghi A, Saiidi MS. Design guidelines for rapid repair of earthquake-damaged circular RC bridge columns using CFRP. *Journal of Bridge Engineering*. 2012;18(9):827-36.
- [12] Eslami A, Ronagh H. Effect of FRP wrapping in seismic performance of RC buildings with and without special detailing–A case study. *Composites Part B: Engineering*. 2013;45(1):1265-74.
- [13] Vincent T, Ozbakkaloglu T. Influence of concrete strength and confinement method on axial compressive behavior of FRP confined high-and ultra high-strength concrete. *Composites Part B: Engineering*. 2013;50:413-28.
- [14] Ozbakkaloglu T. Behavior of square and rectangular ultra high-strength concrete-filled FRP tubes under axial compression. *Composites Part B: Engineering*. 2013;54:97-111.

- [15] Ozbakkaloglu T, Saatcioglu M. Seismic behavior of high-strength concrete columns confined by fiber-reinforced polymer tubes. *Journal of Composites for Construction*. 2006;10(6):538-49.
- [16] Zohrevand P, Mirmiran A. Behavior of ultrahigh-performance concrete confined by fiber-reinforced polymers. *Journal of Materials in Civil Engineering*. 2011;23(12):1727-34.
- [17] Zohrevand P, Mirmiran A. Cyclic behavior of hybrid columns made of ultra high performance concrete and fiber reinforced polymers. *Journal of Composites for Construction*. 2012;16(1):91-9.
- [18] Li B, Zohrevand P, Mirmiran A. Cyclic behavior of FRP concrete bridge pier frames. *Journal of Bridge Engineering*. 2012;18(5):429-38.
- [19] Shi Y, Zohrevand P, Mirmiran A. Assessment of cyclic behavior of hybrid FRP concrete columns. *Journal of Bridge Engineering*. 2012;18(6):553-63.
- [20] El Chabib H, Nehdi M, El Naggar M-H. Behavior of SCC confined in short GFRP tubes. *Cement and Concrete Composites*. 2005;27(1):55-64.
- [21] Yu T, Fang X, Teng J. FRP-Confined Self-Compacting Concrete under Axial Compression. *Journal of Materials in Civil Engineering*. 2013.
- [22] Xiao J, Huang Y, Yang J, Zhang C. Mechanical properties of confined recycled aggregate concrete under axial compression. *Construction and Building Materials*. 2012;26(1):591-603.
- [23] Zhao J, Yu T, Teng J. Stress-Strain Behavior of FRP-Confined Recycled Aggregate Concrete. *Journal of Composites for Construction*. 2014.
- [24] Yan Z, Pantelides CP, Reaveley LD. Posttensioned FRP composite shells for concrete confinement. *Journal of Composites for Construction*. 2007;11(1):81-90.
- [25] Fakhairifar M, Sharbatdar M, Lin Z, Dalvand A, Sivandi-Pour A, Chen G. Seismic performance and global ductility of RC frames rehabilitated with retrofitted joints by CFRP laminates. *Earthquake Engineering and Engineering Vibration*. 2014;13(1):59-73.
- [26] Lin Z, Fakhairifar M, Wu C, Chen G, Bevans W, Gunasekaran AVK, et al. Design, Construction and Load Testing of the Pat Daly Road Bridge in Washington County, MO, with Internal Glass Fiber Reinforced Polymers Reinforcement. 2013.

- [27] Rousakis TC, Tourtouras IS. RC columns of square section–Passive and active confinement with composite ropes. *Composites Part B: Engineering*. 2014;58:573-81.
- [28] Rousakis TC, Kouravelou KB, Karachalios TK. Effects of carbon nanotube enrichment of epoxy resins on hybrid FRP–FR confinement of concrete. *Composites Part B: Engineering*. 2014;57:210-8.
- [29] Anggawidjaja D, Ueda T, Dai J, Nakai H. Deformation capacity of RC piers wrapped by new fiber-reinforced polymer with large fracture strain. *Cement and Concrete Composites*. 2006;28(10):914-27.
- [30] Shimomura T, Phong N. Structural performance of concrete members reinforced with continuous fiber rope. FRPRCS-8 Conference University of Patras, Patras, Greece2007.
- [31] He R, Sneed LH, Belarbi A. Rapid Repair of Severely Damaged RC Columns with Different Damage Conditions: An Experimental Study. *International Journal of Concrete Structures and Materials*. 2013;7(1):35-50.
- [32] Xiao Y, He W, Choi K-k. Confined concrete-filled tubular columns. *Journal of structural engineering*. 2005;131(3):488-97.
- [33] Saatcioglu M, Yalcin C. External prestressing concrete columns for improved seismic shear resistance. *Journal of Structural Engineering*. 2003;129(8):1057-70.
- [34] ElGawady M, Endeshaw M, McLean D, Sack R. Retrofitting of rectangular columns with deficient lap splices. *Journal of Composites for Construction*. 2009;14(1):22-35.
- [35] Micelli F, Angiuli R, Corvaglia P, Aiello MA. Passive and SMA-activated confinement of circular masonry columns with basalt and glass fibers composites. *Composites Part B: Engineering*. 2014;67:348-62.
- [36] Andrawes B, Shin M, Wierschem N. Active confinement of reinforced concrete bridge columns using shape memory alloys. *Journal of Bridge Engineering*. 2009;15(1):81-9.
- [37] Choi E, Kim J-W, Rhee I, Kang J-W. Behavior and modeling of confined concrete cylinders in axial compression using FRP rings. *Composites Part B: Engineering*. 2014;58:175-84.

- [38] Xiao Y, He W, Mao X, Choi K, Zhu P. Confinement design of CFT columns for improved seismic performance. Proceedings of the International Workshop on Steel and Concrete Composite Construction (IWSCCC-2003): Taipei, China; 2003. p. 217-26.
- [39] Xiao Y, Zhang Z, Hu J, Kunnath SK, Guo P. Seismic behavior of CFT column and steel pile footings. *Journal of Bridge Engineering*. 2011;16(5):575-86.
- [40] Mohamed HM, Abdel-Baky HM, Masmoudi R. Nonlinear Stability Analysis of Concrete-Filled Fiber-Reinforced Polymer-Tube Columns: Experimental and Theoretical Investigation. *ACI Structural Journal*. 2010;107(6).
- [41] Wang Y-h, Nie J-g, Cai C. Numerical modeling on concrete structures and steel-concrete composite frame structures. *Composites Part B: Engineering*. 2013;51:58-67.
- [42] Wong Y, Yu T, Teng J, Dong S. Behavior of FRP-confined concrete in annular section columns. *Composites Part B: Engineering*. 2008;39(3):451-66.
- [43] Idris Y, Ozbakkaloglu T. Seismic behavior of high-strength concrete-filled FRP tube columns. *Journal of Composites for Construction*. 2013;17(6).
- [44] Abdelkarim OI, ElGawady MA. Analytical and Finite-Element Modeling of FRP-Concrete-Steel Double-Skin Tubular Columns. *Journal of Bridge Engineering*. 2014.
- [45] Han L-H, Tao Z, Liao F-Y, Xu Y. Tests on cyclic performance of FRP-concrete-steel double-skin tubular columns. *Thin-Walled Structures*. 2010;48(6):430-9.
- [46] Belarbi A, Bae S-W. An experimental study on the effect of environmental exposures and corrosion on RC columns with FRP composite jackets. *Composites Part B: Engineering*. 2007;38(5):674-84.
- [47] Wang J-Y, Yang Q-B. Investigation on compressive behaviors of thermoplastic pipe confined concrete. *Construction and Building Materials*. 2012;35:578-85.
- [48] Pando MA, Ealy CD, Filz GM, Lesko J, Hoppe E. A Laboratory and Field Study of Composite Piles for Bridge Substructures. FHWA-HRT-04-0432006.
- [49] Karbhari VM. *Durability of composites for civil structural applications*: Elsevier; 2007.
- [50] Naghibdehi MG, Sharbatdar M, Mastali M. Repairing reinforced concrete slabs using composite layers. *Materials & Design*. 2014;58:136-44.
- [51] Kurt CE. Concrete filled structural plastic columns. *Journal of the Structural Division*. 1978;104(1):55-63.

- [52] Toutanji H, Saafi M. Durability studies on concrete columns encased in PVC–FRP composite tubes. *Composite structures*. 2001;54(1):27-35.
- [53] Toutanji H, Saafi M. Stress-strain behavior of concrete columns confined with hybrid composite materials. *Materials and Structures*. 2002;35(6):338-47.
- [54] Soliman S, El-kareim A. Behavior of long confined concrete column. *Ain Shams Engineering Journal*. 2011;2(3):141-8.
- [55] Gupta PK. Confinement of concrete columns with unplasticized Poly-vinyl chloride tubes. *International Journal of Advanced Structural Engineering*. 2013;5(1):19.
- [56] Wang J, Yang Q. Experimental study on Mechanical Properties of concrete confined with plastic Pipe. *ACI Materials Journal*. 2010;107(2).
- [57] Nowack R, Otto OI, Braun EW. „60 Jahre Erfahrungen mit Rohrleitungen aus weichmacherfreiem Polyvinylchlorid (PVC-U). *KRV Nachrichten*. 1995:1-95.
- [58] Awham M, Salih ZGM. A Study of some Mechanical Behavior on a Thermoplastic Material.
- [59] Al-Malaika S, Golovoy A, Wilkie CA. *Chemistry and technology of polymer additives*: Blackwell Science; 1999.
- [60] Titow WV. *PVC technology*: Springer; 1984.
- [61] Gupta PK, Verma VK. Study of concrete-filled unplasticized poly-vinyl chloride tubes in marine environment. *Proceedings of the Institution of Mechanical Engineers, Part M: Journal of Engineering for the Maritime Environment*. 2014:1475090214560448.
- [62] Gathimba Naftary K, Oyawa Walter O, Mang'uriu Geoffrey N. Compressive Strength Characteristics of Concrete-Filled Plastic Tubes Short Columns. *International Journal of Science and Research (IJSR)*. 2014;3(9):2168-74.
- [63] Jiang S-F, Ma S-L, Wu Z-Q. Experimental study and theoretical analysis on slender concrete-filled CFRP–PVC tubular columns. *Construction and Building Materials*. 2014;53:475-87.
- [64] Harries KA, Carey SA. Shape and “gap” effects on the behavior of variably confined concrete. *Cement and Concrete Research*. 2003;33(6):881-90.
- [65] ASTM C39/C39M. *Standard Test Method for Compressive Strength of Cylindrical Concrete Specimens*. West Conshohocken (PA): ASTM; 2012. p. 7.

- [66] ASTM C496/C496M. Standard test method for splitting tensile strength of cylindrical concrete. West Conshohocken (PA): ASTM; 2011. p. 5.
- [67] ASTM C78/C78M. Standard test method for flexural strength of concrete (using simple beam with third-point loading). West Conshohocken (PA): ASTM; 2010. p. 4.
- [68] ASTM D1785. Standard Specification for Poly(Vinyl Chloride) (PVC) Plastic Pipe, Schedules 40, 80, and 120. PVC, Schedule. West Conshohocken: ASTM; 2012. p. 11.
- [69] ASTM D3039/D3039M. Standard test method for tensile properties of fiber resin composites. West Conshohocken (PA): ASTM; 2012.
- [70] ASTM D638. Standard Test Method for Tensile Properties of Plastics. ASTM International. West Conshohocken (PA) 2008.
- [71] Tasdemir M, Tasdemir C, Akyüz S, Jefferson A, Lydon F, Barr B. Evaluation of strains at peak stresses in concrete: a three-phase composite model approach. *Cement and Concrete Composites*. 1998;20(4):301-18.
- [72] Vincent T, Ozbakkaloglu T. Influence of fiber orientation and specimen end condition on axial compressive behavior of FRP-confined concrete. *Construction and Building materials*. 2013;47:814-26.
- [73] Shahawy M, Mirmiran A, Beitelman T. Tests and modeling of carbon-wrapped concrete columns. *Composites Part B: Engineering*. 2000;31(6):471-80.
- [74] Lam L, Teng J. Strength models for fiber-reinforced plastic-confined concrete. *Journal of Structural Engineering*. 2002;128(5):612-23.
- [75] Ozbakkaloglu T. Compressive behavior of concrete-filled FRP tube columns: Assessment of critical column parameters. *Engineering Structures*. 2013;51:188-99.
- [76] Chen J, Ai J, Stratford T. Effect of geometric discontinuities on strains in FRP-wrapped columns. *Journal of Composites for Construction*. 2009.
- [77] Fanggi BAL, Ozbakkaloglu T. Compressive behavior of aramid FRP-HSC-steel double-skin tubular columns. *Construction and Building Materials*. 2013;48:554-65.
- [78] Samaan M, Mirmiran A, Shahawy M. Model of concrete confined by fiber composites. *Journal of structural engineering*. 1998;124(9):1025-31.
- [79] Ozbakkaloglu T, Akin E. Behavior of FRP-confined normal-and high-strength concrete under cyclic axial compression. *Journal of Composites for Construction*. 2011;16(4):451-63.

- [80] Yan X, Yali S. Impact behaviors of CFT and CFRP confined CFT stub columns. *Journal of Composites for Construction*. 2012;16(6):662-70.
- [81] Louk Fanggi B, Ozbakkaloglu T. Behavior of Hollow and Concrete-Filled FRP-HSC and FRP-HSC-Steel Composite Columns Subjected to Concentric Compression. *Advances in Structural Engineering*. 2015;18(5):715-38.
- [82] Lim JC, Ozbakkaloglu T. Confinement model for FRP-confined high-strength concrete. *Journal of Composites for Construction*. 2013;18(4).
- [83] Lim JC, Ozbakkaloglu T. Investigation of the Influence of the Application Path of Confining Pressure: Tests on Actively Confined and FRP-Confined Concretes. *Journal of Structural Engineering*. 2014.
- [84] Benzaid R, Mesbah H, Chikh NE. FRP-confined concrete cylinders: axial compression experiments and strength model. *Journal of Reinforced plastics and composites*. 2010;29(16):2469-88.
- [85] Bisby LA, Dent AJ, Green MF. Comparison of confinement models for fiber-reinforced polymer-wrapped concrete. *ACI Structural Journal*. 2005;102(1).
- [86] Lam L, Teng J. Design-oriented stress–strain model for FRP-confined concrete. *Construction and building materials*. 2003;17(6):471-89.
- [87] Shehata IA, Carneiro LA, Shehata LC. Strength of short concrete columns confined with CFRP sheets. *Materials and Structures*. 2002;35(1):50-8.
- [88] Wei Y-Y, Wu Y-F. Unified stress–strain model of concrete for FRP-confined columns. *Construction and Building Materials*. 2012;26(1):381-92.
- [89] Youssef MN, Feng MQ, Mosallam AS. Stress–strain model for concrete confined by FRP composites. *Composites Part B: Engineering*. 2007;38(5):614-28.

Table 1. Test matrix of cylinder specimens

Confinement	<i>D</i> (mm)	<i>H</i> (mm)	FRP type	FRP layers	PVC tube	No. of specimens
FW	152	305	Carbon	1		5
				3		3
			E-Glass	1		3
				3		3
CFPT	168*	305			Grey Schedule 40	5
CCFPT	168*	305	Carbon	1	Grey Schedule 40	4
				3	Grey Schedule 40	3
			E-Glass	1	Grey Schedule 40	7
				3	Grey Schedule 40	3
Total						36

* Outside diameter of PVC tube with a wall thickness of 7.11 mm.

Table 2. Fresh and hardened concrete properties

Property	Cylinder specimens
Air content (%)	1.3
Slump (mm)	92
Unit weight (kg/m ³)	2400
Tensile split cylinder strength (MPa)	2.9 ^a
Flexural strength (modulus of rupture) (MPa)	3.4 ^b
Compressive strength (MPa)	49.5 ^a

^a the average of three cylinders tested according to ASTM C39-12 [65] and C496-11 [66]

^b the average of three beams tested according to ASTM C78-10 [67]

Table 3. Material properties of FRP sheets*

Type	Nominal fiber thickness, t_f (mm ply)	Manufacturer specified			Measured with flat FRP coupon tests		
		Tensile strength, f_f (MPa)	Elastic Modulus, E_f (GPa)	Ultimate tensile strain, ε_f (%)	Tensile strength, f_{frp} (MPa)	Elastic Modulus, E_{frp} (GPa)	Ultimate tensile strain, ε_{frp} (%)
E-Glass	0.373	1517	72.4	2.10	1449	79.18	1.85
CFRP	0.165	3800	227	1.67	3421	251	1.37

* All FRP materials were unidirectional fabrics.

Table 4. Tensile properties of PVC dogbone specimens under tension

PVC specimen	Thickness, t (mm)	Ultimate strength, f_u (MPa)	Modulus of elasticity, E (GPa)	Yield strength at 0.2% offset, $f_{y \text{ offset}}$ (MPa)	Ultimate fracture strain, ϵ_u (%)	Poisson's ratio, ν
Schedule 40	7.11	50.36	4.03	41.26	46	0.419

Table 5. Measured properties of PVC tubes under axial compression

PVC tube	Tube diameter, D_t (mm)	Thickness, t (mm)	Peak axial load, P_t (kN)	Yield stress (MPa)	Ultimate strength (MPa)	Axial strain at peak (%)
Hollow PVC Schedule 40	168.3	7.11	208.5	41.3	50.93	4.27

Table 6. Test results of cylinder specimens

Confinement type	Confinement detail	Specimen designation	f_{ult}/f_{co}	f_{ucl}/f_{co}	f_{cc} (MPa)	f_{cr} (MPa)	ϵ_{cu} (%)	$\epsilon_{cu,sp}$ (%)	f_{ucl}/f_{cc}	$\epsilon_{ucl}/\epsilon_{cc}$	k_c
FW	1 ply CFRP	FW-1C#1	0.15	0.12	65.0	60.4	0.94	1.11	1.30	3.79	0.70
		FW-1C#2	0.15	0.11	67.3	65.3	0.91	1.04	1.35	3.67	
		FW-1C#3	0.15	0.08	63.5	54.6	0.76	0.71	1.27	3.06	
		FW-1C#4	0.15	0.11	64.9	40.2	0.89	1.02	1.30	3.59	
		FW-1C#5	0.15	0.10	62.3	58.6	0.86	0.93	1.25	3.47	
	3 ply CFRP	FW-3C#1	0.45	0.34	99.2	94.9	1.61	1.03	1.98	6.49	0.74
		FW-3C#2	0.45	0.32	99.2		1.42	0.99	1.98	5.72	
		FW-3C#3	0.45	0.33	94.3		1.46	1.01	1.89	5.88	
	1 ply GFRP	FW-1G#1	0.14	0.11	63.1	53.1	1.61	1.41	1.26	6.49	0.71
		FW-1G#2	0.14	0.10	63.8	44.7	1.26	1.29	1.28	5.08	
		FW-1G#3	0.14	0.10	63.3	54.3	1.26	1.25	1.27	5.08	
	3 ply GFRP	FW-3G#1	0.43	0.35	104.2		2.03	1.52	2.08	8.18	0.85
FW-3G#2		0.43	0.39	102.3		2.20	1.68	2.05	8.87		
FW-3G#3		0.43	0.35	102.1		2.05	1.52	2.04	8.26		
CFPT	Sch. 40 PVC	CFPT-G40#1	0.08		52.6	42.0	0.60		1.05	2.42	
		CFPT-G40#2	0.08		49.5	39.6	0.44		0.99	1.81	
		CFPT-G40#3	0.08		47.8	38.2	1.01		0.96	4.07	
	Sch. 40 PVC with 12 mm. gaps at both ends	CFPT-G40-w gap#1	0.08		55.5	44.4	0.50		1.11	2.01	
		CFPT-G40-w gap#2	0.08		58.2	46.6	0.81		1.16	3.26	

Table 7. Average recorded strain reduction factor, k_c , for FW and CCFPT specimens

Confinement type	k_c	SD	No.
All without foam	0.790	0.105	27
FRP confined (FW)	0.744	0.091	14
• CFRP	0.715	0.088	8
• GFRP	0.781	0.087	6
FRP + PVC confined (CCFPT)	0.839	0.100	13
• CFRP + PVC	0.785	0.106	7
• GFRP + PVC	0.903	0.041	6

Table 8. Models used to predict strength and strain enhancement ratios of confined specimens

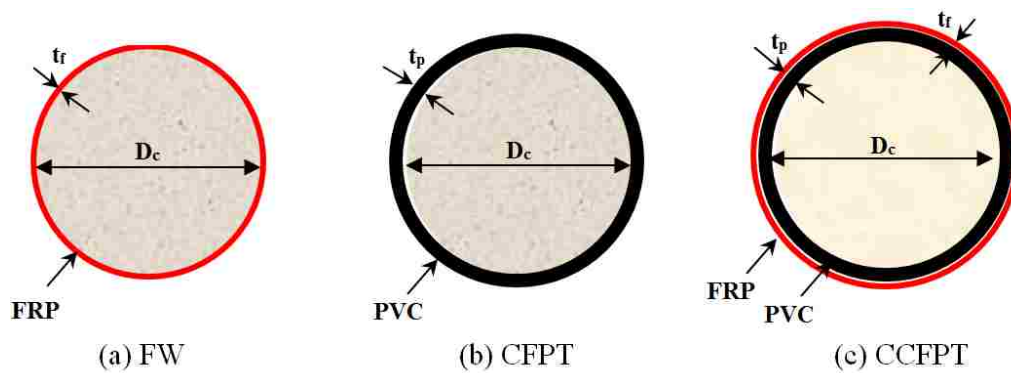
Benzaid et al. [84]	$\frac{f'_c}{f'_c} = 1 + 2.2 \frac{f_{con}}{f'_c}$	$\frac{\epsilon_{con}}{\epsilon_c} = 2 + 7.6 \frac{f_{con}}{f'_c}$
Bisby et al. [85]	$f'_{cc} = f'_c + 3.587 (f'_c)^{0.7}$	$\epsilon_c = \epsilon_{cc} + k_1 \frac{f'_{cc}}{f'_c}$ $k_1 = 0.014$
Lam and Teng [86]	$\frac{f'_{cc}}{f'_c} = 1 + 3.3 \frac{f_{con}}{f'_c}$	$\frac{\epsilon_{cc}}{\epsilon_c} = 1.75 + 3.55 \frac{f_{con}}{f'_c} + \frac{\epsilon_{cc}}{\epsilon_c} \frac{f_{con}}{f'_c}$
Shehata et al. [87]	$\frac{f'_{cc}}{f'_c} = 1 + 2 \frac{f_{con}}{f'_c}$	$\frac{\epsilon_{cc}}{\epsilon_c} = 1 + 0.32 \frac{f_{con}}{f'_c} \frac{f_{con}}{f'_c}$
Ozbakkaloglu and Mirza [88]	$f'_{cc} = \phi_c f'_c + k_1 (f_{con} - f'_c)$	$\epsilon_{cc} = \epsilon_c + k_2 \frac{K}{f'_c} \frac{f_{con}}{f'_c}$
Wei and Wu [88]	$\frac{f'_{cc}}{f'_c} = 1 + 2.2 \frac{f_{con}}{f'_c}$	$\frac{\epsilon_{cc}}{\epsilon_c} = 1.75 + 12 \frac{f_{con}}{f'_c} \frac{f_{con}}{f'_c}$
Youssef et al. [89]	$\frac{f'_{cc}}{f'_c} = 1 + 2.25 \frac{f_{con}}{f'_c}$	$\epsilon_c = 0.003368 + 0.259 \frac{f_{con}}{f'_c} \frac{f_{con}}{f'_c}$

Table 9. Average relative error (%) of strength and strain enhancement ratio predictions

Model	Confinement type	f_{cc}/f_{co}	$\epsilon_{cu}/\epsilon_{co}$
Benzaid et al. [84]	FW	11.8	34.1
	CCFPT	11.7	37.4
Bisby et al. [85]	FW	3.6	25.0
	CCFPT	7.3	34.2
Lam and Teng [86]	FW	7.3	12.7
	CCFPT	8.3	26.4
Shehata et al. [87]	FW	6.3	67.1
	CCFPT	10.1	42.4
Ozbakkaloglu and Lim [4]	FW	10.2	6.97
	CCFPT	10.5	26.3
Wei and Wu [88]	FW	3.6	16.4
	CCFPT	6.8	32.8
Youssef et al. [89]	FW	9.8	12.5
	CCFPT	14.4	29.7



Fig. 1. Preparation of cylinder specimens: (a) PVC tube prior to casting; (b) ground end.



Core concrete diameter, D_c : 152 mm

FRP jacket thickness, t_r : 1 or 3 ply

PVC tube thickness: t_p : 7.10 mm

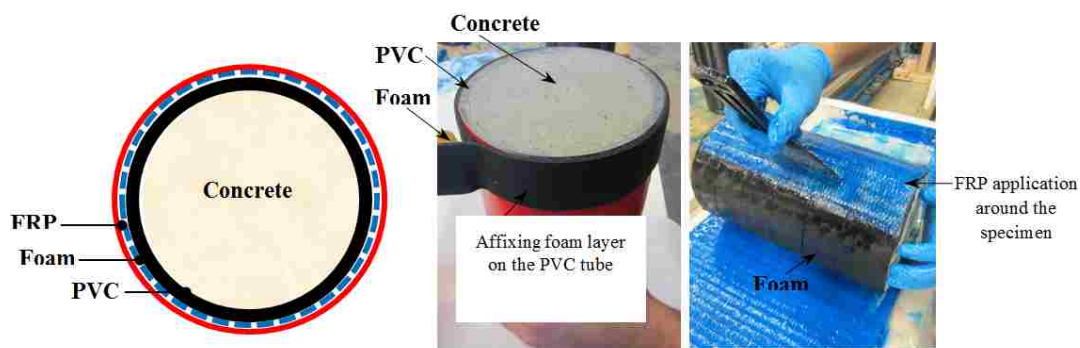
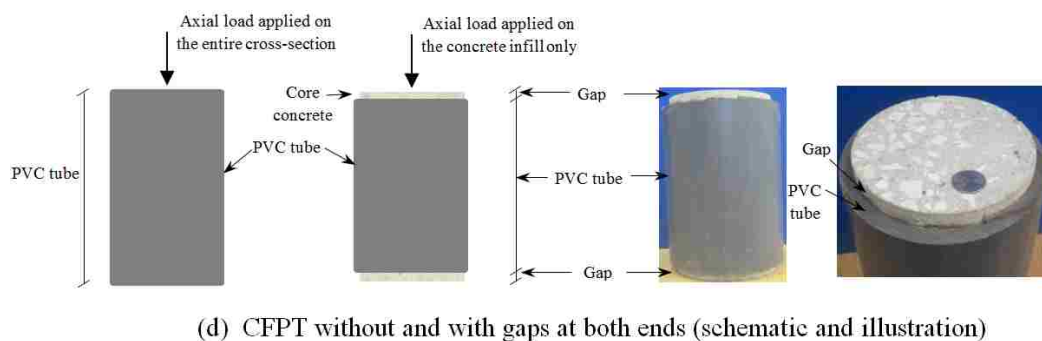


Fig. 2. Details of cylinder specimens: (a) FW; (b) CFPT; (c) CCFPT; (d) CFPT without and with gaps at both ends; and (e) application of a foam layer between PVC tube and FRP wrap in CCFPT system.

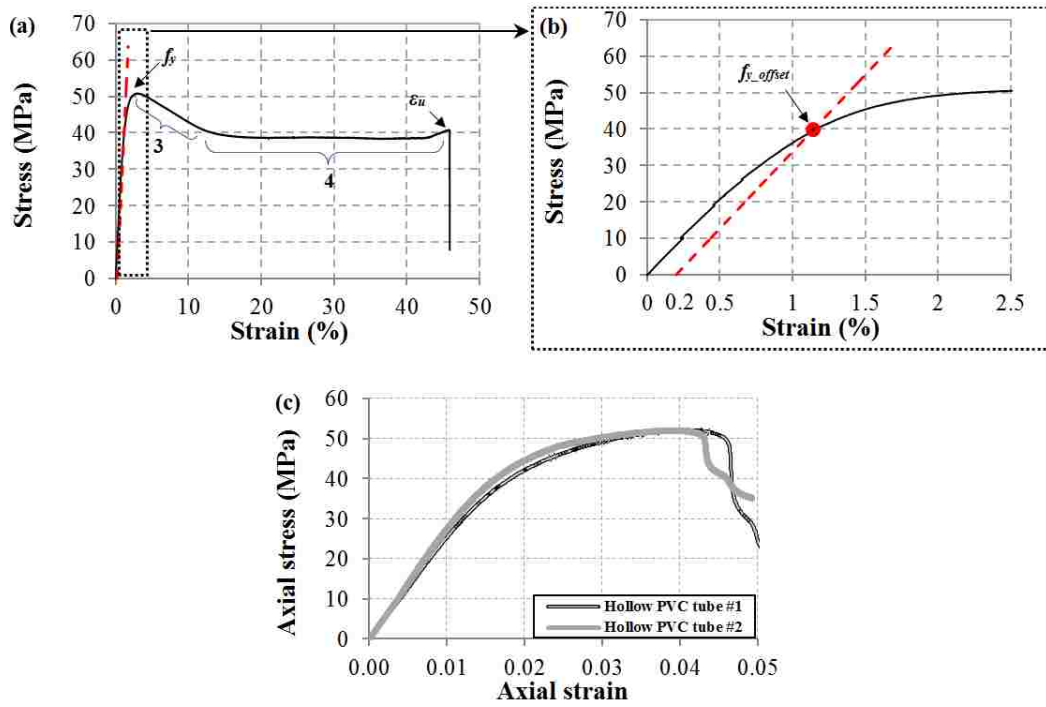


Fig. 3. Experimental stress-strain curves: (a) complete tensile curve up to fracture of a dogbone PVC specimen; (b) pre-peak curve with a 0.2% line offset of the dogbone specimen; and (c) axial compressive behavior of empty PVC tube.

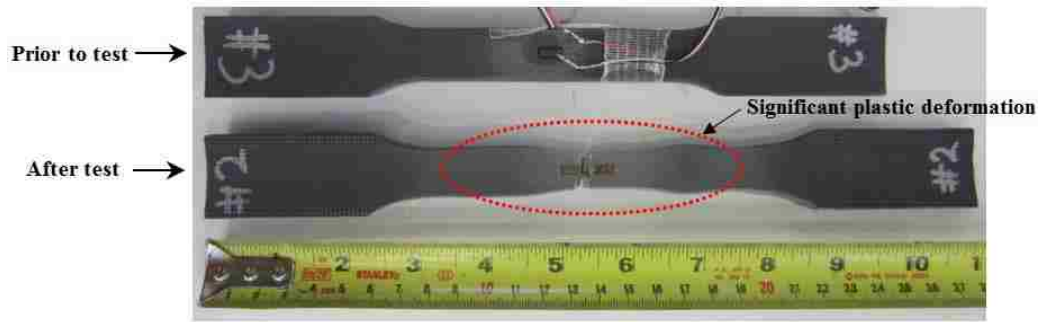


Fig. 4. PVC dogbone test specimen prior to and after tensile test.

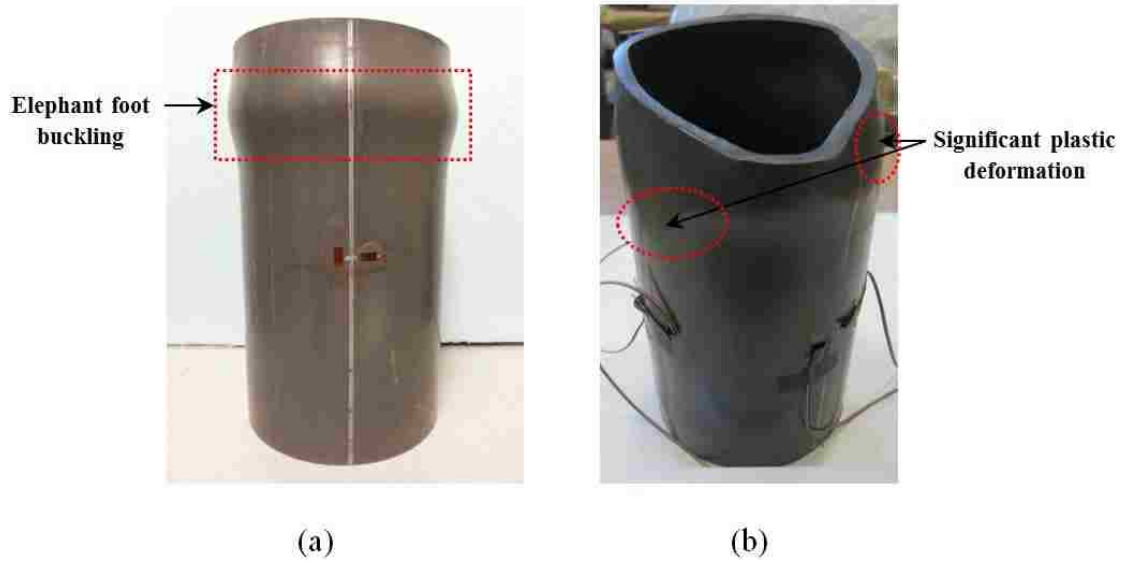
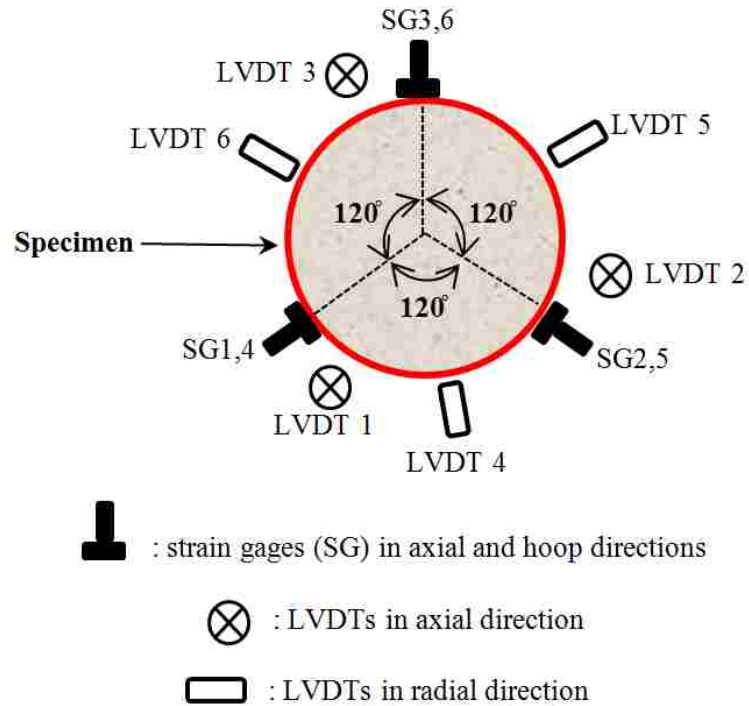
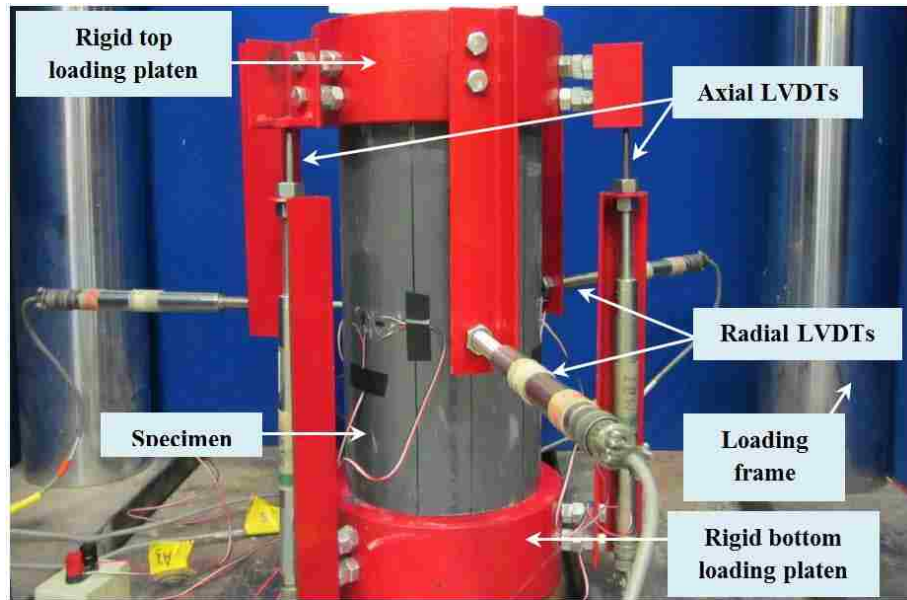


Fig. 5. Hollow PVC tube deformation modes: (a) local elephant foot buckling; (b) global bulging.



(a)



(b)

Fig. 6. Uniaxial compression test: (a) instrumentation; (b) setup.

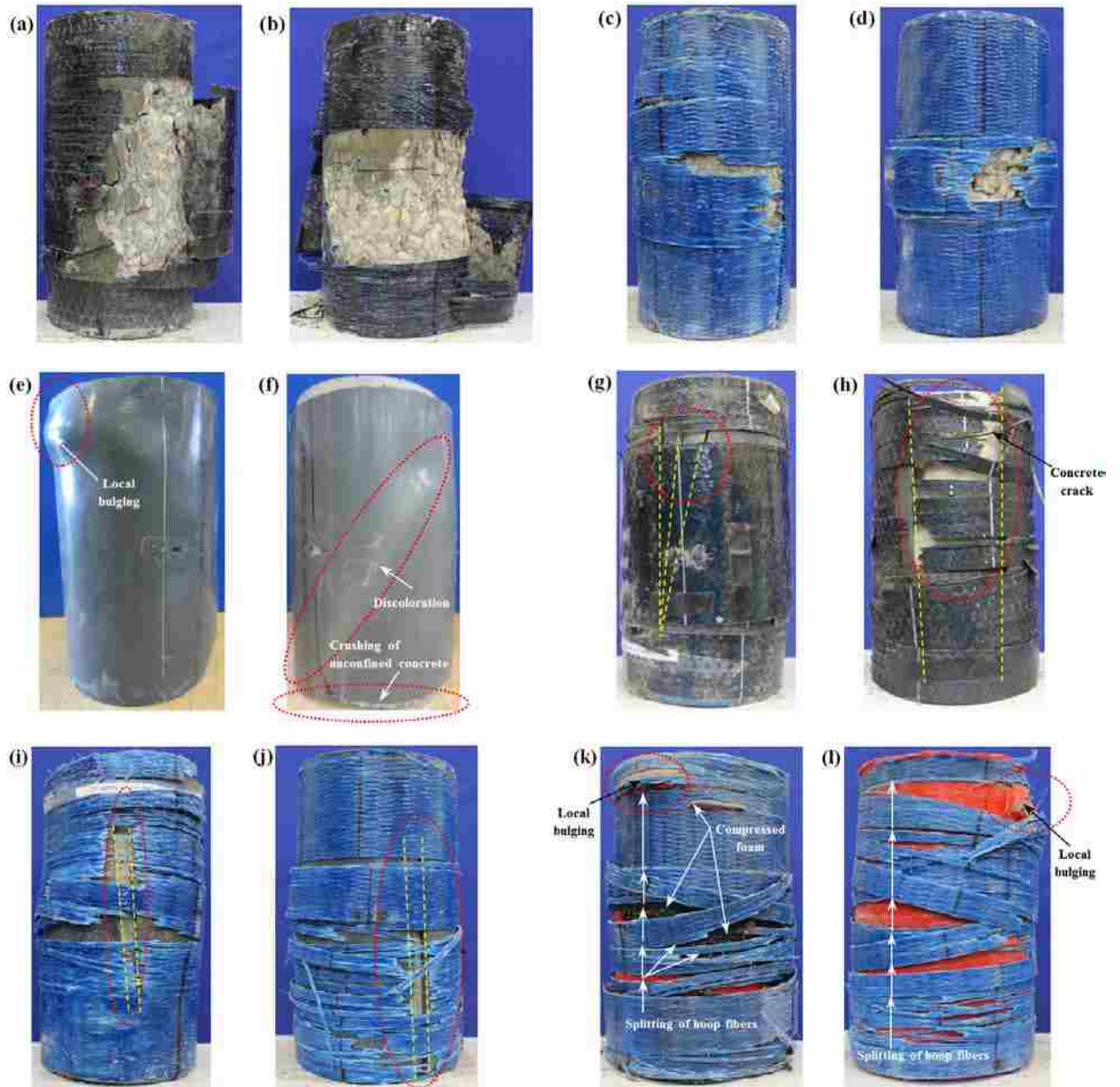
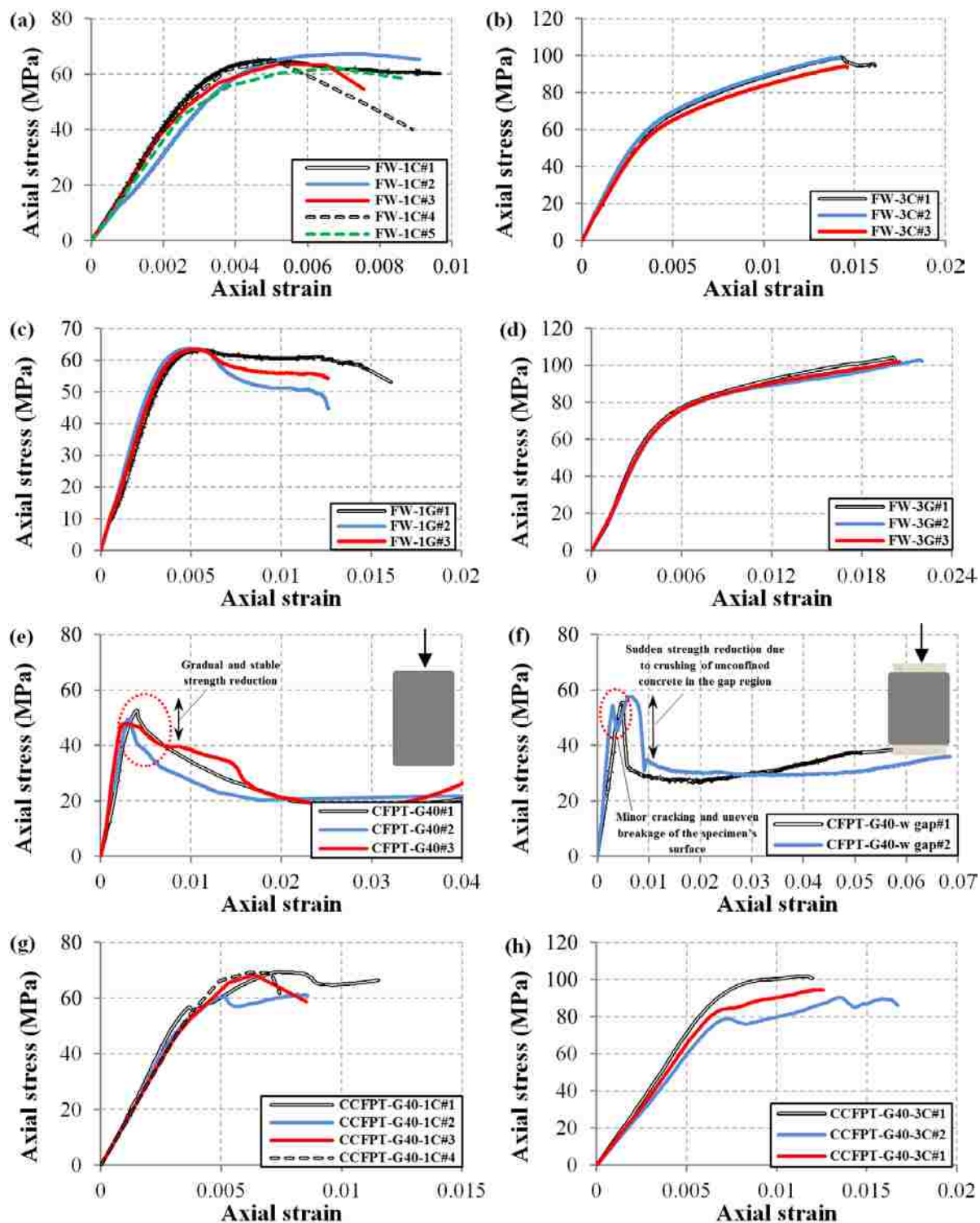


Fig. 7. Typical failure of cylinders under axial compression: (a) FW-1C#1, (b) FW-3C#2, (c) FW-1G#1, (d) FW-3G#3, (e) CFPT-G40#1, (f) CFPT-G40-w gap#1, (g) CCFPT-G40-1C#3, (h) CCFPT-G40-3C#2, (i) CCFPT-G40-1G#1, (j) CCFPT-G40-3G#1, (k) CCFPT-G40-1G-foam#1, and (l) CCFPT-G40-1G-foam#3.

(* Cracks on the PVC tube in CCFPT specimens are marked with yellow dashed lines.)



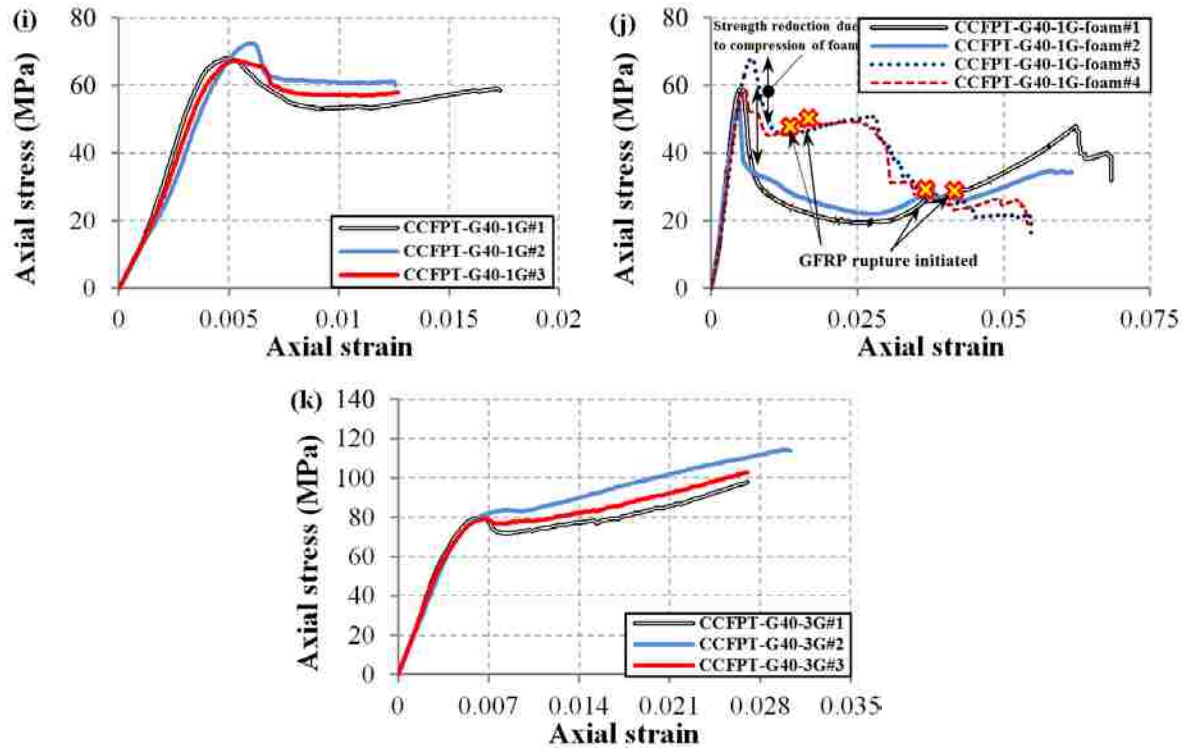


Fig. 8. Axial stress-strain behavior of cylinders: (a) FW-1C, (b) FW-3C, (c) FW-1G, (d) FW-3G, (e) CFPT-G40, (f) CFPT-G40-w gap, (g) CCFPT-G40-1C, (h) CCFPT-G40-3C, (i) CCFPT-G40-1G, (j) CCFPT-G40-1G-foam, and (k) CCFPT-G40-3G.

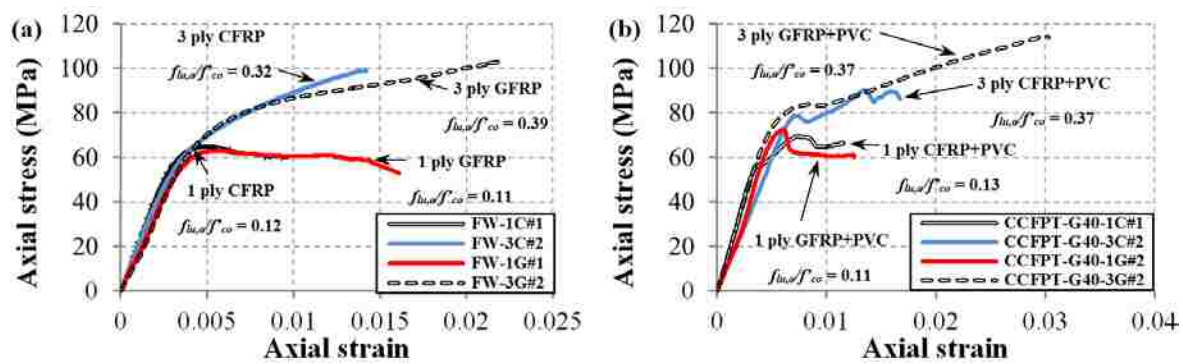


Fig. 9. Influence of confinement pressure on stress-strain behavior of test specimens: (a) FW; (b) CCFPT.

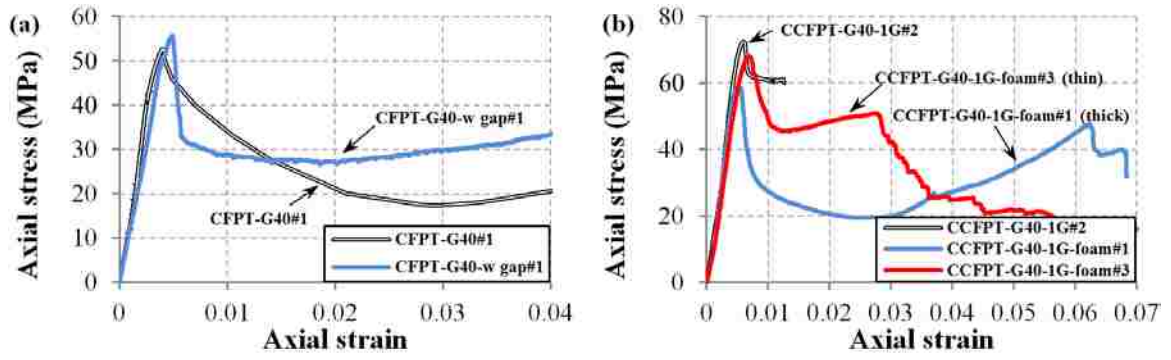


Fig. 10. Influence of confinement detail on stress-strain behavior: (a) presence of gap in CFPT specimens; (b) presence of compressible foam in CCFPT specimens.

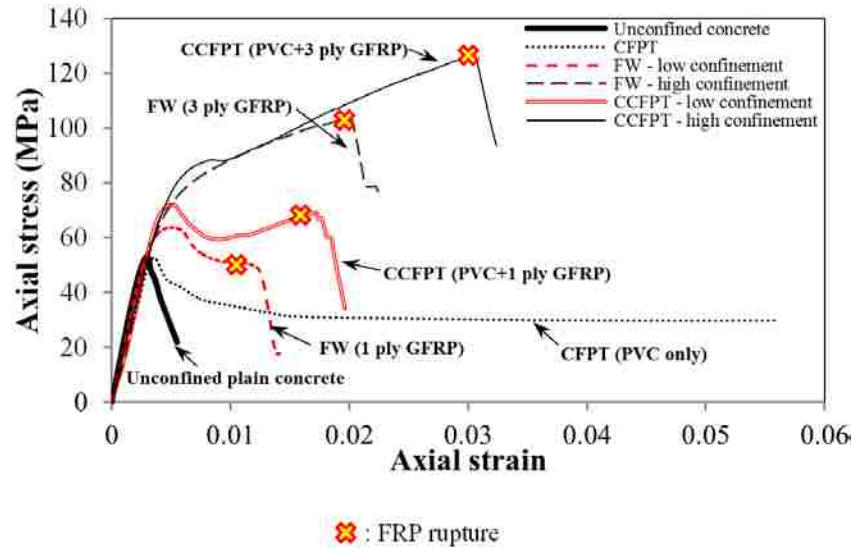


Fig. 11. Comparison of representative axial stress-strain behavior of CFPT, FW, and CCFPT specimens.

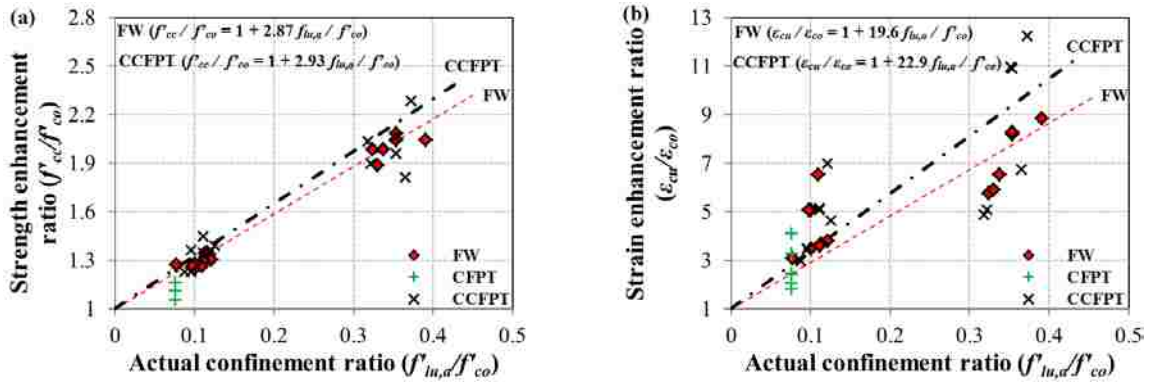


Fig. 12. Influence of confinement type on: (a) strength enhancement ratio; (b) strain enhancement ratio.

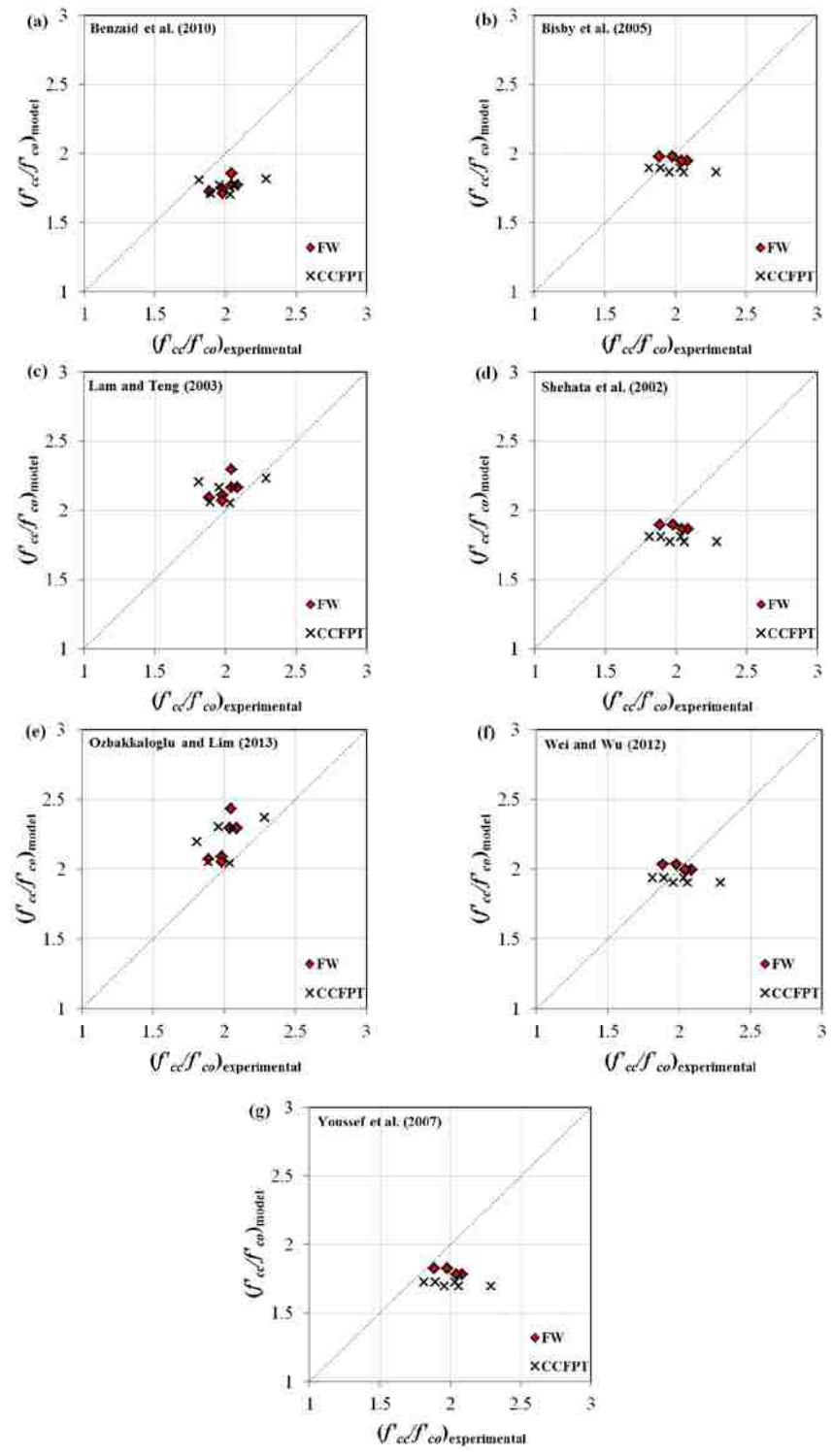


Fig. 13. Performance of various confinement models in predicting strength enhancement ratio (f'_{cc}/f'_{co}) .

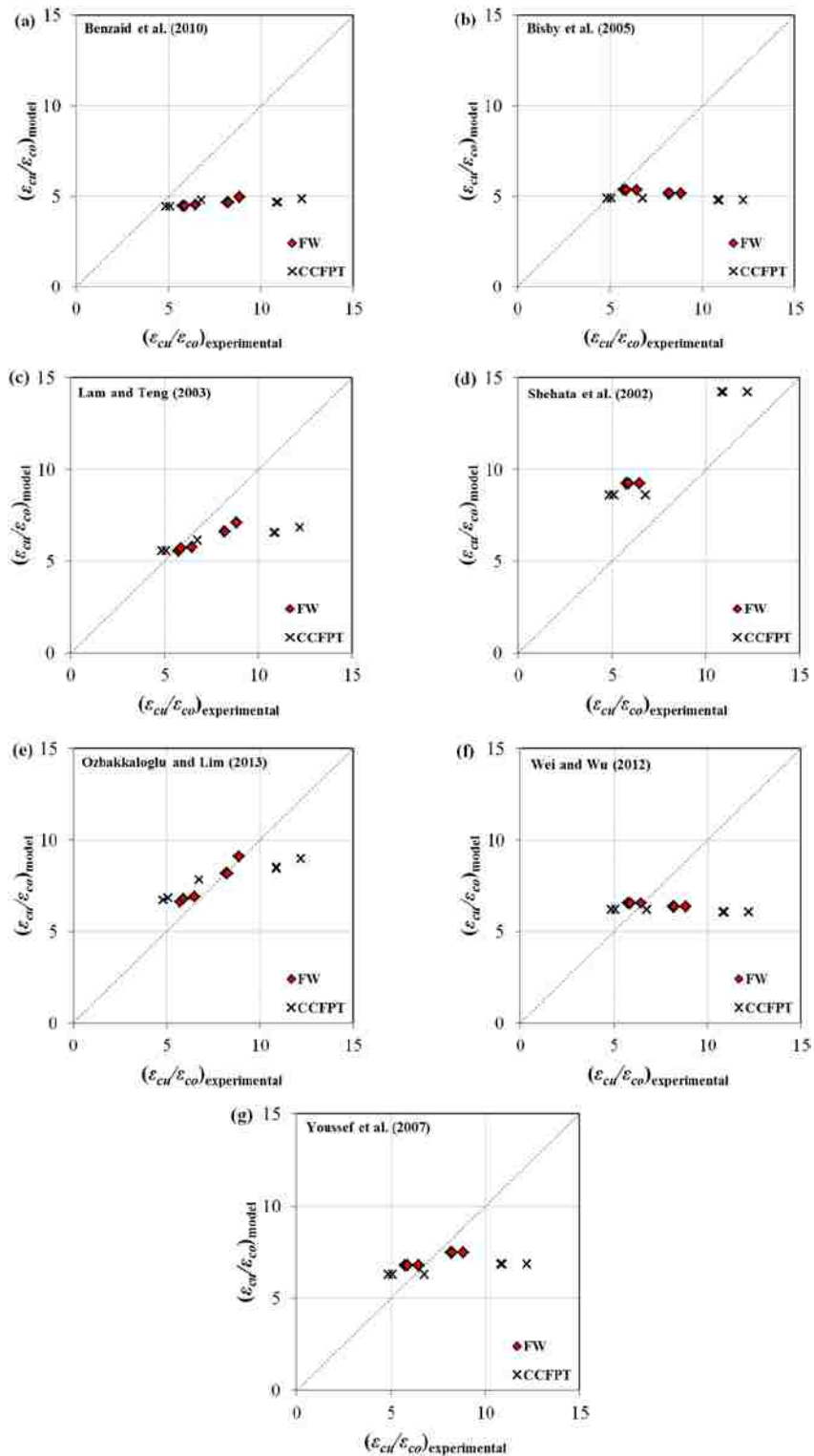


Fig. 14. Performance of various confinement models in predicting strain enhancement ratio $(\epsilon_{cu}/\epsilon_{co})$.

V. CONCRETE FILLED FRP-PVC TUBULAR COLUMNS FOR DUCTILE AND DURABLE BRIDGE BEHAVIOR UNDER EARTHQUAKE LOADS

ABSTRACT

This study is aimed at exploring a new ductile and corrosion-free design concept of confined concrete-filled polyvinyl-chloride tubular (CCFPT) columns. Confinement was provided with the use of a polyvinyl-chloride (PVC) tube and fiber-reinforced polymer (FRP) wrappings or FRP with a sandwiched layer of foam to enhance impact energy reduction due to potential FRP rupture and PVC fracture. Axial and flexural behavior of CCFPT columns was investigated with compressive and flexural tests, respectively, and compared with those of their corresponding concrete-filled polyvinyl-chloride tubular (CFPT) and FRP-wrapped (FW) columns. Test results obtained from 152×305 mm (6×12 in.) stub columns under axial loads and 152×1524 mm (6×60 in.) flexural beams under four-point loads indicated that the CCFPT columns can significantly enhance strength over the CFPT columns and enhance ductility over the FW columns. The transverse confining pressure from FRP wrapping and the interface property between the FRP and PVC proved critical in CCFPT design. Furthermore, the idea of introducing a cushioning foam layer between FRP layers and PVC to lessen the brittleness of FRP rupture in seismic regions proved effective.

KEY WORDS: Bridge, Concrete Column, FRP, PVC, Confinement, Durability.

INTRODUCTION

Past studies have demonstrated the enhanced structural performance of concrete-filled tube (CFT) systems, incorporating steel or FRP confining tubes, as an improved form of gravitational and lateral load resisting system for tall buildings/bridge columns and pile-footings (1; 2). Concrete-filled steel tube (CFST) and concrete-filled FRP tube (CFPT) column systems are the two most common types of CFTs that have been investigated at both member and system level (e.g.(2)). CFT system demonstrate remarkable properties in terms of enhanced structural performance and project economy/constructability (2). Some studies (e.g., (1)) have incorporated the additional confinement provided by FRP wraps in the CFST system, in which the CFST is circumscribed by FRP jacket.

Durability of reinforced concrete (RC) structures and steel-concrete composite structures under severe environmental conditions has always been a major concern (3). It is estimated only in the U.S. over \$1 billion is spent annually for repair and replacement of waterfront piling systems (4). Considering the corrosion of steel tubes (2; 4), durability, and potential long-term bond issues, in addition to brittle failure of FRP materials (5), few research studies investigated other types of confining-tubes. Commercially-available thermoplastic pipes, like high-density-polyethylene (HDPE) and polyvinyl-chloride (PVC) pipes for improved durability of RC structures have been investigated (e.g. (3; 6-8)). Experimental studies on CFPTs have been limited to axial compression tests only (9). PVC materials, exhibiting remarkable mechanical properties compared to other general purpose olefin plastics, demonstrate impressive ratio of cost to performance, specifically remarkable durability (6-8). Investigation of soil-buried PVC pipes dug up after 60 years of active use, indicated no deterioration and likely to have a further life expectancy of 50 years! (10). Thermal conductivity of PVC is only 0.45~0.6% of a steel tube, which provides a stable curing condition for the core concrete to achieve high performance and high durability (8). Study by Gupta and Verma (11) on RC-filled-PVC tubes subjected to harsh environmental condition indicated that no degradation in the strength and ductility of reinforced concrete-filled PVC specimens was observed. Test results on RC-filled-PVC tubes submerged in saturated sea water for 6 months revealed

that the microstructure and chemical composition of the PVC jacket remained nearly identical after exposure to sea water (11). The improved durability of PVC material allows potential applications of this system for wide variety of structural systems exposed to harsh environmental conditions (marine and saline environments).

Aging of the polymer, could affect the behavior of the FRP pipes/tubes and PVC pipes differently (3; 8). Study by Li et al. (12) indicated that environmental conditioning - in a tank with boiled water and UV light for seven days only – resulted in 57-76% loss of strengthening efficacy, and 43-48% stiffness degradation of FRP after conditioning. Study by Jakubowicz et al. (13) on accelerated and natural aging of PVC materials, indicated that aging in air at 80 °C and 90 °C for up to eight weeks caused no significant changes in mechanical properties and elongation at fracture of PVC material. PVC has outstanding anti-corrosion characteristics, and FRP jackets could be applied as additional confinement to compensate for the relatively weak confining properties of PVC pipes, introducing the confined concrete-filled PVC tube (CCFPT), with exceptional durability and mechanical strength.

Against this background, this study is aimed at investigating the structural performance of the CCFPT technology. This composite column consists of an exterior FRP-PVC shell confining the core concrete. This system is lightweight, cost-effective, and features the enhanced strength capacity of FRP materials, in addition to the superior corrosion resistance of PVC, which allows a feasible proposal for its application in pile foundation and harsh environment (acid-based and sea water).

Test results on axial compressive and flexural behavior of CFPT (PVC confined) and CCFPT (FRP+PVC confined) specimens are reported. Companion FRP-wrapped (FW) specimens were also tested to provide a reliable performance comparison between the extensively studied area of FRP-confined-concrete versus the lesser understood areas of PVC-confined and FRP+PVC-confined concrete. Monotonic axial compressive tests on stub column specimens (152×305 mm (6×12 in.)), in addition to simply-supported beam (152×1524 mm (6×60 in.)) tests, on CFPT, CCFPT and FW were undertaken. As illustrated in Figure 1, CCFPT is a combination of FW and CFPT configurations. Companion FW and CFPT have been tested, to identify the potential advantages of the CCFPT system, versus FW and CFPT systems when utilized individually.

EXPERIMENTAL PROGRAM

Axial and Flexural Test Specimens

Axial and flexural behavior of FRP-wrapped (FW), concrete-filled-PVC tube (CFPT), and confined-concrete-filled-PVC tube (CCFPT) specimens has been investigated in this study. A total of twenty one 152×305 mm (6×12 in.) stub cylindrical columns - referred as stub specimens hereafter - were tested under monotonically increasing compression to investigate the confinement effect of the FRP, PVC or FRP+PVC jacket on axially loaded NSC. Seven 152×1524 mm (6×60 in.) cylindrical specimens - referred as beam specimens hereafter - were tested under transverse four-point bending to investigate the flexural capacity of the FW, CFPT and CCFPT systems. Self-consolidating concrete (SCC) mix was used to cast the beam specimens. This would replicate using SCC mix for casting deep-concrete-pile-foundations to alleviate air cavities and soil pockets in field applications. All of the specimens included plain NSC without internal reinforcement.

All the CFPT, CCFPT, and FW specimens were manually manufactured. For CFPTs, the PVC pipe was cut to the required length (305 mm (12 in.) and 1524 mm (60 in.) for stubs and beams, respectively), followed by affixing a wood board at the bottom of the tube, which functioned as a stay-in-place formwork during concrete casting. For FW and CCFPT specimens, FRP sheets were applied using a manual wet-layup process, which required wrapping epoxy-resin-impregnated fibers around precast-concrete cylinders (for FWs) or PVC (for CCFPTs). For all the FW and CCFPT stub specimens, the FRP wraps were applied in the hoop direction only. To avoid direct axial stress transfer from the steel loading platens onto the FRP, the FRP jackets were recessed by 5 mm (0.2 in.) at both ends. For FW and CCFPT beam specimens, details on fibers orientation are reported later in the paper.

The stub column test matrix as shown in Table 1 included six FWs, five CFPTs, and ten CCFPTs. Table 1 also includes the designation of specimens for later reference. The bearing effect of PVC on the axial load carrying capacity of column specimens was investigated by recessing the PVC tube from both ends as illustrated in Figure 1(d). The two specimens with gap at each end were designated as CFPT-G40-w gap#1 and 2.

Additional CCFPTs (CCFPT-G40-1G-foam#1, 2, 3 and 4 specimens) were included in the stub test matrix, in which presence (or absence) of a cushioning soft layer between the PVC tube and FRP wrap was evaluated (Figure 1(e)). This cushion was basically a soft and compressible foam layer to: (1) delay the engagement of the FRP wrap and thus obtain larger axial deformation prior to rupture of the FRP jacket, (2) inhibit the PVC tube from immediate fracture after the FRP rupture, and (3) control the unnecessary strength enhancement. This system was tested to examine its efficacy for regions of high seismicity to avoid the undesirable brittle failure of FRP at ultimate limit state.

The flexural beam test matrix as shown in Table 2 included two FWs, one CFPT, and four CCFPTs. Table 2 also details the orientation and number of FRP plies, stacking sequence of FRP plies, and presence (or absence) of foam layer between the PVC tube and FRP wrap in CCFPT columns or between the FRP layers in FW columns. For FW-1, two plies of longitudinal FRP were applied directly on a precast-concrete beam and then confined by 3-ply of FRP in hoop direction. FW-2 was the same as FW-1 except that a foam layer was introduced after installation of the first longitudinal FRP and reinforced by a second longitudinal FRP layer before 3-ply of hoop fibers were installed. CFPT-1 represented a PVC tube filled with concrete. CCFPT-1 included 3-ply of FRP wrapped around the CFPT-1 in hoop direction. In CCFPT-2, foam was applied on the PVC tube before the 3-ply of hoop fibers were applied. CCFPT-3 included 2-ply of longitudinal FRP applied on the PVC tube and wrapped by 3-ply of FRP in hoop direction. CCFPT-4 is the same as CCFPT-3 except a foam layer was applied on the PVC tube before 2-ply of longitudinal and 3-ply of hoop fibers were installed.

Material Properties

Concrete

Two different NSC mixes with a target unconfined compressive strength (f'_{co}) of 50 MPa (7.0 ksi); and 25 MPa (3.6 ksi) at 28 days were used in the manufacture of stub column and flexural beam specimens, respectively. Plain concrete cylinders with 152×305 mm (6×12 in.) dimensions were tested at selected time intervals to determine the in-place unconfined concrete strength. The measured average compressive strength of

stub and beam specimens during the period of testing was 49.5 (7.0) and 24.12 (3.5) MPa (ksi), respectively.

FRP

Two types of glass FRP (GFRP) were used to fabricate stub column and beam specimens. Properties of GFRPs used in the manufacture of specimens were obtained from flat coupon tests. GFRP used to manufacture stub specimens had the following properties: tensile strength (f_{frp})= 1,228 MPa (178 ksi), elastic modulus (E_{frp})= 79.18 GPa (11,484 ksi), and ultimate tensile strain (ε_{frp})= 1.55%, with a nominal thickness of (t_f)= 0.373 mm/ply (0.015 in./ply). GFRP used for beam specimens had the following properties: f_{frp} = 431 MPa (62.5 ksi), E_{frp} = 27.2 GPa (3,945 ksi), ε_{frp} = 1.59%, and t_f = 1.3 mm/ply (0.05 in./ply). For the FW and CCFPT specimens, a thin layer of epoxy resin was applied to the concrete or PVC tube surface prior to manually wrapping the epoxy-impregnated FRP. Specimens with 1 and 3 layers of FRP were wrapped with 1 continuous sheet with 1 overlap zone. To prevent premature debonding failure, the FRP sheets were wrapped around the PVC or precast concrete cylinders continuously, with an additional overlap length of 152 mm (6 in.) and 144 mm (5.7 in.) for CCFPT and FW specimens, respectively, corresponding to 30% of the specimen's circumference.

PVC

Commercially available Grey schedule 40 PVC pipe used for water supply with nominal pressure of 1.24 MPa (180 psi) was used to manufacture the stub and beam CFPTs and CCFPTs. The selected PVC pipe had grey color, with an inside diameter of 152 mm (6 in.) with a minimum wall thickness of 7.10 mm (0.28 in.), as shown in Figure 1. All the CFPT, CCFPT, and FW specimens had a concrete infill of 152 mm (6 in.) in diameter, measured at the concrete core. Mechanical properties of the PVC pipe was specified by testing a minimum of five tensile dogbone coupon specimens, as illustrated in Figure 2(a). The PVC coupons exhibited significantly ductile behavior reaching to an average fracture strain of 46%. The tensile coupon PVC specimens had the following properties: ultimate tensile strength at yield ($f_{y,pvc}$)= 50.36 MPa (7.3 ksi), modulus of elasticity (E_{pvc})= 4.03 GPa (585 ksi), ultimate fracture strain ($\varepsilon_{u,pvc}$)= 46%, and Poisson's

ratio (ν)= 0.419. Besides, two similar hollow PVC tubes having the same height as the stub specimens were tested under axial compression. The axial stress-strain relationships are illustrated in Figure 2(b), and the following properties were obtained under axial compression: peak axial load sustained= 208.5 kN (46.9 kips), yield stress= 41.3 MPa (6 ksi), peak stress= 50.93 MPa (7.4 ksi), and axial strain at peak= 4.27%.

Instrumentation and Testing Procedure

Stub Specimens Under Compression

The specimens were tested under a constant displacement control regimen at approximately 0.50 mm (0.02 in.) per minute. For the CFPT and CCFPT specimens, the load was applied to the entire specimens' cross section. The in-place strengths of the unconfined concrete (f'_{co}) were measured at the time of testing, and the corresponding axial strain (ϵ_{co}) was calculated according to the expression given by Tasdemir et al. (14) as shown below.

$$\epsilon_{co} = (-0.067 f'_{co} + 29.9 f'_{co} + 1053) \times 10^{-6} \quad (1)$$

where f'_{co} is in MPa.

For each specimen, three vertical linear variable differential transformers (LVDTs) were utilized to measure the axial deformations, which were placed equidistantly at 120-degree increments between the top and bottom supporting steel plates, as shown in Figure 3(a). In addition, three horizontal LVDTs located at the specimens' mid-height were used to capture the lateral dilation (radial expansion) of the specimens. Moreover, specimens were instrumented at the mid-height with three strain gages to measure axial strains. Hoop strains were measured by three strain gages that were spaced equidistantly around the perimeter at the specimen's mid-height outside the overlap region. For FW and CCFPT specimens, one additional hoop strain gage was installed on the overlap region of the FRP wrap.

The stub specimens under axial compressive loading were identified according to the confinement material, where the FRP type, number of FRP layers, and PVC type are specified. Confinement tube is designated as either FW, CFPT, or CCFPT. The symbol G is used to represent the type of FRP, namely: glass (G) preceded by the number of layers.

For CFPT and CCFPT specimens the letter G was used in specimens designation to specify the PVC pipe schedule/color followed by a number that determines the PVC pipe schedule. As stated earlier, the gray Schedule 40 PVC pipe was used in this study, hence the G40 designation was used accordingly. A final number was provided to identify between nominally identical specimens. Details on all the stub specimens are presented in Table 1. For example, a FRP-wrapped specimen confined with one layer of GFRP, which is the first in its group would be FW-1G#1. A CFPT specimen encased by the gray Schedule 40 PVC tube, and is third in its group would be labelled as CFPT-G40#3. Lastly, a CCFPT specimen encased by the gray Schedule 40 PVC tube and one layer of GFRP, and is the first in its group would be CCFPT-G40-1G#1.

Two companion CFPT specimens with 12-mm gap at both ends (CFPT-G40-gap#1 and 2) were tested (Figure 1(d)). Stub specimens with foam layer between the PVC tube and FRP wrap (CCFPT-G40-1G-foam#1, 2, 3 and 4 specimens) were also included (Figure 1(e)). For CCFPT-G40-1G-foam#1 and 2 a 4.175-mm (0.16 in.) foam was utilized, wherein for the CCFPT-G40-1G-foam#3 and 4 a 1-mm (0.04 in.) foam layer was used.

Beam Specimens Under Transverse Bending

The 1.321 m (52 in.) long beams (clear span-length) were tested as simply supported, using a four-point bending setup as shown in Figure 3(b). The beam specimens were instrumented with linear position transducers (LPTs) at mid-span, and at quarter points, to record the vertical displacements along the beam. Strain gages in the hoop and longitudinal directions at mid-span were installed on the top and bottom surfaces. Additionally, a strain rosette was installed at mid-distance between the loading points and supports. The load was transferred from the actuator to the test beam through a transfer loading beam at two locations spaced 0.508 m (20 in.) apart. The load was applied monotonically in displacement control (5 mm (0.2 in.) per minute).

RESULTS AND DISCUSSION

Stub Specimens Failure Modes

The typical failure modes of all stub column specimens reported in Table 1 are illustrated in Figure 4. All the FW and CCFPT specimens exhibited brittle rupture of the FRP wrap, which was either a continuous rupture along the specimen's height (Figure 4(c, i)), or localized FRP rupture at the mid-height (Figure 4(a, b)). FWs and CCFPTs failed by rupture of the FRP wrap, immediately followed by failure of the core concrete due to loss of confinement. Catastrophic failure was observed for these two types of specimens. Figure 4(d) exemplifies the extensive concrete damage and fracture of the PVC tube after removing the FRP. Unlike FWs and CCFPTs, the CFPTs exhibited a very ductile behavior with gradual post-peak strength degradation – evident from their recorded stress-strain relationships discussed later in the paper- where the core concrete continued to crush causing the PVC tube to bulge and sustain very large axial strains. The highly stressed regions on the PVC tube, due to non-uniform dilation of the concrete, correspond to discoloration (white patches due to flow of resin) on the PVC tube (Figure 4(f)). Specifically, two types of failures, namely: shear type and drum type were observed for CFPTs, as shown in Figures 4(g) and 4(h), respectively. Both failures were ductile, and no fracture of the PVC tube was observed. The core concrete was thoroughly crushed and somewhat pulverized, while the PVC tube still retained its integrity. Shear failure of the PVC tube is characterized by damage of the concrete by shear stress developed in one direction due to the relatively weak confining effect of the PVC. The shear crack direction could be interpreted from the appearance of the distorted specimen (Figure 4(g)). In drum type failure, concrete did not crack in one direction, and multiple bulging of the tube was observed (Figure 4(h)). Nonetheless, all the CFPTs exhibited highly ductile behavior.

CCFPTs with foam demonstrated a ductile behavior similar to their CFPT counterparts, where no distinct FRP rupture could be defined. The FRP rupture was gradual due to slow fracture of the FRP wrap as fibers progressively ruptured that caused tearing and splintering along the specimen's height (Figure 4(i)). In these specimens, the PVC tube remained intact upon FRP rupture, and catastrophic failure was not observed.

Stub Specimens Stress-Strain Relationship

The ultimate condition, which consists of the ultimate axial strength (f'_{cu}) recorded at failure of the specimen, corresponding axial strain (ϵ_{cu}) and FRP hoop rupture strain ($\epsilon_{h,rupt}$), of each specimen is reported in Table 1, and the axial stress-strain relationships are presented in Figure 5.

For specimens that their stress-strain relationship consisted of a descending post-peak branch, so that the ultimate stress (f'_{cu}) was lower than the recorded peak stress (f'_{cc}), then both the ultimate stress and the peak stress are reported. For specimens exhibiting a monotonically increasing second branch, the ultimate stress (f'_{cu}) and peak stress (f'_{cc}) were equal, thus only a single value is reported under f'_{cc} in Table 1. For specimens with decreasing second branch, the ultimate conditions (f'_{cu} , ϵ_{cu} and $\epsilon_{h,rupt}$) presented in Table 1 correspond to 20% drop below the recorded peak stress.

The ultimate hoop rupture strain ($\epsilon_{h,rupt}$) of each specimen obtained from the average of the lateral strain gages is tabulated in Table 1. Past studies have indicated that the hoop rupture strains obtained from FRP-confined concrete specimens, are usually smaller than the tensile strain of the component fiber advertised by the manufacturers (ϵ_{fu}) (e.g. (15)). The strain reduction factors, k_ϵ , calculated from Eq. (2), were established for FW and CCFPT specimens and are presented in Table 1.

$$k_\epsilon = \frac{\epsilon_{h,rupt}}{\epsilon_{fu}} \quad (2)$$

Comparison of Stress-Strain Behavior

The CFPTs exhibited a ductile strain-softening post-peak response without sudden strength loss (Figure 5(c)). Unlike CFPTs, the FWs and CCFPTs when adequately confined (3-ply FRP), exhibited a monotonically ascending strain-hardening response up to FRP's rupture (Figures 5(b, g)). For lightly confined FW and CCFPT specimens (1-ply FRP) the strength (f'_{cc}/f'_{co}) and strain ($\epsilon_{cu}/\epsilon_{co}$) enhancement ratios were significantly smaller compared to their companion ones with adequate confinement (3-ply FRP), as reported in Table 1.

The CFPTs with gaps at both ends demonstrated very similar behavior to their companion CFPTs up to the peak strength. Nevertheless, upon reaching the peak strength, the unconfined concrete outside the PVC tube started to crush resulting in rapid and unstable post-peak strength degradation (Figure 5(d)). However, the PVC tube in these series of specimens still demonstrated a ductile behavior, similar to CFPTs with full-height tube. Figure 5(i) compares the stress-strain relationships of a CFPT with full-height PVC (CFPT-G40#1) versus CFPT with gap (CFPT-G40-w gap#1). The peak strength is very similar for both types of specimens.

The CCFPTs with foam exhibited distinct axial stress-strain relationship due to the cushioning properties of foam. CCFPTs with foam demonstrated similar behavior to CCFPTs without foam up to peak stress, with gradual post-peak strength reduction (Figure 5(f)). Representative stress-strain responses of CCFPTs with foam are compared with a CCFPT without foam (CCFPT-G40-1G#2) in Figure 5(j). Post-peak strength reduction for CCFPTs with foam was stable, and it was due to the compression of the foam between the PVC and FRP, wherein the FRP wrap was not significantly strained as the foam material was continually compressed. The effect of the foam thickness becomes significant on the second region of the stress-strain relationship. For CCFPT-G40-1G-foam#1 and 2 with the thicker foam, larger strength drop was observed before the FRP wrap starts to provide the confining pressure. In these specimens larger gap is provided by the foam, in which it allows greater dilation of the concrete before the FRP wrap becomes engaged. Presence of the foam layer delayed the onset of FRP rupture as marked on Figure 5(f).

Increasing in the number of FRP layers in the FW and CCFPT specimens lead to increase in ultimate conditions (f'_{cu} and ε_{cu}), tabulated in Table 1, and improve the strength (f'_{cu}/f'_{co}) and strain ($\varepsilon_{cu}/\varepsilon_{co}$) enhancement ratios. Figure 5(h) illustrate the influence of confinement pressure (f_{lu}) provided by different number of FRP layers on the axial stress-strain relationships of FWs and CCFPTs. The nominal confinement ratio (f_{lu}/f'_{co}) is the ratio of lateral confinement pressure by the confining jacket to the in-place unconfined concrete strength, calculated by the following equation:

$$\frac{f_{lu}}{f'_{co}} = \frac{2t_f f_{fu}}{Df'_{co}} = \frac{2t_f E_f \varepsilon_{fu}}{Df'_{co}} \quad (3)$$

where t_f = total nominal thickness; E_f = the modulus of elasticity; ε_{fu} = ultimate tensile strain of the fibers; and D = the diameter of the confined concrete. As stated earlier, FRP hoop-rupture strain ($\varepsilon_{h,rupt}$) are often lower compared to the ultimate rupture-strain of fibers (ε_{fu}) obtained from flat-coupon tests and/or reported by manufacturers. Therefore, the actual confinement ratio ($f_{lu,a}/f'_{co}$) was also calculated and presented in Table 1, by the following equation:

$$\frac{f_{lu,a}}{f'_{co}} = \frac{2t_f f_{fu} k_\varepsilon}{Df'_{co}} = \frac{2t_f E_f (\varepsilon_{fu} k_\varepsilon)}{Df'_{co}} = \frac{2t_f E_f \varepsilon_{h,rupt}}{Df'_{co}} \quad (4)$$

The actual confinement ratio for FW and CCFPTs with 1-ply and 3-ply of FRP are equal to 0.11 and 0.37, respectively. It is clear that the shapes of the axial stress-strain relationship for FWs and CCFPTs with similar level of confining pressure are very close (Figure 5(h)). However, CCFPTs experience greater strength (f'_{cu}/f'_{co}) and strain ($\varepsilon_{cu}/\varepsilon_{co}$) enhancement ratios, compared to their companion FWs with identical number of FRP layers. As presented in Table 1, significant gains in strain capacity (ε_{cu}) for CCFPTs compared to FWs, irrespective of the number of FRP layers could be observed. Table 1 indicates that CCFPTs consistently exhibited larger strain reduction factors (k_ε) compared to their FW companion specimens. Hence, considerably higher strain enhancement ratios were observed for CCFPTs. This could be attributed that in CCFPTs the PVC pipe provides a relatively uniform stress distributing medium, where concrete is maintained and contained integral upon concrete cracking, thus the stress concentrations due to uneven concrete cracking is reduced on the FRP wrap. Additionally, substrate for the FRP wrap in CCFPTs is the PVC tube which compared to concrete surface is very uniform that may enhance the bond between the FRP for the CCFPT.

Flexural Specimens Failure Modes

Figure 6 illustrates the condition of core concrete, after removal of the FRP/PVC shell. Depending on the confinement detail and presence of the foam, ductile or brittle failures—evident from their recorded load-mid-span deflection relationships discussed later in the paper—were observed. CFPT-1 experienced uniform flexural cracking distributed along the beam's length (Figure 6(a)). Similarly, presence of the foam

between PVC and FRP in CCFPT-2 resulted in uniform distributed flexural cracking (Figure 6(c)). Plastification of PVC tube in CFPT-1 and CCFPT-2 along the constant moment region of the beams was observed. On the contrary, in CCFPT-1, 3, and 4, the damaged region is localized and limited to one or two cross sections only (Figures 6(b), (d) and (e)).

Flexural Specimens Load-Displacement Relationship

As shown in Figure 7, either bi-linear or linear-elastic load-deflection relationships were observed. The peak load (P_{peak}), recorded mid-span deflection at the peak load (Δ_{peak}), mid span deflection at ultimate (Δ_{ult}) where 20% drop from the peak load was recorded, and load at ultimate (P_{ult}) are reported in Table 2. Peak moment (M_{peak}) calculated from the recorded loads are also reported. For specimens exhibiting monotonically increasing behavior, the peak load (P_{peak}) and load at ultimate (P_{ult}), and similarly the mid-span deflection at peak load (Δ_{peak}) and mid-span deflection at ultimate (Δ_{ult}), were equal, thus only a single value is reported under P_{peak} and Δ_{peak} in Table 2. In Figure 7, the lateral load-mid span displacement relationships with a deflection range from 0 to 180 mm (7 in.) and from 0 to 80 mm (3.1 in.) are illustrated, respectively, so that the post-peak behavior and the onset behavior of the load-displacement curves can be analyzed more clearly.

The CFPT-1 and CCFPT-2 specimens demonstrated ductile bi-linear load-deflection with smooth transition from the linear-elastic to the nonlinear second region. Specimens with FRP in longitudinal direction (FW-1, CCFPT-3 and 4), except FW-2, demonstrated linear elastic behavior with brittle failure.

The effect of the additional confinement for CFPTs through FRP wraps was investigated by comparing CFPT-1 and CCFPT-1. The effect of presence of the foam between the FRP wrap and PVC tube was investigated by comparing the CCFPT-1 and CCFPT-2. CFPT-1 demonstrated the most ductile response compared to all of the beam specimens. However, it demonstrated the smallest flexural strength as shown in Table 2, except for CCFPT-1. While it was anticipated that CCFPT-1 should experience enhanced load carrying capacity compared to CFPT-1 due to the additional confinement provided from 3-ply of hoop FRP, however, upon entering to the nonlinear behavior of CCFPT-1,

cracking at the fibers-resin interface resulted in fracture of the PVC tube. A sudden snap sound was heard and the specimen lost its flexural strength, as if the PVC experienced a brittle fracture. Comparison of test results from stub specimens on companion CFPTs versus CCFPTs with FRP wraps demonstrated very promising results. However, contrary to the expected outcome, flexural beam test results indicated the importance of the interface between FRP-wrap and PVC-tube. Bridge piers and soil-buried-piles are expected to undergo inelastic excursions under lateral forces, experiencing significant flexural deformations. Additional tests are strongly recommended to further understand this new composite system.

Comparison of CCFPT-2 against CFPT-1 indicates that due to presence of foam, CCFPT-2 could demonstrate a ductile behavior with considerable plastic deformations. Similar to CFPT-1, the CCFPT-2 demonstrated gradual strength degradation upon reaching its peak-strength. The additional confinement in CCFPT-2 resulted in increase of the initial stiffness and flexural strength. CCFPT-2 developed a peak load of 78.6 kN (17.7 kips) at 79.3 mm (3.1 in.) mid-span deflection, whereas CFPT-1 was able to sustain a peak load of 67.9 kN (15.3 kips) at 129.6 mm (5.1 in.) mid-span deflection.

Difference between FWs and CCFPTs was investigated by comparing FW-1 and CCFPT-3. For identical fiber architectures, presence of PVC in CCFPT-3 resulted in enhancement of peak strength and initial stiffness (peak load increased from 158.1 kN (35.5 kips) for FW-1 to 169.6 kN (38.1 kips) for CCFPT-3). However, both specimens demonstrated significantly reduced ultimate deflection compared to CFPT-1, with brittle failure.

The concept of introducing foam between longitudinal FRP-plyies to lessen the brittleness of the composite system upon rupture of longitudinal FRP was investigated by comparing FW-2 and CCFPT-4. Load-deflection curves with similar trends were observed, with post-peak strength degradation due to longitudinal-FRP rupture. FW-2 demonstrated promising results in terms of inhibiting the brittle failure and exhibiting some level of ductility. In FW-2, upon rupture of the first longitudinal layer of FRP, only a 22% drop in the load carrying capacity was observed and the specimen recovered to undergo additional deflection and sustained additional load without failure. Contrary to FW-1 with brittle failure, FW-2 demonstrated a two-peak staged-type failure. Presence of

foam for CCFPT-4 proved to be less significant, and resulted in three strength drops as marked in Figure 7(b). However, strength loss at peak was significant that resulted in fracture of the PVC.

CONCLUSIONS

This paper reports the axial and flexural behavior of FRP-confined concrete-filled PVC tubular columns and compares their performance with those of concrete-filled PVC tubular columns and FRP-wrapped columns. Based on the test results and visual observations, the following conclusions can be drawn:

- PVC tube provided low confinement on concrete columns but can undergo significant plastic deformation to cope with concrete dilation. Additional confinement provided by FRP wraps with fibers oriented in hoop direction made the columns sufficiently ductile for potential applications in column design. The FRP wraps can effectively inhibit local buckling of the PVC tube and restrain the lateral dilation of the encased concrete.
- PVC tube contributed little to the axial strength of concrete columns, but FRP wraps with fiber oriented in longitudinal direction can significantly strengthen the columns.
- PVC tube fractured right after the rupture of its immediate FRP wraps resulting in a sudden loss of load carrying capacity. This brittle failure mode can be prevented by introducing an energy absorption foam layer between the PVC tube and the FRP wraps. In this case, the strength was gradually reduced in steps.
- Introduction of foam between FRP layers proved to be an effective method to lessen the brittleness, and obtainment of relatively ductile member's response upon FRP rupture.

ACKNOWLEDGMENTS

Financial support for this study was provided by the U.S. National Science Foundation under Award No. CMMI-1030399. The views, findings, and conclusions reflected in this paper are those of the authors only and do not necessarily reflect the official views or policies of the sponsor.

REFERENCES

1. Xiao, Y., W. He, and K.-k. Choi. Confined concrete-filled tubular columns. *Journal of structural engineering*, Vol. 131, No. 3, 2005, pp. 488-497.
2. Fam, A. Z., and S. H. Rizkalla. Concrete-filled FRP tubes for flexural and axial compression members. *Proceedings of ACMBS-3, Ottawa, Canada, 2000*, pp. 315-322.
3. Wang, J.-Y., and Q.-B. Yang. Investigation on compressive behaviors of thermoplastic pipe confined concrete. *Construction and Building Materials*, Vol. 35, 2012, pp. 578-585.
4. Pando, M. A., C. D. Ealy, G. M. Filz, J. Lesko, and E. Hoppe. A Laboratory and Field Study of Composite Piles for Bridge Substructures. In *FHWA-HRT-04-043*, 2006.
5. Karbhari, V. M. *Durability of composites for civil structural applications*. Elsevier, 2007.
6. Kurt, C. E. Concrete filled structural plastic columns. *Journal of the Structural Division*, Vol. 104, No. 1, 1978, pp. 55-63.
7. Toutanji, H., and M. Saafi. Durability studies on concrete columns encased in PVC-FRP composite tubes. *Composite structures*, Vol. 54, No. 1, 2001, pp. 27-35.
8. Wang, J., and Q. Yang. Experimental study on Mechanical Properties of concrete confined with plastic Pipe. *ACI Materials Journal*, Vol. 107, No. 2, 2010.
9. Jiang, S.-F., S.-L. Ma, and Z.-Q. Wu. Experimental study and theoretical analysis on slender concrete-filled CFRP-PVC tubular columns. *Construction and Building Materials*, Vol. 53, 2014, pp. 475-487.
10. Nowack, R., O. I. Otto, and E. W. Braun. „60 Jahre Erfahrungen mit Rohrleitungen aus weichmacherfreiem Polyvinylchlorid (PVC-U). *KRV Nachrichten*, 1995, pp. 1-95.
11. Gupta, P. K., and V. K. Verma. Study of concrete-filled unplasticized polyvinyl chloride tubes in marine environment. *Proceedings of the Institution of Mechanical Engineers, Part M: Journal of Engineering for the Maritime Environment*, 2014, p. 1475090214560448.

12. Li, G., S.-S. Pang, J. E. Helms, D. Mukai, S. I. Ibekwe, and W. Alaywan. Stiffness degradation of FRP strengthened RC beams subjected to hygrothermal and aging attacks. *Journal of composite materials*, Vol. 36, No. 7, 2002, pp. 795-812.

13. Jakubowicz, I., N. Yarahmadi, and T. Gevert. Effects of accelerated and natural ageing on plasticized polyvinyl chloride (PVC). *Polymer degradation and stability*, Vol. 66, No. 3, 1999, pp. 415-421.

14. Tasdemir, M., C. Tasdemir, S. Akyüz, A. Jefferson, F. Lydon, and B. Barr. Evaluation of strains at peak stresses in concrete: a three-phase composite model approach. *Cement and Concrete Composites*, Vol. 20, No. 4, 1998, pp. 301-318.

15. Vincent, T., and T. Ozbakkaloglu. Influence of fiber orientation and specimen end condition on axial compressive behavior of FRP-confined concrete. *Construction and Building Materials*, Vol. 47, 2013, pp. 814-826.

List of tables:

TABLE 1 Summary of stub column specimens test results

TABLE 2 Summary of flexural beam specimens test results

List of figures:

FIGURE 1 Details of studied specimens: (a) FRP-wrapped (FW), (b) concrete filled PVC tube (CFPT), (c) confined concrete filled PVC tube (CCFPT), (d) CFPT with and without gaps at both ends, and (e) application of foam layer between PVC tube and FRP wrap.

FIGURE 2 Measured mechanical properties of PVC pipes: (a) tensile stress-strain curve of PVC pipe coupon up to fracture, and (b) compressive behavior of empty PVC tubes.

FIGURE 3 Test setup: (a) stub column, and (b) flexural beam.

FIGURE 4 Typical failure modes of stub columns: (a) FW-1G#2, (b) FW-3G#2, (c) CCFPT-G40-1G#2, (d) CCFPT-G40-1G#2 after FRP removal, (e) CCFPT-G40-3G#3, (f) CFPT-G40-w gap#1, (g) CFPT-G40#1, (h) CFPT-G40#2, and (i) CCFPT-G40-1G-foam#3.

FIGURE 5 Axial stress-strain curves of stub specimens: (a) FW-1G, (b) FW-3G, (c) CFPT-G40, (d) CFPT-G40-w gap, (e) CCFPT-G40-1G, (f) CCFPT-G40-1G-foam, (g) CCFPT-G40-3G, (h) FW versus CCFPT, (i) CFPT for gap effect, and (j) CCFPT for foam effect.

FIGURE 6 Core concrete conditions of CFPT and CCFPT beam specimens after test: (a) CFPT-1, (b) CCFPT-1, (c) CCFPT-2, (d) CCFPT-3, and (e) CCFPT-4.

FIGURE 7 Load-deflection curves of flexural beams.

TABLE 1 Summary Of Stub Column Specimens Test Results

Confinement type	Confinement detail	Specimen	f_w/f_{cs}	f_w/f_{cs}	f_{cs} (MPa)	f_{cs} (MPa)	ϵ_{cu} (%)	$\epsilon_{cu,avg}$ (%)	f_w/f_{cs}	$\epsilon_{cu}/\epsilon_{cc}$	k_c
FRP-wrapped	1 ply GFRP	FW-1G#1	0.14	0.11	63.1	53.1	1.61	1.41	1.26	6.49	0.71
		FW-1G#2	0.14	0.10	63.8	44.7	1.26	1.29	1.28	5.08	
		FW-1G#3	0.14	0.10	63.3	54.3	1.26	1.25	1.27	5.08	
	3 ply GFRP	FW-3G#1	0.43	0.35	104.2		2.03	1.52	2.08	8.18	0.85
		FW-3G#2	0.43	0.39	102.3		2.20	1.68	2.05	8.87	
		FW-3G#3	0.43	0.35	102.1		2.05	1.52	2.04	8.26	
Concrete filled PVC tube	Sch. 40 PVC	CFPT-G40#1	0.08		52.6	42.0	0.60		1.05	2.42	
		CFPT-G40#2	0.08		49.5	39.6	0.44		0.99	1.81	
		CFPT-G40#3	0.08		47.8	38.2	1.01		0.96	4.07	
	Sch. 40 PVC with 12 mm gaps at both ends	CFPT-G40-w gap#1	0.08		55.5	44.4	0.50		1.11	2.01	
		CFPT-G40-w gap#2	0.08		58.2	46.6	0.81		1.16	3.26	
Confined concrete filled PVC tube	Sch. 40 PVC+1 ply GFRP	CCFPT-G40-1G#1	0.13	0.12	68.0	58.5	1.73	1.73	1.36	6.97	0.88
		CCFPT-G40-1G#2	0.13	0.11	72.4	60.2	1.26	1.58	1.45	5.08	
		CCFPT-G40-1G#3	0.13	0.11	67.4	57.8	1.27	1.59	1.35	5.12	
	Sch. 40 PVC+1 ply GFRP with foam between PVC tube and FRP wrap	CCFPT-G40-1G-foam#1	0.13	0.13	58.7	47.0	0.62	1.84	1.17	2.50	0.97
		CCFPT-G40-1G-foam#2	0.13	0.13	54.0	43.2	0.53	1.80	1.08	2.14	
		CCFPT-G40-1G-foam#3	0.13	0.12	68.0	54.4	0.89	1.77	1.36	3.59	
		CCFPT-G40-1G-foam#4	0.13	0.12	58.8	47.0	0.90	1.78	1.18	3.63	
	Sch. 40 PVC+3 ply GFRP	CCFPT-G40-3G#1	0.39	0.35	97.9		2.70	1.68	1.96	10.88	0.92
		CCFPT-G40-3G#2	0.39	0.37	114.3		3.03	1.77	2.29	12.21	
		CCFPT-G40-3G#3	0.39	0.35	103.0		2.71	1.67	2.06	10.92	

TABLE 2 Summary Of Flexural Beam Specimens Test Results

Confinement type	Specimen	FRP fibers orientation		Stacking sequence	Foam	P_{peak} (kN)	M_{peak} (kN.m)	Δ_{peak} (mm)	P_{ult} (kN)	Δ_{ult} (mm)
		Longitudinal	Hoop							
FRP-wrapped	FW-1	2	3	2 long / 3 hoop	-	158.1	32.1	41.1		
	FW-2	2	3	1 long / foam / 1 long / 3 hoop	Between long. FRP	93.6	19.0	30.3	74.9	31.0
Concrete filled PVC tube	CFPT-1	-	-	-	-	67.9	13.8	129.6	54.3	166.8
Confined concrete filled PVC tube	CCFPT-1	-	3	3 hoop	-	35.9	7.3	14.8		
	CCFPT-2	-	3	Foam / 3 hoop	Between PVC and hoop FRP	78.6	16.0	79.3	62.9	111.7
	CCFPT-3	2	3	2 long / 3 hoop	-	169.6	34.5	30.6		
	CCFPT-4	2	3	Foam / 2 long / 3 hoop	Between PVC and long. FRP	128.7	26.2	58.0		

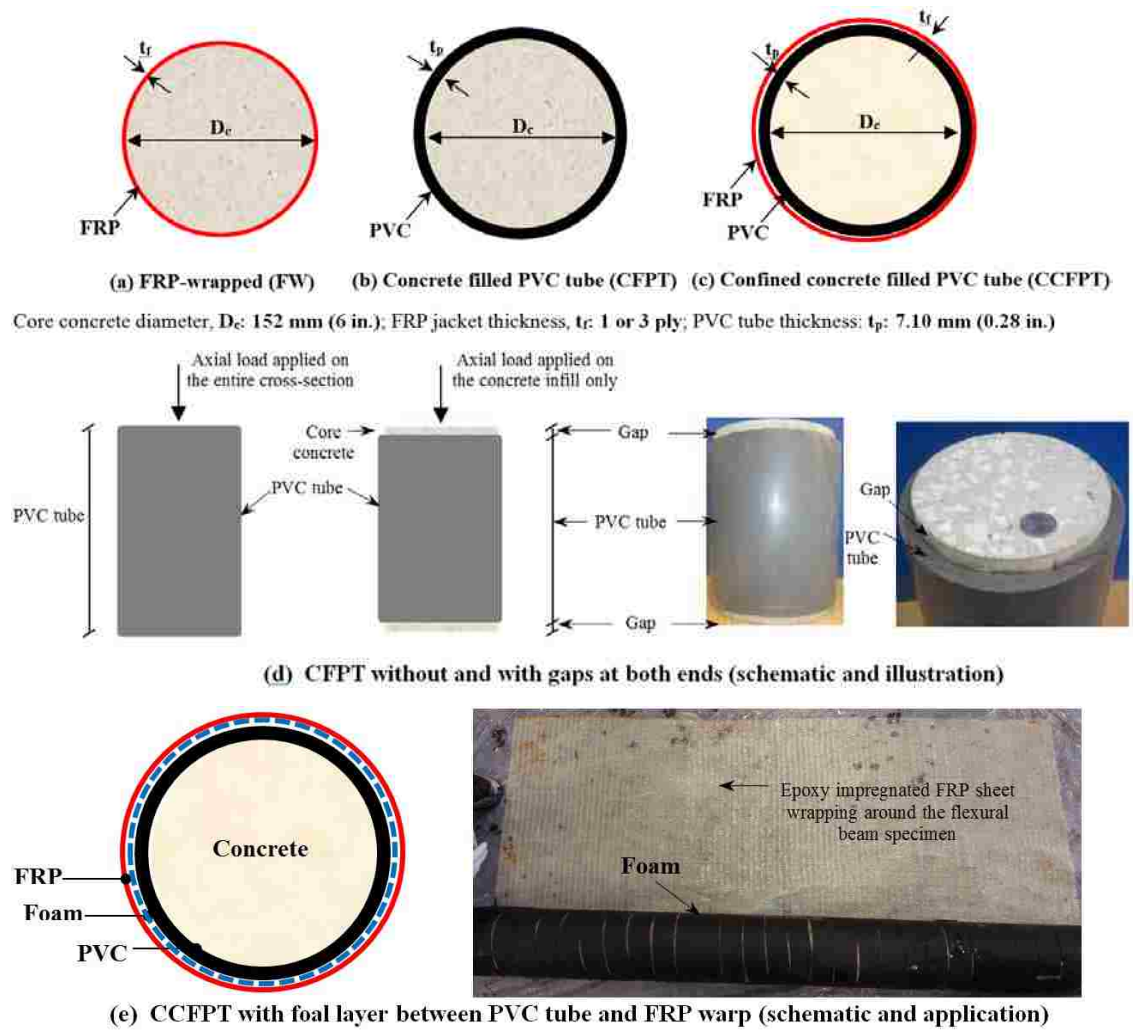


FIGURE 1 Details of studied specimens: (a) FRP-wrapped (FW), (b) concrete filled PVC tube (CFPT), (c) confined concrete filled PVC tube (CCFPT), (d) CFPT with and without gaps at both ends, and (e) application of foam layer between PVC tube and FRP wrap.

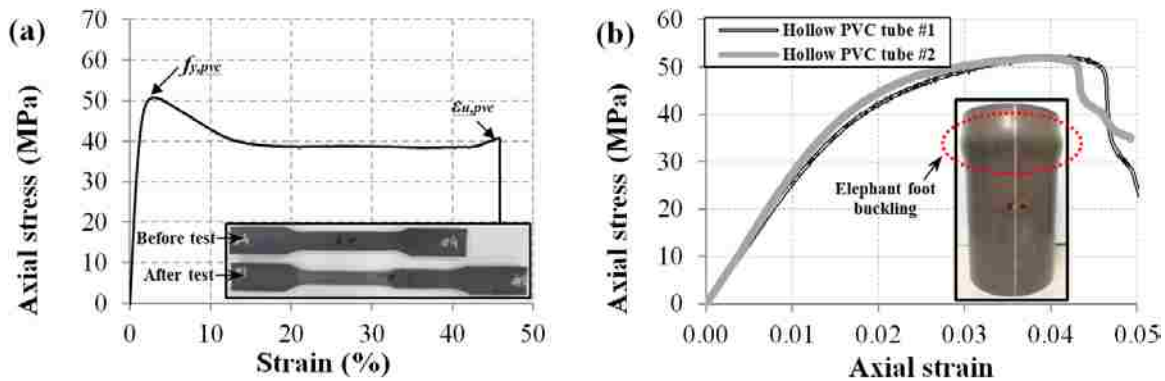


FIGURE 2 Measured mechanical properties of PVC pipes: (a) tensile stress-strain curve of PVC pipe coupon up to fracture, and (b) compressive behavior of empty PVC tubes.

Conversion: 1 MPa = 145 psi

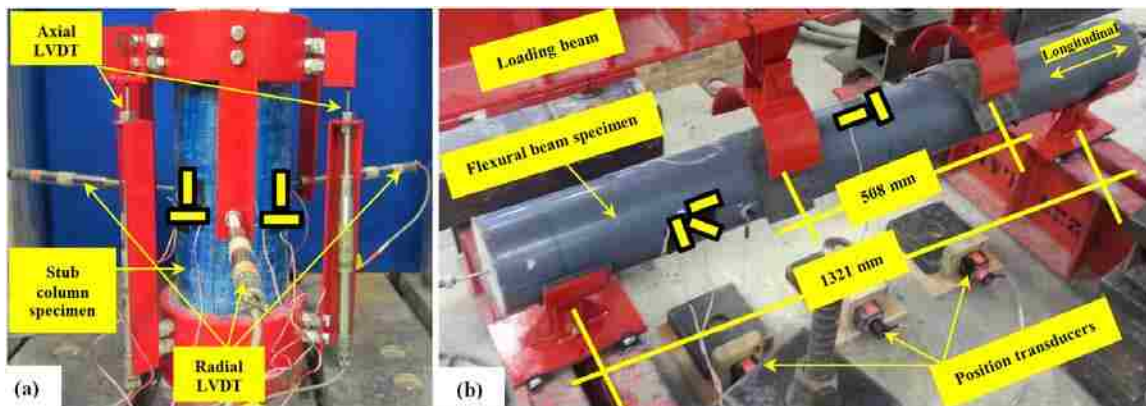



FIGURE 3 Test setup: (a) stub column, and (b) flexural beam. ( : strain gage)

Conversion: 1 mm = 0.04 in.

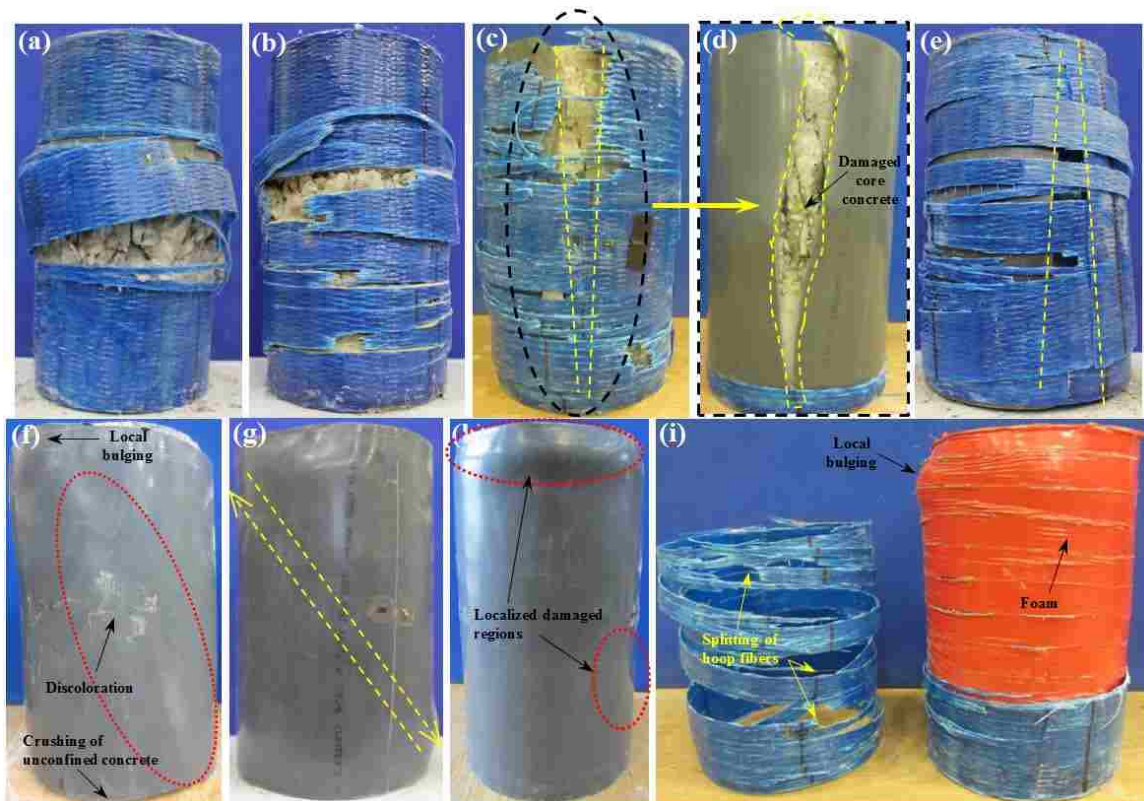


FIGURE 4 Typical failure modes of stub columns: (a) FW-1G#2, (b) FW-3G#2, (c) CCFPT-G40-1G#2, (d) CCFPT-G40-1G#2 after FRP removal, (e) CCFPT-G40-3G#3, (f) CFPT-G40-w gap#1, (g) CFPT-G40#1, (h) CFPT-G40#2, and (i) CCFPT-G40-1G-foam#3.

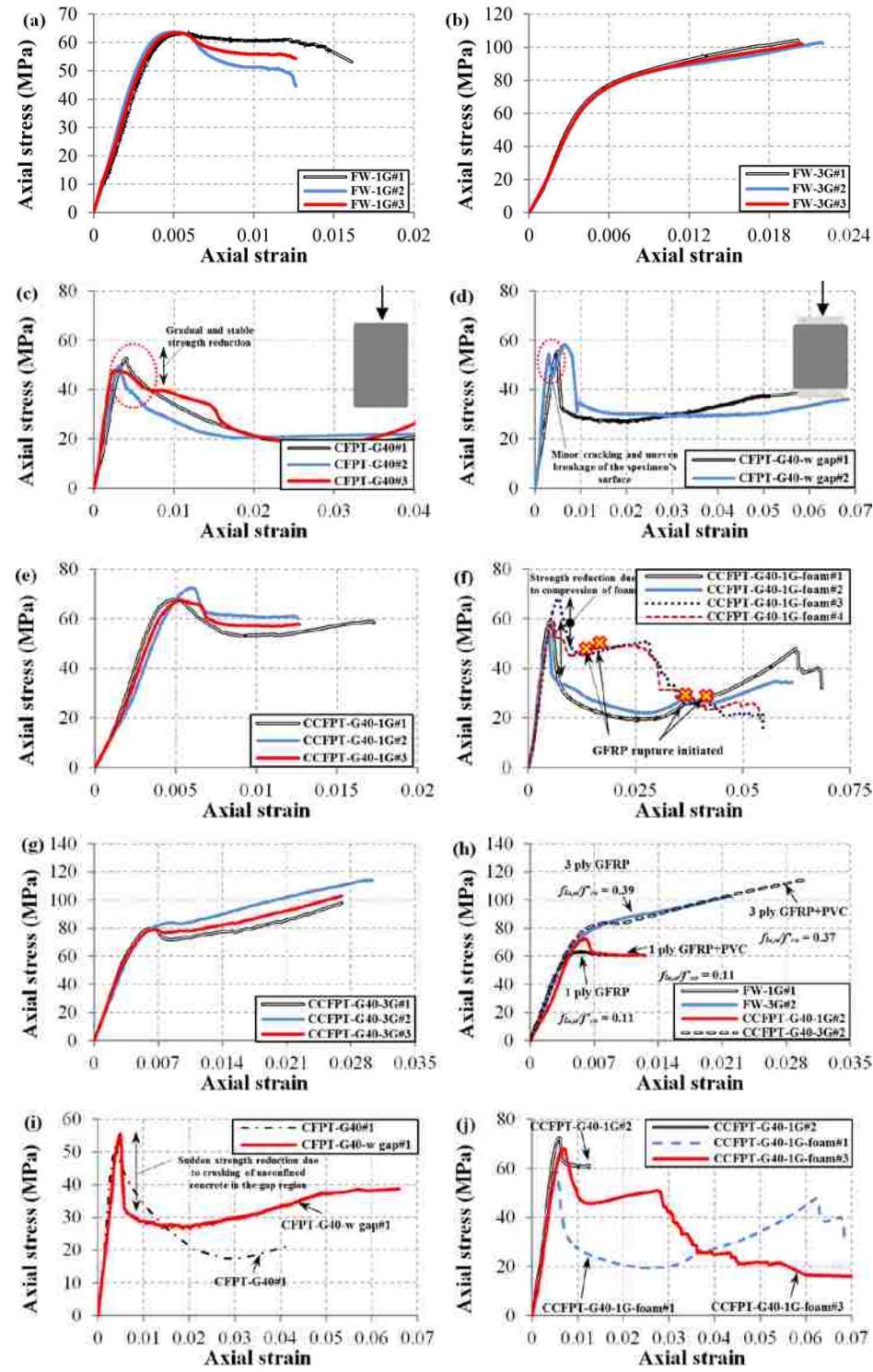


FIGURE 5 Axial stress-strain curves of stub specimens: (a) FW-1G, (b) FW-3G, (c) CFPT-G40, (d) CFPT-G40-w gap, (e) CCFPT-G40-1G, (f) CCFPT-G40-1G-foam, (g) CCFPT-G40-3G, (h) FW versus CCFPT, (i) CFPT for gap effect, and (j) CCFPT for foam effect.

Conversion: 1 MPa = 145 psi

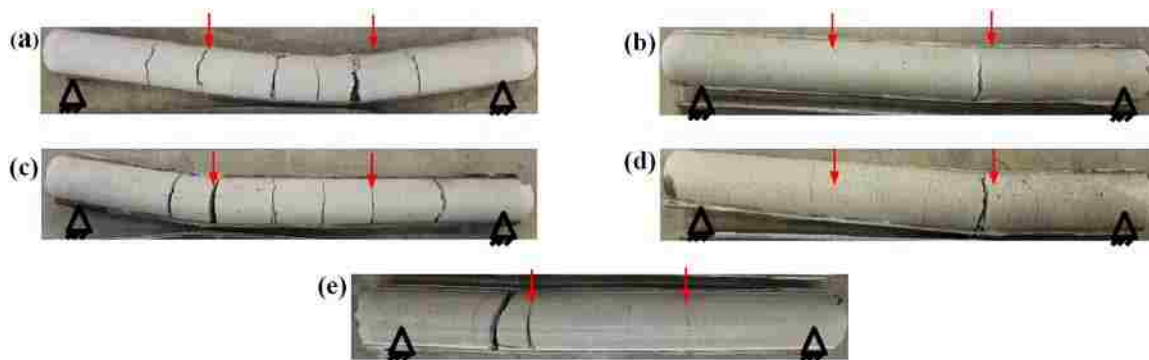


FIGURE 6 Core concrete conditions of CFPT and CCFPT beam specimens after test: (a) CFPT-1, (b) CCFPT-1, (c) CCFPT-2, (d) CCFPT-3, and (e) CCFPT-4.

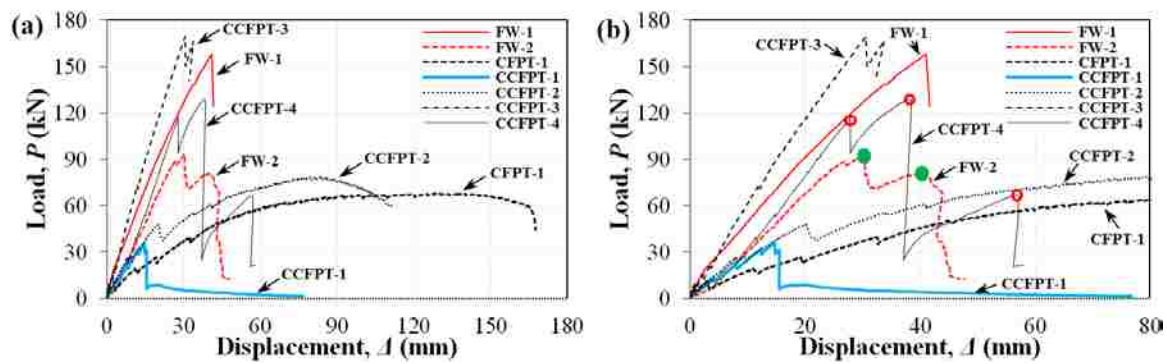


FIGURE 7 Load-deflection curves of flexural beams

Conversion: 1 kN = 225 lbf; 1 mm = 0.04 in.

SECTION

2. SUMMARY, CONCLUSIONS AND RECOMMENDATIONS

2.1. SUMMARY OF RESEARCH WORK

The primary objective of this study was developing, characterizing and validating an integrated composite confinement system of conventional jackets for: (1) repair and retrofit of existing bridge columns; and (2) construction of new bridge columns, subjected to earthquake excitations.

The first objective was to develop the composite steel confinement jacket for effective and rapid repair of earthquake damaged RC bridge columns, and the results of the experimental and analytical investigations conducted were presented in the sections “Paper I”, “Paper II”, and “Paper III”.

The experimental study involved repair of two 1/2-scale severely damaged lap-spliced circular RC bridge columns (Column 1 and Column 2) tested to failure under reversed cyclic loading. The two columns were designed with the same geometric and material properties, except that the longitudinal reinforcement of the second column included enamel coated rebar. Both columns included $20d_b$ lap-spliced reinforcement (d_b = rebar diameter) at column-footing interface. Both columns were tested under constant axial load and incrementally increasing cyclic load to complete failure. Both specimens failed due slip of dowel and column bars in the lap-spliced region. After the original test, severe damage in the plastic hinge region of the columns was observed. Damage included cover concrete cracking and spalling, core concrete crushing, lap-splice failure, reinforcement bar yielding in both columns. Reinforcement buckling was also observed in the second column.

Considering the repair performance objectives, and availability of the repair materials the two columns were repaired for two performance levels, namely service and ultimate limit state. Column 1-R refers to Column 1 after repair in which repair was designed for service limit state. Column 2-R refers to Column 2 after repair in which repair intervention was designed for ultimate limit state. Repair material consisted of a

quick set repair grout and the composite (hybrid) steel jacket. The quick set grout was used to repair the damaged concrete and restore the original column cross section. The composite steel jacket, which is also referred to as hybrid or prestressed steel jacket in this text, consisted of a thin steel sheet wrapped and welded around the column circumscribed by discrete prestressing hoops joined at the ends through Dywidag twisted ring anchors manufactured by Dywidag Systems International®. The column cross section was restored first prior to application of the jacket in order to validate the applicability and efficacy of the proposed jacket for retrofit applications of existing columns where dry bond exists between the column surface and jacket. However, it was feasible to place the thin sheet jacket around the column and fill it with the repair grout. Moreover, for rapid application of the proposed jacket, epoxy injection was not used to seal the existing cracks. No surface preparation/treatment or adhesive epoxy application was conducted on the column surface prior to jacket application to better simulate condition of a field application. After restoring the column cross section, the thin sheet metal was wrapped around the column and welded. Then ten prestressing strands were placed over the sheet metal and column, and tensioned to the required level of prestressing pressure.

The first column (Column 1) was designed for rapid repair (Column 1-R) considering the service limit state. The second column (Column 2) was repaired (Column 2-R) for ultimate limit state considering permanent repair requirement. Hence, a carefully designed/detailed force transfer mechanism using headed anchor reinforcement was designed and implemented for the second column. Both columns were repaired at the 1220-mm bottom in the plastic hinge region only using the proposed composite steel jacket. The headed dowel anchor reinforcements for the second column were designed to restore the initial stiffness of the repaired column, considering the footing flexural capacity and the reserved shear capacity of the damaged column. Moreover, the headed dowel anchor reinforcements were designed to form the plastic hinge region at the column footing interface, similar to the original column specimen. The repaired columns were then re-tested under similar loading protocol applied to the as-built original columns.

Measured data were analyzed to investigate the effectiveness of the proposed repair technique on the performance of the repaired columns compared to the corresponding original column responses. The repair method was proved effective in repairing both columns considering the repair performance objectives. Repair jacket for the first column completely restored and even improved the response of the repaired column in terms of strength and ductility, compared to the original column. However, service stiffness of the repaired column was lesser compared to the original column due to the existing damage in the concrete and reinforcement from original test. Nonetheless, the repair method was still regarded as effective, since rapid repair was the primary goal for the first column and strength and ductility were completely restored and improved. Additionally, the unstable in-cycle strength degradation of the original column was improved to more stable cyclic strength degradation. The second column repaired for ultimate limit state, better suited as a permanent repair method, demonstrated dramatic improvement in terms of strength and ductility compared to the original column. The second repaired column demonstrated excellent stable hysteresis cycles and could reach to drift ratio close to 7%. In both columns the prestressed strands had effectively confined the lap-spliced joint and dowel connection from the column to its footing and no adhesive was required to bind the jacket with the repair grout. Additionally, in both columns, the steel sheet confined by prestressed strands inhibited the concrete spalling and prevented strands from penetrating into the concrete cover even at large drift angles. Strain measurements verified that the active confining pressure provided by prestressed strands remained effective throughout the tests for both columns. Eventually, seismic performance of mainshock-damaged RC columns repaired with different confinement jackets, namely conventional thick steel, FRP, and the proposed hybrid jacket subjected to series of aftershock attacks were investigated. Extensive series of incremental dynamic analysis (IDA) by subjecting a prototype bridge to sequences of mainshock-aftershocks of various intensities (moderate and severe intensity) from different earthquake types (near-fault and far-fault) were conducted. Analytical results obtained from adequately calibrated refined fiber finite element models indicated the effectiveness of the proposed repair technique under severe mainshock-severe aftershock attacks.

The second objective of this study was to develop the composite FRP/PVC confinement system for construction of new bridge columns, and the results of the experimental and analytical investigations conducted were presented in the sections “Paper IV”, and “Paper V”.

This objective involved investigating a new composite confinement system of a fiber reinforced polymer (FRP) sheet wrapped around a polyvinyl chloride (PVC) tube with energy dissipation medium in between for new bridge columns construction. This composite system is essentially a FRP-confined concrete filled PVC tube, featuring exceptional durability and anti-corrosion properties of PVC materials in addition to high strength of the FRP fabrics. In the proposed confined concrete filled PVC tube (CCFPT) confinement was provided with the use of a PVC tube and FRP wrappings or FRP with a sandwiched layer of foam to enhance impact energy reduction due to potential FRP rupture and PVC fracture. Experimental study involved axial and flexural behavior of CCFPT columns through uniaxial compressive and flexural tests, and compared with those of their corresponding concrete filled PVC tube (CFPT) and FRP-wrapped (FW) columns. Experimental test results obtained from stub columns under axial loads and flexural beams under four-point loads indicated that the CCFPT columns can significantly enhance strength over the CFPT columns and enhance ductility over the FW columns. The transverse confining pressure from FRP wrapping and the interface property between the FRP and PVC proved critical in CCFPT design. Furthermore, the idea of introducing a cushioning foam layer between FRP layers and PVC to lessen the brittleness of FRP rupture in seismic regions proved effective.

Analytical studies involved assessing seven existing strength and strain models from previous studies verified against the obtained experimental test results from FRP-wrapped and CCFPT test results. The average relative error (ARE) was used as statistical measure to assess the efficacy and overall accuracy of the existing models. Relations were also derived to predict the ultimate strength and strain conditions of the proposed CCFPT system.

2.2. CONCLUSIONS

The following section summarizes the conclusions from both the experimental and analytical studies, related to the composite confinement systems studied in this research.

2.2.1. Composite Steel Confinement for Repair/Retrofit. Based on the results of this study, the following conclusions can be made:

- The hybrid jacket is a lightweight system of steel materials with no curing requirement. It can be manually installed by a two-member crew in 4 h after fast setting cementitious grout to replace loose concrete in the damaged column has been cured in 8 h. It is a cost-effective technique for post-earthquake emergency repair.
- The confining pressure exerted by prestressing strands is adequate for shear transfer between the steel jacketing and column; no adhesive epoxy or dowel reinforcement is required.
- Sheet metal provides the required bearing strength and prevented cover concrete spalling and penetration of the prestressing cables.
- When repaired with the hybrid jacket, the ultimate strength and displacement ductility of the damaged column were respectively restored to 115% and 140% of those of Column 1 in as-built condition.
- The hybrid jacket can effectively prevent the premature lap-splice failure of the repaired Column 1-R. The initial stiffness of the damaged column, however, was partially restored (84% of that of the as-built column) since the jacket was designed to restore the ultimate strength and ductility only. The jacket applies sufficient passive and active confining pressure on the column surface to prevent cover concrete from spalling.
- The 1.27-mm-thick steel sheet provides the required shear strength to sustain the potential penetration of the 12.7-mm-diameter seven-wire strands that were spaced 102 mm and 152 mm within and outside the spliced region, respectively. The strands in turn restrain the thin steel sheet from potential buckling.

- The prestressing forces in various strands or the active confinement applied on the repaired column suffered little or no loss up to 8% drift. Therefore, the friction force between the sheet metal and the column remained steady throughout the test and effectively restrained flexural cracks in the plastic hinge region from widening.
- Both the as-built and repaired columns with lap splice deficiency did not exhibit appreciable hardening behavior beyond the yield strength, irrespective of the level of confining pressure in the plastic hinge region.
- When repaired with the hybrid jacket and anchored dowel bars, the ultimate strength, initial stiffness, and displacement ductility of the damaged column were restored to 156%, 100%, and 239% of those of Column 2 in as-built condition. Ten 12.5-mm-diameter headed bars, which were anchored into the footing by 250 mm deep and embedded in 25-mm-thick cementitious grout, added significant stiffness in the lap-spliced region of the column and thus provided an effective load transfer mechanism that can compensate for potential lap splice failures.
- Hybrid jacket is shown to be more cost effective compared to conventional thick steel and FRP jackets for rapid repair of earthquake-damaged RC columns.
- Test results indicated that the developed composite confinement jacket was effective as an emergency repair method for the damaged RC columns.

Based on the analytical study, the following conclusions are presented:

- The accumulated damage of bridges under multiple earthquakes is closely related to the intensity of seismic events. Although adequate for a single severe MS event, RC bridges designed with modern seismic codes can significantly degrade when subjected to severe MS-severe AS sequences. Confining repair jackets, including CFRP, can increase the post-repair collapse capacity of severely MS-damaged columns by approximately 20% under severe AS events.
- Moderate AS events results in a slight decrease of the residual collapse capacity of the damaged bridge columns previously attacked by a severe MS.

Therefore, confining repair jackets are insignificant and not required for severely damaged bridge columns under moderate AS events unless post-earthquake high-volume traffic induced fatigue loads are a concern.

- The confining pressures provided by CFRP, steel and hybrid jackets are comparable in improving the post-repair collapse capacity of damaged columns subjected to AS events. Repair interventions that provide only lateral confining pressure (including CFRP, steel and hybrid jackets) cannot restore the stiffness of the repaired column to that of the original column. In comparison with the CFRP jacket, both steel and hybrid jackets provide more energy dissipation and relatively higher stiffness of repaired columns (attracting larger ductility demand in turn). In the case of CFRP repair, bidirectional FRP jackets are recommended for severe MS-damaged columns subjected to severe AS.
- For severe-MS damaged bridge columns subjected to severe AS, an appropriately designed (i.e., not exceeding the residual shear strength of the damaged column, the flexural capacity and the overturning capacity of the original footing due to increased force demands) force transfer system (such as FRP or double headed steel anchors) is recommended to improve the efficacy of repair intervention. Anchorage could compensate for the loss of reduced steel reinforcement properties and could restore and even improve the flexural capacity of the repaired column compared to that of the original column.
- Compared to far-fault ground motions, near-fault ground motions resulted in smaller collapse capacity for the original bridge with no prior damage under severe MS events but larger capacity for the damaged bridge under severe MS-severe AS and severe MS-moderate AS sequences, irrespective of repair methods. This is due to the potential match of the lengthened vibration period of the damaged bridge with the pulse duration in near-fault motions.

2.2.2. Composite FRP/PVC Confinement for New Construction. Based on the results of this study, the following conclusions can be made:

- The PVC tube in a CFPT cylinder added little to axial load capacity due to its low modulus of elasticity. Even so, leaving a small PVC gap at two ends of the cylinder resulted in rapid post-peak strength degradation due to crushing of the unconfined concrete. The PVC tube also provided a relatively low confining pressure on the cylinder. But it can cope with significant concrete dilation and make the concrete cylinder ductile with a strain softening post-peak response. No fracture or crack was observed in PVC tubes tested.
- By introducing additional confinement, the FRP wrap on a CCFPT cylinder can effectively delay outward local buckling of the confined PVC tube and restrain the lateral dilation of the encased concrete, thus increasing both strength and strain capacities of the cylinder.
- The post-peak stress-strain behavior of a CCFPT cylinder is mainly affected by the confining pressure from FRP wrap. When adequately confined by FRP, both carbon and glass FRP resulted in a monotonically increasing stress-strain behavior with an ascending second region. In comparison with carbon wraps, glass wrapping provided significantly greater strain enhancement for the CCFPT cylinder.
- PVC tube fractured right after the rupture of its immediate FRP wraps resulting in a sudden loss of load carrying capacity. This brittle failure mode can be prevented by introducing an energy absorption foam layer between the PVC tube and the FRP wraps. In this case, the strength was gradually reduced in steps.
- The stress-strain curves of CCFPT specimens without compressible foam resembled those of FW specimens with slightly larger ultimate strength and significantly larger ultimate strain. Therefore, the energy dissipation ability of the CCFPT specimens is significantly higher than that of the FW specimens.
- Seven of the most accurate existing stress-strain models from literature were assessed and proved to predict the ultimate strength of axially-loaded CCFPT columns with an average relative error of less than 15%.

2.3. RECOMMENDATIONS

Based on the conclusions listed in the preceding sections, the following aspects for future research on the two types of composite confinement systems are recommended.

Recommendations on composite steel confinement for repair/retrofit:

- Assess the effectiveness of the developed composite repair technique on earthquake-damaged RC bridge columns with shear failure;
- Evaluate the applicability and efficacy of the proposed composite jacket for retrofit (undamaged) applications of existing bridge column;
- Implement shape memory alloy (SMA) hoops instead of prestressing seven-wire steel strands to apply the confining pressure;
- Evaluate the capacity of the bridge system subjected to subduction, interface and in-slab record sets;
- Investigate the effectiveness of the repair between mainshock-aftershock on the bridge post-repair response subjected to near-fault mainshocks and far-fault aftershocks and vice versa.
- Include the load path history effect on the performance limit states used for aftershock analysis.

Recommendations on composite FRP/PVC confinement for new construction:

- Investigate application of other types of concretes including high strength, self-consolidating, and fibrous high performance concretes in confined concrete filled PVC tube (CCFPT) system to produce high-performance, anti-corrosion RC bridge columns;
- Study the axial compressive behavior of CCFPT system under cyclic axial compression;
- Perform large-scale CCFPT columns reinforced with internal steel or FRP rebars under reserved cyclic loading;
- Study the effect of different FRP types and PVC schedules on the CCFPT system;
- Perform durability studies on CCFPT and companion similar CFTP and FRP-wrapped configuration to assess the long term performance of the system.

REFERENCES

- [1] Laplace PN, Sanders DH, Saiidi MS, Douglas BM, El-Azazy S. Performance of concrete bridge columns under shaketable excitation. *ACI structural journal*. 2005;102(3).
- [2] Priestley MN. *Seismic design and retrofit of bridges*: John Wiley & Sons; 1996.
- [3] Mes D. *Seismic retrofitting of concrete bridge columns by external prestressing*. Ottawa, Ontario, Canada: University of Ottawa (Canada); 1999.
- [4] Priestley M, Seible F. Design of seismic retrofit measures for concrete and masonry structures. *Construction and Building Materials*. 1995;9(6):365-77.
- [5] Chai I YH, Priestley MN, Seible F. Seismic retrofit of circular bridge columns for enhanced flexural performance. *ACI Structural Journal*. 1991;88(5).
- [6] ElGawady M, Endeshaw M, McLean D, Sack R. Retrofitting of rectangular columns with deficient lap splices. *Journal of Composites for Construction*. 2009;14(1):22-35.
- [7] Saatcioglu M, Yalcin C. External prestressing concrete columns for improved seismic shear resistance. *Journal of Structural Engineering*. 2003;129(8):1057-70.
- [8] Vosooghi A, Saiidi MS. Design guidelines for rapid repair of earthquake-damaged circular RC bridge columns using CFRP. *Journal of Bridge Engineering*. 2012;18(9):827-36.
- [9] Laplace P, Sanders D, Saiidi M, Douglas B. *Experimental Study and Analysis of Retrofitted Flexure and Shear Dominated Circular Reinforced Concrete Bridge Columns Subjected to Shake Table Excitation*: Center for Earthquake Engineering Research, Department of Civil Engineering, University of Nevada, Reno; 2001.
- [10] Vosooghi A, Saiidi MS. Shake-table studies of repaired reinforced concrete bridge columns using carbon fiber-reinforced polymer fabrics. *ACI Structural Journal*. 2013;110(1).
- [11] Xiao Y, He W, Choi K-k. Confined concrete-filled tubular columns. *Journal of structural engineering*. 2005;131(3):488-97.
- [12] Xiao Y, He W, Mao X, Choi K, Zhu P. Confinement design of CFT columns for improved seismic performance. *Proceedings of the International Workshop on Steel and Concrete Composite Construction (IWSCCC-2003)*: Taipei, China; 2003. p. 217-26.

- [13] Xiao J, Huang Y, Yang J, Zhang C. Mechanical properties of confined recycled aggregate concrete under axial compression. *Construction and Building Materials*. 2012;26(1):591-603.
- [14] Xiao Y, Zhang Z, Hu J, Kunnath SK, Guo P. Seismic behavior of CFT column and steel pile footings. *Journal of Bridge Engineering*. 2011;16(5):575-86.
- [15] Ozbakkaloglu T. Behavior of square and rectangular ultra high-strength concrete-filled FRP tubes under axial compression. *Composites Part B: Engineering*. 2013;54:97-111.
- [16] Ozbakkaloglu T, Saatcioglu M. Seismic behavior of high-strength concrete columns confined by fiber-reinforced polymer tubes. *Journal of Composites for Construction*. 2006;10(6):538-49.
- [17] Shi Y, Zohrevand P, Mirmiran A. Assessment of cyclic behavior of hybrid FRP concrete columns. *Journal of Bridge Engineering*. 2012;18(6):553-63.
- [18] Zohrevand P, Mirmiran A. Behavior of ultrahigh-performance concrete confined by fiber-reinforced polymers. *Journal of Materials in Civil Engineering*. 2011;23(12):1727-34.
- [19] Li B, Zohrevand P, Mirmiran A. Cyclic behavior of FRP concrete bridge pier frames. *Journal of Bridge Engineering*. 2012;18(5):429-38.
- [20] Zohrevand P, Mirmiran A. Cyclic behavior of hybrid columns made of ultra high performance concrete and fiber reinforced polymers. *Journal of Composites for Construction*. 2012;16(1):91-9.
- [21] Zaghi AE, Saiidi MS, Mirmiran A. Shake table response and analysis of a concrete-filled FRP tube bridge column. *Composite Structures*. 2012;94(5):1564-74.
- [22] Mohamed HM, Abdel-Baky HM, Masmoudi R. Nonlinear Stability Analysis of Concrete-Filled Fiber-Reinforced Polymer-Tube Columns: Experimental and Theoretical Investigation. *ACI Structural Journal*. 2010;107(6).
- [23] Teng J, Lam L. Behavior and modeling of fiber reinforced polymer-confined concrete. *Journal of Structural Engineering*. 2004;130(11):1713-23.
- [24] Yu T, Fang X, Teng J. FRP-Confined Self-Compacting Concrete under Axial Compression. *Journal of Materials in Civil Engineering*. 2013.
- [25] Zhao J, Yu T, Teng J. Stress-Strain Behavior of FRP-Confined Recycled Aggregate Concrete. *Journal of Composites for Construction*. 2014.

- [26] Ozbakkaloglu T, Lim JC. Axial compressive behavior of FRP-confined concrete: Experimental test database and a new design-oriented model. *Composites Part B: Engineering*. 2013;55:607-34.
- [27] Ozbakkaloglu T, Lim JC, Vincent T. FRP-confined concrete in circular sections: Review and assessment of stress–strain models. *Eng Struct*. 2013;49:1068-88.
- [28] Vincent T, Ozbakkaloglu T. Influence of concrete strength and confinement method on axial compressive behavior of FRP confined high-and ultra high-strength concrete. *Composites Part B: Engineering*. 2013;50:413-28.
- [29] Wang Y-h, Nie J-g, Cai C. Numerical modeling on concrete structures and steel–concrete composite frame structures. *Composites Part B: Engineering*. 2013;51:58-67.
- [30] Wong Y, Yu T, Teng J, Dong S. Behavior of FRP-confined concrete in annular section columns. *Composites Part B: Engineering*. 2008;39(3):451-66.
- [31] Idris Y, Ozbakkaloglu T. Seismic behavior of high-strength concrete-filled FRP tube columns. *Journal of Composites for Construction*. 2013;17(6).
- [32] Abdelkarim OI, ElGawady MA. Analytical and Finite-Element Modeling of FRP-Concrete-Steel Double-Skin Tubular Columns. *Journal of Bridge Engineering*. 2014.
- [33] Han L-H, Tao Z, Liao F-Y, Xu Y. Tests on cyclic performance of FRP–concrete–steel double-skin tubular columns. *Thin-Walled Structures*. 2010;48(6):430-9.
- [34] Belarbi A, Bae S-W. An experimental study on the effect of environmental exposures and corrosion on RC columns with FRP composite jackets. *Composites Part B: Engineering*. 2007;38(5):674-84.
- [35] Wang J-Y, Yang Q-B. Investigation on compressive behaviors of thermoplastic pipe confined concrete. *Construction and Building Materials*. 2012;35:578-85.
- [36] Pando MA, Ealy CD, Filz GM, Lesko J, Hoppe E. A Laboratory and Field Study of Composite Piles for Bridge Substructures. FHWA-HRT-04-0432006.
- [37] Nanni A, Norris M, Bradford N. Lateral confinement of concrete using FRP reinforcement. *ACI Special Publication*. 1993;138.
- [38] Nanni A, Bradford NM. FRP jacketed concrete under uniaxial compression. *Construction and Building Materials*. 1995;9(2):115-24.
- [39] Karbhari VM. *Durability of composites for civil structural applications*: Elsevier; 2007.

- [40] Naghibdehi MG, Sharbatdar M, Mastali M. Repairing reinforced concrete slabs using composite layers. *Materials & Design*. 2014;58:136-44.
- [41] Li Y, Song R, Van De Lindt JW. Collapse Fragility of Steel Structures Subjected to Earthquake Mainshock-Aftershock Sequences. *Journal of Structural Engineering*. 2014;140(12).
- [41] Ribeiro FL, Barbosa AR, Neves LC. Application of Reliability-Based Robustness Assessment of Steel Moment Resisting Frame Structures under Post-Mainshock Cascading Events. *Journal of Structural Engineering*. 2014;140(8).
- [43] Terzic V, Stojadinovic B. Evaluation of Post-Earthquake Axial Load Capacity of Circular Bridge Columns. *ACI Structural Journal*. 2014;111(1-6).
- [44] Li Y, Song R, van de Lindt J, Nazari N, Luco N. Assessment of wood and steel structures subjected to earthquake mainshock-aftershock. 15th World Conf on Earthquake Engineering 2012.
- [45] Di Sarno L. Effects of multiple earthquakes on inelastic structural response. *Engineering Structures*. 2013;56:673-81.
- [46] Mander JB, Priestley MJ, Park R. Theoretical stress-strain model for confined concrete. *Journal of structural engineering*. 1988;114(8):1804-26.
- [47] Lopez A, Galati N, Alkhrdaji T, Nanni A. Strengthening of a reinforced concrete bridge with externally bonded steel reinforced polymer (SRP). *Composites Part B: Engineering*. 2007;38(4):429-36.
- [48] Teng J, Chen J, Smith ST, Lam L. Behaviour and strength of FRP-strengthened RC structures: a state-of-the-art review. *Proceedings of the ICE-Structures and Buildings*. 2003;156(1):51-62.
- [49] Fam AZ, Rizkalla SH. Confinement model for axially loaded concrete confined by circular fiber-reinforced polymer tubes. *ACI Structural Journal*. 2001;98(4).
- [50] Eslami A, Ronagh H. Effect of FRP wrapping in seismic performance of RC buildings with and without special detailing—A case study. *Composites Part B: Engineering*. 2013;45(1):1265-74.
- [51] El Chabib H, Nehdi M, El Naggar M-H. Behavior of SCC confined in short GFRP tubes. *Cement and Concrete Composites*. 2005;27(1):55-64.
- [52] Yan Z, Pantelides CP, Reaveley LD. Posttensioned FRP composite shells for concrete confinement. *Journal of Composites for Construction*. 2007;11(1):81-90.

- [53] Fakharifar M, Sharbatdar M, Lin Z, Dalvand A, Sivandi-Pour A, Chen G. Seismic performance and global ductility of RC frames rehabilitated with retrofitted joints by CFRP laminates. *Earthquake Engineering and Engineering Vibration*. 2014;13(1):59-73.
- [54] Lin Z, Fakhairfar M, Wu C, Chen G, Bevans W, Gunasekaran AVK, et al. Design, Construction and Load Testing of the Pat Daly Road Bridge in Washington County, MO, with Internal Glass Fiber Reinforced Polymers Reinforcement. 2013.
- [55] Rousakis TC, Tourtouras IS. RC columns of square section–Passive and active confinement with composite ropes. *Composites Part B: Engineering*. 2014;58:573-81.
- [56] Rousakis TC, Kouravelou KB, Karachalios TK. Effects of carbon nanotube enrichment of epoxy resins on hybrid FRP–FR confinement of concrete. *Composites Part B: Engineering*. 2014;57:210-8.
- [57] Anggawidjaja D, Ueda T, Dai J, Nakai H. Deformation capacity of RC piers wrapped by new fiber-reinforced polymer with large fracture strain. *Cement and Concrete Composites*. 2006;28(10):914-27.
- [58] Shimomura T, Phong N. Structural performance of concrete members reinforced with continuous fiber rope. FRPRCS-8 Conference University of Patras, Patras, Greece2007.
- [59] He R, Sneed LH, Belarbi A. Rapid Repair of Severely Damaged RC Columns with Different Damage Conditions: An Experimental Study. *International Journal of Concrete Structures and Materials*. 2013;7(1):35-50.
- [60] Micelli F, Angiuli R, Corvaglia P, Aiello MA. Passive and SMA-activated confinement of circular masonry columns with basalt and glass fibers composites. *Composites Part B: Engineering*. 2014;67:348-62.
- [61] Andrawes B, Shin M, Wierschem N. Active confinement of reinforced concrete bridge columns using shape memory alloys. *Journal of Bridge Engineering*. 2009;15(1):81-9.
- [62] Choi E, Kim J-W, Rhee I, Kang J-W. Behavior and modeling of confined concrete cylinders in axial compression using FRP rings. *Composites Part B: Engineering*. 2014;58:175-84.
- [63] Fakharifar M, Chen G, Sneed L, Dalvand A. Seismic performance of post-mainshock FRP/steel repaired RC bridge columns subjected to aftershocks. *Composites Part B: Engineering*. 2014.

- [64] He R, Yang Y, Sneed LH. Seismic Repair of Reinforced Concrete Bridge Columns: Review of Research Findings. *Journal of Bridge Engineering*. 2015;04015015.
- [65] Haroun MA, Elsanadedy HM. Fiber-reinforced plastic jackets for ductility enhancement of reinforced concrete bridge columns with poor lap-splice detailing. *Journal of Bridge Engineering*. 2005;10(6):749-57.
- [66] Buckle I, Friedland I, Mander J, Martin G, Nutt R, Power M. Seismic retrofitting manual for highway structures: part 1-bridges. 2006.
- [67] Koch GH, Brongers MP, Thompson NG, Virmani YP, Payer JH. Corrosion cost and preventive strategies in the United States. 2002.
- [68] Hollaway LC, Leeming M. Strengthening of reinforced concrete structures: Using externally-bonded FRP composites in structural and civil engineering: Elsevier; 1999.
- [69] Weyers RE, Prowell BD, Sprinkel MM, Vorster M. Concrete bridge protection, repair, and rehabilitation relative to reinforcement corrosion: A methods application manual. *Contract*. 1993;100:103.
- [70] Ghasemi H, Otsuka H, Cooper JD, Nakajima H. Aftermath of the kobe earthquake. *Public Roads*. 1996;60(2).
- [71] Itani R. Effects of retrofitting applications on reinforced concrete bridges. 2003.
- [72] Caltrans S. Caltrans Seismic Design Criteria. California Department of Transportation, Sacramento, CA. 2010.
- [73] Chai Y. AN ANALYSIS OF THE SEISMIC CHARACTERISTICS OF STEEL-JACKETED CIRCULAR BRIDGE COLUMNS. *Earthquake engineering & structural dynamics*. 1996;25(2):149-61.
- [74] Mitchell D, Bruneau M, Saatcioglu M, Williams M, Anderson D, Sexsmith R. Performance of bridges in the 1994 Northridge earthquake. *Canadian Journal of Civil Engineering*. 1995;22(2):415-27.
- [75] Aboutaha RS, Engelhardt MD, Jirsa JO, Kreger ME. Retrofit of concrete columns with inadequate lap splices by the use of rectangular steel jackets. *Earthquake Spectra*. 1996;12(4):693-714.
- [76] Bett BJ, Klingner RE, Jirsa JO. Lateral load response of strengthened and repaired reinforced concrete columns. *ACI Structural Journal*. 1988;85(5).
- [77] Rodriguez M, Park R. Seismic load tests on reinforced concrete columns strengthened by jacketing. *ACI Structural Journal*. 1994;91(2).

- [78] Priestly M, Seible F. Repair of shear column using fiberglass/epoxy jacket and epoxy injection. Rep No 93-04, Job No 90. 1993;8.
- [79] Saadatmanesh H, Ehsani MR, Jin L. Seismic strengthening of circular bridge pier models with fiber composites. *ACI Structural Journal*. 1996;93(6).
- [80] Seible F, Priestley MN, Hegemier GA, Innamorato D. Seismic retrofit of RC columns with continuous carbon fiber jackets. *Journal of composites for construction*. 1997;1(2):52-62.
- [81] Saadatmanesh H, Ehsani M, Jin L. Seismic retrofitting of rectangular bridge columns with composite straps. *Earthquake Spectra*. 1997;13(2):281-304.
- [82] Xiao Y, Ma R. Seismic retrofit of RC circular columns using prefabricated composite jacketing. *Journal of structural engineering*. 1997;123(10):1357-64.
- [83] Sheikh SA, Yau G. Seismic behavior of concrete columns confined with steel and fiber-reinforced polymers. *ACI Structural Journal*. 2002;99(1).
- [84] Cheng C-T, Yang J-C, Yeh Y-K, Chen S-E. Seismic performance of repaired hollow-bridge piers. *Construction and Building Materials*. 2003;17(5):339-51.
- [85] Li Y-F, Sung Y-Y. Seismic repair and rehabilitation of a shear-failure damaged circular bridge column using carbon fiber reinforced plastic jacketing. *Canadian Journal of Civil Engineering*. 2003;30(5):819-29.
- [86] Belarbi A, Silva PF, Bae S-W. Retrofit using CFRP composites of RC bridge columns under combined loads. Proc, 4th Int Symp on FRP Composites in Civil Engineering (CICE): EMPA Duebendorf, Switzerland; 2008.
- [87] Vosooghi A, Saiidi M, Gutierrez J. Rapid repair of RC bridge columns subjected to earthquakes. Proceedings of 2nd international conference on concrete repair, rehabilitation, and retrofitting 2008. p. 397-8.
- [88] Vosooghi A, Saiidi M. Rapid repair of high-shear earthquake-damaged RC bridge columns. Proceedings of 25th US–Japan bridge engineering workshop, Tsukuba, Japan 2009.
- [89] ElSouri AM, Harajli MH. Seismic repair and strengthening of lap splices in RC columns: carbon fiber–reinforced polymer versus steel confinement. *Journal of Composites for Construction*. 2011;15(5):721-31.
- [90] Sun Z, Wang D, Du X, Si B. Rapid repair of severely earthquake-damaged bridge piers with flexural-shear failure mode. *Earthquake Engineering and Engineering Vibration*. 2011;10(4):553-67.

- [91] Rutledge ST, Kowalsky MJ, Seracino R, Nau JM. Repair of reinforced concrete bridge columns containing buckled and fractured reinforcement by plastic hinge relocation. *Journal of Bridge Engineering*. 2013;19(8):A4013001.
- [92] Yang Y, Sneed LH, Morgan A, Saiidi MS, Belarbi A. Repair of RC bridge columns with interlocking spirals and fractured longitudinal bars—An experimental study. *Construction and Building Materials*. 2015;78:405-20.
- [93] Yang Y, Sneed L, Saiidi MS, Belarbi A, Ehsani M, He R. Emergency Repair of an RC Bridge Column with Fractured Bars using Externally Bonded Prefabricated Thin CFRP Laminates and CFRP Strips. *Composite Structures*. 2015;133:727-38.
- [94] Coffman HL, Marsh ML, Brown CB. Seismic durability of retrofitted reinforced-concrete columns. *Journal of Structural Engineering*. 1993;119(5):1643-61.
- [95] Lin Y, Gamble W, Hawkins N. Report to ILLDOT for Testing of Bridge Piers, Poplar Street Bridge Approaches. Internal Report, Department of Civil Engineering, University of Illinois at Urbana-Champaign; 1994.
- [96] Priestley MJN, Seible F, Chai YH. Design guidelines for assessment retrofit and repair of bridges for seismic performance: Dept. of Applied Mechanics & Engineering Sciences, University of California, San Diego; 1992.
- [97] Yalcin C. Seismic evaluation and retrofit of existing reinforced concrete bridge columns. Ottawa: University of Ottawa (Canada). 1998.
- [98] Beauséjour P. Seismic retrofit of concrete columns with splice deficiencies by external prestressing. Ottawa: University of Ottawa (Canada). 2000.
- [99] Yarandi MS. Seismic retrofit and repair of existing reinforced concrete bridge columns by transverse prestressing [PhD thesis]. Ottawa: University of Ottawa; 2007.
- [100] Sabri A. Seismic Retrofit of Concrete Columns by Transverse Prestressing. Ottawa: University of Ottawa; 2013.
- [101] Miyagi T, Yamakawa T, Li W, Rahman M. A Study on Emergency Retrofit using Prestressing Bars and Steel Plates for Damaged Column. 13th World Conference on Earthquake Engineering 2004. p. 1-6.
- [102] Nesheli K, Meguro K. External prestressing concrete columns with fibrous composite belts. 7th Int Symp on Fiber-Reinforced Polymer for Concrete Structures (FRPRCS-7): American Concrete Institute Farmington Hills, MI; 2005. p. 1631-46.

- [103] Nesheli KN, Meguro K. Seismic retrofitting of earthquake-damaged concrete columns by lateral pre-tensioning of FRP belts. Proc, 8th US National Conf on Earthquake Engineering: Earthquake Engineering Research Institute (EERI) El Cerrito, CA; 2006.
- [104] Kyoda N, Yamakawa T, Nakada K, Javadi P, Nagahama A. Emergency Retrofit for Damaged RC Columns by Fiber Belts Prestressing and Plywoods. *Advances in FRP Composites in Civil Engineering*: Springer; 2011. p. 801-5.
- [105] Zhou C, Lu X, Li H, Tian T. Experimental study on seismic behavior of circular RC columns strengthened with pre-stressed FRP strips. *Earthquake Engineering and Engineering Vibration*. 2013;12(4):625-42.
- [106] Hawkins G, Patel N, Steckel G. Failure analysis of highway bridge column composite overwraps. *First International Conference on Composites in Infrastructure*1996.
- [107] Shin M, Andrawes B. Emergency repair of severely damaged reinforced concrete columns using active confinement with shape memory alloys. *Smart Materials and Structures*. 2011;20(6):065018.
- [108] Shin M, Andrawes B. Lateral cyclic behavior of reinforced concrete columns retrofitted with shape memory spirals and FRP wraps. *Journal of Structural Engineering*. 2010;137(11):1282-90.
- [109] Kurt CE. Concrete filled structural plastic columns. *Journal of the Structural Division*. 1978;104(1):55-63.
- [110] Toutanji H, Saafi M. Durability studies on concrete columns encased in PVC–FRP composite tubes. *Composite structures*. 2001;54(1):27-35.
- [111] Wang J, Yang Q. Experimental study on Mechanical Properties of concrete confined with plastic Pipe. *ACI Materials Journal*. 2010;107(2).
- [112] Nowack R, Otto OI, Braun EW. „60 Jahre Erfahrungen mit Rohrleitungen aus weichmacherfreiem Polyvinylchlorid (PVC-U). *KRV Nachrichten*. 1995:1-95.
- [113] Awham M, Salih ZGM. A Study of some Mechanical Behavior on a Thermoplastic Material.
- [114] Al-Malaika S, Golovoy A, Wilkie CA. *Chemistry and technology of polymer additives*: Blackwell Science; 1999.
- [115] Titow WV. *PVC technology*: Springer; 1984.
- [116] Toutanji H, Saafi M. Stress-strain behavior of concrete columns confined with hybrid composite materials. *Materials and Structures*. 2002;35(6):338-47.

- [117] Soliman S, El-kareim A. Behavior of long confined concrete column. *Ain Shams Engineering Journal*. 2011;2(3):141-8.
- [118] Gupta PK. Confinement of concrete columns with unplasticized Poly-vinyl chloride tubes. *International Journal of Advanced Structural Engineering*. 2013;5(1):19.
- [119] Gupta PK, Verma VK. Study of concrete-filled unplasticized poly-vinyl chloride tubes in marine environment. *Proceedings of the Institution of Mechanical Engineers, Part M: Journal of Engineering for the Maritime Environment*. 2014:1475090214560448.
- [120] Gathimba Naftary K, Oyawa Walter O, Mang'uriu Geoffrey N. Compressive Strength Characteristics of Concrete-Filled Plastic Tubes Short Columns. *International Journal of Science and Research (IJSR)*. 2014;3(9):2168-74.
- [121] Jiang S-F, Ma S-L, Wu Z-Q. Experimental study and theoretical analysis on slender concrete-filled CFRP-PVC tubular columns. *Construction and Building Materials*. 2014;53:475-87.
- [122] Fam AZ, Rizkalla SH. Concrete-filled FRP tubes for flexural and axial compression members. *Proceedings of ACMBS-3, Ottawa, Canada*. 2000:315-22.
- [123] Li G, Pang S-S, Helms JE, Mukai D, Ibekwe SI, Alaywan W. Stiffness degradation of FRP strengthened RC beams subjected to hygrothermal and aging attacks. *Journal of composite materials*. 2002;36(7):795-812.
- [124] Jakubowicz I, Yarahmadi N, Gevert T. Effects of accelerated and natural ageing on plasticized polyvinyl chloride (PVC). *Polymer degradation and stability*. 1999;66(3):415-21.
- [125] Newman E, Stark T. Ten-year PVC geomembrane durability. *Geosynthetics International*. 2009;16(2):97-108.
- [126] Punj B, Singh G. Current trends in pipe coating technology and applications. *Internal and External Protection of Pipes--Proceedings of the 8 th International Conference 1989*. p. 49-64.
- [127] Matthys S, Toutanji H, Audenaert K, Taerwe L. Axial load behavior of large-scale columns confined with fiber-reinforced polymer composites. *ACI Structural Journal*. 2005;102(2).
- [128] Vincent T, Ozbakkaloglu T. Influence of fiber orientation and specimen end condition on axial compressive behavior of FRP-confined concrete. *Construction and Building materials*. 2013;47:814-26.

VITA

Mostafa Fakharifar was born in Tehran, Iran. He received his M.S. degree in Civil Engineering with emphasis on Earthquake Engineering from Semnan University working on nonlinear dynamic analysis of retrofitted reinforced concrete frames with FRP wraps under earthquake excitations in 2010. His research work during his masters involved experimentation and simulation of various reinforced concrete structural members rehabilitated with fiber reinforced composites. After graduation with master degree, he worked as the head of structural engineering department of [Vima Company](#), a subsidiary to [Kayson Company](#). He was involved in the design and construction of a wide range of civil engineering structures such as steel space frame structures, industrial structures, buildings and bridges.

He joined Missouri S&T in August 2011 to pursue his Ph.D. studies. He was a Civil-Structural Engineering Ph.D. student in Civil, Architectural, and Environmental Department at the Missouri University of Science and Technology (Missouri S&T). During his Ph.D. program he worked on several projects dealing with full scale construction and experimentation on FRP-reinforced bridge girders and slabs, repair of large scale earthquake damaged bridge columns, material characterization of various composite systems, developing corrosion-free composite column systems using fiber reinforced composites and polyvinyl chloride materials, collapse analysis and finite element simulations of bridge structures subjected to earthquake excitations. In May, 2016, he received his PhD in Civil Engineering with emphasis on Structural Engineering from Missouri University of Science and Technology.